Advanced Control of Renewable Energy Microgrids with Hybrid Energy Storage System

by

Felix Garcia Torres

Microgrids Laboratory
Simulation and Control Unit
(Centro Nacional del Hidrogeno)

Department of Systems Engineering and Automation
Escuela Técnica Superior de Ingenieros
(Universidad de Sevilla)

A thesis submitted for the degree of

Doctor Ingeniero Industrial por la Universidad de Sevilla

Supervisor: Dr. Carlos Bordons Alba

Seville, Spain, 2015

A Gloría, a Miriam y a Esther por el tiempo que os he robado...
A mis padres, hermanos y madrina, en el fondo todo lo que soy os lo debo a vosotros

Abstract

ADVANCED CONTROL OF RENEWABLE ENERGY MICROGRIDS WITH HYBRID ENERGY STORAGE SYSTEM
by Felix Garcia Torres

Supervisor: Dr. Carlos Bordons Alba.

Renewable energy will play an important role in the transition to a new energetic model which, along with other developments of the digital age, will probably bring about the Third Industrial Revolution. However, the change to this new energetic model is subject to overcoming technological barriers, namely the sporadic nature of renewable sources. Which in turn affects both, power quality and economic competitiveness.
The imbalance of active and reactive power that renewable energies introduce in the grid causes variation in the voltage supply, grid frequency, harmonics, as well as producing other power quality issues. Energy storage systems appear to be a key factor in compensating generation and demand.
The lack of controllability and the penalty for deviations in the regulation market hinder the economic competitiveness of renewable energy. Energy storage systems will be the technological solution enabling controllability in renewable energies, allowing their introduction in the spot energy market.
Redesigning the grid into smaller, more manageable units based on microgrids appears as a solution to the outlined problems. In these microgrids, stored energy compensates both the intermittent nature of renewable generation and the randomness of the consumer's behaviour. Traditionally, energy storage has been developed by large hydropower-regulation plants, however, these kinds of plants are subject to natural emplacements and their implementation is subject to environmental impact grades. The high energy density of hydrogen as an energy carrier will play an important role in this new energetic paradigm. However, robust performance and the transient response are the main barriers for its technological implantation and, usually, hydrogen-based systems have a useful life that is sometimes too limited to buffer the associated cost. Batteries and supercapacitors have a better transient response, however, their low energy density

does not provide enough autonomy to the system. The design of a hybrid energy storage system, having advanced control systems in charge of taking advantage of each storage system and avoiding the causes of degradation and/or limitations of them, emerges as a technological solution to the problems commented.
The high number of constraints and variables to be optimized increases the complexity of the associated control problem, making it necessary to deploy advanced control algorithms. In this thesis, the development of optimal controllers for renewable energy microgrids with hybrid energy storage systems is explored using Model Predictive Control (MPC). The control system is introduction on different time scales resulting in an optimal control solution for the economic dispatch and the power quality of the microgrid. Meanwhile, degradation issues of energy storage systems are analyzed and minimized, improving the longevity of the whole energy storage system.

Estación de FF.CC. "La Alhondiguilla", Córdoba, 2015

Acknowledgements

Esta tesis doctoral es fruto de las experiencias que he recibido a lo largo tanto de mi vida profesional como personal, es por ello, que en estos momentos deseo detenerme y expresar mis agradecimientos a todas las personas que han contribuido a que este trabajo haya sido realizado.

En primer lugar, quiero agradecer a Carlos, como director de la tesis, por su actitud siempre constructiva, así como, por su paciencia sin límites durante todo este tiempo. No sólo quiero agradecerle todo lo que me ha aportado a nivel técnico, sino también todo lo que me ha aportado como persona.

Desearía agradecer a toda la plantilla del Centro Nacional del Hidrogeno, pues en el fondo todos han aportado su granito de arena a esta tesis doctoral, de manera muy especial a Lourdes Rodriguez Mayor, como directora, quien siempre apoyó e impulsó la realización de este trabajo. Querría hacer una mención especial a María Jaén y a Ana Cortecero, por su amistad y el ánimo que me prestaron en los momentos más difíciles de esta tesis. A Carlos, a Dani y a Ernesto como compañeros de unidad, por sus multiples comentarios y aportaciones a esta tesis doctoral. De mi estancia en la Universidad, quiero agradecer la ines-timable ayuda de Luis Valverde en las pruebas experimentales de la microrred y de Sergio Vázquez en la parte de electrónica de potencia. De la misma forma expresar mis agradecimientos a las correciones que Selina Martínez Keogh realizó para que la tesis pudiese ser presentada en inglés. No me gustaría olvidar a la gente de GreenPower, donde aprendí muchos conceptos de electrónica de potencia y de quienes hoy aun recibo muestras de amistad y compañerismo. De la misma forma, recordar el año inolvidable que pasé en el IAI, dando especial agradecimiento al Dr. Domingo Guinea y a Eugenio Villanueva con quienes empecé esta etapa de la vida. Je voudrais aussi me rappeler de mes premières collègues de travail et superviseurs, Jean

Pierre Belliard, Bernard Cottiers et Fabrice Thebault, aujourd'hui, je finis ça que avec vous j'ai commencé.

Realizar un especial recuerdo a mis compañeros de la escuela, Antonio, Manolo, Fran, Castro, Félix, Edu, Cordobés, Chico, Isa, Gema, Carolina, Alberto, Alicia, Victor, Dani y Jorge, entre otros, es un lujo que diez años más tarde siga manteniendo vuestra amistad.

Para terminar me gustaría hacer mención a aquellos amigos de la infancia, adolescencia y vida actual que consiguieron este hito o no perdieron el ideal de alcanzarlo, como el Dr. Jorge Alcantara, el Dr. Kike Doblas, el Dr. Gustavo Becerra, el Dr. Miguel Romero, el Dr. Rafael Llompart y la aspirante a doctora Carmen Díaz, vuestro ímpetu siempre me sirvió de aliento para terminar este trabajo.

Do or do not. There is no try
Master Yoda
Star Wars: Episode V
The Empire Strikes Back

Glossary

Roman Symbols

A_i Surface Area (cm^2)

C_i Capacity (Wh)

CC Capital Cost (€)

$Cost$ Hourly economic Cost (€/h)

$Cycles$ Number of life cycles (Cycles)

F Faraday Constant (96485 C)

h_i Hour i

$Hours_i$ Number of life hours

I_i Current (A)

I_o Exchange Current (A)

LOH Level of Hydrogen (Nm^3)

m_j Minute j

N_i^{cell} Number of cells ($cells$)

P_i Electric Power (W)

R Universal Gas Constant (8.3145 $J/(mol \cdot K)$)

R_{ohm} Ohmic Resistor (Ω)

SH Schedule Horizon

SOC_i State of Charge ($p.u.$)

t_k Generic Instant

T_s Sample period (s)

z_i Electric power formulated as MLD variable (W)

Greek Symbols

δ_i on/off state

η_i Performance ($p.u$)

χ_i Logical degradation state

ϑ_i MLD power variation in degradation state (W)

ς_{elz} Electrolyzer Consumption (Nm^3/kWh)

ς_{fc} Fuel Cell Consumption (kWh/Nm^3)

σ_i Logical variable start up/shut down state

Γ_i Energy price(€)

Λ_i Logical order signal to start up

φ_i Constant time to start up of the system

Superscripts

max Maximum Value

min Minimum Value

off Off State

on On State

ref Reference

sch Schedule

$shutdown$ Shut Down

$startup$ Startup

DM Daily Market

IM Intraday Market

RM Regulation Service Market

Subscripts

bat Battery

ch Charge

$degr$ Degradation

dev Deviation

dis Discharge

$down$ Down

elz Electrolyzer

fc Fuel Cell

$grid$ Main grid

h_2 Hydrogen

$load$ Load

pur Purchase of energy

pv Photovoltaic system

reg Regulation

rem Remaining power

$sale$ Sale

uc Ultracapacitor

up Up

wt Wind turbine

$\mu grid$ Microgrid

Acronyms

AC Altern Current

ARMA Auto-Regressive Moving Average

BDOS Base Daily Operating Schedule

BESS Battery Energy Storage System

BOP Balance of Plant

BOS Base Operating Schedule

BSP Balance Service Provider

CAES Compressed-Air Energy Storage

CERTS Consortium for Electric Reliability Technology Solutions

CSC Current Source Converter

DC Direct Current

DER Distributed Energy Resources

DG Distributed Generation

DS Distributed Storage

ELZ Electrolyzer

EMS Energy Management System

ENTSO-E European Network of Transmission System Operators for Electricity System

ESS Energy Storage System

EWEA European Wind Energy Association

EU European Union

FBESS Flow Battery Energy Storage System

FC Fuel Cell

FESS Flywheel Energy Storage System

HESS Hydrogen Energy Storage System

HF High Frequency

HV High Voltage

ICE Internal Combustion Engine

ICT Information and Communications Technology

IGBT Insulated Gate Bipolar Transistor

IPS Intelligent Power Switch

LQR Lineal Quadratic Regulator

LMP Locational Marginal Pricing

LV Low Voltage

MIBEL Iberian Electricity Market

MLD Mixed Logic Dynamic

MIQP Mixed Integer Quadratic Programming

MPPT Maximum Power Point Tracking

MV Medium Voltage

MPC Model Predictive Control

NRA National Regulatory Authority

PHS Pumped Hydro-Storage

SMES Superconducting Magnetic Energy Storage

SOC State of Charge

TSO Transmission System Operator

UESS Ultracapacitor Energy Storage System

UPS Uninterrupted Power System

VSI Voltage Source Inverter

2L-VSI Two Level Voltage Source Inverter

Contents

List of Figures

List of Tables

Chapter 1

Introduction

Renewable energy will play an important role within a society that is not only increasingly more energy dependent but is also more aware of environmental problems. At the end of the last century and the beginning of the 21th, our society has taken part in one of the historic episodes in which more technological developments have ever been witnessed.

The First and Second Industrial Revolutions were a conjunction of energy resource use, social consciousness and technological developments. The end of the fossil fuel age, respect for the environment and the introduction of the digital age are concepts in the use of the energy which appear as catalysers of the Third Industrial Revolution, as several authors or economists, such as Jeremy Rifkin, begin to prophesy [1].

Considering both previous revolutions, it is essential to realise the impor-tance of energy storage. The use of coal and petrol were decisive for the develop-ment of the First and Second Industrial Revolutions. But coal and petrol have been one of ways in which nature has been storing solar energy for years. The control-lability of fossil fuels stored energy has allowed our electric power system based on power plants to develop. These electric systems produce energy according to end-user needs, transmitting the energy through transport and distribution lines. The economy of producing energy in this way has created a centralised generation based system. Nowadays, natural energy-stored resources are coming to their end, which will globally change the way our society manages energy. In this new energetic paradigm, energy use will be limited to its availability in time. Losses associated with energy transport should be avoided, so in this context energy should be produced beside the load consumption. Once renewable energy technology has been developed, energy can be produced anywhere thanks to re-newable resources. Nowadays, natural energy stored in fossil fuels is coming to

its end. This fact will globally change the way our society manages energy. In this new energetic paradigm, energy use will be limited to its availability in time. The losses associated to the energy transport should be avoided, in this context, energy should be produced beside the load consumption. Once the renewable energy technology has been developed, the energy can be produced in everywhere with renewable resources. Resources will be limited to the time in which they are available. This availability can be obtained through an appropriate ESS (Energy Storage System). This has begun to change the traditional conception of a centralised generation system towards one system is increasingly more distributed. This model minimises transport losses if the generation is produced next to the consumption. This new scheme is known as DG (Distributed Generation). The benefits of renewable energy and DG, have been manifested in several studies and projects but the randomness associated to this kind of energy has still has to overcome several challenges [2].

High penetration of renewable energy produces energy imbalances in the grid with the associated problems in power quality supply, such as, flickers, sags, variations in frequency and voltage level of the main grid. On the other hand, the increasing level of electronic loads in the grid requires even greater levels of power quality [3, 4].

The electricity market rules determine the energy price in the spot energy market, matching offers from generators to bids from consumers to develop a classic supply and demand equilibrium price, usually on an hourly interval. The unpredictability of renewable energy joined with the penalty deviations used in the regulation market make it difficult for clean energy to play an important role in the system. The definitive technological implementation of renewable energies will be subject to its economic competitiveness.

1.1 Energy Storage in Smart Grids

The latest progress (technical and regulatory) in renewable energy is reaching high penetration of wind and solar energy in the different national grids. This fact should be positive for our society, but management of these random power inputs in the grid is beginning to be a barrier in the management of the grid. The intrinsic characteristics of non-dispatchability, unpredictability and intermittency highlight the need for new schemes to control the grid [2, 3, 5].

In this context, dividing the grid into smaller, more management units, such as microgrids, appears to be a structural solution. Different accepted defini-tions of a microgrid exist, the Consortium for Electric Reliability Technology Solutions

(CERTS) defines a microgrid as an *aggregation of loads and microsources operating as a single system providing both power and heat* [5]. The term microgrid is usually used to describe a customer-owned installation containing generation, as well as consumption, where there is large controllability of the power exchange between the microgrid and the rest of the grid [3, 4].

A consistent definition of smart grid does not currently exist, but this term is used to introduce Information and Communications Technology (ICT) when managing the grid. At the moment, a consistent definition of smart grid, but this term is used to introduce the Information and Communications Technology (ICT) in the form of managing the grid. According to the European Technology Platform for Smart Grids, the concept of Smart grids was developed in 2006 and concerns an electricity network that can intelligently integrate the actions of all users connected to it - generators, consumers and those that do both - in order to efficiently deliver sustainable, economic and secure electricity supplies. A smart grid employs innovative products and services together with intelligent monitoring, control, communication, and self-healing technologies in order to:

- Better facilitate the connection and operation of generators of all sizes and technologies
- Allow consumers to play a part in optimizing the operation of the system
- Provide consumers with greater information and options for choice of supply
- Significantly reduce the environmental impact of the whole electricity supply system
- Maintain or even improve the existing high levels of system reliability, quality and security of supply
- Maintain and improve the existing services efficiently
- Foster market integration towards an European integrated market.

Smart grids deployment must include not only technology, market and commercial considerations, environmental impact, regulatory framework, standardization usage, ICT and migration strategy but also societal requirements and governmental edicts. The grid is becoming a distributed generation scheme which is witnessing an increase in Distributed Energy Resources (DER) and how the end-user is beginning to acquire an active participation. From this point of view, the transition to the new energetic paradigm has begun with the introduction of smart meters in the grid. The introduction of an advanced metering infrastructure and

two-way communication technologies can provide both consumers and operators with a virtual platform to make decisions [3, 4]. Since Nicola Tesla introduced the concept of the current electric power system, the system has taken shape in an environment where production capacity and the consumption demand were two different issues. Controllability of the traditional power plants based on the stored energy of fossil fuels, has allowed the system to manage generation and demand through a daily spot market. The imbalances are corrected with economic penalisation in the regulation market in the most common way, storing energy in large hydropower-regulation plants. However, these kinds of plants are subject to natural emplacements and their implementation is dependent on environmental impact grades.

The automation system of the traditional power system is still based on the design and operation of the system as it was decades ago [3, 4]. The introduction of the ICT, will upgrade all the power system automation (including transmission, distribution, substation, individual feeders using the latest technology). These aspects will completely change the conception of the grid, becoming more active where even the customer can monitor their own voltage and power and manage their energy consumption, for example based on the electricity prices [3, 4]. But the change does not finish here, the decreasing costs of renewable energies, the continuous introduction of energy storage technologies, linked to a virtual platform based on ICT, will allow the end-user to not only produce their own energy, but also to decide if they prefer to sell to the grid, to buy from the grid and also to have the possibility to store it.

Energy storage technologies will compensate the imbalances introduced by renewable energy fluctuations in the grid, giving the end-loads the appropriate power quality. A new grid architecture based on microgrids can even decide if the microgrid must work connected to the grid, or change into an islanded mode if the power quality of the main grid is not satisfactory [3, 4].

Storage is not only a technical solution for network management and ensuring real-time load levelling but it is also a mean of efficiently utilising renewable resources by avoiding load shedding in times of over production. Coupled with local renewable energy generation, decentralised storage could also improve power network sturdiness through a network of energy [6].

The high energy density of hydrogen will make this technology play an important role in this new paradigm. This aspect is reinforced by the fact that it is the most abundant element in nature. However, the reduced life time associated to the main hydrogen technologies (electrolyzers and fuel cells) is still a technological barrier for its definitive technological introduction. The behavior against transitory conditions is also a constraint. Electrolyzers and fuel cells degrade if

the time response is not accurately controlled. Batteries have a better and faster response against transient conditions yet they have high current stress in charge and discharge can cause degradation in their life time. Also batteries have less energy density, having better power density than fuel cells and electrolyzers. Ultracapacitors even have a better transient response than batteries, more power density and higher cycles. They have almost no degradation effects for load cycling, but this technology does not have enough energy density to supply power in long time periods. In [7] a comparative study of the different ESS technologies was carried outsee figure 1.1).

The design and development of an advanced control system is crucial for the proper operation of hybrid ESSs. The control strategy can take advantage of the features of each storage systems, avoiding degradation issues and/or limitations therefore, it appears as a technological solution to increase the efficiency, autonomy and life time problems of ESSs.

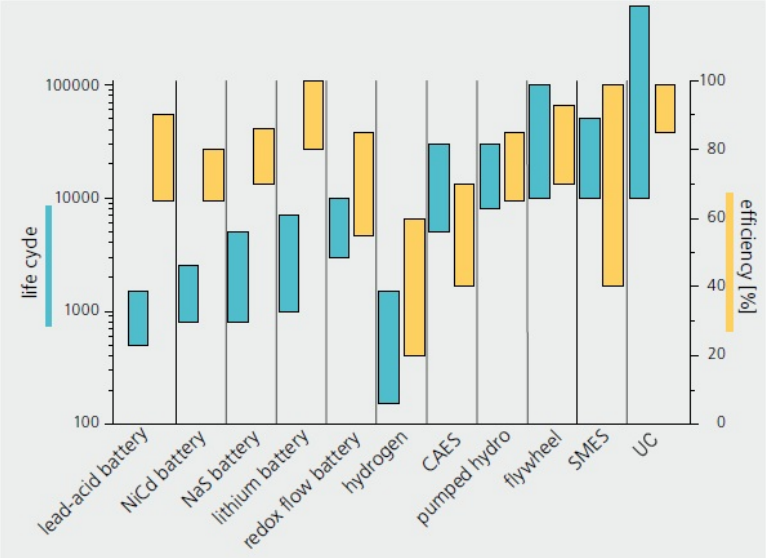

Figure 1.1. Overall efficiency and lifetime of storage systems(Source: Adapted from [7])

1.2 Current Challenges in Control of Microgrids and Hybrid Storage

Only a reduced number of publications have applied hybrid storage to renewable microgrids. Sharing power methods with several ESSs have been applied in the field of electric vehicle giving satisfactory results which took into account efficiency, global degradation and behaviourbehavior against transient conditions. The main challenge of controlling hybrid storage is how to manage the power density of each with the energy density. The time response is linked to power density in each ESS but t autonomy of the ESS or the energy storage capacity depends of energy density (see figure 1.2, page 6). The hybrid ESS control system must consider the limitations of each ESS ,taking into account time response, load cycling degradation, power density and energy density constraints. The high number of constraints and variables to be optimized hinders the control problem making advanced control algorithms necessary. In turn, Model Predictive Control (MPC) appears as the optimal solution to solve the high computational cost of the associated algorithm.

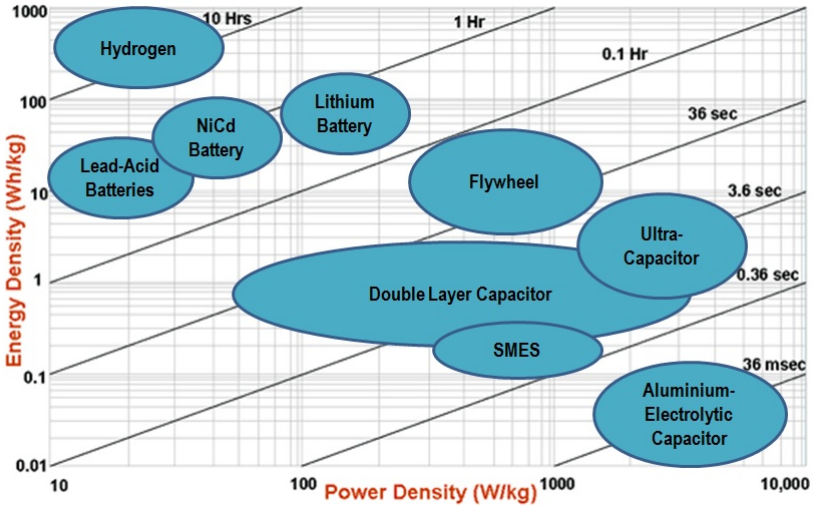

Figure 1.2. Ragone's plot. (Adapted from US Defense Logistic Agency [8])

.

In figure 1.2 the relationship between energy density versus power density in the different ESSs can be observed. According to this relationship in figure 1.3, different fields of application and implementation of the different energy storage systems can be seen. To be noted is the fact that systems with very low storage periods(seconds) and high power density are used for grid stabilisation in

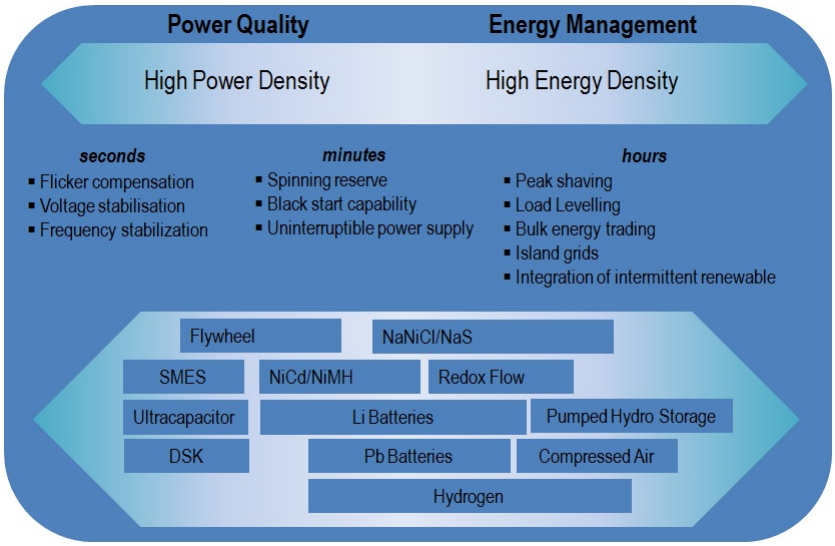

Figure 1.3. Energy storage applications (Adapted from Fraunhofer Institute for Environmental [7])

.

aspects of power quality. One example includes ultracapacitor technology which shows high power ratings for low levels of stored electricity. At the other end of the spectrum, we can find an ESS with the ability to store significant amounts of energy, e. g. pumped hydro or hydrogen systems. They possess enough capacity to store energy for periods of severalhours or more and compensate for the fluctuating integration of energy, such as wind power, and are able to smooth peak demand loads. The intermediate spectrum operates at intervals of minutes ensuring uninterruptible power supply, black start and spinning reserve [7]. Long-term quality problems in the control system, for instance a shut down in the main grid, are detected as short-term problems that must be managed as a long-term problem. The control system must manage the time response of each ESS, correctly mitigating the problem in order to minimize its affectation of the power quality given to the load.

The introduction of ESSs gives the opportunity for a better management of the economic dispatch of renewable energies. There are several ways to store the energy but each ESS has its own advantages and disadvantages considering economic cost, energy rating, power rating, lifetime and degradation issues. The use of hybrid storage systems appears as a solution to mitigate the disadvantages of energy storage. The control strategy must have the ability to decide which ESS to use at every moment in order to minimize general costs of energy storage.

1.3 Thesis Motivation

The definitive introduction of renewable energies as an energetic model will not only need smaller management units but will also require an effective ESS. This effectiveness must not be judged on its efficiency but also on its robustness. A correct transient response must be even more important than an efficiency efficient behaviourbehavior. The life cycle of the energy storage system must be another criterion to be taken into account. The integration problem of renewable energy must be focused on economic and technical aspects:

1. From the technical point of view, the ESS must compensate the imbalances introduced by renewable sources into the grid reaching optimal performance. This performance must be fulfilled in the short, medium and long term. The minimization criterion of degradation and functional costs of the ESS must be introduced in the control algorithm, considering the constraints of power density and energy density for each ESS. However, in order to correctly balance the power quality in the microgrid, the control response must manage the control periods in the order of microseconds. The transient response of the associated power converter must be fast enough and possess a minimum transient response.

2. Regarding the economic aspect of the microgrid, the ESS must allow renewable energy to become competitive as opposed to fossil fuel-based technologies, in their participation in the electrical market. Reaching competitiveness is linked to increasing the life cycle of the ESS. The economical cost associated to the degradation process of each ESS must be integrated inside the control algorithm. The electricity market rules are managed in the day-ahead-spot energy market, so the control algorithm must be scheduled 38 hours before the real-time control decisions are taken.

1.4 Research Objectives

The main objective of this thesis is to develop several optimal control algorithms of a renewable energy microgrid with Photovoltaic generator (PV) and Wind Turbine (WT) generation and a hybrid energy storage system composed by Hydrogen Energy Storage System (HESS), Battery Energy Storage System (BESS) and Ultracapacitor Energy Storage System (UCESS). The dissertation has the following specific objectives:

1. To develop a model of renewable energies in the microgrid to predict associated behaviourbehavior to wind power and solar power generation, as well as the load consumption and the energy price prediction.

2. To develop a model of the energy storage system in the microgrid that includes all the constraints of the hybrid ESS, taking into account degradation causes, energy and power density, and the transient response for each ESS that integrates the microgrid.

3. To carry out an optimal economic management of the microgrid using MPC, that minimizes t global functional costs of the hybrid ESS.

4. To improve the power quality in the microgrid through an optimal control algorithm of the power electronic devices associated with the ESS minimizing the transient response using MPC techniques.

1.5 Dissertation Layout

This dissertation focuses on the current problems of integration of the renewable energy from two main points of view: technical and economic. Both problems are solved in a microgrid structure with energy storage. An optimal ESS does not exist and each ESS has its own advantages and disadvantages, in aspects such as degradation causes, energy density, power density or transient response. To consider all these factors, the number of variables and constraints associated to the control problem is too high to be solved with classic methods. An advanced control for the economic dispatch and power quality improvement is carried out using MPC techniques.

The thesis is structured in six chapters. In the **first chapter** an introduction to energy storage technology, its application and its future importance in the implementation of smart grids, is explained, pertaining the control problem associated.

In the **second chapter**, a literature review is made. The literature review is focused on three main aspects: control of hybrid storage system, economic control algorithms applied to renewable energy microgrids and power quality management in microgrids.

The **third chapter** focuses on the model and analysis of the component of the microgrid.Also the plant model of the microgrid is developed. An analysis of each component to be solved, the different problems associated, such as forecast difficulties, power quality issues or degradation causes, are analysed.

The algorithm for the optimal economical dispatch of the microgrid, using MPC is implemented in the **forth chapter**. Daily market, intradaily market, regulation market control and real scenario load sharing problems are solved. In order to model both continuous/discrete dynamics and switching between different operating conditions, the plant is modeled with the framework of Mixed Logic Dynamic (MLD). Taking into account the presence of integer variables the MPC problem is solved as MIQP (Mixed Integer Quadratic Programming).

An optimal solution for power quality management is carried out in the **fifth chapter**, where new control algorithms for power converters associated to ESSs are developed for both cases: grid-connected and islanded mode . The **last chapter** of the thesis summarizes the main conclusion obtained. The main contributions and future research lines are also explained.

Chapter 2

Context and Literature Review

2.1 Introduction

The transition to the smart grid will change the energy scenario that is now occurring in the traditional grid. An outline of the new technologies which are appearing in the smart grid is shown in figure 2.1. In the new smart grid framework more distributed energy resources (DER) will appear every day. The main change will be outcome by the decreasing presence of fossil fuel generation and the growing in the relevance of renewable generation. This fact is introduced and discussed in section 2.2. The ESSs appear as key solution to the inherent randomness of renewable energy. But a perfect ESS does not exist; each one has its own advantages and disadvantages. For this reason, each ESS must be used to solve a determined problem of the overall issue that renewable energy introduces. A survey of the different possibilities and limitations that ESSs provide is carried out in section 2.3. Using hybrid ESSs will allow the control system of the microgrid to maximize the advantages of each technology while the disadvantages are neglected. But this fact increases the complexity of the associated-control problem, making the use of advanced control algorithms necessary

A discussion of the proposed solutions for microgrid control according to the literature is included in section 2.4. Introducing renewable energy on the grid must be done from an economic and technical point of view. Thus existing economic dispatch control algorithms and power quality enhancement in the microgrids are revised.

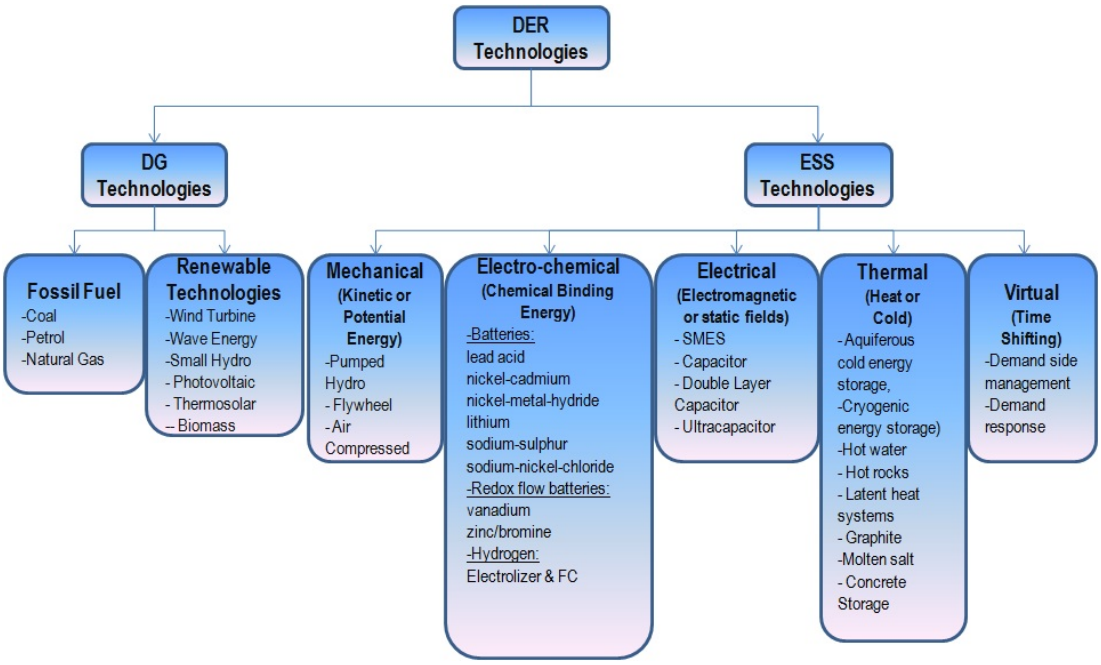

Figure 2.1. Different types of DG technologies and classification(Source: Adapted from [7] and [9])

2.2 Distributed Energy Resources

The smart grid will integrate several means of producing energy, given that depleting fossil fuel reserves will encourage renewable technologies to have an increasingly important role in the new energetic model. In this section a thorough analysis of the current situation for each kind of generation is provided.

2.2.1 Fossil Fuels Generation

Small capacity combustion turbines, which can operate using natural gas, propane, petrol, coal and other fuels, are also an option for DG. They consist of a compressor, combustor, recuperator, small turbine and a generator. At times they have only one moving shaft, and use air or oil for lubrication. Unlike traditional combustion turbines, micro turbines operate at lower temperatures and pressure, and faster speed (up to 150,000 rpm), which sometimes requires no gearbox. Their small size is a great benefit of these systems thanks to the use of high-speed turbines with airfoil bearings. As a result of low-priced natural gas, low installation and low maintenance costs, micro-turbines are one of the most numerous DG energy sources today [9].

The controllability and autonomy of this kind of system have been its major advantage but the increasing price of fossil fuels and the environmental impact will cause this tenhnology to play a less important role in the smart grid.

2.2.2 Renewable Energy Generation

The number of ways to produce renewable energy is increasing with the closeof the end of the fossil fuel age. Both wind and photovoltaic generation are becoming relevant in the current grid. Alongside traditional wind and photovoltaic technologies, we now have emerging technologies such as high temperature solar plants, wave energy plants and small hydro, which is increasingly more present in the electrical grid [10]-[12].

Biomass can be regarded as a hybrid way of energy generation, considering it operateswith a combustion engine as fossil fuels technologies do. Several studies are considering this technology as a way to manage the fluctuations of renewable energies. Taking into account their global cycle, this technology must be not contemplated as a greenhouse impacting technology [11, 13]. Biomass is also a way in which nature stores energy naturally.

Small hydro is a further potential technology to be considered if its possibility to be stored is contemplated. However, the associated ecosystem impact must also be taken into account with this kind of energy generation.

Focusing on the two main renewable energy methods photovoltaic systems and wind turbines the legal framework for the overall increase of renewable energy sources in the EU was established with Directive 2009/28/EC and with the associated National Renewable Energy Action Plans (NREAPs) of the 27 Member States. These guidelines have specific photovoltaic solar energy targets adding up to 84.5 GW in 2020 [14, 15, 16]. The average annual growth rate for photovoltaic generation between 2000 and 2015 was 75 % (Figure 2.2). Hence, the European Commissions Joint Research Centre concluded that *"The main issue to realise such ambitious targets is not whether or not the PV industry can supply the needed systems, but whether or not the electricity grid infrastructure will be able to absorb and distribute the solar-generated electricity"* [14, 16].

Similar developments can be observed with the wind energy penetration in Europe and according to the statistics given by the European Wind Energy Association (EWEA) in 2014, the installed wind power capacity in the European Union totaled 117,300 megawatts (MW). The EU wind industry has had a compound annual growth rate of 10% between the years 2000 and 2014. In 2014, a total of 11,159 MW of wind power was installed, representing 32% of all new power capacity. In a normal wind year the wind power capacity installed by early

2014 would produce 284 TWh of electricity, enough to supply 10.2% of the EUs electricity consumption[17].

A review of the projected PV and wind contribution to final electricity demand in 6 key countries until 2030 is shown in figure 2.2. This figure just draws on the need for new ways to manage energy flows in the grid.

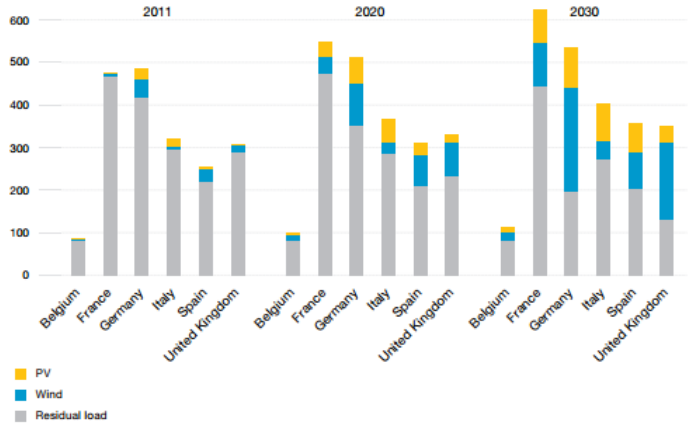

Figure 2.2. Projected photovoltaic and wind contribution to final electricity demand in 6 key countries until 2030 [15]

2.3 Distributed Energy Storage System

Microgrids will benefit from the deployment of efficient and cost effective energy storage technology, which will provide an additional degree of flexibility to the Microgrid operators (in particular in the presence of a large number of renewable energy sources) [18]. The integration of fluctuating renewable energies such as wind and photovoltaic power generates severe load variations in the grid. To compensate for these variations and to assure reliability and steadiness, it is not only necessary to reinforce the grids but also to provide backup and reserve power which, in the medium term, calls for energy storage. Both real and virtual energy storage systems can charge energy in the event of excess renewable power, and are also able to integrate power into the grid during periodic levelling [7].

In Europe, the installed energy storage capacity amounts to 46 GW. This is in absolute and relative terms, with 6.6% being the highest global amount of the world. The most significant differences emerge between different power plant parks and as a result of regional restrictions on electricity grids [7].

The current status of energy storage in the grid is not clear enough. The stoRE project has recently been created by the European Commission in order to deal with the non-technological barriers of energy storage. Therefore, creating the right regulatory and market conditions that incentivize the development of energy storage infrastructure to the extent necessary for the accommodation of the planned renewable energy installations to the electricity grid [19].

A consensus among all key actors was reached about the necessary adaptation of the European Energy framework and policies, developing concrete recommendations and planning their implementation. Similar work was carried out in the six target countries (Austria, Denmark, Germany, Greece, Ireland and Spain), leading to improvements of the policies, legislation and market mechanisms [19]. In the following paragraphs, there will be a summary of the deliverable D.4.2 - European Regulatory and Market Framework for Electricity Storage Infrastructure, in which the different actions to regularize Energy Storage Systems are collected and explained.

The Directive 2009/72/EC concerning common rules for the internal market in electricity establishes common rules for the generation, transmission and distribution of electricity, unfortunately the concept of electricity storage is not mentioned. The European Commission invites the Agency for the Cooperation of Energy Regulators (ACER) to develop framework guidelines, which set out general principles for the rules that regulate, who may use the electricity networks to transport energy across borders and under which conditions. Network codes are then drafted by the European Network of Transmission System Operators for Electricity (ENTSO-E) in coherence with the principles that ACER sets out in the framework guidelines. Network codes can be made legally binding by a separate Commission decision [19].

The Framework Guidelines on Electricity Balancing were adopted on the 18th of September 2012. They address the roles and responsibilities of stakeholders involved in electricity balancing, the procurement of frequency restoration reserves and replacement reserves, the activation of balancing energy from frequency restoration reserves and replacement reserves, and the imbalance settlement [19].

In these Framework Guidelines, the ACER intends to limit the Transmission System Operator's (TSO) responsibility strictly on organising balancing markets in the most effective and efficient manner and encourage cooperation with each other in order to achieve this. With regards to which market player shall provide the required balancing services it is mentioned: The Network Code on Electricity Balancing shall require that each TSO is responsible for procuring the required balancing services from Balance Service Providers (BSPs) and is not allowed to

offer the balancing services itself except, subject to National Regulatory Authority's (NRA) approval, if system security is threatened due to insufficient bids from BSPs [19].

The first full preliminary draft Network Code on Balancing has been completed and further issues will be discussed with regulators and stakeholders through organised meetings and workshops prior to, during and after a public consultation. Then in November 2012 a communication was adopted addressing specifically the progress with the internal energy market. In this communication importance was placed on storage, even included in the introduction: *we urgently need to invest in generation, transmission and distribution infrastructure, as well as storage.*. The "Guidelines for trans-European energy infrastructure" proposal aims at ensuring that strategic energy networks and storage facilities are completed by 2020. To this end, the Commission has identified 12 priority corridors and areas covering electricity, gas, oil and carbon dioxide transport networks. It proposes a regime of "common interest" for projects contributing to implementing these priorities and having obtained this label. In general storage has a prominent position in the proposed regulation as it is always mentioned together with transmission. On the 5th of July 2012, the Ten Year Network Development Plan (TYNDP) was completed by ENTSO-E and submitted to ACER. The importance of storage is highlighted in a dedicated full page text box (page 84), recognising that storage is a complementary and not competitive approach to grid development: *As a conclusion, storage facilities might be a complement, and not an alternative way, to the grid development in order to allow: resolution of grid congestions, peak shaving, reserve for the electricity system and primary frequency regulation* [19].

The "Energy 2020" Communication, which identifies the energy priorities for the period up to 2020, deals with: *Re-establishing Europes leadership on electricity storage (both large-scale and for vehicles). Ambitious projects will be developed in the fields of hydro capacity, compressed air storage, battery storage, and other innovative storage technologies such as hydrogen. These will prepare the electricity grid at all voltage levels for the massive uptake of small-scale decentralised and large-scale centralised renewable electricity* [19].

The Energy Roadmap 2050, analysis of the scenarios concludes that *Storage technologies remain critical. Storage is currently often more expensive than additional transmission capacity, gas backup generation capacity, while conventional storage based on hydro is limited. Greater efficiencies in their use and competitive costs require improved infrastructure for integration across Europe. With sufficient interconnection capacity and a smarter grid, managing the variations of wind and solar power in some local areas can be provided also from renewables elsewhere in Europe. This could diminish the need for storage, backup*

capacity and base load supply[19]. It also recognises that: *One challenge is the need for flexible resources in the power system (e.g. flexible generation, storage, demand management) as the contribution of intermittent renewable generation increases... Ensuring that market arrangements offer cost-effective solutions to these challenges will become increasingly important. Access to markets needs to be assured for flexible supplies of all types, demand management and storage as well as generation, and that flexibility needs to be rewarded in the market. All types of capacity (variable, base load, flexible) must expect a reasonable return on investment* [19].

The last paragraphs portray an image of the relevance of ESS in future decades. In this new outline (see figure 2.1), several technologies have been appearing to store energy. A classification can be based on the way in which energy is stored: mechanically, electrically, electrochemically, thermally or virtually. Choosing an ESS must be carried out by weighing benefits and disadvantages, a brief description of every technology is carried out. In tables 2.1 and 2.2 a summary of the main characteristics of each ESS can be consulted.

Table 2.1. Comparison of technical characteristics of EES systems (I). [a]

Systems	Power rating and discharge time		Storage duration		Capital Cost		
	Power Rating	Discharge Time	Self discharge per day	Suitable storage duration	$/kW	$/kWh	cents/kWh per cycle
PHS	100-5000 MW	1-24 h+	Very small	Hours-months	600-2000	5-100	0.1-1.4
CAES	5-300 MW	1-24 h+	Small	Hours-months	400-800	2-50	2-4
Flywheel	0-250 kW	1e-3s -15 min	100%	Seconds-minutes	250-350	1000-5000	3-25
Capacitor	0-50 kW	1e-3s -60 min	40%	Seconds-hours	200-400	500-1000	-
UCESS	0-300 kW	1e-3s -60 min	20-40%	Seconds-hours	100-300	300-2000	2-20
SMES	0.1-10 MW	1e-3s - 8s	10-15%	Minutes-hours	200-300	1000-10,000	-
Lead-acid	0-20 MW	Second-hours	0.1-0.3%	Minutes-days	300-600	200-400	20-100
Ni-Cd	0-40 MW	Second-hours	0.2-0.6%	Minutes-days	500-1500	800-1500	20-100
Li-ion	0-100 kW	Minutes-hours	0.1-0.3%	Minutes-days	1200-4000	600-2500	15-100
FBESS	30 kW-3 MW	Seconds-10h	Small	Hours-Month	600-1500	150-1000	5-80
HESS [b]	0-50 MW	Seconds-24 h+	Almost zero	Hours-months	12,000+	-	3-5 [c]
HT-TES	0-60 MW	Seconds-24 h+	0.05-1.0%	Minutes-months	-	30-60	-

[a] Source: Modified from [20]

[b] HESS formed by electrolizer and fuel cell

[c] Cost in cents per hour

Table 2.2. Comparison of technical characteristics of EES systems (II). [a]

Systems	Energy and Power Density				Life Time and Cycles		Influence on the enviroment	
	Wh/kg	W/kg	Wh/L	W/L	Years	Cycles	Influence	Description
PHS	0.5-1.5	-	-	0.5-1.5	40-60	-	Negative	Destruction of green land
CAES	30-60	-	3-6	0.5-2	20-40	-	Negative	Emissions from combustion of natural gas
Capacitor	0.05-5	∼1e5	2-10	1e5+	∼5	5e4+	Small	Little amount of remains
UCESS	2.5-15	500-5000	2-10	1e5+	20+	1e6+	Small	Little amount of remains
SMES	0.5-5	500-2000	0.2-2-5	1000-	20+	1e3-4e3	Negative	Strong magnetic fields
Lead-Acid	30-50	75-300	50-80	10-400	5-15	500-1000	Negative	Toxic remains
NiCd	50-75	150-300	60-150	-	10-20	2000-2500	Negative	Toxic remains
Li-Ion	75-200	150-315	200-500	-	5-15	1e3-10e3	Negative	Toxic remains
FBESS	10-30	-	16-33	-	5-10	12e3	Negative	Toxic remains
HESS [b]	800-10e3	500+	500-3000	500+	5-15	1000+	Nearly null	Remains of component
HT-TES	80-200	-	120-500	-	5-15	-	Small	-

[a] Source: Modified from [20]

[b] HESS formed by electrolyzer and fuel cell with renewable energy system

2.3.1 Mechanical Storage

2.3.1.1 Pumped Hydro Storage

Pumped Hydro-Storage (PHS) is the oldest and largest of all of the commercially available energy storage technologies. Traditionally it has been the ESS used in the common grid. PHS consists of two large water reservoirs positioned at different elevations. During off-peak hours the water is pumped from the lower reservoir to the higher one. In this way, excess energy from the grid is stored in potential energy. When it is necessary to generate electricity, the water is then returned to the lower reservoir, passing through hydraulic turbines and generating electrical power. Its self-discharge is very low so this ESS is quite appropriate for long term energy storage. There are also many small hydro schemes of less than a megawatt and even just a few kilowatts, which are normally in isolated grids [7, 20, 21, 22].

As can be observed in tables 2.1 and 2.2, PHS is a technology with a long life cycle, high- efficiency conversion and low cost. However, low energy d and power density require large green land spaces which entail the destruction of trees and associated ecosystems.

2.3.1.2 Compressed Air Energy Storage

Compressed air energy storage (CAES) (see figure 2.3) plants store energy by compressing air into subterranean caverns. During peak loads, the compressed air is directly coupled to a conventional gas turbine with higher ratings because no energy is needed for compressing the combustion air. CAES is the only other commercially available technology (besides pumped-hydro) able to provide the very large system energy storage deliverability (above 100 MW in single unit sizes) to use for commodity storage or other large-scale settings [7, 20, 22, 23].

CAES works on the basis of conventional gas turbine generation. It decouples the compression and expansion cycles of a conventional gas turbine into two separated processes and stores the energy in the form of elastic potential energy of compressed air. During low demand, energy is stored by compressing air into an air tight space, typically 4.0-8.0 MPa. To extract the stored energy, compressed air is drawn from the storage vessel, heated and then expanded through a high-pressure turbine, which captures some of the energy in the compressed air. The air is then mixed with fuel and combusted with the exhaust expanded through a low-pressure turbine. Both the high- and low-pressure turbines are connected to a generator to produce electricity [20, 23].

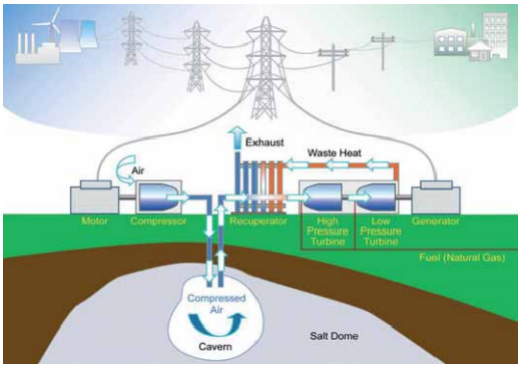

Figure 2.3. Compressed air energy storage system (Source: Ridge Energy Storage & Grid Services L.P)

CAES systems also have improved environmental characteristics in com-parison with conventional intermediate generating units. CAES has a relatively long storage period, low capital costs and high- efficiency but CAES are only designed to work with fossil fuel generation technologies, so its associated impact with the environment is its main disadvantage [20, 23].

2.3.1.3 Flywheel

A flywheel energy storage system (FESS) stores energy through accelerating a rotor up to a high rate of speed and maintaining the energy in the system as kinetic energy. Instead of generating potential energy, flywheels store kinetic energy. Flywheels release the energy by reversing the process and using the motor as a generator. As the flywheel releases its stored energy, the flywheels rotor slows until it is fully discharged. Advanced composite materials are sometimes used for the rotor to lower its weight while allowing for the extremely high speeds. Flywheels material degrades when an upper speed limit is overcome [7, 20, 22, 24].

Flywheels have the ability to charge and discharge rapidly, and are almost immune to temperature fluctuations. They take up relatively little space, have lower maintenance requirements than batteries, and have a long life span. Flywheel devices are relatively tolerant of abuse, i.e. the lifetime of a flywheel system will not be shortened by a deep discharge unlike a battery. As can be seen in figure 1.2, flywheels occupy an intermediate position between batteries and ultracapacitors in relation to power and energy densities[25].

Although most of the flywheel technology was developed in the auto and aerospace industry, flywheels have seen most commercial success targeted for

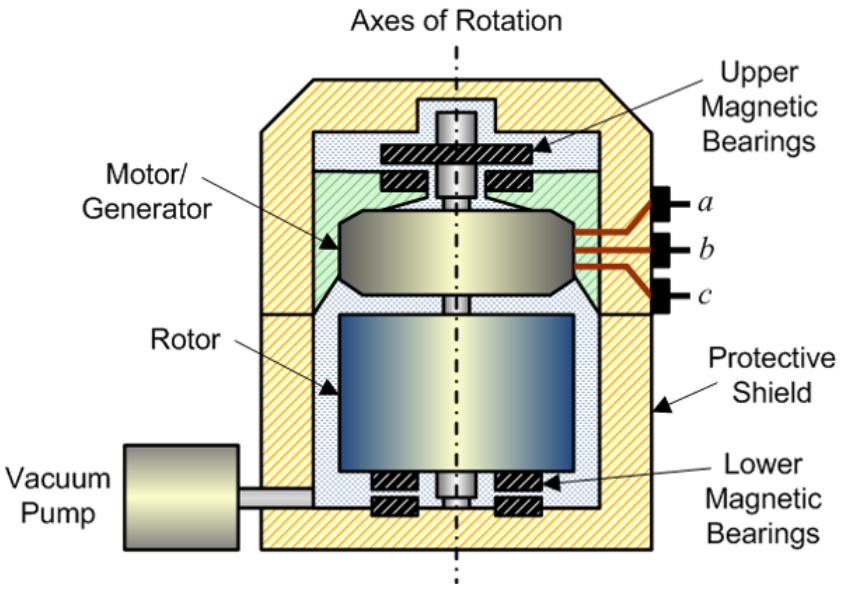

Figure 2.4. Flywheel [25]

power delivery capabilities in the 150 kW-1MW range. These systems are compact and have lower maintenance costs and requirements than battery systems. The main focus for development of this technology has been the power quality and reliability market [22].

2.3.2 Electrical Storage

2.3.2.1 Capacitors

Capacitors can be considered the most direct way to store electrical energy. A capacitor consists of two metal plates separated by a non-conducting layer called a dielectric (see figure 2.5). When one plate is charged with electricity, the other plate will induce an opposite charge[7, 20, 25, 26]. Capacitors can be charged substantially faster than conventional batteries and cycled tens of thousands of times with a high efficiency. Conventional capacitors have been developed for daily peak load in summer for less than 1 h with small capacities (1kW). However, the main problem presented by conventional capacitors is the low energy density, although the new topologies of double-layer capacitors or ultracapacitors increase this factor (see figure 1.2). This technology is only appropriate for short-term storage application [7, 20, 25, 26]

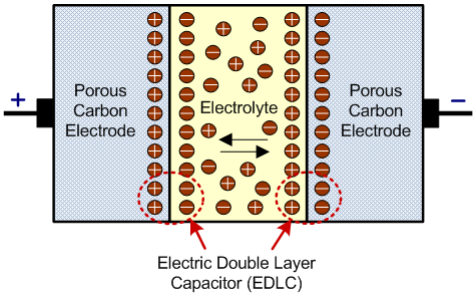

Figure 2.5. Ultracapacitor [25]

2.3.2.2 Superconducting Magnetic Energy Storage

SMES is a large superconducting coil capable of storing electric energy in the magnetic field generated by DC current flowing through it. Since energy is stored as circulating current, energy can be drawn from an SMES unit with almost instantaneous response with energy. An SMES (figure 2.6) unit consists of a large super-conducting coil at the cryogenic temperature. Niobium-Titanium (NbTi) is the material commonly used to mould the superconductor. This temperature is maintained by a cryostat or a dewar that contains helium or nitrogen liquid vessels, being its operation temperature one of its limitations [27, 28, 29]. As

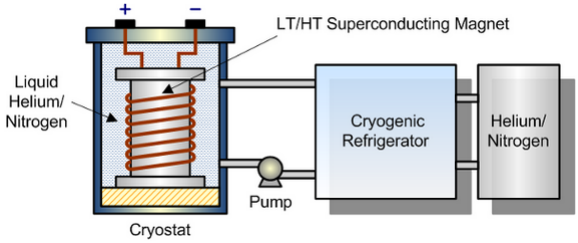

Figure 2.6. Superconducting magnetic energy storage system [25].

can be seen in figure 1.2, page 6, SMES are an ESS with high-power density but with low-energy density. In figure 1.1 we can observe the high efficiency and long life time of SMES, due to its fast response, its possibility both absorb and generate active and reactive power. SMESs are highly suitable for power quality applications such as those including load leveling, dynamic stability, transient stability, voltage stability, frequency regulation, transmission capability enhancement, power quality improvement, automatic generation control, uninte-rruptible power supplies, etc. [7, 27].

The fast response time (under 100 ms) of these systems is one of its greatest advantages, making them ideal for regulating network stability. These facilities

currently range in size up to 3 MW units and are generally used to provide grid stability in a distribution system and power quality at manufacturing facilities requiring ultra-clean power [22]. However their overall cost as a result of the refrigerating system and the operating temperature, is one of the limitations for the application of this kind of ESS.

2.3.3 Electrochemical Storage

2.3.3.1 Batteries

Battery Energy Storage Systems (BESS) have been the classical electrochemical way to store energy. A battery (see figure 2.7) is comprised of one or more electrochemical cells and each cell consists of a liquid, paste, or solid electrolyte together with a positive electrode (anode) and a negative electrode (cathode). During discharge, electrochemical reactions occur at the two electrodes generating a flow of electrons through an external circuit. The reactions are reversible, allowing the battery to be recharged by applying an external voltage across the electrodes [20, 30]. Batteries are in some ways ideally suited for electrical energy

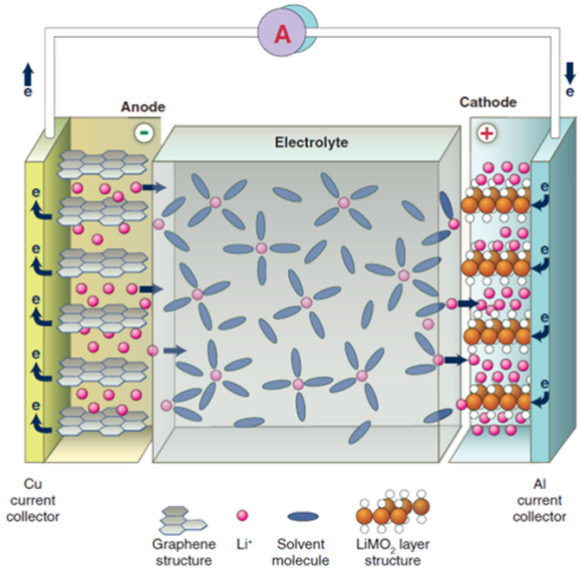

Figure 2.7. Lithium-Ion batteries [31]

.

storage applications. The technology of batteries has matured during the last century, searching for a better ratio between energy density and power density

as can be observed in figure 1.2. This evolution has resulted in a wide variety of typologies of batteries classified according to their electrolytes. Lithium-ion batteries are technologically best positioned but there are still economical barriers when implementing them in large-scale storage. Batteries have also a negative impact on the environment as most batteries contain toxic materials.

From the technical point of view, batteries occupy an intermediate place between large-term storage and short-term storage (see figure 1.3). Batteries degrade when high stress current of charge and discharge are applied [32, 33].

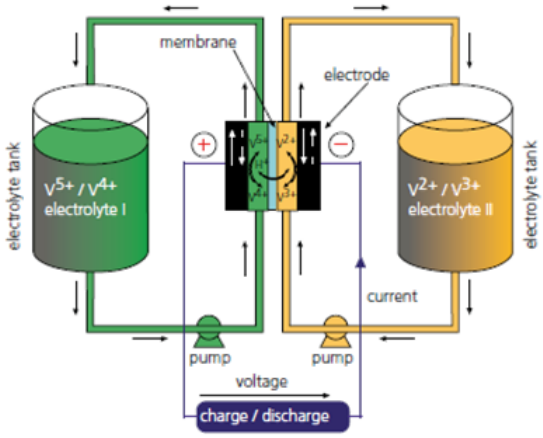

Figure 2.8. Vanadium Redox-Flow battery [7].

2.3.3.2 Flow Batteries

Contrary to conventional batteries in fixed units with traditional electrodes and electrolytes, redox flow batteries have separated parts for conversion (power conversion system PCS) and storage (storage system). Each power conversion system contains two electrodes and a membrane in between to form a single cell. These cells are connected to form a stack which is comparable to the stacks in fuel cells. The storage of electrolytes takes place in external tanks, so that the power conversion system and the storage system are separated. This makes it possible to adapt them individually to the application. Advantages of this system include: uncontaminated electrolytes due to the transferability through the membrane, an aqueous reaction which increases speed, and the potential of such systems to reach efficiencies of 70%. This is an emerging technology that is beginning to be relevant in energy storage aspects, the downside being that flow batteries have an

environmental impact because the electrolyte usually used is a toxic component such as Vanadium, Zinc bromine or Polysulphide bromide [7, 20].

2.3.3.3 Hydrogen

Hydrogen offers a range of benefits as a clean energy carrier (if produced by clean sources), which are receiving ever greater attention as policy priorities. But hydrogen is just an energy carrier and although it is the most abundant element in the universe it is often not found in nature in its free state. However, it can be found in a combined state in water, sugar, cellulose, acids, proteins, fats and hydrocarbon. To have the complete hydrogen energy storage system (HESS), a hydrogen production system, a hydrogen storage system and a hydrogen to energy transformation system must be assembled [34, 35, 36].

Hydrogen can be produced from fossil fuels, nuclear and renewable energy sources by a number of processes such as water electrolysis, natural gas reforming, gasification of coal and biomass, water-splitting by high-temperature heat, photo-electrolysis and biological processes. The majority of the produced hydrogen is obtained from fossil fuels. But this way of hydrogen generation cannot be considered as a clean ESS. The possibility to produce hydrogen coupling electroly-zers (ELZ) to renewable sources is increasing its interest in the smart grids development [34, 35].

Hydrogen can be transformed into energy using an internal combustion engine (ICE) or a fuel cell (FC). The ICE has several advantages as opposed to the FC because it is a mature technology with lower costs and a higher life cycle. But ICEs are limited by the Carnot limit, being its main disadvantage versus FCs.

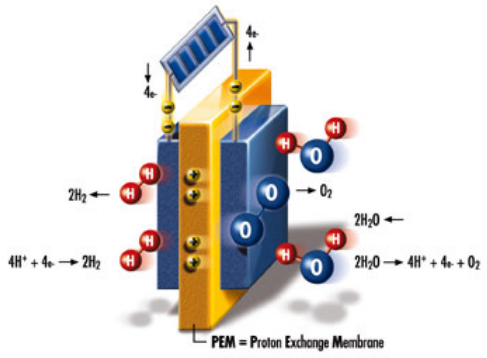

Figure 2.9. Electrolyzer (Source: Terran Cell Renewable Energy Solutions)

The power density and energy density of a HESS will depend of the hydrogen storage system considered. Another difficulty of hydrogen being energy carrier is

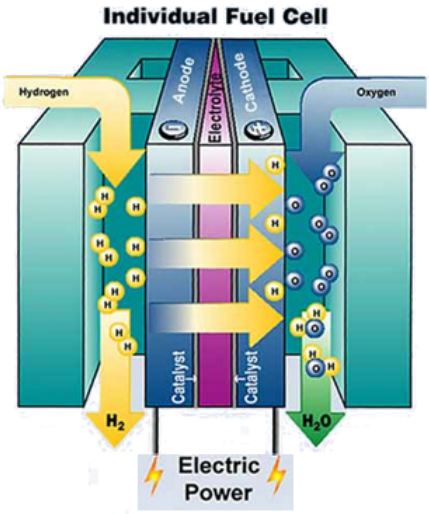

Figure 2.10. Fuel cell (Source: Hygen Industries)

its low critical temperature of 33 K (i.e. hydrogen is a gas at ambient temperature. Hydrogen can be stored using six different methods and phenomena: (1) high-pressure gas cylinders (up to 800 bar), (2) liquid hydrogen in cryogenic tanks (at 21 K), (3) adsorbed hydrogen on materials with a large specific surface area (at $T < 100K$), (4) absorbed on interstitial sites in a host metal (at ambient pressure and temperature), (5) chemically bonded in covalent and ionic compounds (at ambient pressure), or (6) through oxidation of reactive metals, e.g. Li, Na, Mg, Al, Zn with water. The most common storage systems are high-pressure gas cylinders with a maximum pressure of 20 MPa (200 bar) [36]. The latest electrolyzer developments have been focused on reaching the pressure of 350-700 bar.

HESS has almost no impact on nature if it is produced from renewable energies and obtained from water, but there are still two barriers to be overcome. The first barrier is economical as hydrogen technologies are not mature enough to be competitive. The second one is a technical barrier due to its short life time. Concerning the main causes of degradation in electrolyzers and fuel cells, it must be said that both degrade in the start up and shut down cycles. The life cycle of electrolyzers and fuel cells could be longer if they were exposed to a non-fluctuating profile [37]-[41].

2.3.4 Thermal Storage

Thermal energy can be stored as (i) Low temperature energy storage (Aquiferous cold energy storage, cryogenic energy storage); (ii) High temperature energy storage (sensible heat systems such as steam or hot water accumulators, graphite, hot rocks and concrete, latent heat systems such as phase change materials). Low-temperature energy storage and latent heat systems are not used for electric energy uses but are important in the heating and cooling of building comfort systems. High-temperature energy storage technologies such as molten salt storage and Room Temperature Ionic Liquids are beginning to have a relative importance in research projects on high-temperature solar thermal power plants [20].

2.3.5 Virtual Energy Storage

Virtual energy storage systems compensate for off-peak and peak loads, just like real storage systems. In contrast to real storage systems, which are charged or discharged depending on supply and demand, virtual storage systems manage non-fixed load with time. Time-shifting is used in order to supply power to these kinds of loads in moments when an exceeding power generation exists. The efficiency of this kind of storage is 100 % and it has no impact on the environment as well as having almost no economic cost.[7]

2.4 Control of Microgrids

This section gives an overview of the existing microgrid algorithms, focusing on the importance of power and energy management strategies linked to the different control levels of the microgrid and its association with the control strategies of the hybrid ESS. An introduction to the main global aspects of microgrids and smart grids is also included.

2.4.1 Global Concepts

The final objective of an electric power system consists of the generation and transmission of energy from the generation point to the end-user. This is achieved by maintaining a sinusoidal electric field. This electric field is determined by the frequency and the effective voltage value.

Frequency is related with the active power balance in the system. This is due to the fact that the employed generating technology is generally formed by a set of synchronous turbines (machine). At the instant when an increase in the

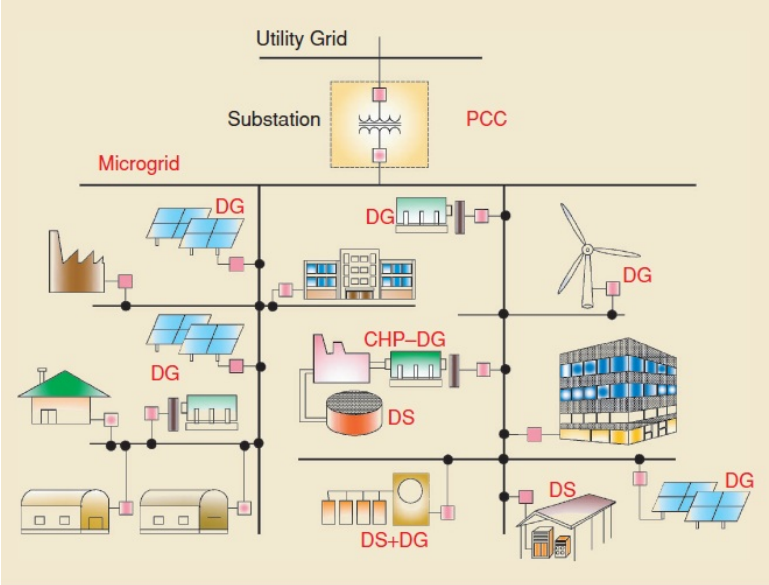

Figure 2.11. Typical microgrid structure(Source: Adapted from [2])

demanded electric power is produced, the turbine torque is suddenly applied to the shaft, which will result in a decrease of the rotation speed and consequently, also the frequency of the wave generated. Meanwhile, the effective voltage value , is closely related to the excitation of the synchronous machine. That is, it can be seen that it is important for the active power control implemented through the turbine, while the control voltage is the excitation of the machine. This explains why both problems are studied in a decoupling problem, but in reality they are not at all, the latter being particularly important when producing transient phenomena[42].

In simplistic terms, a microgrid can be conceived as an auto-managed portion of the grid where energy sources, loads and ESS work together. Although this study is centered around electric energy management of microgrids, microgrids should not only be studied from the point of electric energy but also from the point of heat energy. Heating and cooling energies generate great portion of the final energy consumption by end-user. An introduction to microgrids was carried out in [43].

Figure 2.11 gives an overview of the microgrid concept, where some DGs and some distributed ESSs are connected downstream of the PCC (Point of Common Coupling) with the utility grid. For the grid, the microgrid is just seen as a unit in which electric power exchange is done. DER units are connected usually in LV or MV [2].

Every DER unit that is integrated into the microgrid has its own output characteristics concerning voltage and current that must be homologated into a same voltage characteristic defined by the microgrid bus. From a topological point of view there are two main distinctions in microgrids, DC or AC microgrids depending of the coupling voltage of the bus in the microgrid [44].

Microgrids have two main operating modes depending on whether the microgrid is connected to main grid or whether it operates in islanded mode. Several control aspects change depending on its operating mode, taking into account economic or power quality aspects [5]. Two classifications can be made according to the way DER units are connected to the common bus of the microgrid [2]:

- **Conventional DG units**: These kind of units do not require the use of an electronic power converter to be coupled to the common bus of the microgrid (e.g., a synchronous generator driven by a reciprocating engine or an induction generator driven by a fixed-speed wind turbine (WT)). The rotating machine converts the power from the primary energy source to the electrical power and also acts as the interface medium between the source and the microgrid.

- **Electronically Coupled DG units**: These kind of units require a power converter to transform its power output into the normalized one by the AC or DC bus of the microgrid. This provides an increase in complexity but can provide another layer of conversion and/or control such as voltage and frequency.

Attending to the controllability of the DER, it must be made the differentiation between dispatchables and non-dispatchables DER units. In the dispatchable DER units the power that flows with the microgrid can be controlled through a supervisory control which can set the operating-point of every dispatchable DER, considering the global requirement of whole microgrid in order to match generation and consumption in the microgrid. On the other hand, the non-dispatchable DER control, for example a wind turbine or a photovoltaic array, are operated under its MPPT (Maximum Power Point Tracking) in order to obtain the maximum energy into the microgrid. Generally all the renewable energy sources are non-dispatcha-bles, being this aspect one of the disadvantages in comparison with the fossil fuel DG [2].

Pedrasa [45] carried out a survey of techniques used to control microgrids with ESSs during island operation, considering the voltage and frequency management, the balance between supply and demand, power quality, microsources issues and the communication among microgrid components. The different algorithms that were studied in this article were solved using classical methods.

Controlling a microgrid entails various aspects which should be taken into account. The majority of the articles, dissertations and paper reviewed can be classified into three main families, (i)hybridization management among ESSs in microgrids (ii)authors who focus their work on the economic dispatch (iii)power quality in microgrids. As explained in section 2.12 there is an ongoing discussion about the different control levels that the microgrid must have. The next sections give an overview of the current situation in regards to every commented aspect of the microgrid control.

2.4.2 Hierarchical Control of Microgrids

The microgrid is usually conceived to operate within three control hierarchical levels (similar to the grid). These levels are shown in figure 2.12 and are explained in dept in [2],[46]-[48]. The primary and secondary control levels are related with the power quality operation of the microgrid while the tertiary level is related with the economic dispatch.

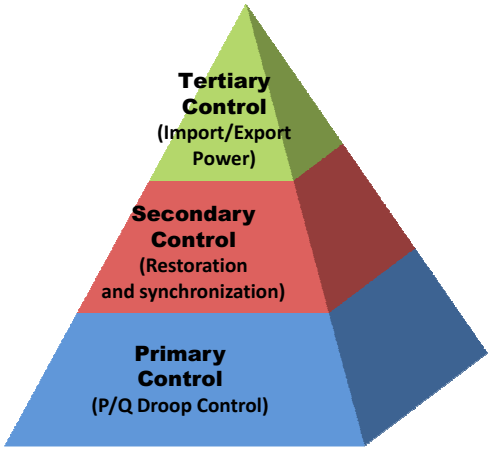

Figure 2.12. Hierarchical control levels of a microgrid [46, 47]

The proposed algorithm by Guerrero *et al.* [47] adapts that of the ISA-95 to control a microgrid, adopting zero to three levels: (i) The third level controls the power flow between the microgrid and the grid. (ii) The second level ensures that the electrical levels in the microgrid are inside the required values. In addition, it includes a synchronisation control loop to seamlessly connect or disconnect the microgrid to the distribution system. (iii) The first level provides a droop

control method that emulates the physical behaviours that make the system stable and more damped. (iv) Level zero is formed by the inner control loops where regulation issues of each module are integrated. Current and voltage, feedback and feedforward and linear and nonlinear control loops are performed to regulate the output voltage and to control the current, while the system is maintained stable. The control problem is formulated with a classic method solving every level with PI-Controllers, aspects related to sharing power between ESSs are not taken into account. Guerrero also introduces the difficulties associated withAC microgrids: the need for synchronization of the distributed generators, the inrush currents due to transformers, reactive power flow, harmonic currents, and three-phase unbalances. Furthermore, this author also discusses the increasing interest in integrate prime movers with DC output such as photovoltaic modules or fuel cells in DC microgrids.

The proposed algorithm by Brabandere *et al.* [48] is also composed of a three level control structure over the microgrid. The primary droop control ensures reliable operation in the microgrid even when communication fails. The second and third levels are in charge of power quality aspects and economic optimization through classical PI-control methods.

The work carried out by Yang Wang *et al.*, in [50], describes a four-stage hierarchical control system for the microgrid. Firstly there is a physical level consisting of the hard-ware and the corresponding control software of each DER and protection system, moving into a second and third control levels dedicated to power quality and economic dispatch, and the last stage provdes a user application level to make customers participate in the microgrid control more conveniently. The control algorithm is solved through heuristic method.

In [51], the major issues and challenges in the microgrid control are discussed, and a review of state-of-the-art control strategies and trends is presented; a general overview of the main control principles (e.g., droop control, model predictive control, multi-agent systems) is also included. The paper classifies microgrid control strategies into three levels: primary, secondary, and tertiary, where primary and secondary levels are associated with the operation of the microgrid itself, and tertiary level pertains to the coordinated operation of the microgrid and the host grid. There is an important number of articles dedicated to the management of several microgrids such as [52]-[55]. This could be considered as another control level of the microgrid however, this control level is not the object of this dissertation.

2.4.2.1 Primary Control

The interfaces between the different components of the microgrids are often based on power electronics converters acting as voltage source inverter, VSI, in case of AC microgrids [49, 56]. These power electronics converters are parallel connected through the microgrid. In order to avoid circulating currents among the converters without the use of any critical communication between them, the droop control method is often applied [49], [57]-[60].

In case of paralleling inverters, the droop method consist of subtracting proportional parts of the output average active and reactive power to the frequency and amplitude of each module to emulate virtual inertias. These control loops, also called $P-f$ and $Q-U$ droops (see equations 2.1 and 2.2), have been applied to parallel connected uninterrupted power systems (UPS) [61]-[64].

$$f - f^{ref} = G_P(s) \cdot (P - P^{ref}) \tag{2.1}$$

$$U - U^{ref} = G_Q(s) \cdot (Q - Q^{ref}) \tag{2.2}$$

where f and U are the output frequency and amplitude of the output voltage reference, P and Q denote the active and reactive power, and G_P and G_Q their corresponding transfer functions, are typically proportional gains m and n.

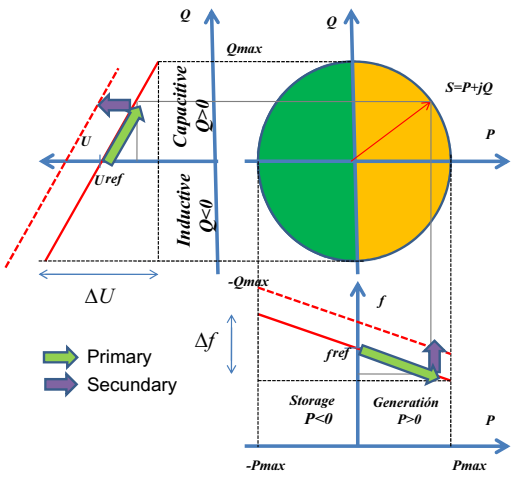

Figure 2.13. $P-Q$ circle and $Q-E$ control droop [49]

Figure 2.13 shows the relationship between the $P-Q$ circle of a distributed generation unit. The parameters m and n regarding the ESS introduction in the

microgrid can be determined as follows:

$$m = \frac{\Delta f}{2P_{max}} \tag{2.3}$$

$$n = \frac{\Delta V}{2Q_{max}} \tag{2.4}$$

However, although this technique achieves high reliability and flexibility, it has several drawbacks that limit its application, overall when non-linear loads are shared, because the control units should take into account harmonic currents, and, at the same time, to balance active and reactive power. Another important disadvantage of the droop method is its load-dependent frequency and amplitude deviations. In order to solve this problem, a secondary controller is implemented in the microgrid central control can restore the frequency and amplitude in the microgrid [49].

2.4.2.2 Secondary Control

In order to compensate for the frequency and amplitude deviations, a secondary control can be used. The secondary control ensures that the frequency and voltage deviations are regulated towards zero after every change of load or generation inside the microgrid. The frequency and voltage amplitude levels in the microgrid $f_{\mu grid}$ and $U_{\mu grid}$ are sensed and compared with the references f^{ref} and U^{ref}, the errors that are processed through compensators (δf and δU) are sent to all the units to restore the output voltage frequency and amplitude [49]. This control can also be used for microgrid synchronization with the main grid before performing the interconnection after a transition between islanded to grid connected mode [46]. The difference action between primary and secondary control can be observed in figure 2.13.

2.4.2.3 Tertiary Control

This can be considered as the economic level of the microgrid. No technology will be definitively integrated in society if it does not have economic benefits in comparison with its predecessor. This control is used to regulate the active and reactive power exchange between the microgrid and the main grid according to economic dispatch developed for the microgrid.

2.4.3 Hybrid ESS Management

The technological maturity of energy storage technologies with a short lifetime is still a barrier for its technological implantation, being the economic revenue by their use usually lower than the investment carried out in their acquisition. In this aspect, a correct use of the selected ESS where degradation causes were taken into account can improve their economic profitability and as a result their useful life.

The importance of power sharing in hybrid ESSs, management of the energy density versus power density, transient response and autonomy, respecting the degradation causes have been discussed in several studies. The existing literature exposes how the use of hybrid ESSs can satisfy a major range of applications, improving the lifetime of the single components. The optimal use of the hybrid ESS requires the development of a controller which takes into account all the constraints, limitations, degradation issues and the economic cost of each ESS.

The majority of these studies have focused on fuel cell electrical vehicles (FCEV) such as [33], [65]-[69] and just a few apply hybridization between ESSs and microgrids or stationary applications. Two main scenarios can be differentiated in microgrids, excess or deficit of energy. The energy system of a FCEV can be regarded as a microgrid in the energy deficit scenario where the ESS has to supply the power to the load (electrical engine of the vehicle). The concept of respecting degradation issues for every ESS can be applied in scenarios of both excess or deficit of energy.

Each technology has its own degradation causes that should mark the operating limits or the associated degradation costs of exposing the ESS to these operating conditions must be considered. The dissertation presented by Stevens [33] analyses the physical causes of degradation in fuel cells and batteries applied in FCEVs, resulting in a mere model as the hybridization control algorithm is not developed. In the same way, the thesis carried out by Bergen and Roy [37, 38] studies the main causes of degradation of a electrolyzer according to the power profile applied without developing a control algorithm.

The main causes of degradation in batteries have been object of study in several articles and dissertations. The study carried out by Sikha *et al.* [32] makes an analysis of different protocols of charging and discharging lithium-ion batteries. This dissertation establishes that the rate capability loss is proportional to the value of the average current used, not being possible to avoid this apparent increase of the capacity fade when the battery is charged at fast rates. The study concludes that material degradation can be eliminated by using an optimized current profile. Similar results can be found in [33, 70].

A lot of information relating to the degradation or associated use problems of ultracapacitors cannot be found, maybe due to their high number of life cycles (See table 2.2). The thesis presented by Flores-Oropeza [71] concluded with the associated problematic of the high discharge ratio of UCESSs. In high discharges UCESSs behave like a short circuit, so a high current ratio is applied to the associated power converter.

Several studies and projects has been carried out in reference to microgrids. Heuristic methods with classical controllers are applied in [72]-[75], managing renewable energy microgrids with hybrid ESSs considering the system dynamics of each ESS. The study presented by Tao Zhou *et al.* [76] proposes a hybrid ESS between HESS and UCESS, where the UCESS absorbs the transients that HESS dynamic cannot absorb are managed through the ultracapacitor. The articles presented by Garcia *et al.* and Schaltz *et al.* [69, 77] use a control method to manage the hybridization between different ESSs, using frequency filters which generate good results. Lin *et al.* [78] propose a strategy based o adaptive control using neural networks.

Thounthong *et al.* apply hybridization between a FC, a BESS and UCESS in [79, 80] which is used in an electric vehicle and a microgrid taking into account dynamic and degradation aspects of each ESS. In the studies completed by Thounthong *et al.*, the energy in the hybrid system is balanced by the DC bus voltage regulation. A ultracapacitor module, working as a high dynamic and high power density device, functions for supplying energy to regulate a DC bus voltage. A battery module, as a high energy density device, operates to supply energy to a supercapacitor bank to keep it charged. An FC, as a slowest dynamic source in this system, functions to supply energy to a battery bank in order to keep it charged. Therefore, there are three voltage control loops: DC bus voltage regulated by a supercapacitor bank, supercapacitor voltage regulated by a battery bank, and battery voltage regulated by an FC. As explained by Pukrushpan and Suh in [40, 41] transient response is a key characteristic feature of ESSs, sometimes more critical than efficiency, due to the importance of accepting rapidly changing, uncertain electric loads. Fast transient response is essential for autonomy in start-up and fast power response but concepts such as long-term autonomy in order to have the lower level of dependence with the main grid must be also considered. An optimal ESS which would be able to respond in the short, medium and long term still does not exist. Hybrid ESSs with an optimal algorithm for sharing power, minimizing the cost function of the whole ESS, and managing the different time scales in the renewable energy microgrid are required. Advanced control are required in order to consider the large number of control variables that must be studied to minimize degradation aspects in

hybrid ESSs. The dissertation presented by Kyung Wons Suh in [40] solves the hybridization control problem with the following objectives: (i) protect the fuel cell system from abnormal load including transient (ii) maintain state of charge of the battery (iii) maintain the DC bus voltage (iv) regulate the current (from both the fuel cell and battery) to the optimized values if supervisory control demand exists through LQR strategies.

Vahidi and Greenwell [81] and [82] applied the MPC in their studies to control the load sharing of a hybrid ESS composed of a fuel cell and an ultracapacitor, including some degradation issues. However, these studies do not include the connection to the grid or the start up/shut down degradation issues associated with the fuel cell. Similar developments have been advanced in the hybridization of a fuel cell and a battery by Arce *et al.* and Bordons *et al.* in [83, 84].

2.4.4 Economic Dispatch

The electricity market rules determine the energy price in the Day-Ahead market, matching offers from generators to bids from consumers to develop a classic supply and demand equilibrium price, usually on an hourly interval. With the liberalization of electricity markets, renewable energy producers have the possibility to dispatch their production through electricity pools. The main characteristic of these markets is that one has to propose bids in advance, and is then charged for any imbalance, defined here after as the deviation between the actual production and the energy bid. The Regulation Service corrects for short-term changes in electricity use that might affect the stability of the power system. It helps match generation and load and adjusts generation output to maintain the desired frequency [85, 86, 87]. Regulation power is more expensive than the bulk power available at the market. This is because it is only, used at short intervals and has to be kept ready so that continuous production by that capacity cannot be sold to the electricity spot market. Paying extra for regulation is also one incentive for the market actors to maintain their power balance. The intermittency of renewable energy, as well as difficulties with prediction, will need a great amount of regulation power in the system.

The economic costs of each storage system are introduced by Geer *et al.*s research [88], in which an evaluation of the economics of operating a wind/hydrogen-bus system is explained. Dufo *et al.* [89] consider a strategy applied to a standalone microgrid composed of renewable sources (wind, PV and hydro), batteries, a fuel cell, an AC generator and an electrolyzer, all of which optimize the control of the hybrid system while minimizing the total cost throughout their lifetime using genetic algorithms. Heuristic algorithms applied to the economic

dispatch of microgrids are presented by Chakraborty and Simoes [90], who solve the economic dispatch of a PV-microgrid where only batteries are used as energy storage. In [91]-[93] a dead-band hysteresis algorithm is used to decide the use of the battery ESS or the hydrogen ESS. Gu *et al.* [94] make an optimization control algorithm for the combined heat and power of a microgrid with batteries and a fuel cell fed with natural gas neglecting degradation aspects of the ESS. In [95] and [96] different strategies in the control of microgrids with hybrid storage using heuristical methods are presented. Advanced scheduling to encourage customers not only to participate in energy generation but also in efficient electricity consumption is proposed by Adika and Wang [97]. In the paper presented by Ferrari-Trecate *et al.* [98] the development of MPC for hybrid cogeneration power plants is carried out introducing the MLD framework. MPC applied to distributed energy resources with a battery ESS is developed by Negenborn *et al.* [99] introducing an MLD model but without taking into account other kinds of ESSs or the degradation issues associated with the battery. Korpås [87] uses MPC to integrate hydrogen ESSs in the electrical market not considering other ESS possibilities, neglecting degradation issues associated with the ESS. Del Real *et al.* [100] and Valverde *et al.* [101] develop MPC strategies applied to the field of microgrid optimisation without considering the degradation issues of the ESS. Mixed Integer Linear Programming (MILP) including operational costs in the ESS is used in [102]-[105] without integrating the degradation issues in the ESS. A comprehensive detailed model for a stand-alone hybrid energy system with wind turbine and solar energy conversion, an electrolyzer, a fuel cell, and hydrogen storage components was developed. A supervisory controller for proper power management and a set of local controllers for efficient hydrogen generation and consumption were implemented in [106]. Mixed-Integer Programming techniques are used by Palma-Behnke *et al.* in [107] in a microgrid with BESS including the State of Health of the battery in the cost function. Microgrid optimal scheduling considering multi-period islanding constraints is solved using Mixed-Integer programming in the study carried out by Khodaei [108]. A self-organizing computing framework, based on self-organizing agents, for solving the fundamental control and monitoring problems of a microgrid is presented in [109]. The control problem of coordinated energy management of networked microgrids is dealt with in [110]. Jiang and Fei [111] propose an energy ecosystem facilitated by microgrid management with hierarchical agents and optimization, where updated external information and users task preference are considered to make the control decisions. Nguyen and Le [112] suggest a framework for optimizing energy trading operations of a microgrid aggregator in the energy market.

There are almost no studies where the application of the tri-hybrid ESS ultracapacitor-battery-hydrogen in the field of the smart grid is considered.

2.4.5 Power Quality

Main grid lines have a high inductive component and are mostly fed by rotary generators; therefore, there is usually an association between frequency control (active power balance) and between voltage control (reactive power balance). Special units to compensate frequency and voltage unbalances that acted when necessary existed in the traditional power system. Future smart grids will be mainly composed by renewable generation. Renewable generation is characteristically instable and fluctuant. This makes it necessary to have advanced control architecture to enhance power quality and reliability for the consumer. Benefits of ESSs with renewable sources in power quality enhancement have been studied in [113] - [117].

An introduction to power quality aspects in microgrids can be found in [3, 4]. Power quality aspects can be grouped in three main concepts: frequency control, voltage control and harmonic control. Depending of the time scale of the perturbation, several classifications can be made, such as variations and events. While variations are continuously measured and evaluated, unpredictable events occur in general and require a trigger action to be measured. Important variations (cf. EN 50160) are: slow voltage changes, harmonics, flicker and unbalance. Important events are rapid voltage changes, dips, swells and interruptions. The power quality in the microgrid will be a result of the interaction between the main grid, the generator connected to the microgrid and the load fed by the microgrid. A description of the main problems and solutions of power quality in microgrids, distributed energy storage systems, and AC/DC hybrid microgrids are discussed by Guerrero et al in [49, 118]. The study developed by Wasiak *et al.* [119] deals with the application of energy storage connected to the low-voltage microgrid by coupling inverter for simultaneous energy management and ancillary services that include the compensation of power quality disturbances.

The power quality control problem in microgrids has recently been the object of study by several authors. Heuristic and classic controllers to eliminate power fluctuation in a stand-alone microgrid are used by Ahmed in [120]. Li [121] studied the frequency fluctuations resulting mainly from real power imbalances and applied the BESS and HESS system to smooth the power fluctuation of microgrids power system presenting a fuzzy control strategy of micro-grid power system.

The dissertation carried out by Vasquez [46] studies different control structures based on droop control. Vasquez proposes a control method with a dynamic model based on adaptive droop methodology using Padé approximation. The proposed control method injects the desired active and reactive power independently into the grid for a large range of impedance grid values using an identification algorithm. The proposed method decouples active and reactive power flows. Vasquez also focuses his research on the phase and amplitude synchronization algorithm in the transition between the islanded operation mode to the connected mode when a fault in the main grid is detected and cleared. Vasquez carried out a small-signal stability study to give guidelines for properly adjusting the control system parameters according to the desired dynamic response.

The thesis presented by Majumder [122] study different problems with power quality in microgrids. An angle droop controller is proposed to share power amongst converter interfaced DGs in the microgrid. An enhanced frequency and voltage droop controller is offered as a better dynamic response and a smooth transition between grid connected and islanded modes of operation of the microgrid. This thesis also proposes a frequency and voltage isolation technique between the microgrid and the utility by using a back-to-back converter. For accurate load sharing, a supplementary droop controller is proposed. A small signal model of the system is developed. Two methods are put forward for load sharing with minimal communication and without communication.

A smooth transition between the grid connected and islanded mode assures a stable operation of the system. A hierarchical control scheme is proposed by Savaghebi [123] for the enhancement of Sensitive Load Bus (SLB) voltage quality in microgrids. The control structure consists of primary and secondary levels. The primary control level comprises Distributed Generators (DGs) local controllers. Each of these controllers includes a selective virtual impedance loop which is considered to improve the sharing of fundamental and harmonic components of load current among the DG units. The sharing improvement is provided at the expense of increasing voltage unbalance and harmonic distortion. Therefore, the secondary control level is applied to manage the compensation of SLB voltage unbalance and harmonics by sending proper control signals to the primary level. DGs compensation efforts are controlled locally at the primary level. Ghosh [124] describes the operation of a microgrid that contains a custom power park (CPP). The park may contain an unbalanced and/or nonlinear load and the microgrid may contain many distributed generators (DGs). One of the DGs in the microgrid is used as a compensator to achieve load compensation. A new method is proposed for current reference generation for load compensation, which takes into account the real and reactive power to be supplied by the DG connected

to the compensator. The real and reactive power from the DGs and the utility source is tightly regulated assuming that dedicated communication channels are available. Therefore this scheme is most suitable in cases where the loads in CPP and DGs are physically located close to each other. In [125], the standard IEEE 34 bus distribution feeder is adapted and managed as a microgrid by adding distributed generations and load profiles. Supervisory power management has been defined to manage the transitions and to minimize the transients on voltage and frequency. Detailed analyses for islanding, reconnection, and black start are presented for various conditions. The economic problem linked to technical problems of power quality is treated in [126], and the problem is solved using an evolutionary game theory and classic PI-control methods.

Delghavi [127] carried out his research on advanced islanded-mode control of microgrids. This dissertation is focused on the modelling, control stability and power management of electronically interfaced DER units for microgrids. The thesis proposes a voltage and frequency regulation strategy for islanded DER systems, regulating the frequency by controlling the q-axis component of the terminal voltage of the DER system. The research proposes a discrete-time adaptive feedforward compensation strategy that alters the dynamic couplings between a DER system and its host microgrid. Finally, the thesis puts forward a unified control strategy for both islanded and connected operation modes.

In his dissertation, Mohamed proposes [9] new controls for the DG interface. A deadbeat current regulation scheme is proposed for the inverter giving good results for the injection of high power quality. The developed algorithm utilized the maximum dynamic performance of the inverter in a way that provides a high bandwidth and decoupled control performance for the outer control loops. The adaptive interface relies on a new interface-monitoring unit that gives accurate and fast estimation of the interfacing impedance parameters and the gird voltage vector at the PCC. A new voltage control scheme targeting the fast load voltage regulation and mitigation of fast voltage disturbances is carried out. A sharing method to preserve the dynamic performance and stability of each inverter unit at different loading conditions is also established.

The control problem of parallel inverters is mentioned in [46, 128]. Jiang [128]. This research presents an active power and voltage control scheme for the inverters that operate in the islanding mode which can regulate both the active power and the magnitude of the voltage of the inverters through PI-controllers. The MPC controller for power inverters have also been used by Rodriguez and Gever [129, 130]. Kwan [131] presents a hybrid fuel cell and an ultracapacitor MPC controller for power quality improvement. The different associated problems with the islanded-mode of microgrids are discussed in the studies developed

by Lopes *et al.* [132] and Pedrasa *et al.* [45]. Different developments can be found in the field of the voltage/ frequency control in the islanded mode of microgrids. Sao *et al.*[133] and Karimi *et al.* [134] developed models and control strategies based on pre-specified, balanced, linear, load circuit configurations voltage-droop controllers. The controller proposed by Li *et al.* [135] contains inner voltage and current loops and external power control loops for controlling real and reactive power flow, facilitating power sharing between the paralleled DG systems when a utility fault occurs and the microgrid islands. Jiang and Xunwei[128] present an active power and voltage control scheme for inverters and a droop control method for the power sharing among the parallel inverter-interfaced distributed energy resources. Delghavi and Yazdani [136] propose a control strategy which utilizes a combination of deadbeat and repetitive control to enhance the performance of the control system under unbalanced and/or distorted load currents. Escobar *et al.* [137] solve the control algorithm using adaptive control and Willmann *et al.* [138] use a multiple-loop H-infinity control. A multi-functional grid-tied inverter with Objective-Oriented Power Quality Compensation for microgrids application is presented in [139].For microgrid in islanded operations, due to the effects of mismatched line impedance, the reactive power could not be shared accurately with the conventional droop method. To improve the reactive power sharing accuracy, the paper proposed by Han *et al.* [140] presents an improved droop control method. The proposed method mainly includes two important operations: error reduction operation and voltage recovery operation. The sharing accuracy is improved by the sharing error reduction operation, which is activated by the low-bandwidth synchronization signals. In [141] an enhanced islanding microgrid reactive power, imbalance power, and harmonic power sharing scheme is discussed. The proposed method utilizes the frequency droop as the link to compensate reactive, imbalance, and harmonic power sharing errors. A decentralized control of voltage source converters in microgrids based on the application of instantaneous power theory is presented by Ovalle *et al.* in [142]. A new strategy to control microgrids highly penetrated by VSCs and operating in stand-alone mode is proposed. The strategy is based on the instantaneous measurements and calculations of voltages and currents and the application of instantaneous power theory. This approach employs each VSC along with an LC filter as a current source. The grid parameters are not known by the controller; only the filter inductance and capacitance are known. The approach is capable of giving an approximation of the equivalent impedance of the system seen from the filter output, without difficult procedures or measurements. A critic-based self-tuning PI structure for active and reactive power control of VSCs in microgrid systems is presented in [143].

From the point of view of power quality, the energy supply must be provided respecting the necessary compatibility between all the devices connected to the same grid. High penetration of renewable energy produces energy imbalances in the grid resulting in serious problems in power quality, such as, flickers, sags, variations in frequency and voltage magnitude of the main grid. This fact is due to fluctuating systems and their inherent intermittency . This makes more precise requirements on the power balance control algorithm, from primary control to the operational planning necessary. This fact requires higher effectiveness in reference tracking for the electronic power associated to the ESS. Moreover, it is necessary to establish new control algorithms different from the classical PI-PWM controllers which present slow response and a long transient period until the references are reached.

The MPC technique applied to power converters are introduced by Rodriguez *et al.* [129] which are known by the fast dynamic response. MPC needs a model of the plant to predict the output in the control horizon utilized by the controller. A review of MPC applications in power electronics can be found in [144] and [145]. The MPC technique has been applied to the voltage control of inverters with an output LC filter by Cortés *et al.* in [146] and [147]. In these papers the problem to estimate the current for the next instant is manifested. This estimation problem is mainly due to the fact that the connected load to the inverter is unknown to be modelled and predicted.

2.5 Summary

In this chapter an analysis of the main technologies that are appearing for DG has been presented. The great problem regarding generation is how to manage the non-dispatchable DER, such as, photovoltaic generators and wind turbines. The control of the microgrid, based on these kinds of technologies, will be developed in the next chapter. A critical review of the main ESSs used is also explained. According to the study carried out, the most appropriate technologies in the short, medium and long storage time are the ultracapacitor, the battery and the HESS (composed by an electrolyzer and a fuel cell). Degradation causes must be avoided by the control algorithm in order to maximize their lifetime. A complete analysis of the main causes of degradation in the selected technologies must be done, as well as a model of the generation in the microgrid that includes the forecast of the wind and solar generation. To complete the model of the microgrid, a prediction model of energy prices and load consumption must be considered. There are just a few authors who propose a global algorithm for the

microgrid that includes the economic point of view and the power quality aspects of renewable energy microgrids. Those authors who have carried out this advance use heuristic or classic PI-controllers.

The main shortage found in the literature review is the fact that degradation issues of the ESSs are not included in the control algorithm of the microgrid. A global MPC controller for the microgrid, including the minimization of degradation causes in a hybrid ESS that manages the long, medium and short time control aspects in the microgrid, will be developed in the following chapters.

From the point of view of power quality, the ESS appears to be a key solution to the power quality problems introduced by a grid with high penetration of renewables. But usually, ESSs are interfaced with inverters where the control algorithm is based on classic methods whose transient response under fluctuating conditions could even introduce more power quality problems while the reference is reached. In order to improve the power quality in these kinds of applications, new control strategies will be implemented for the power electronics associated to ESSs.

Chapter 3

Modelling and Analysis of the Microgrid Components

3.1 Introduction

The purpose of this chapter is to develop the physical model of each component of the microgrid, in order to analyse the different advantages and disadvantages introduced by each one in the microgrid. The microgrid, object of this dissertation, is composed by a photovoltaic generator and a wind turbine, in order to analyse the problem introduced by the most classic ways of renewable generation. It can also work in grid-connected or islanded mode. It has three ways to store energy: in ultracapacitors, batteries or hydrogen. It has also domestic load connected to the microgrid. The schematic view of the microgrid and the components value are shown in figure 3.1 and table 3.1. The microgrid of the Centro Nacional del Hidrogeno (object of this study) was not fully operational at the end of this thesis. For this reason the microgrid of the Escuela Tecnica Superior de Ingeniería of Seville was used to validate the models and the controller explained in Chapter 4. This plant can be observed in figure 3.2. The experimental plant has not got physically the PV-pannels, the wind turbine, the ultracapacitor. These components were emulated using a power source and a electronic load. The forecast difficulties and power quality issues in the case of photo-voltaic array and wind turbine generation are also studied. In the case of the different ESSs, an analysis of the degradation issues is carried out in order to be minimized by the whole control algorithm.

The model to be used at each control level of the microgrid will depend of the time-scale applied (see table 3.2). Aspects such as energy forecasting that

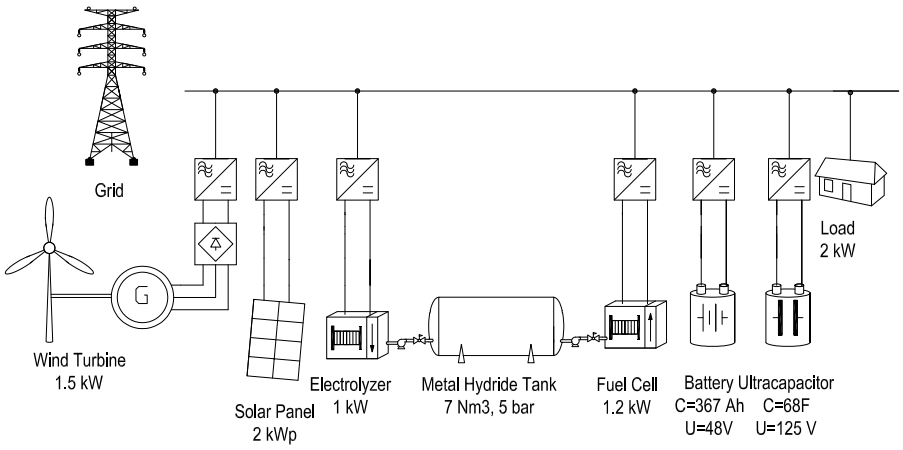

Figure 3.1. Microgrid object of this study

Table 3.1. Microgrid components

Microgrid Component	**Manufacturer**	**Model**	**Rated Capacity**
Photovoltaic Pannel	ISOFOTON	Isofoton-150	2.1kWp
Wind Turbine	BORNAY	INCLIN 1500	1.5kW
Ultracapacitor	MAXWELL	BMOD0063P125B08	68 F, 125V, 228.55 Wh
Battery	EXIDE	Pb-Acid	C_{120}=367 Ah, 17616 Wh
Electrolyzer	HAMILTON-STD	PEM	0.23 Nm^3/h, 1kW
Metal Hydride Storage	LABTECH	-	7 Nm^3, 5 bar
Fuel Cell	Heliocentris	Nexa 1200	1.2kW

has a stronger influence in the long term while time-response of the dispatchable components has a clear importance in the very short or immediate term. If the control problem is associated to the economical schedule, a forecasting model must be used. When power quality issues are being solved the model must be based on the power electronics of the component. While for real-time optimal load sharing, the most important aspect is the physical model.

Table 3.2. Time-scale in control of microgrids. [a]

Time Horizon	**Range**	**Application**	**Model**
Inmediatus term	$10^{-6} - 1$sec	- Power Quality - Active and Reactive Balancing	- Power Electronic
Short term	$1sec - 10min$	- Electricity Market Clearing - Regulation Actions	- Response Time - Energy Density Limit - Power Density Limit - Load Cycling Degradation
Medium term	$10min - 1h$	- Regulation Market Planning - Load Increment/Decrement	- Energy Forecast - Load Cycling Degradation - Energy Density Limit - Power Density Limit
Long term	$1h - 6h$	- Intradaily Market Planning	- Energy Forecast - Load Cycling Degradation - Energy Density Limit - Power Density Limit
Very Long term	$6h - 1week$	- Daily Market Planning	- Energy Forecast - Load Cycling Degradation - Energy Density Limit - Power Density Limit

[a] Source: Modified from [148]

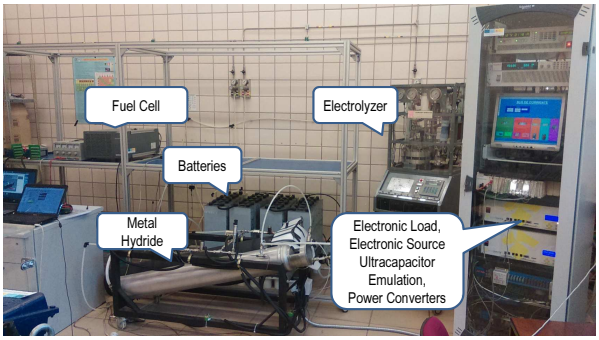

Figure 3.2. Experimental set-up of the microgrid

3.2 Photovoltaic Generator

Solar energy is one of the most promising renewable resources to be introduced in the future smart grid. The high penetration level that this kind of energy generation has obtained in the last decades endorses this hypothesis. Two main technologies of solar generation are thermosolar and photovoltaic. For the thermosolar generation large power generation plants are needed thus the use of photovoltaic in microgrids is more logical. The benefits of the low cost of sun generation are manifested in several projects, articles and dissertations but photovoltaic technology still has several problems that hinder its correct integration in the grid. In the literature several models of the photovoltaic array can be found and in this section the photovoltaic model is presented by analyzing the main problems associated to the integration of this technology in the grid.

A photovoltaic generator is mainly composed by a matrix of PV cells in array disposition. Through the photovoltaic effect the sunlight is converted to DC-power. The output DC-power of the matrix of PV arrays is converted to AC-power with a power inverter (see figure 3.3). In the next section every part of the PV power generation process will be detailed.

3.2.1 Sunlight Resource

Irradiance or insolation is the instantaneous solar power received on a units surface area and is normally given in W/m^2. The global irradiance G that the photovoltaic panel receives at a particular moment will depend on the solar coordinates and the meteorological conditions at this moment. Solar irradiation is almost constant throughout the year. The solar constant B_0, can be defined as

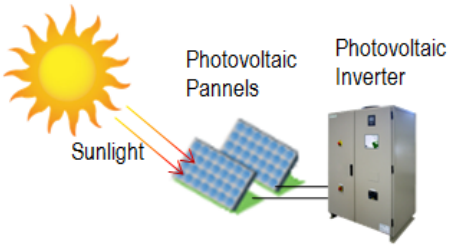

Figure 3.3. Solar energy transformation thought a photovoltaic generator

the proceeding irradiance from the sun which has an impact on a surface situated perpendicular to the propagation direction of the solar radiation, located out of the atmosphere and in a distance with a equivalent value to the average distance between the Earth and the Sun. The value of this constant is $B_0 = 1353W/m^2$ [89, 149].

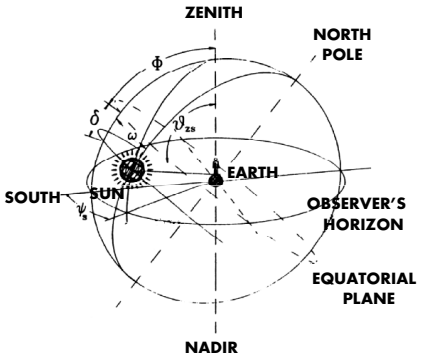

Figure 3.4. Celestial sphere and coordinate system attached to a point on the Earth. Source: Adapted from [89, 149]

The Earth makes a daily rotation on itself and the equatorial plane is not parallel with the Earth's orbital plane around the Sun (ecliptic). The Earths equatorial plane maintains the same direction throughout the year, presenting a fixed inclination of $23^o\ 27'$ on the ecliptic plane, so that the solar declination δ (sun straight angle - flat land with the Equator), ranges from $23^o\ 27'$(summer solstice) to $-23^o\ 27'$(winter solstice). The solar declination follows the next expression for every day of the year:

$$\delta = 23.45 \cdot \sin\left(\frac{360}{365} \cdot (d_n + 284)\right) \tag{3.1}$$

where, d_n is the number of the day of the year being 1 the first day of the year (1st of January) and 365 the last one (31th of December). The distance between the Sun and the Earth varies throughout the year because of the eccentricity of the ecliptic (ε_0), which can be estimated by the equation:

$$\varepsilon_0 = \left(\frac{r_o}{r}\right)^2 = 1 + 0.033 \cdot \cos\left(\frac{360 \cdot d_n}{365}\right) \tag{3.2}$$

where r_o is the average distance between the Sun and the Earth and r is the distance at the moment when the calculus is carried out. The latitude (ϕ) can be defined as the angular distance north or south from the Equator of a point on the Earth's surface, measured on the meridian of the point. In an axis-solidary system with a point of the Earth two angles are defined to locate a point at the celestial sphere (see figure 3.4).

- The solar zenith angle (θ_z) is the angle measured from directly overhead to the geometric centre of the sun's disc, as described using a horizontal coordinate system. The solar elevation angle is the altitude of the sun, the angle between the horizon and the centre of the sun's disc. Its complementary angle is called solar elevation (γ).

- The azimuth angle (ψ) defines in which direction the sun is, whereas the solar zenith angle or its complementary angle solar elevation define how high the sun is.

At a certain instant the zenith angle and the azimuth angle of the sun can be calculated as a function of the latitude with the following equations:

$$\cos\theta_{zs} = \sin\delta \cdot \sin\phi + \cos\delta \cdot \cos\phi \cdot \cos\omega = \sin\gamma \tag{3.3}$$

$$\cos\psi_s = \frac{\sin\gamma \cdot \sin\phi - \sin\delta}{\cos\gamma \cdot \cos\phi} \tag{3.4}$$

where γ is the elevation and ω is the hourly angle of the solar time.

Solar irradiance over a perpendicular surface to the solar rays (B_{0n}) and irradiance over horizontal surfaces ($B_{0i}(0)$) can be obtained with the subsequent equations (see figure 3.5):

$$B_{0n} = \varepsilon_0 \cdot B_0 \tag{3.5}$$

$$B_{0i}(0) = B_0 \cdot \varepsilon_0 \cdot \cos(\theta_{zs}) \tag{3.6}$$

The different components of the atmosphere decompose solar irradiance over a surface in three components:

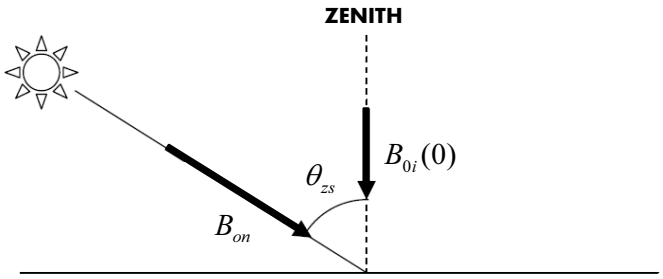

Figure 3.5. Normal irradiance and irradiance over horizontal surface. Source: Adapted from [89]

- Direct radiation (B) which is also sometimes called "beam radiation" or "direct beam radiation". It is used to describe solar radiation traveling on a straight line from the sun down to the surface of the earth.
- Diffuse radiation (D), on the other hand, describes the sunlight that has been scattered by molecules and particles in the atmosphere but that has still made it down to the surface of the earth.
- Reflected radiation (R) describes sunlight that has been reflected off of non-atmospheric things such as the ground.

Global radiation over a surface can be obtained by adding the three terms as indicated in equation 3.7.

$$G_i(\beta, \alpha) = B_i(\beta, \alpha) + D_i(\beta, \alpha) + R_i(\beta, \alpha) \tag{3.7}$$

where β and α define the angles of inclination and azimuth of the receptor surface. The diffuse fraction (K_D) and the clearness index (K_T) can be defined with the following equations which can be calculated using several correlations such as Graham-Hollands or Liu-Jordan [89]:

$$K_D = \frac{D_i(0)}{G_i(0)} \tag{3.8}$$

$$K_T = \frac{G_i(0)}{B_{oi}(0)} \tag{3.9}$$

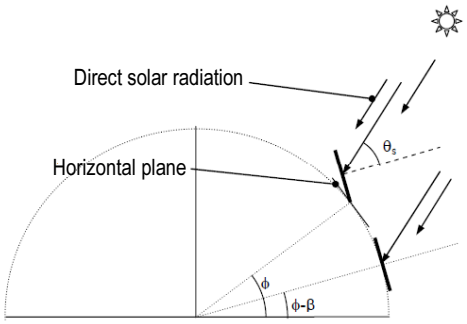

Figure 3.6. Angle of incidence of the solar radiation on an inclined surface. Source: Adapted from [89]

In figure 3.6 the angle of incidence of the solar radiation on an inclined surfaceis shown, if this surface is rotated an azimuth angle α, the cosine of the solar incidence can be calculated with the following expression:

$$\begin{aligned}\cos\theta_s &= \sin\delta\cdot\sin\phi\cdot\cos\beta + \cos\delta\cdot\cos\phi\cdot\cos\omega\cdot\cos\beta \\ &- \sin\delta\cdot\cos\phi\cdot\sin\beta\cdot\cos\alpha + \cos\delta\cdot\sin\omega\cdot\sin\beta\cdot\sin\alpha \\ &+ \cos\delta\cdot\sin\phi\cdot\cos\omega\cdot\sin\beta\cdot\cos\alpha\end{aligned} \tag{3.10}$$

The direct radiation over a surface with the angles α and β can be obtained with the subsequent expression:

$$B_i(\beta,\alpha) = \frac{B_i(0)\cdot\max(0,\cos\theta_s)}{\cos\theta_{zs}} \tag{3.11}$$

Reflected radiation depends on the albedo or reflection coefficient (ρ_{alb}) which is the diffuse reflectivity or reflecting power of the ground where the solar panel is installed, a typical value is 0.2 [89].

$$R_i(\beta,\alpha) = G_i(0)\cdot\left(\frac{1-\cos\beta}{2}\right)\cdot\rho_{alb} \tag{3.12}$$

The modulation factor or anisotropy index is defined with

$$K_2 = K_T\cdot(a_G + b_G\cdot\cos\omega - K_D) \tag{3.13}$$

where the coefficients a_G and b_G are defined with the following empiric formulae:

$$a_G = 0.409 - 0.501\sin(\omega_s + \pi/3) \tag{3.14}$$

$$b_G = 0.6609 + 0.4767 \sin(\omega_s + \pi/3) \tag{3.15}$$

where ω_s is the exit angle of the sun (in this instant $\theta_{zs} = 90^o$)

$$\omega_s = -\arccos(-\tan\delta \cdot \tan\phi) \tag{3.16}$$

3.2.2 Model of the Components

A phovotolvotaic cell directly converts the sunlight into electricity [89, 150]. The equivalent circuit of a photovoltaic cell is shown in figure 3.7. In this figure, the photovoltaic cell is represented by a series resistor, parallel resistor and a diode, see figure 3.7. This components represents [89]:

- Series resistance (R_s): This component of the circuit represents the losses due to the electrical contact and the resistivity of silicon.
- Parallel resistance (R_p): It is associated to the losses produced in p-n junction
- Diode current (I_d): Diode current when it is direct polarized
- Photovoltaic current (I_{pv}): It is the generated current due to the incidence of the sunlight over the photovoltaic cell. This is proportional to the received irradiance over the cell.
- Generated current (I): Existent current at the output of the photovoltaic cell.

Figure 3.7 represents the equivalent circuit of the ideal PV cell. The basic equation from the theory of semiconductors that mathematically describes the IV characteristic of the ideal PV cell is [150, 151]:

$$\begin{aligned} I &= I_{pv,cell} - I_d \\ &= I_{pv,cell} - I_{o,cell}\left[exp\left(\frac{qU}{akT}\right) - 1\right] \end{aligned} \tag{3.17}$$

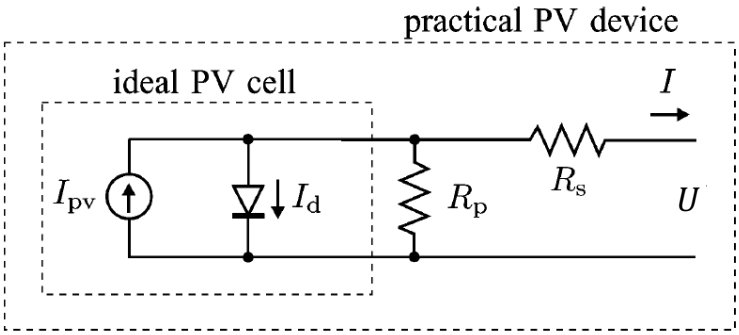

Figure 3.7. Single-diode model of the theorical PV cell and equivalent circuit of a practical PV device including the series and parallel resistances [150]).

is connected with N_p cells in parallel and N_s cells in series, the PV array is formed and the next relationships are satisfied [151], being q the charge of electron a which is the ideality factor of the diode and K the Boltzman constant:

$$\begin{aligned} I_{pv} &= I_{pv} - I_d - I_p \\ &= N_p \cdot I_{pv,cell} - N_p \cdot I_{o,cell} \cdot e^{\left(\frac{U+R_s \cdot I}{U_t \cdot a}\right)-1} - \frac{U + R_s \cdot I}{R_p} \end{aligned} \tag{3.18}$$

where I_{pv} and I_o are the photovoltaic (PV) and saturation currents, respectively of the array and $U_t = N_s kT/q$ is the thermal voltage of the array with N_s cells connected in series. Cells connected in parallel increase the current and cells connected in series provide greater output voltages. R_s and R_p represent the equivalent series and parallel resistance of the array. The light generated current (I_{pv}) of the PV cell depends linearly on solar irradiation and it is also influenced by temperature according to the following expression [150, 152, 153],:

$$I_{pv} = (I_{pv,n} + K_I \Delta T)\frac{G}{G_n} \tag{3.19}$$

where $I_{pv,n}$ is the light generated current at nominal condition (usually 25^oC and $1000W/m^2$),$\Delta T = T - T_n$ (T and T_n are the actual and the nominal temperature), G is the actual irradiation on the device surface, and G_n is the nominal irradiation. The diode saturation current I_0 and its dependence with the temperature can be expressed as [150, 152, 154]:

$$I_0 = I_{0,n}\left(\frac{T_n}{T}\right)^3 exp\left[\frac{q \cdot E_g}{a \cdot K}\left(\frac{1}{T_n} - \frac{1}{T}\right)\right] \tag{3.20}$$

where E_g is the bandgap energy of the semiconductor and $I_{0,n}$ is the nominal saturation current:

$$I_{0,n} = \frac{I_{sc,n}}{\exp\left(U_{oc,n}/aU_{t,n}\right) - 1} \tag{3.21}$$

being U_t, n the thermal voltage of N_s series-connected cells at nominal temperature. The model can be improved if in equation 3.21 the voltage and current correction factors K_U and K_I are included.

$$I_0 = \frac{I_{sc,n} + K_I \Delta T}{\exp\left((U_{oc,n} + K_U \Delta T)/aU_{t,n}\right) - 1} \tag{3.22}$$

The results of the model can be observed in figure 3.8. In table 3.3 the parameters used for the photovoltaic model are explained. The comparison of the result of the model and that which was supplied by the manufacturer can be observed in figure 3.8.

Finally, an inverter is associated as described in figure 3.3. The inverter is modeled with a Maximum Power Point Tracking (MPPT). A review of the different MPPT associated to photovoltaic inverters can be found in [155]. In this dissertation the model chosen is based on the perturbation and observation method.

Table 3.3. Parameters of the photovoltaic panel model

Parameter	Value
Number of parallel panels N_p	1 $[p.u]$
Number of serial panels N_s	14 $[p.u]$
Light-generated current at nominal conditions $I_{pv,n}$	8.71 $[A]$
Short-circuit current at nominal conditions $I_{sc,n}$	8.8 $[A]$
Open-circuit current at nominal conditions $U_{oc,n}$	22.6 $[V]$
Current/Temperature correction factor K_I	0.0032 $[A/K]$
Voltage/Temperature correction factor K_V	-0.1230 $[V/K]$
Constant diode ideality a	1.3 $[p.u]$
Equivalent Series Resistance R_s	0.223 $[\Omega]$
Equivalent Parallel Resistance R_p	415 $[\Omega]$

3.2.3 Forecast Difficulties

The power output of solar plants varies in a deterministic way. This is caused by the change of the sun incidence angle on a diurnal and seasonal basis. It can also

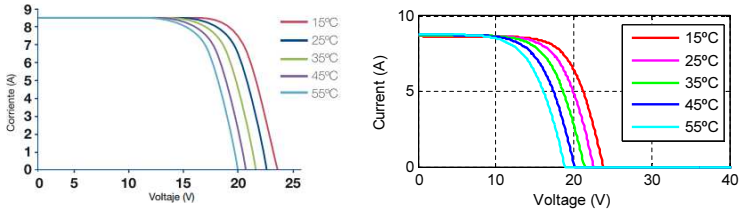

Figure 3.8. Comparison between the photovoltaic curve given by the manufacturer and the one obtained by the model

vary in a stochastic way, as a result of changes induced by cloud movements and temperature variations. Stochastic changes are not easily predictable, and forecasts play a significant role in helping grid operators manage variability and allow for expected power ramps caused by changing PV production. One of the principal concerns about PV generation from is its variability. Deterministic variability such as day-night fluctuation must be distinguished from stochastic variability, brought about by cloud movement and errors in short-term forecasting, which is of greatest concern to system operators. These short-time variability issues are to be further distinguished from long-time variability caused by the seasonal variation in output as the Earth moves around the Sun throughout the year. Different concepts are needed to overcome these fluctuations in a more economical manner, bearing in mind that variability is becoming an increasingly important daily occurrence in power systems with high penetration of fluctuating renewables. Variability increases the amount of necessary balancing resources and the associated balancing cost. For a power plant that is large enough that a cloud moving across it will not cover all the modules simultaneously, the power output of the plant will not drop instantaneously by the plants nominal capacity, but will do so gradually as the cloud covers more and more modules. It should not be forgotten that even if the modules are completely covered by a cloud that prevents the direct sunlight from reaching them, the diffuse irradiance will still be present so that at least some power output is still expected. PV plants can produce even more electricity after the cloud moves away than they were producing before the cloud moved in, due to increased efficiency of the solar cells caused by them cooling down during the absence of direct sunlight [14].

The principal cause of concern that arises from an erroneous forecast is the inadequacy of reserve generation in the system. The risk is then that there are not sufficient reserves in the given time frame to adjust for the discrepancy between the scheduled and actual generation. This problem tends to be worse

for markets with longer dispatch blocks, as shorter time frames allow to include short-term changes in forecast output of PV and readjust the plants scheduling. The time scales on which forecasts are made are typically for the day-ahead (for unit commitment planning process), and hours-ahead (for accounting for ramping requirements and taking measures for additional ramping capabilities). Nowadays deviations from forecast generation levels are primarily handled by the balancing reserves constituted by conventional generation units. Newer, more sophisticated measures such as demand-side management and virtual power plants, in which a number of geographically-dispersed producers using different technologies, storage and controllable demand can be united to provide a significantly higher capacity factor than individual PV installations, will gain in importance with increasing PV penetration levels. Overestimates in forecasting for solar or wind resources may lead to missing balancing reserves, whereas under-forecasting is less of a problem from the power system operation perspective as long as excess resources can be stored or curtailed [14].

3.2.4 Power Quality Issues

From the technical point of view the grid integration of the PV generators has the following challenges [14]:

- **Voltage Variations in Distribution Networks due to PV**: One of the problems for the integration of large amounts of PV in the networks is the possibility of local overvoltage due to high generation. The maximal PV capacity that can be added to the distribution system depends on the short-circuit power of the connection point (network impedance) and the present load. If the loads and generation profiles do not coincide, an overvoltage is possible even when there is enough load installed to consume the excess power production. Rapid changes in PV output can also lead to fast voltage variations, also known as flicker, which can be visible to the human eye from an electric bulb.

- **Harmonic Distortion**: As is the case with other power electronic devices, PV inverters are non-linear loads, and contribute to harmonic distortion in the network. The primary concern of these studies is that additional injection of harmonic currents by PV inverters will lead to an increase in the voltage distortion in the network. At present, most of the electrical power is generated by synchronous generators, and the main contributors to the voltage distortion are non-linear loads. In a scenario where considerable power is generated by PV inverters two changes need to be considered: 1)

Harmonic emission of PV inverters, which at the moment act as current sources of distortion 2) Equivalent impedance of inverters, because inverters behave as mainly capacitive elements in contrast with directly-coupled electrical machines which are inductive.

- **Voltage Support During Short Circuits (Voltage Dips)**: With the increasing number of distributed generators in the network, these systems are required to support the bulk generation. This means that they need to contribute to the frequency and voltage stability and provide voltage support during short-circuits. Voltage support during dips is an inherent characteristic of all synchronous and asynchronous generators (large-scale thermal power plants, CHP, directly-coupled wind generators), but the short-circuit contribution of converter-interfaced generators highly depends on their control algorithms. For this reason, it is important to investigate the potential for voltage support of PV inverters, which could help in the definition of fault ride through requirements for PV inverters. During short-circuits in the power system, synchronous generators provide very high currents limited only by their short circuit impedances and the network impedance until the location of the fault. Their short circuit current may be harmful for the generator itself and the series network elements, but it has two positive effects: 1) For protection as it is easy to distinguish short circuits from load variations, inrush currents, etc. 2) It provides voltage support until the fault clearance; due to this, the voltage level does not fall down to zero for all network close to the fault location. Inverter-interfaced generators do not exhibit such short-circuit behavior. When voltage support is expected from an inverter, it has to be built in as a special control function. In the past, it was a standard practice to allow all inverter-based devices to disconnect immediately when they detect a grid fault. As the number of inverter interfaced generators is increasing in the network, this generates the concern that voltage support in the network will decrease due to the synchronous and asynchronous generators being displaced by the inverter based generators. This will cause more severe voltage dips on locations close to the fault, and decrease the remaining voltage level on average. This would lead to additional financial losses caused by voltage dips. At present, connection requirements for renewable generators demand fault ride- through capability in Germany and other countries in high and medium voltage systems (in the future it is expected to be extended to low voltage units as well). It is expected that such requirements will be implemented in all countries anticipating high penetration levels of renewables.

3.3 Wind Turbines

Wind generation is a technological and economical mature way of energy generation. But as well as solar generation outlines problems in the aspects of economical and technical introduction in the grid. Wind forecast is even more difficult to be predicted than solar energy. Similarly, from the point of view of power quality wind generation has also more problems than photovoltaic because the wind turbine is subjected to the inertia of the associated electric generator, which is of great relevance when the wind turbine generator is exposed to voltage dips. The operation of wind turbines has an impact on the power quality of the connected grid. Depending on the grid configuration and the type of wind turbine used, different power quality problems may arise. All wind turbines have an uneven power production following the natural variations of the wind. The power fluctuations caused by the turbine may cause flicker disturbances, harmonic injection, voltage and frequency imbalances in the grid [156].

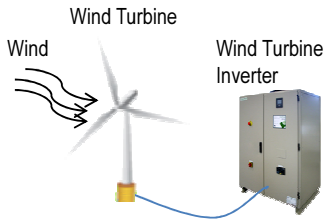

Figure 3.9. Wind energy transformation thought a wind turbine generator

3.3.1 Wind Resource

The movement of air masses in the atmosphere is perceived as wind and has various causes. The first and most important of these is the heating of the Earth by the Sun. Wind energy utilization is therefore, an indirect way of using solar energy. Radiation from the sun is absorbed by the Earths surface and then returned to the atmosphere above. Since the Earths surface is not heterogeneous solar energy varies both with respect to geographic distribution and with respect to the time of the day and the annual distribution. This non-uniform heat absorption produces great differences in the atmosphere with respect to temperature,

density and pressure so that the result forces will move air masses from one place to another [157].

Coriolis forces produced by the rotation will deflect air masses to the right in the northern hemisphere and to the left in the southern hemisphere. This process causes the familiar spiral movements of air equalization from the cloud pictures of the low pressure regions [157].

The second effect of the Earths rotation becomes effective at a medium altitude. Each air particle has an angular momentum that is directed form west to east. If the particle is moving in the direction of the poles, it will approach the Earths rotational axis more closely. The law of conservation of momentum causes an increase in the velocity component form west to east as compensation for the increasingly closer approach to the pole. This effect is less in the vicinity of the equator and causes the so-called west *drift* that is opposite to the global wind direction [157].

Close to the ground, surface friction produces a decrease in wind velocity, which also reduces coriolis forces. Over the sea friction is lower because of the relatively smooth surface. Since the equalization between the different pressure regions takes place mainly by means of the deflected wind close to the surface, the low-pressure regions, for example, will persist longer over the sea and are also accompanied by higher wind velocities. Apart from these global movements of air equalization in the atmosphere, the wind flows are also influenced by small-scale topographic situations [157].

3.3.2 Model of the Components

As described in figure 3.11, a wind turbine-generator is composed of a wind turbine, a gearbox and a permanent magnet synchronous generator which is connected to two VSI's in order to rectify the output frequency and translate the frequency into the magnitude of the grid as a second step [158, 159]:

- Wind Turbine
- Gearbox
- Permanent Magnet Synchronous Generator

The wind turbine extracts power from wind and then converters it into mechanical power. The amount of aerodynamic torque is related to the wind speed as follows [158]:

$$T_w = 0.5 \cdot \pi \cdot \rho_{air} \cdot R_{blade}^3 \cdot v_w^2 \cdot C_p(\theta, \lambda)/\lambda \tag{3.23}$$

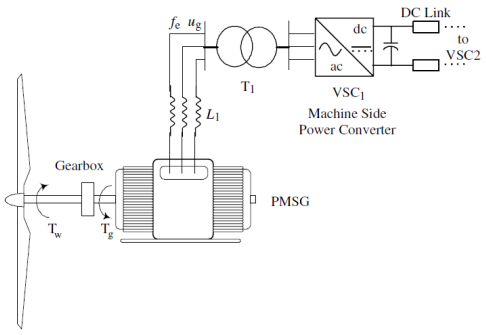

Figure 3.10. Wind energy transformation through a wind turbine generator [158]

$$\lambda = \frac{\omega_w \cdot R_{blade}}{v_w} \tag{3.24}$$

where ρ is air density, R_{blade} is the turbines radius, v_w is the wind speed and C_p is the power coefficient, θ is the pitch angle of the rotor, λ is the tip speed ratio and ω_w is the turbine rotor speed. Different authors use interpolation tables to calculate the coefficient C_p. This coefficient can be approached with the following equations [158]:

$$\beta = \frac{1}{\frac{1}{\lambda + b_1 \cdot \theta} - \frac{b_2}{\theta^3 + 1}} \tag{3.25}$$

$$C_p = c_1 \cdot \left(\frac{c_2}{\beta} - c_3 \cdot \theta - c_4 \right) \cdot e^{(c_5/\beta)} \tag{3.26}$$

where coefficients b_i and c_j are adjusted to match the curves approach of the manufacturer. Energy transmission to the permanent magnet synchronous generator through the gearbox can be expressed with the following relationships. Further description about this model can be found in [159]:

$$T_{gen} - T_w = J_{wt} \frac{d\omega_w}{dt} \tag{3.27}$$

Different models of the PMSG can be obtained in [160]. To complete the model, as in the photovoltaic case, an MPPT control algorithm applied to the wind turbine must be chosen. There are different methods to acquire the MPPT value for the wind turbine. A review of this methods can be found in Shirazi *et al.* [161]. In this dissertation both the model of the wind turbine and the model of the photovoltaic generator will be used for the energy forecast in the microgrid. This will be done in Chapter 4. According to this assumption the power coefficient

is taken as a constant. The values used for the wind turbine model may be consulted in table 3.4. The model of the wind turbine will only be used for the wind energy forecast (see Chapter 4). In order to simplify the model, it will be assumed that C_p has a constant value. So the output power of the wind turbine can be modeled with the subsequentequation:

$$P_{wt} = 0.5 \cdot \pi \cdot \rho_{air} \cdot C_p \cdot R_{blade}^2 \cdot v_w^3 \tag{3.28}$$

Table 3.4. Parameters of the model of the wind turbine

Parameter	Value
Air Density ρ_{air}	1.293 $[kg/m^3]$
Turbine Radio R_{blade}	1.43 $[m]$
Power coefficient C_p	0.25 $[Ws^3/m^2kg]$

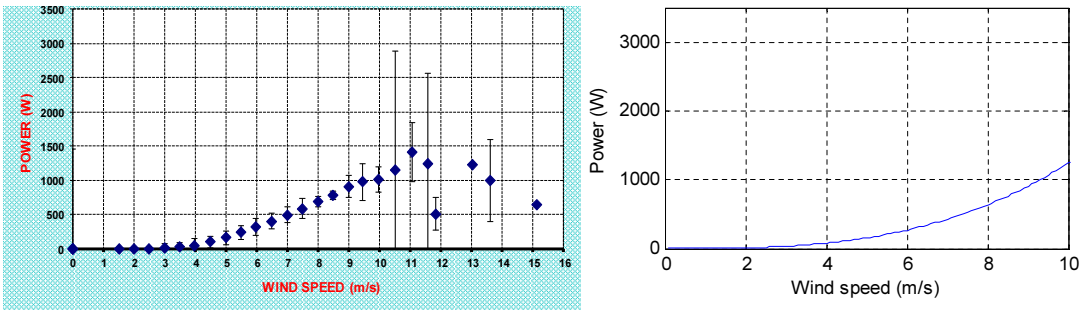

Figure 3.11. Comparison between the manufacturer's curve of the wind turbine and the one obtained by the model

3.3.3 Forecast Difficulties

Intermittency of wind is the biggest challenge to Introduce wind-energy as a reliable autonomous source of electric power [148]. From the point of view of system operators and wind power traders, forecasting of wind speed and power is of fundamental importance. In the deregulated electricity market, power generators may be penalized if their actual generation in a given time span is too far below or above the generation level contracted. Political support systems may broaden tolerance margins specifically for wind power plants, before penalties are

induced. However, with increasing penetration of wind power, accurate forecasting will increase the economical and ecological value of wind power considerably [116].

As stated in [162], the requirements for wind power prediction accuracy and time span depend on the specific power market system in the considered zone, rather than on physical criteria. In Denmark and Germany, for instance, predictions are used mainly for the day-ahead market closing at noon in Denmark (i.e. 12 to 36 hours before time of delivery) and at 3 p.m. in Germany (9 to 33 hours). Unlike the spot market in Great Britain which closes only one hour before the time of delivery, according to the British New Electricity Trading Arrangement. In Scandinavia, the market operation requires a 36-hours forecast horizon, which is technically not strictly necessary as the hydro system (mostly in Sweden) can adjust generation within a fraction of an hour. Various wind speed and power forecast systems exist, developed by different research institutes [162]. Basically wind speed forecast systems use either a physical or a statistical method, or a combination of both [116].

- The physical method simulates large-scale wind flows starting from numeric weather predictions (NWP), and further predicts local wind power generation using physical equations. This method offers insight in the physical processes, allowing a solid theoretical basis for predictions.

- The statistical method mostly also starts from NWP, and further uses statistics, artificial neural networks or fuzzy logic instead of physical equations to calculate local wind power generation. They have the advantage of being able to learn from experience. The disadvantage is that they need a large dataset to be trained properly, and that extreme values of wind power will be more difficult to foresee.

3.3.4 Power Quality Issues

Grid-connected wind turbines do affect power quality. The power quality depends on the interaction between the grid and the wind turbine. The main power quality issues in wind turbines are described below [163]:

- **Voltage variations on the grid**: They are mainly caused by variations in load and power production units. When wind power is introduced, voltage variations also emanate from the power produced by the turbine. The power production from wind turbines may vary widely and not only due to variations in the wind. It may also momentarily go from full to zero power

production in the event of an emergency stop or vice versa at a start under high wind conditions. All kinds of wind turbines cause voltage variations. Voltage variations are due to the variation in the energy content of the wind.

- **Flickers**: The flickers phenomenon is caused by power fluctuations. Power fluctuations mainly emanate from variations in the wind speed, the tower shadow effect and mechanical properties of the wind turbine. Pitch-controlled turbines also have power fluctuations caused by the limited bandwidth of the pitch mechanism. Switching operations will also produce flicker. Typical switching operations are the start and shut down of wind turbines. Start, stop and switching between generators or generator windings will cause a change in the power production. The change in the power production will cause voltage changes at the point of common connection (PCC).

- **Voltage harmonics**: They are virtually always presented on the utility grid. Non-linear loads, power electronic loads, rectifiers and inverters in motor drives etc., are some sources which produce harmonics. The effects of the harmonics include overheating and equipment failure, faulty operation of protective equipment, nuisance tripping of a sensitive load and interference with communication circuits.

- **Transients**: Transients seem to occur mainly during the start and shut down of fixed-speed wind turbines. The start-up sequence of a fixed-speed wind turbine is performed in two steps. First, the generator is switched. To avoid a large inrush current a soft starter is used. As the soft starter begins operating and the generator is connected to the grid the shunt capacitor banks is switched. The shunt capacitor banks are switched directly to the grid without any soft switching devices. As the shunt capacitor banks are connected, a large current peak occur.

- **Frequency variations**: The intermittent power production from wind turbines can produce changes in the grid frequency.

3.4 Ultracapacitor

3.4.1 Principles of the Technology

Capacitors store energy by charge separation. The simplest capacitors store energy in a thin layer of dielectric material that is supported by metal plates that

act as terminals for the device. The energy stored in a capacitor is given by

$$E = \frac{1}{2}CU^2 \tag{3.29}$$

where C is its capacitance (Farads) and U is the voltage between the terminal plates. The maximum voltage of the capacitor is dependent on the breakdown characteristics of the dielectric material. Charge Q (coulombs) stored in the capacitor is given by the product of the capacity and the voltage. The capacitance of the dielectric capacitor depends on the dielectric constant K and the thickness (th) of the dielectric material and its geometric area A [164].

$$C = \frac{K \cdot A}{th} \tag{3.30}$$

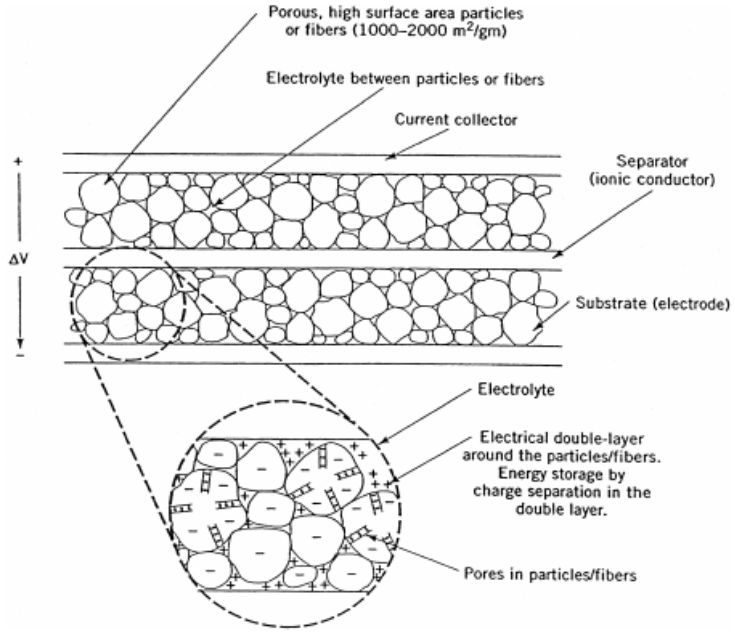

Figure 3.12. Schematic diagram of a double-layer ultracapacitor [164]

Energy is stored in the double-layer capacitor as charge separation in the double-layer formed at the interface between the solid electrode material surface and the liquid electrolyte in the micropores of the electrodes. A schematic diagram of an ultracapacitor is shown in figure 3.12. The ions displaced in forming the double-layers in the pores are transferred between the electrodes by diffusion

through the electrolyte. The capacitance is dependent primarily on the characteristics of the electrode material surface area and pore size distribution . The specific capacitance of an electrode material can be written as follows [164]:

$$C/g = [F/cm^2]_{act}[cm^2/g]_{act} \tag{3.31}$$

where the surface area referred to is the active area in the pores on which the double-layer is formed. In simplistic terms, the capacitance per unit of active area is given by [164]:

$$[F/cm^2]_{act} = [K/\text{thickness of the double-layer}]_{eff} \tag{3.32}$$

The cell voltage of the ultracapacitor is dependent on the electrolyte used. For aqueous electrolytes, the cell voltage is about 1 V and for organic electrolytes, the cell voltage is 3−3.5 V [164]. The main advantages of using an ultracapacitor-based ESS are:

1. Longer life expectancy than batteries/hydrogen in terms of charge/discharge cycles [165].

2. Higher specific power than batteries, specifically in the ability to accept higher power during charge (resulting more effective in the frequent charge/discharge cycles during regenerative braking and motoring modes of operation) [165].

3. Higher efficiency than batteries due to lower internal resistance (thus also generating less heat than batteries). One of the key advantages of ultracapacitors is that they are symmetric with respect to charge and discharge throughout their complete operating range of voltage and that they have high round-trip efficiency ($> 90\%$) even when operated at very high rates (>1kW/kg). For ultracapacitors, the peak power quoted usually has a 95% efficient discharge in which only 5% of the energy from the device is dissipated in heat [164].

4. Can generally operate over a wider temperature range than batteries [166].

5. Since stored energy is expressed by equation (3.29), the ultracapacitor SOC_{uc} can be determined from the voltage, enabling the control system to be simplified [165].

3.4.2 Degradation Issues

The overall performance and lifetime of ultracapacitors are significantly affected by their operating conditions. For example, while operating at a reasonably high working voltage DC bus, many capacitors must be stacked in series resulting in the need for efficient charge balancing circuits and charging circuits that do not overcharge any individual capacitor bank in the series. To further improve their performance, reliability and lifetime, it is important that these capacitors are not overheated due to high ripple voltage or ripple current from the charging circuit. Switch mode PWM converters used for charging ultracapacitors can often result in high voltage and current ripple and thus cause temperature rise and lifetime reduction of these ultracapacitors. Similarly when using ultracapacitors as energy storage buffers for downstream PWM converters, the resulting voltage and current ripple in them can also cause temperature rise and lifetime reduction [167]. Ultracapacitors consist of two metal plates separated by a non-conducting layer called a dielectric. When one plate is charged with electricity, the other plate will have induced in it a charge of the opposite sign. Ultracapacitors can be charged substantially faster than conventional batteries and can have a higher number of life cycles. But ultracapacitors have low energy density and behave like a short circuit when they are exposed to low levels of state-of-charge. High states of charge can also damage this technology [164].

The switching circuits in the downstream converter can cause over-charging of the ultracapacitor. The reflected voltage ripple and capacitor temperature rise due to charging and discharging ripple current may result in the reduction in lifetime of ultracapacitors. If the rated nominal working voltage of these capacitors is exceeded during their charging then it often results in a reduction of their lifetime due to gas generation inside the capacitor. Moreover, though the standard temperature rating for ultra-capacitors is -25^{o}C to 70^{o}C, ambient temperature rises along with charging voltage also reduces their lifetime. In general, raising ambient temperature by 10^{o}C will decrease their lifetime by at least a factor of two. Thus the charging voltage should be reduced with increasing ambient temperature.

Overheating of ultra-capacitors can occur by high charging ripple current or over voltage charging, leading to increased gas generation, decreased lifetime, leakage, venting or rupture. Though for highest energy storage, the ultracapacitor must be charged to its maximum rated nominal working voltage, it should be ensured that the charging voltage ripple does not overcharge the capacitor. Moreover, as ultracapacitors have a higher ESR compared to aluminum electrolytic capacitors, they are more susceptible to internal heat generation when exposed to higher ripple current. In order to ensure a long lifetime, it is recommended

that the maximum ripple current should not increase the surface temperature of the ultracapacitor by more than 3^oC above ambient temperature. Thus reducing this voltage ripple and ripple current, by selecting appropriate component parameters for the above mentioned switch mode charging converter, are the keys to improving capacitor lifetime. Moreover, reducing the charging ripple current will also help reduce the charging ripple voltage.

3.4.3 Model of the Components

The main variables of the ultrapacitor model are voltage U_{uc}, current I_{uc} and the state-of-charge SOC_{uc}. These three variables are related with the following expressions [168, 169]:

$$U_{uc}(t) = \frac{N_{s,uc}C_{uc}(t)x_{2,uc}}{N_{p,uc}N_{l,uc}\varepsilon\varepsilon_o A_{uc}} + \frac{N_{l,uc}N_{s,uc}2RT_{uc}(t)}{F}\sinh\left(\frac{C_{uc}(t)}{N_{p,uc}N_{l,uc}A_{uc}\sqrt{8RT_{uc}(t)\varepsilon\varepsilon_o M_{uc}}}\right) - R_{uc}\cdot i_{uc}(t). \tag{3.33}$$

where $N_{s,uc}$ is the number of series supercapacitors, C_{uc} is the capacity of the ultracapacitor (F), $x_{2,uc}$ is the molecular radius, $N_{p,uc}$ is the number of parallel supercapacitors, $N_{l,uc}$ is the number of layers of electrodes, ε is the permittivity of material, ε_o is the permittivity of free space, A_{uc} is the interfacial area between electrodes and electrolyte (m^2), R is the ideal gas constant, T_{uc} is the operating temperature of the ultracapacitor (K), F is the Faraday's constant, M_{uc} is the molar concentration (mol m^{-3}) and R_{uc} is the total resistance (Ω).

$$i_{uc}(t) = A_{uc}i_{o,uc}(t)\exp\left(\frac{\alpha_{uc}F\left(\frac{U_{uc}(t)-U_{uc,max}}{N_{s,uc}} - \Delta U_{uc}(t)\right)}{RT}\right)N_{l,uc} \tag{3.34}$$

where i_{uc} is current density of the ultracapacitor (A/cm^2), $i_{o,uc}$ is the exchange current density, α_{uc} is the charge transfer coefficient of the Tafel's equation ($0< \alpha_{uc} <1$). The capacity of the ultracapacitor C_{uc} and state-of-charge of the ultracapacitor SOC_{uc} can be expressed as follows:

$$C_{uc}(t) = C_{uc}(t_0) + \int_{t_0}^{t} I_{uc}(t)dt \tag{3.35}$$

$$\mathrm{SOC}_{uc}(t) = \frac{C_{uc}(t)}{C_{uc,max}} \tag{3.36}$$

In table 3.5 and figure 3.13 the parameters of the ultracapacitor can be found

Table 3.5. Parameters of the model of the ultracapacitor

Parameter	Value
Rated Capacity C_{uc}	68 $[F]$
Number of series capacitors $N_{s,uc}$	2 $[p.u]$
Number of parallel capacitors $N_{p,uc}$	1 $[p.u]$
Equivalent DC Series Resistance R_{uc}	2.1 $[m\Omega]$
Rated Voltage U_{uc}	110 $[V]$
Nominal Voltage $U_{uc,n}$	125 $[V]$
Nominal Voltage $U_{uc,n}$	125 $[V]$
Molecular radius (Helmholtz layer length) $x2, uc$	1.23e-9 $[m]$
Permittivity of material ε	6.021e-10 $[p.u]$
Charge transfer coefficient α_{uc}	0.3 $[p.u]$
Over potential ΔU_{uc}	0.3 $[V]$

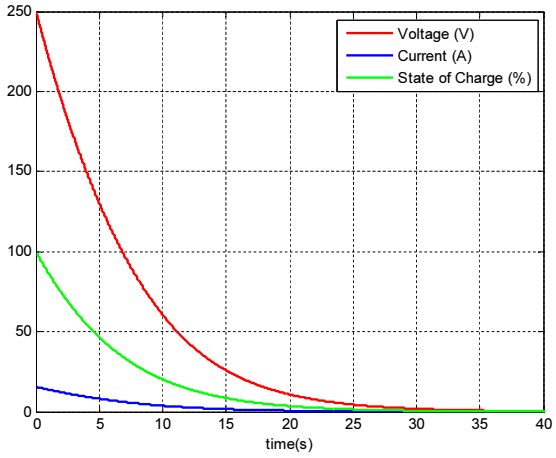

Figure 3.13. Evolution of the variables U_{uc}, I_{uc}, C_{uc} under a constant load $P = 6000W$

utilized in the model, as well as the results of the model under a constant charge of 6000 W.

3.5 Batteries

3.5.1 Principles of the Technology

Battery Energy Storage Systems (BESSs) has been the classical electrochemical way to store energy. A battery comprised of one or more electrochemical cells with each cell consisting of a liquid, paste, or solid electrolyte together with a positive electrode (anode) and a negative electrode (cathode). During discharge, electrochemical reactions occur at the two electrodes generating a flow of electrons through an external circuit. The reactions are reversible, allowing the battery to be recharged by applying an external voltage across the electrodes. The balance of plant for a battery is limited to control and is used as a coolant in circuits [170].

A battery has three main usage phases: charging, discharging, and resting. During the charging phase, electrical energy is supplied from an outside source and is stored as charged chemical species within the electrodes of the cell. During the discharge phase, the storage reaction is reversed, and energy is transferred from the chemical species to an external circuit. When the cell is at rest, no energy is transferred in or out of the cell; however, a small amount can be lost through self-discharge[170]. An schematic view of the process of charge and discharge of a battery can be seen in figure 3.14.

Charging is usually done in several phases. If the battery is at a low state-of-charge (SOC), then it can accept a relatively large charging current without harm. The battery is typically charged at a constant current (CC), where the limiting factor is usually the maximum amount of current the charging circuit can supply. After the battery reaches a certain voltage, continuous high currents will damage it. Therefore, charging is done at a constant voltage (CV) to prevent overvoltage conditions. As the battery approaches full charge, it is sometimes given current pulses, which are designed to allow the cells to equalize. Once the battery has reached full charge, it is often trickle charged, which means that a small pulsed or constant current is applied to the battery. Trickle charging is often used to ensure the cell is at 100% charge capacity and to counteract self-discharge within the cells. There are other charge strategies that can also be used [170, 171].

A typical Battery Management System (BMS) consists of a battery, sensors to monitor the state of the battery, a battery model or charge estimator, and a controller. A BMS must monitor the battery to ensure that the battery is

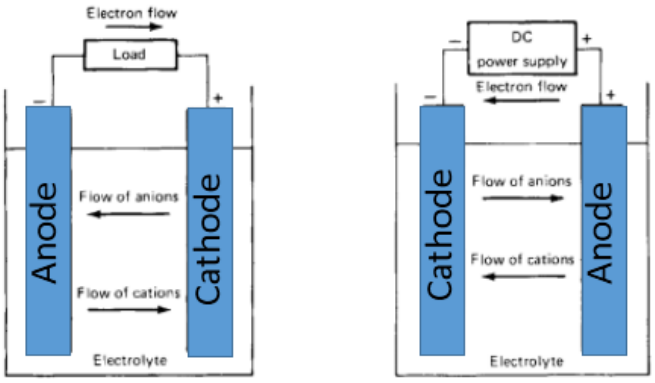

Figure 3.14. A schematic view of the charge and discharge processes of a battery [171]

operating within safe limits. Typically, the important sensed variables are voltage, current, and temperature. For some battery types, such as NiH2, the internal cell pressure is also measured. In a simple BMS, voltage could be monitored using a simple comparator. This comparator circuit could be used to disable the circuit when the voltage goes outside the operational limits specified by the manufacturer. In a more advanced BMS, the voltage, current, and temperature can be monitored by a microprocessor system and used to correct the state-of-charge estimate or be recorded for long-term trending of battery performance [170].

The primary purpose of the BMS is to control the battery to ensure that its operation stays within the designed limits so as to minimize damage. During charging, damage can occur to the battery if one of several conditions takes place. For example, if the temperature of the battery gets too high gassing will occur, resulting in a loss of electrolytes and in a shorter life of the battery. If charging is continued after the battery has reached full charge, electrolysis of the electrolyte occurs which also shortens the batterys life. In cases of extreme overcharging, high temperature, electrolysis, and gassing can lead to the explosion of the cell [170, 172].

3.5.2 Degradations Issues

A significant number of degradation studies have been performed on the lithium technology. These results have shown that capacity and power fade is affected by temperature, SOC window, End of Charge Voltage (EOCV), End of Discharge

Voltage (EODV), charge current, and discharge current. Batteries exhibit two forms of degradation: capacity fade and power fade. Capacity fade represents a gradual loss in energy capacity for a given current. Power fade represents a gradual increase in battery impedance, and subsequent decay in apparent voltage for a given current. Capacity fade is generally measured in Amperes-hours while power fade is measured in Volts [33, 170].

Both capacity and power fade each have two major implications. For capacity fade, the first is that a decrease in useable capacity represents larger State-Of-Charge (SOC) swings in charge-sustaining operation for a given load cycle, further contributing to accelerated degradation. Secondly for capacity fade, the battery capacity has a direct correlation to charge-depleting range of the application. Considering power fade, the first implication is that the minimum and maximum high voltage bus limits will be achieved at lower battery discharge and charge currents respectively. As a result, the maximum discharge and charge power of the battery is reduced, resulting in less power available during accelerations and less ability to recapture power during regenerative braking. Since the load cycle determines the required power, the second implication of power fade is a further decrease in useable battery capacity as a given power will require additional current to compensate for a lower terminal battery voltage [33]. The capacity fade measurements are dependent on the test current temperature, and definition of start and end point. Power fade measurements are also dependent on the test current, temperature, and the state of charge of the battery during the test. While these challenges limit the ability to derive quantifiable relationships between operational factors and degradation, qualitative relationships may be obtained. Key degradation variables include, state-of-charge, energy throughput, and pulse power levels [173].

Batteries have different degradation issues that must be avoided: one of the degradation modes identified is the formation of permanent oxides during the overcharging of the battery pack at high SOC. This mechanism produces a loss of electrode active material, more predominately at the anode. Causes include fracture of the graphite plane due to excessive mechanical stresses on the lattice during intercalation (charging to high SOC) causing electrical isolation. But the specific degradation mechanism in batteries is associated to an increase in the resistance related to electrode-electrolyte interfacial interference, caused by surface film growth. Since these processes are diffusion controlled and slow, it is necessary to use a low charging rate. The rate capability loss is proportional to the value of the average current used. Thus, one cannot avoid this apparent increase of the capacity fade when the battery is charged at fast rates. However, the material degradation can be eliminated by using an optimized current profile

[32, 33, 70]. This film grown can be expressed with the following expression [70]:

$$\frac{d\iota}{dt} = \kappa \cdot |I_{bat}(t)| \tag{3.37}$$

where ι is the thickness of the film, κ is a constant which depends on the battery and I_{bat} is the current of the battery.

AC ripple causes ohmic heating that is a major contributor to battery heating. There is evidence that these microcycles might lead to a capacity loss and a lower state-of-charge under the operating conditions of renewable energy systems, which is likely to be caused by changes in the current distribution and the microstructure of the active materials. By minimizing AC ripple and with careful attention to battery cabinet layout, product float life can be maximized. The inverter design is crucial to the reduction of battery current microcycles. It is recommended that a two-stage converter with capacitive energy storage is used in order to minimize AC battery currents, and reduce battery wear [174].

3.5.3 Model of the Components

The voltage of the battery U_{bat} can be expressed as a function of the state-of-charge of the battery SOC_{bat} and the current of the battery I_{bat} [175]:

$$\begin{aligned} U_{bat}(t) = U_{o,bat} &- K_{1,bat}\frac{C_{120,bat}}{C_{120,bat} - C_{bat}(t)} I_{bat,ch}(t) \\ &+ K_{1,bat}\frac{C_{120,bat} \cdot (\delta_{bat,ch} - \delta_{bat,dis})}{C_{120,bat} - C_{bat}(t)} C_{bat}(t) \\ &- K_{1,bat}\frac{C_{120,bat}}{C_{120,bat} + 0.1C_{bat}(t)} I_{bat,dis}(t) \\ &- K_{2,bat} \cdot e^{(K_{3,bat} \cdot C_{bat}(t))} + R_{ohm,bat} \cdot I_{bat}(t) \end{aligned} \tag{3.38}$$

where $U_{o,bat}$ is the batterys internal voltage (V), $C_{120,bat}$ is the maximum battery capacity (Ah), C_{bat} is the capacity of the battery (Ah), $K_{i,bat}$ are internal parameters of the battery and $R_{ohm,bat}$ is the internal ohmic resistor of the battery. The model differs for the states-of-charge and discharge of the battery, so the binary variables of the state of the battery are introduced $\delta_{bat,dis}$ and $\delta_{bat,ch}$. The capacity (Ah) of a battery can be expressed with the following expression

$$C_{bat}(t) = \int_0^t I_{bat}(t)dt \tag{3.39}$$

Finally, the state-of-charge of the battery is related with the capacity in the following equation:

$$\mathrm{SOC}_{bat}(t) = \frac{C_{bat}(t)}{C_{120,bat}} \tag{3.40}$$

Finally the parameters utilized to feed the model, as well as, the comparison of the results obtained by the model and those obtained with experimental results can be found in figure 3.15.

Table 3.6. Parameters of the model of the batteries

Parameter	Value
Rated Capacity $C_{120,bat}$	367 $[Ah]$
Battery Internal Voltage $U_{o,bat}$	51.58 $[V]$
Exponential voltage $K_{1,bat}$	0.006215 $[V]$
Polarization constant $K_{2,bat}$	11.053 $[V]$
Exponential capacity $K_{3,bat}$	2.452 $[Ah^{-1}]$

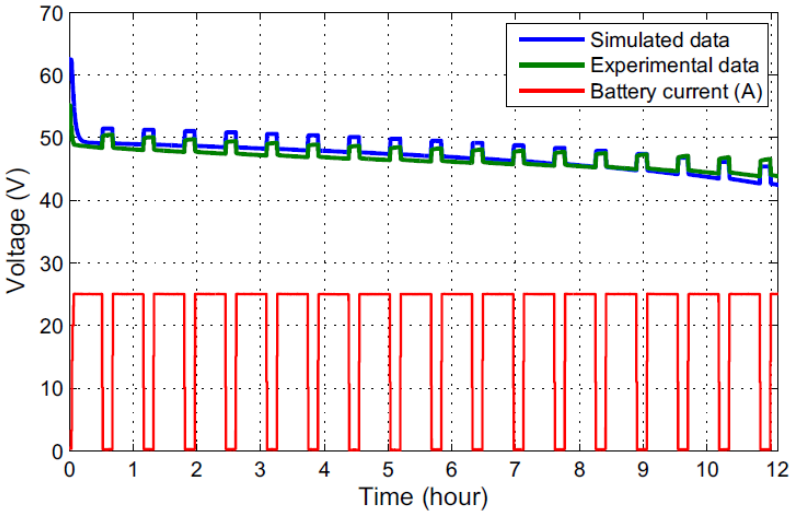

Figure 3.15. Comparison between battery experimental voltage and battery model voltage while a discharging test is carried out [175]

3.6 Electrolyzer

3.6.1 Principles of the Technology

Electrolyzers are electrochemical devices which are able to separate hydrogen and oxygen in the H_2O molecule when a direct current is applied. Electrolysis is the process of using an electric current to breakdown a compound by chemical conversion. The compound must be in a fluid state, either dissolved or molten, to permit the flow of electricity. This fluid is called an electrolyte. The ions (charged particles) within the electrolyte carry the current, unlike electricity in a metal conductor, where electrons are responsible. A negatively charged ion is called an anion and a positively charged ion is known as a cation. Electrolysis was first performed by William Nicholson (1753-1815) and Anthony Carlisle in 1800. Using Alessandro Volta's recently-invented Voltaic pile battery, they immersed two electrodes into water and allowed electricity to flow. This caused the water to break down into its two components; hydrogen and oxygen. As hydrogen ions were converted into hydrogen atoms, they combined to form hydrogen molecules that bubbled off.

Among the other types of electrolyzers PEM electrolyzers are very simple and compact, and they are able to supply hydrogen at higher pressures. They also ensure high purity and efficiency at high current density levels. In PEM electrolyzer, water is supplied by the channels of the anode and the cathode of the electrolysis cells, when DC voltage is supplied the catalysis action of the platinum produces the conduction of proton exchange (H_3O^+) through the polymeric membrane which separates the anode and the cathode. This electro-chemical reaction allows the decomposition of the water molecule into oxygen through the anode and hydrogen through the cathode. These reactions are produced in the stack of electrolysis cells. The output of the anode is driven to the oxygen separator and in a similar way the output of the cathode is linked with the hydrogen separator. To eliminate the residual water in oxygen and hydrogen flows a condenser is situated in the output of each one [176, 177]. The different components of the electrolyzer balance of plant (BOP) are shown in figure 3.16.

3.6.2 Degradation Issues

Electrolyzers have different degradation mechanisms. Fluctuations in the current applied to electrolyzers produce: i) variations in the differential pressure, producing reverse conduction of hydrogen to the oxygen separator or vice-versa ii) small concentrations of hydrogen in oxygen or oxygen in hydrogen ($> 4\%$)

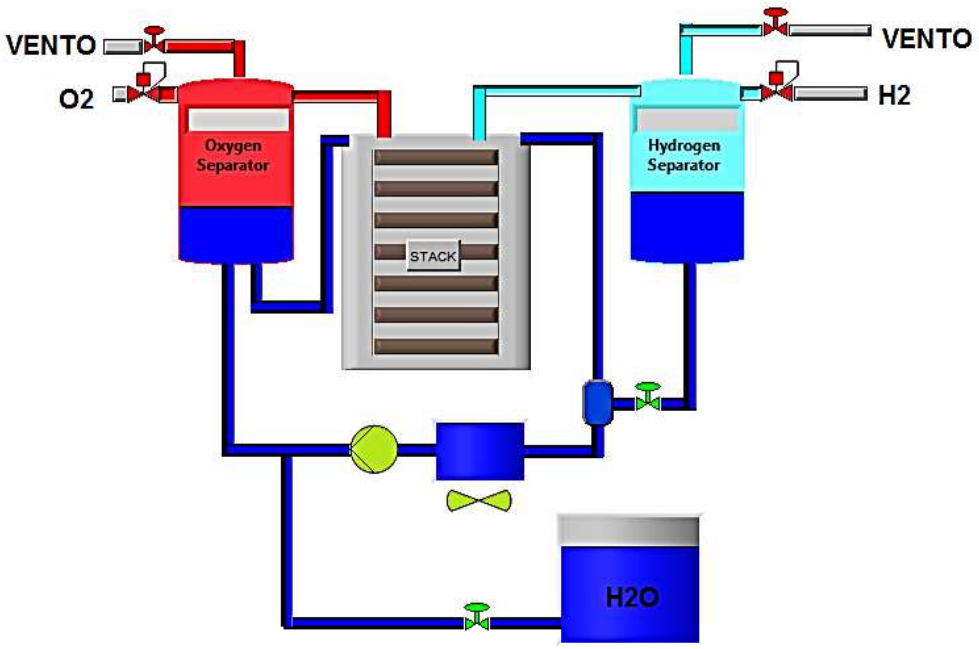

Figure 3.16. Balance of plant of the electrolyzer

which can produce highly explosive reactions iii) losses in the mechanical wear of the membrane, iv) chemical degradation of the membrane via radical attack. On/Off cycling of electrolyzers produces: i) chemical and mechanical degradation due to the temperature and pressure cycling, ii) chemical degradation caused by uncontrolled stack polarity, iii) production of hydrogen peroxide at cathode after turn off with following membrane and carbon carrier oxidation. In the same way electrolyzers need to be maintained over an optimal-working temperature (55^oC). The electrolyzer management system (ELMS) is charged to maintain the correct water level in the separator in order to avoid drying conditions in the membrane, feeding the stack with enough water to produce the electrolysis reaction. Before the electrolyzer is in the state of hydrogen production the ELMS realizes the stages of water filling of the separators, nitrogen purge in all the gas circuit and a preheating to 55^oC of the stack. Further description about PEM electrolyzers can be found in [176, 177, 178]. Electrolyzers have similar current ripple degradation issues than the explained for fuel cells in the next section.

3.6.3 Model of the Components

3.6.3.1 Model of the Stack

The electrolyzer of the experimental plant was modeled in the previous work carried out by Valverde *et al.*[175], where the polarization curve of the electrolyzer was modeled. The stack voltage of the electrolyzer $U_{elz}(t)$ (V) can be expressed as the product of the number of electrolysis cells N_{elz}^{cell} and the voltage of a single cell U_{elz}^{cell}.

$$U_{elz}(t) = N_{elz}^{cell} \cdot U_{elz}^{cell}(t) \tag{3.41}$$

The voltage of a single cell can be expressed with the following equation:

$$U_{elz}^{cell}(t) = U_{elz,o}^{cell}(t) + U_{elz,act}^{cell}(t) + U_{elz,ohm}^{cell}(t) + U_{elz,conc}^{cell}(t) \tag{3.42}$$

where $U_{elz,o}^{cell}$ is the reversible potential or "Nernst" voltage, $U_{elz,act}^{cell}(t)$ is the activation overpotencial, $U_{elz,act}^{cell}(t)$ is the ohmic overvoltage and $U_{elz,conc}^{cell}$ are the losses due to concentration mass. Hence, the voltage drop is a sum of four terms that can be expressed with the following expressions:

$$\begin{aligned} U_{elz,o}^{cell}(t) = E_{elz}^{o} + \frac{\Delta S_{elz}^{o}}{2F}\left(T_{elz}(t) - T_{elz}^{o}\right) \\ + \frac{2.3 \cdot R \cdot T_{elz}(t)}{2F} \ln\left(\frac{p_{H_2}(t) \cdot p_{O_2}^{1/2}(t)}{p_{H_2O}(t)}\right) \end{aligned} \tag{3.43}$$

$$\begin{aligned} U_{elz,act}^{cell}(t) = \frac{R \cdot T_{elz}(t)}{F}\left[\sinh^{-1}\left(\frac{I_{elz}(t)}{2 \cdot A_{elz} \cdot i_{a_o,elz}}\right)\right. \\ \left. + \sinh^{-1}\left(\frac{I_{elz}(t)}{2 \cdot A_{elz} \cdot i_{c_o,elz}}\right)\right] \end{aligned} \tag{3.44}$$

$$U_{elz,ohm}^{cell}(t) = R_{ohm} \cdot I_{elz}(t) \tag{3.45}$$

$$U_{elz,conc}^{cell}(t) = K_{1,elz}^{conc} \cdot e^{\left(K_{2,elz}^{conc} \cdot I_{elz}(t)\right)} \tag{3.46}$$

where T_{elz} is the electrolyzer stack temperature, R is the ideal gas constant, F is Faradays constant, p_{H_2} is the hydrogen partial pressure, p_{O_2}, is the oxygen partial pressure, I_{elz} is the electrolyzers current density, $i_{ao,elz}$ is the anode current density, $i_{co,elz}$ is the cathode current density and $K_{1,elz}^{conc}$ and $K_{2,elz}^{conc}$ are the concentration-losses factors of the electrolyzer.

Taking into account the reaction produced in the electrolysis stack the hydrogen and oxygen mass flows can be modeled with the next expressions:

$$W_{elz}^{H_2,pro}(t) = N_{elz}^{cell}\frac{I_{elz}(t)}{2 \cdot F} \tag{3.47}$$

$$W_{elz}^{O2,pro}(t) = N_{elz}^{cell}\frac{I_{elz}(t)}{4 \cdot F} \tag{3.48}$$

3.6.3.2 Model of the Cathode

The hydrogen separator is directly connected to the cathode of the stack. The pressure in the separator can be modeled with the next equations:

$$\begin{aligned} n_{sep_{H2}}^{H_2}(t) = n_{sep_{H2}}^{H_2}(t_0) + \int_{t_0}^{t} \Big(& W_{elz}^{H2,pro}(t) \\ & - W_{elz}^{H2,out}(t) \Big) \end{aligned} \tag{3.49}$$

The output mass flow is regulated by a back pressure regulator. This back pressure regulator is only opened when the pressure of the hydrogen separator is higher than 7 bar. The logical variable $\delta_{elz}^{H2,check}$ models this fact. There is a relationship between the output difference pressure and the mass flow over the valve given by the constant $K_{elz}^{H2,BPR}$. As can be observed in [175] the pressure of the metal hydride tank can be considered constant in relation to the previous instant:

$$\begin{aligned} & W_{elz}^{H2,out}(t_{k+1}) = \\ & \delta_{elz}^{H2,check}(t_k) \cdot K_{elz}^{H2,BPR} \cdot (p_{sep_{H_2}}(t_k) - p_{tank}(t_k)) \end{aligned} \tag{3.50}$$

To calculate the final pressure inside the hydrogen separator as opposed to the pressure given by the number of moles of hydrogen in the separator, the vapor pressure must be also added.

$$p_{sep_{H_2}}(t_{k+1}) = p_{sep_{H_2}}^{H_2}(t_{k+1}) + p_{sep_{H_2}}^{H_2O,v}(T_{sep_{H_2}}(t_k)) \tag{3.51}$$

The vapor pressure can be consulted in the thermodynamic tables of the water. The pressure due to the quantity of hydrogen moles can be expressed with the following equation:

$$p_{sep_{H_2}}^{H_2}(t_{k+1}) = Z^{H_2}\frac{m_{sep_{H2}}^{H_2}(t_{k+1}) \cdot R \cdot T_{sep_{H_2}}(t_k)}{V_{sep_{H_2}}^{gas}(t_{k+1})} \tag{3.52}$$

where Z^{H_2} denotes the compressibility factor of hydrogen and $V^{gas}_{sep_{H_2}}$ is the volume of gas in the separator, which can be obtained with the following equation:

$$V^{gas}_{sep_{H_2}}(t_{k+1}) = V_{sep_{H_2}} - \rho^{H_2O(l)} \cdot m^{H_2O(l)}_{sep_{H_2}}(t_{k+1}) \tag{3.53}$$

where $V_{sep_{H_2}}$ is the physical volume of the separator and $m^{H_2O(l)}$ is the water mass at each instant inside the separator. The water quantity in the separator can be modeled with the next expression where $\delta^{v,H_2O}_{sep_{H_2}}(t_k)$ and $Q^{v,H_2O}_{sep_{H_2}}$ are the logical variables on/off of the feeding pump and the flow of the pump when it is active.

$$\begin{aligned} m^{H_2O(l)}_{sep_{H_2}}(t_{k+1}) &= m^{H_2O(l)}_{sep_{H_2}}(t_k) \\ &+ M^{H_2O} N^{cell}_{elz} \frac{I_{elz}(t_{k+1})}{F} T_s - \delta^{v,H_2O}_{sep_{H_2}}(t_k) Q^{v,H_2O}_{sep_{H_2}} T_s \end{aligned} \tag{3.54}$$

3.6.3.3 Model of the Anode

The oxygen separator is directly connected to the anode of the stack. The output flow is governed by a back pressure regulator and a check valve. Considering that the discharge is done into the P_{amb}, it can be developed to obtain the expression for $W^{O2,out}_{elz}(t_{k+1})$.

$$\begin{aligned} n^{O_2}_{sep_{O2}}(t_{k+1}) = n^{O_2}_{sep_{O2}}(t_k) + T_s \cdot \Big(& W^{O2,pro}_{elz}(t_{k+1}) \\ & - W^{O2,out}_{elz}(t_{k+1} \Big) \end{aligned} \tag{3.55}$$

$$p_{sep_{O_2}}(t_{k+1}) = p^{O_2}_{sep_{O_2}}(t_{k+1}) + p^{H_2O,v}_{sep_{O_2}}(T_{sep_{O_2}}(t_k)) \tag{3.56}$$

$$p^{O_2}_{sep_{O_2}}(t_{k+1}) = Z^{O_2} \frac{n^{O_2}_{sep_{O2}}(t_{k+1}) \cdot R \cdot T_{sep_{O_2}}(t_k)}{V^{gas}_{sep_{O_2}}(t_{k+1})} \tag{3.57}$$

$$V^{gas}_{sep_{O_2}}(t_{k+1}) = V_{sep_{O_2}} - \rho^{H_2O(l)} \cdot m^{H_2O(l)}_{sep_{O_2}}(t_{k+1}) \tag{3.58}$$

$$\begin{aligned} m^{H_2O(l)}_{sep_{O_2}}(t_{k+1}) &= m^{H_2O(l)}_{sep_{O_2}}(t_k) \\ &+ \delta^{Pump,H_2O}_{elz}(t_k) \cdot \rho_{H2O} \cdot Q^{Pump,H_2O}_{elz} \cdot T_s \\ &- 3 \cdot M^{H_2O} \cdot N^{cell}_{elz} \frac{I_{elz}(t_{k+1})}{2F} \cdot T_s \end{aligned} \tag{3.59}$$

3.6.3.4 Model validation

The electrolyzer model was validated applying a fluctuant current to the electrolyzer and measuring the obtained voltage as well as comparing it with the results given by the developed model. This results are exposed in figures 3.17, 3.18 and 3.19. The utilized parameter to feed the model of the electrolyzer can be observed in table 3.7.

Table 3.7. Parameters of the model of the electrolyzer

Parameter	Value
Stack Area A_{elz}	212.5 $[cm^2]$
Anode current density i_{ao}	1.0631 $[\mu A/cm^2]$
Cathode current density i_{co}	1 $[mA/cm^2]$
Membrane thickness d_B	1.78 $[\mu m]$
Membrane conductivity s_B	0.14 $[S/cm]$
Number of cell N_{elz}^{cell}	6 $[p.u]$
Volume of the hydrogen separator $V_{sep,H2}$	0.000555 $[m^3]$
Volume of the oxygen separator $V_{sep,O2}$	0.00050 $[m^3]$
Back pressure regulator of oxygen separator $K_{elz}^{O2,BPR}$	=0.00068 $[mol/bar]$
Back pressure regulator of hydrogen separator $K_{elz}^{H2,BPR}$	0.0001385 $[mol/bar]$

3.7 Fuel Cell

3.7.1 Principles of the technology

PEM fuel cells are electrochemical devices whose function is complementary to the electrolyzer's one: receiving a hydrogen flow by the anode and an oxygen flow through the cathode the PEM cells are able to produce electricity. The main component of the PEM fuel cell system is the stack of PEM cells where electricity production from hydrogen and oxygen is carried out. The biggest difference of PEM fuel cells from the other types of fuel cells is their capability to work directly with air in the cathode. The fuel cell principle was discovered in 1839 by William R. Grove, a British physicist [179]. A fuel cell consists of an electrolyte sandwiched between two electrodes. The electrolyte has a special property that allows positive ions (protons) to pass through while blocking electrons. Hydrogen gas passes over one electrode, called an anode, and with the help of a catalyst,

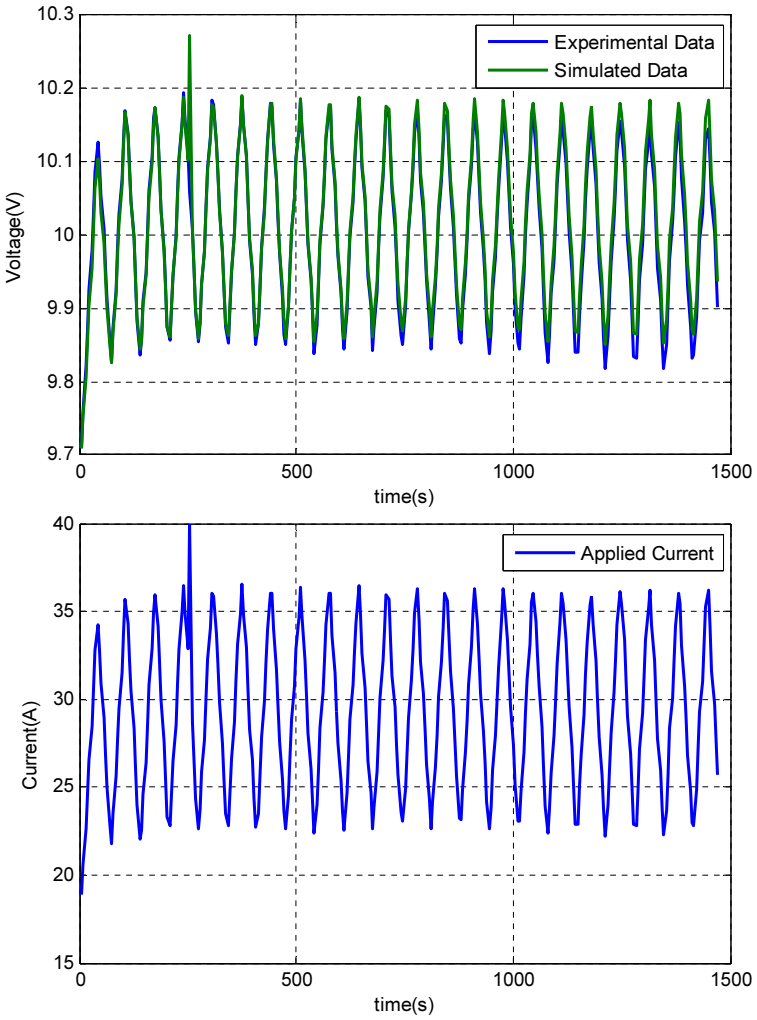

Figure 3.17. Electrolyzer voltage model validation under fluctuant load-current

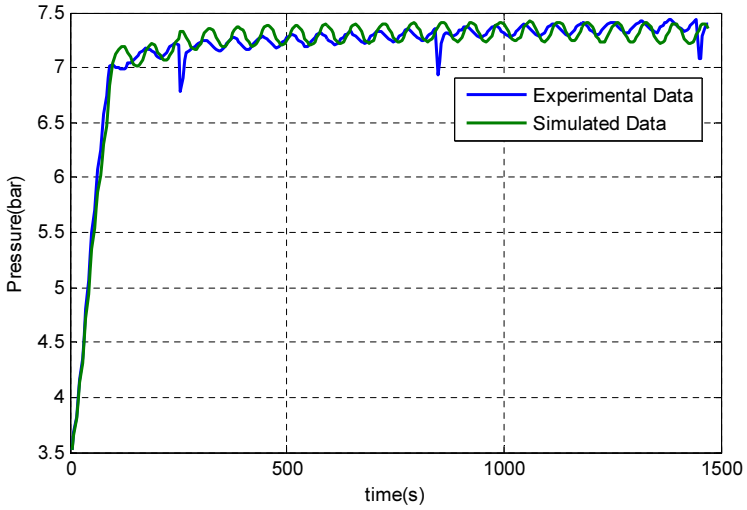

Figure 3.18. Electrolyzer hydrogen separator pressure model validation under fluctuant load-current

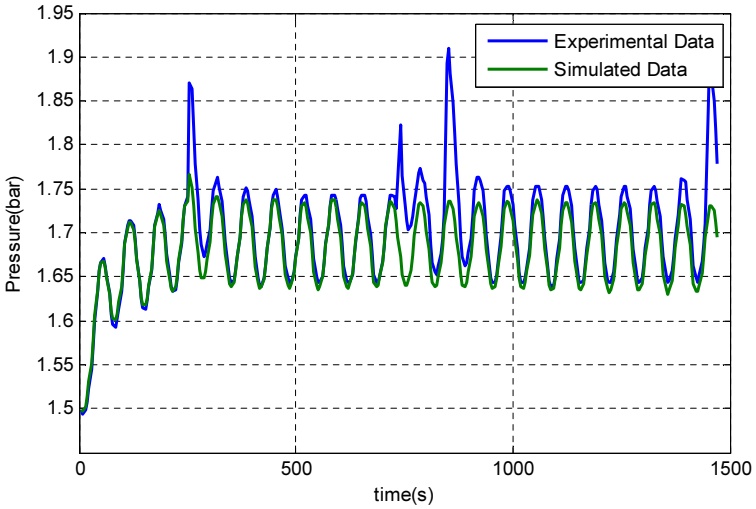

Figure 3.19. Electrolyzer oxygen separator pressure model validation under fluctuant load-current

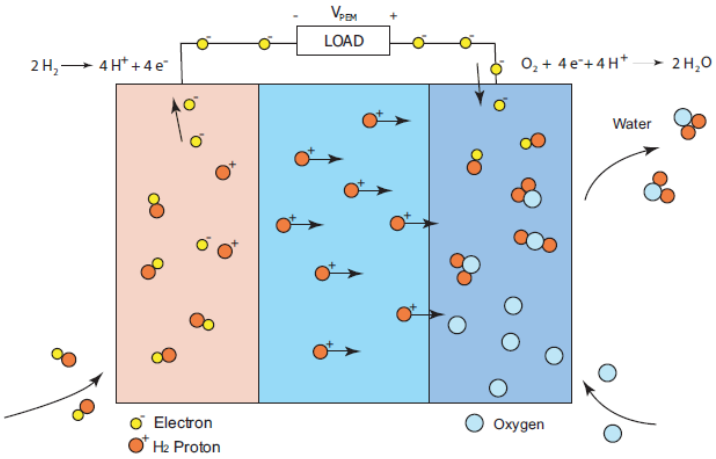

Figure 3.20. Fuel cell reaction [41]

separates into electrons and hydrogen protons (Figure 3.20). Hydrogen gas passes over one electrode, called an anode, and with the help of a catalyst, separates into electrons and hydrogen protons [41]:

$$2H_2 \Rightarrow 4H^+ + 4e^- \tag{3.60}$$

The protons flow to the other electrode, called a cathode, through the electrolyte while the electrons flow through an external circuit, thus creating electricity. The hydrogen protons and electrons combine with oxygen flow through the cathode, and produce water [41]:

$$O_2 + 4H^+ + 4e^- \Rightarrow 2H_2O \tag{3.61}$$

The overall reaction of the fuel cell is therefore [41]:

$$2H2 + O_2 + 4H^+ + 4e^- \Rightarrow 2H_2O \tag{3.62}$$

A PEM fuel cell system has ancillary services like the membrane humidifier whose function is to maintain correct humidity in the membrane, the water separator whose function is to separate the water in the output oxygen flow, the cooling and heating system whose function is to control the working temperature at 55^oC and the compressor charged to inject the correct proportion of air to produce the desired output power. Open-cathode PEMFCs differ from typical PEMFCs in that they have cathode channels exposed to the atmosphere whereas typical PEMFCs are usually operated with a closed-cathode structure. In closed-cathode PEMFCs, the air is supplied by a compressor at pressures from near

ambient to approximately 6 atm. On the other hand, open-cathode PEMFCs are usually operated at around atmospheric pressure with the air being supplied either by convection or low-power fans. Higher pressures in closed-cathode PEMFCs require cathode pressure regulation in order to match the anode pressure [180, 181]. However, in open-cathode PEMFC systems, due to near-atmospheric operating pressures, pressure regulation is not required. It should also be noted that although operating at higher pressures results in better performance and higher voltages, it induces considerable parasitic loads (e.g., compressor, cooling system, humidification system). Open-cathode PEMFCs, on the contrary, owe their popularity to their portability and reduced number of required Balance- Of-Plant (BOP) components; no compressors, supply or return manifolds, no cooling system components such as pumps and radiators, and no humidifiers [181].

There are two open-cathode PEMFC system Configurations: air-breathing and air-forced. The air-breathing open-cathode PEMFC system does not have any components for air flow management; thus, air is acquired by diffusion and natural convection from the surrounding atmosphere [181, 182]. Also, the produced water in the cathode is removed via evaporation. This configuration is suitable for applications such as cell phone emergency chargers. However, for higher powers, the generated heat needs to be actively dissipated and therefore, more air is required for the cathodic reaction. In this case, air-forced systems in which the cathode system consists of a fan or a blower to provide airflow [181, 182, 183].

In open-cathode fuel cells, fans are usually placed at the cathode entry in order to generate air flow through the cathode channels. These fans not only provide the required air for the fuel cell reaction but they are also used for thermal management in the cathode channels. That is, the amount of air passing through the cathode channels can be regulated so that proper heat dissipation is achieved inside the cathode channels. Therefore, the control of air delivery system through fans is challenging in open-cathode fuel cell systems [181].

The hydrogen tank is used in order to provide pure hydrogen required for the PEMFC operation. The pressure regulator guarantees a safe operating hydrogen pressure in the anode. The hydrogen supply valve and mass flow controller, which are placed before the anode entry, are usually employed in order to control the flow and amount of hydrogen. The purge valve at the anode exit is used in order to expel the unused hydrogen, nitrogen, and generated water in the fuel cell. Efficient control of purging is vital to ensure proper fuel cell performance while maintaining minimal hydrogen losses [181]. An schematic view of the used open cathode fuel cell can be observed in figure 3.21.

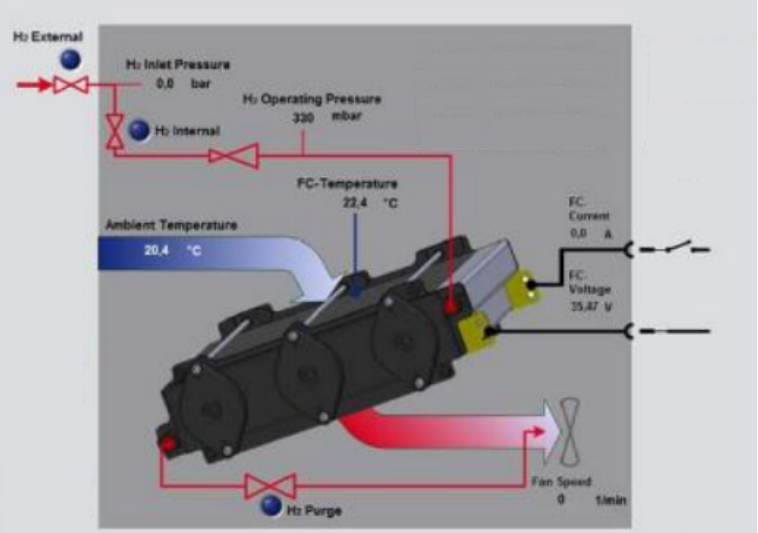

Figure 3.21. Open cathode fuel cell schematic view (From Nexa 1200 Instruction Manual - Heliocentris)

3.7.2 Degradation Issues

In a similar way to the electrolyzer, start up and shut down cycles have degradation effects on the catalyst layer. A fluctuating operation of the fuel cell can produce the loss of the correct humidity in the membrane and overall the process know as starvation, where the output power demanded to the fuel cell is higher than the correspondent air flow at the cathode input, degrades serially the fuel cell. Both the electrolyzer and the fuel cell response, are limited by the complex dynamics associated with mass and heat balances inside and outside the stack which results in a slow transient response [33, 40]. A detailed model and description of each component of the fuel cell can be found in [41]. The control of a PEM fuel cell mainly consists of reactant supply, water/temperature, and power management. Lack of robustness in control can cause cross-coupled failures during dynamic load changes in fuel cell system. Proton exchange membrane fuel cells, when operating with low air flow to minimize parasitic loss associated with powering the flow device, are prone to oxidant starvation during dynamic load changes even with optimized flow field design. The temporarily low oxidant stoichiometry produces cell voltage drop, resulting in local temperature increase. Insufficient gas flow associated with dynamic load may cause accumulation of excess water, possibly blocking reactant diffusion. Anomalous operating conditions can cause not only reversible performance decrease but irreversible degradation . Also, fuel cells are required to have an excessive amount of oxygen and hydrogen flow into

the stack to avoid stagnant vapor and nitrogen films covering the electrochemical area [40]. A review of the causal degradation model is developed based upon the fuel cell degradation studies which is exposed in the dissertation of Stevens [33]. The studies shown significantly different degradation rates as a result of membrane construction, operating temperature, and load profile (constant current versus cycled current). Membrane construction is not a function of the load cycling applied and is therefore not considered in the causal degradation model. The fuel cell temperatures observed during fuel cell operation were significantly lower than those present during most of the degradation studies described. The degradation rate for steady state operation was approximately 10 V/hr, whereas cyclic operation exhibited approximately 90 V/hr. In considering this trend and given the desire to have a simple model the degradation rate is manifested as a decrease in open circuit voltage (U_{decay}) according to the following equation [33]:

$$\frac{\partial U_{decay}(t_k)}{\partial t} = -a_1 \cdot stdev\left(P_{fc}(t_{k-4}) \cdot P_{fc}(t_{k-3}) \cdot P_{fc}(t_{k-2}) \cdot P_{fc}(t_{k-1}) \cdot P_{fc}(t_k)\right) - a_2 \tag{3.63}$$

where the degradation rate is driven by the standard deviation of the power outputs for the five previous seconds, being the coefficients a_1 and a_2 dependent on the fuel cell modeled. Fuel cell degradation causes can be summarized as follows: fluctuant load cycling of fuel cells produces: i) catalyzer (platinum) particles dissolving in the cathode due to the potential cycling, ii) mechanical wear of the membrane due to thermal and humidity cycling iii) chemical degradation of the membrane via radical attack due to the time at open circuit voltage, iv) starvation phenomena when the current drawn from a fuel cell is not in the correct proportion to the reacted oxygen, v) losses in the correct humidity in the membrane. Start/Stop cycling produces: i) carbon corrosion in the electrodes ii) deactivation of the catalysis layer. [33, 40, 184]. The complex and slow dynamic of the fuel cell joined to this current ripple located at the output of the stack can produce the loss of the correct humidity in the membrane. It is also the cause of the starvation process where the output power demanded to the fuel cell is higher than the correspondent air flow at the cathode input; these operations seriously and irreversibly degrade the fuel cell, reducing the overall system efficiency. Manufacturers recommend current 100/120 Hz to be limited to within 15% [185].

3.7.3 Model of the Components

3.7.3.1 Model of the Stack

The stack polarization curve and the linear relationship between the stack current and oxygen cathode pressure were found. The stack voltage for the next instant and the oxygen cathode pressure can be expressed with the next equations, assuming that T_{fc} and $p_{an,fc}^{H_2}$ are constant respect to the used sample period which can be expressed with the following equation [41, 181, 186]:

$$U_{fc}(t) = N_{fc}^{cell} \cdot U_{fc}^{cell}(t) \tag{3.64}$$

$$U_{fc}^{cell}(t) = U_{fc,o}^{cell}(t) - U_{fc,act}^{cell}(t) - U_{fc,ohm}^{cell}(t) - U_{fc,conc}^{cell}(t) \tag{3.65}$$

$$U_{fc,o}^{cell}(t) = E_{fc}^{o} + \frac{\Delta S^{o}}{2F}\left(T_{fc}(t) - T_{fc}^{o}\right) + \frac{R \cdot T_{fc}(t)}{2F} ln\left(\frac{p_{H_2}(t) \cdot p_{O_2}^{1/2}(t)}{p_{H_2O}(t)}\right) \tag{3.66}$$

$$U_{fc,act}^{cell}(t) = -K_{1,act} \cdot (1 - e^{-I_{fc}/K_{2,act}}) \tag{3.67}$$

$$U_{fc,ohm}^{cell}(t) = R_{ohm} \cdot I_{fc}(t) \tag{3.68}$$

$$U_{fc,conc}^{cell}(t) = K_{1,fc}^{conc} \cdot e^{K_{2,fc}^{conc} \cdot I_{fc}(t)} \tag{3.69}$$

3.7.3.2 Model of the Cathode

In order to control the fluid dynamics restriction given by the starvation process, the oxygen excess ratio equation (3.70) [41] is set with the MPC controller into a reference point.

$$\lambda_{fc}^{O_2}(t_{k+1}) = \frac{W_{ca,fc}^{O_2}(t_{k+1})}{W_{fc}^{O_2,react}(t_{k+1})} = \frac{\frac{p_{ca,fc}^{O_2}(t_{k+1}) \cdot V_{ca,fc}}{R \cdot T_{fc}(t_k)}}{N_{fc}^{cell}\frac{I_{fc}(t_{k+1})}{4 \cdot F}} \tag{3.70}$$

In open cathode PEMFCs, the pressure drop, imposing the air flow by the air channels can be expressed with the next expression [181]:

$$\Delta p_{total}(t) = \frac{\rho v^2(t)}{2}\left(f\frac{l_c}{D_H} + K_{L,entry} + K_{L,exit}\right) \tag{3.71}$$

Furthermore, the relationship between air velocity and air volumetric flow rate is:

$$Q(t) = A_{ca} v(t) \tag{3.72}$$

For any rotational speed, the fan's operating point is:

$$Q(t) = \omega(t) \frac{Q_n}{\omega_n} \tag{3.73}$$

At the same time, the flow rate is related with the demanded power to the fuel cell. Due to the absence of data to model correctly the cathode pressure an empirical formula using the toolbox *Curve Fitting Tool* from Mathworks® where $p_{ca,fc}^{O_2}(t_{k+1})$ can be predicted as follows:

$$p_{ca,fc}^{O_2}(t_{k+1}) = 0.0001409 - 0.0000001824 \cdot z_{fc}(t_{k+1}) + 0.9718 \cdot p_{ca,fc}^{O_2}(t_k) \tag{3.74}$$

where z_{fc} is the MLD expression of the fuel cell stack power P_{fc}, which will be introduced in Chapter 4.

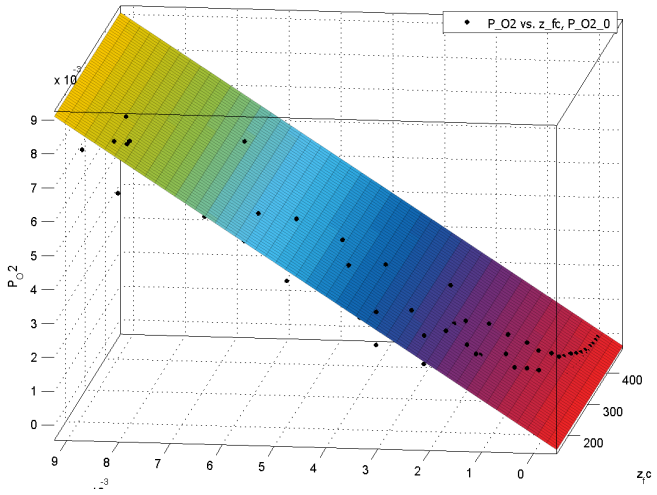

Figure 3.22. Linear surface obtained for $p_{ca,fc}^{O_2}(t_{k+1})$ vs $p_{ca,fc}^{O_2}(t_k)$ and $z_{fc}(t_{k+1})$ using the toolbox *Curve Fitting Tool* from Mathworks®

3.7.3.3 Model of the Anode

The hydrogen consumed in the fuel cell can be modeled with the next equation [41]:

$$W_{fc}^{H_2,reacted}(t_{k+1}) = N_{fc}^{cell} \frac{I_{fc}(t_{k+1})}{2 \cdot F} \tag{3.75}$$

In the fuel cell the consumption of hydrogen is not only due to reaction in the fuel cell, but also because a purge is carried out by the system every φ_{fc}^{purge} seconds. In order to model this consumption of hydrogen a term is added with a logical variable which is active when the purge is carried out. During the start-up procedure the Fuel Cell System emits in 4s a volume of ca 0.55 l_n of hydrogen. During the normal operation the system emits every 20s in 0.5s an amount of ca 0.045 l_n of hydrogen.

$$W_{fc}^{H_2,purge}(t_{k+1}) = \delta^{H_2,purge}(t_{k+1}) \cdot K^{H_2,purge}(t_{k+1}) \tag{3.76}$$

Table 3.8. Parameters of the model of the fuel cell

Parameter	Value
Stack Area N_{fc}^{cell}	36 [cell]
Stack Area A_{fc}	110 $[cm^2]$
Anode current density i_{ao}	1.0631 $[\mu A/cm^2]$
Cathode current density i_{co}	1 $[mA/cm^2]$
Ohmic Resistor R_{ohm}	0.47 $[\Omega]$
Activation Coefficient 1 $K_{1,act}$	-0.998 $[V]$
Activation Coefficient 2 $K_{2,act}$	0.03249 $[A]$
Concentration Coefficient 1 $K_{1,conc}$	0.027
Concentration Coefficient 2 $K_{2,conc}$	9.001

3.7.3.4 Model validation

As done in the case of the electrolyzer, the fuel cell model was validated applying a fluctuant current to the fuel cell and measuring the obtained voltage, as well as, comparing it with the results given by the developed model. This results are exposed in figures 3.23, 3.24. The utilized parameter to feed the model of the fuel cell can be observed in table 3.8.

3.8 Conclusions

The analysis and modeling of all the components of the microgrid are carried out in this chapter. Focusing mainly on the power sources, the model shows the

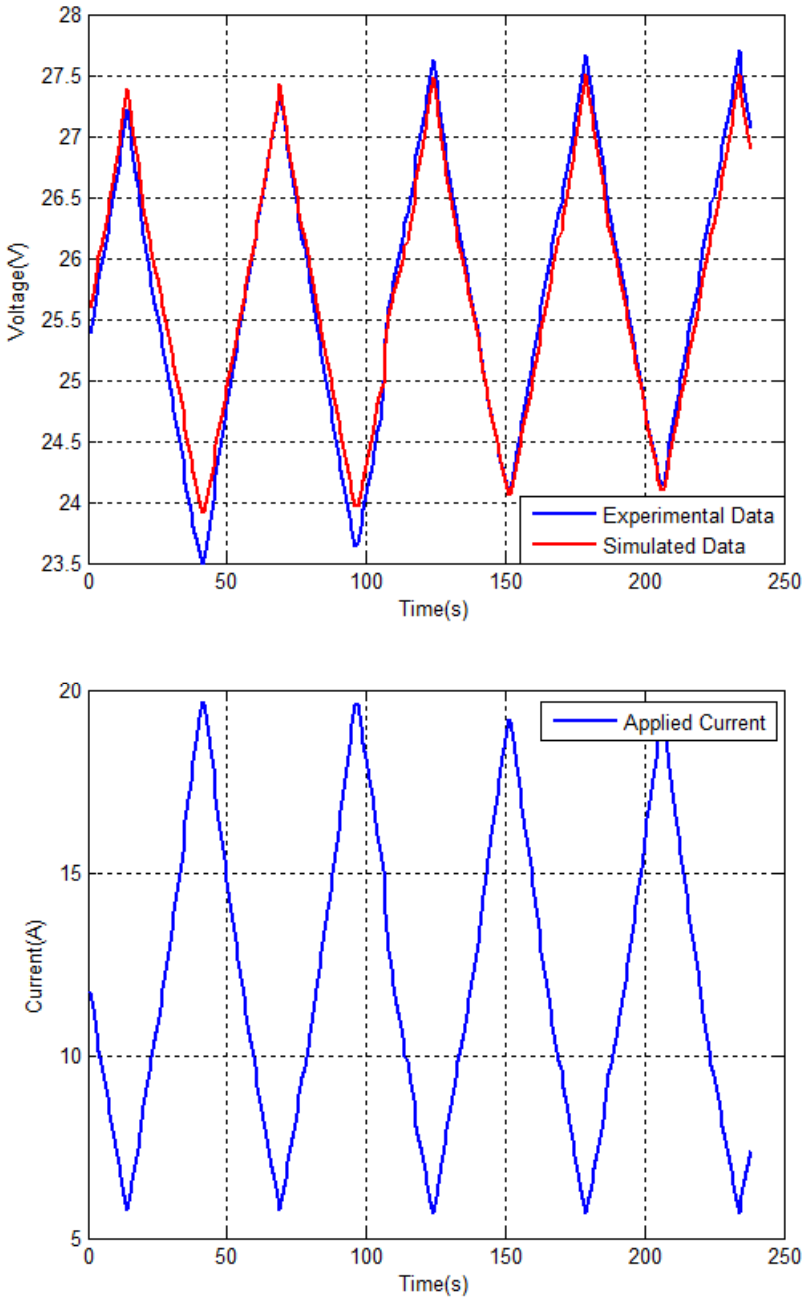

Figure 3.23. Fuel cell voltage model validation under fluctuant-load conditions

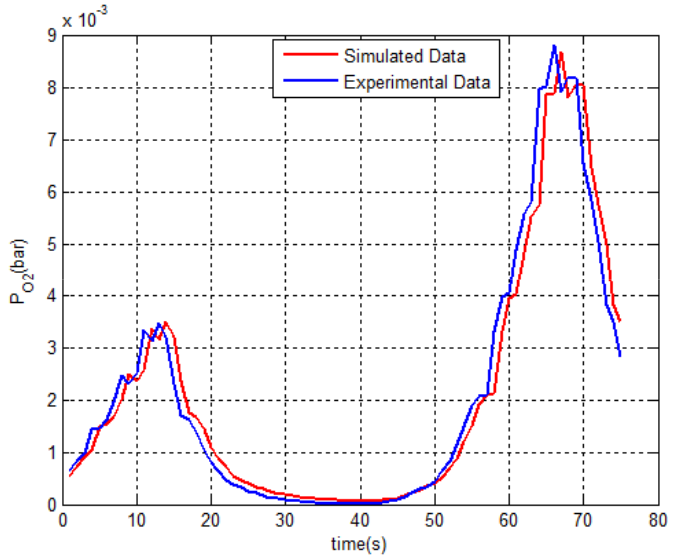

Figure 3.24. Fuel cell cathode pressure model validation under fluctuant-load conditions

dependency on meteorological variables of the produced power by the sources. The randomness of this variable is the cause of not being able to predict the production of this kind of generation to act in the electrical market. It is also the cause of unbalances in the power quality of the associated grid where they are connected. ESSs appear as a key-solution to integrate renewable energy sources. But each energy storage system (ESS) has its own limitations in the relationship between energy and power density, although degradation issues or anomalous working conditions must be also considered. In the case of the ultracapacitor overcharge can damage the technology and undercharge can damage the power electronic associated. In the case of batteries overcharge or undercharge can also degrade the technology. This technology is even more restrictive due to the fact that high stress charge/discharge ratio affects the growth of the internal resistance of the battery. Both electrolyzers and fuel cells are damaged by the start up and shut down cycles. But also power fluctuations most be avoided. Current ripple is another factor to take into account in the ESS integration.

Chapter 4

Optimal Economic Dispatch of the Microgrid

4.1 Introduction

The electricity market is a complex process where the electricity production system provides a total amount of electricity, in each instant, corresponding to a varying load of the electricity consumption. Electricity exchanges first take place in the day-ahead (spot) market, where participants[1] (sellers and buyers) have to propose, before gate closure, their quantity-price bids over the following delivery period. Participants are then financially responsible for any deviation from the contract. Certain electricity pools also integrate intraday markets, where it is possible to take corrective actions. The regulation market, which is managed by the system operator[2], ensures real-time balance between generation and load. For the fast load variations, and unforeseen problems with production capacity, there are reserves at the system operators disposal [85, 86].

With the liberalization of electricity markets, renewable energy producers have the possibility to dispatch their production through electricity pools. But the unpredictability of renewable energy joined to the penalty deviations used in the

[1]Market participants are undertakings that are authorized to act directly in the electric power market as buyers and sellers of electricity.

[2]The role of the system operator in a wholesale electricity market is to manage the security of the power system in real time and co-ordinate the supply of and demand for electricity, in a manner that avoids fluctuations in frequency or interruptions of supply. On the other hand, the market operator is in charge of the wholesale transactions (bids and offers) in the day-ahead and intraday markets.

regulation market make it difficult for clean energy to play an important role in the electricity market. However, the reduction of fossil fuel reserves and its associated increased price will trigger the switch to a continuous introduction of renewable energy in the grid. The randomness of consumers behavior is also an added problem. These facts will require the use of energy storage to balance the generation and demand curve in power networks where sources, loads and energy storage systems must act like a unit. This is to be doneinside a microgrid structure so as to reduce management efforts of the system operator in the smart grid.

As explained in Chapter 3, there are several ways to store energy but each energy storage system has advantages and disadvantages regarding economic costs, energy rating, power rating, life and degradation issues. The high energy density of hydrogen as an energy carrier will play an important role in the new energetic paradigm of microgrids and smart grids. However, the robust performance under transient conditions and slow response are the main barriers for its technological implantation. Batteries and ultracapacitors have better transient responses, however, their low energy density does not give enough autonomy to the system. The use of hybrid storage systems appears as a solution to mitigate the disadvantages of energy storage.

In this chapter, the optimization problem of energy inside a renewable energy microgrid, with different kinds of energy storage systems, which exchanges energy with the main grid, is developed and solved with MPC techniques. The controller includes the operational cost, degradation issues and constraints associated to hybrid ESSs, resulting in the main contribution of the study. All the schedule steps of the market operator and the system operator are considered in comparison with previous works which have only solved one of the steps of the electricity market. The use of MPC techniques allows us to maximize the economic benefit of the microgrid, minimizing degradation causes of each storage system, fulfilling the different system constraints at the same time. In order to capture both continuous/discrete dynamics and to switch between different operating conditions, the plant is modeled with the framework of Mixed Logic Dynamic (MLD). Taking into account the presence of integer variables, the MPC problem is solved within Mixed Integer Quadratic Programming (MIQP). This method was presented in [187, 188, 189].

The modeling criterion will depend on the component, from this standpoint two main component classes can be considered. The first are the non-controllable components of the microgrid, such as, photovoltaic arrays or the wind turbines. The grid together with the randomness of energy prices could also be modeled as a non-dispatchable element in the microgrid. Non-dispatchable elements of

the microgrid are modeled with an ARIMA model of the microgrid. The second class of the models in the microgrid corresponds to the components which can be considered dispatchable. The functional cost of the non-dispatchable components cannot be controlled directly but can be compensated with dispatchable components in order to harness the whole benefit of the microgrid.

4.2 Management in the Electricity Markets

Electricity markets are not only addressed to the day-ahead markets that receive buying and selling bids each day to plan the operation of the system for the next day. The economic schedules obtained for each hour of the next day will have to be validated together with the relevant bilateral contracts by the System Operator. If congestion happens, these schedules have to be changed to enforce technical constraints. When we refer to these markets, we are in fact talking about active power. As it is known, this only corresponds to part of the problem because the safe and reliable operations of power systems require a number of other services, usually known as Ancillary Services. The definition, the scope and the method of scheduling and contracting these services is not harmonized in different countries. Namely in Western Europe or even in countries that have common electricity markets, as for instance Portugal and Spain. In any case, the focus on active power can be explained by two main reasons. The price of generating active power together with the regulated transmission and distribution costs correspond to more than 90% of the final end user tariff which means that outside readers may consider that a reduced impact of Ancillary Services in the final price just reflects their lack of relevance [190].

It would be quite difficult to establish an international electricity market model description in order to apply a generalized advanced control. For example, in Europe, although in 2006, the European Commission created the Electricity and Gas Regional Initiatives with the purpose of facilitating the integration of regional electricity and gas markets, by means of concrete actions, nowadays seven regional markets exist and four integration initiatives (see figure 4.1) [191]:

- Central-West: Germany, Belgium, France, Luxembourg, Netherlands
- Central-South: Germany, Austria, France, Greece, Italy, Slovenia
- South-West: Spain, France, Portugal
- France-United Kingdom-Ireland

Each region brings together regulators, companies, Member States, the European Commission and other stakeholders to focus on developing and implementing solutions to improve the way in which regional energy markets develop. The seven regions have similar aims (integrating fragmented national electricity markets into regional markets) but their priorities and achievements reflect their different regional concerns. An overall monitoring process at EU level ensures that progress towards a single EU market is not hampered, and that there is convergence and coherence across regions. In Directive 2009/72/EC, of 13th July 2009, Concerning Common Rules for the Internal Market in Electricity, the MIBEL (Iberian Electricity Market) initiative in the Iberian market is taken as reference [191].

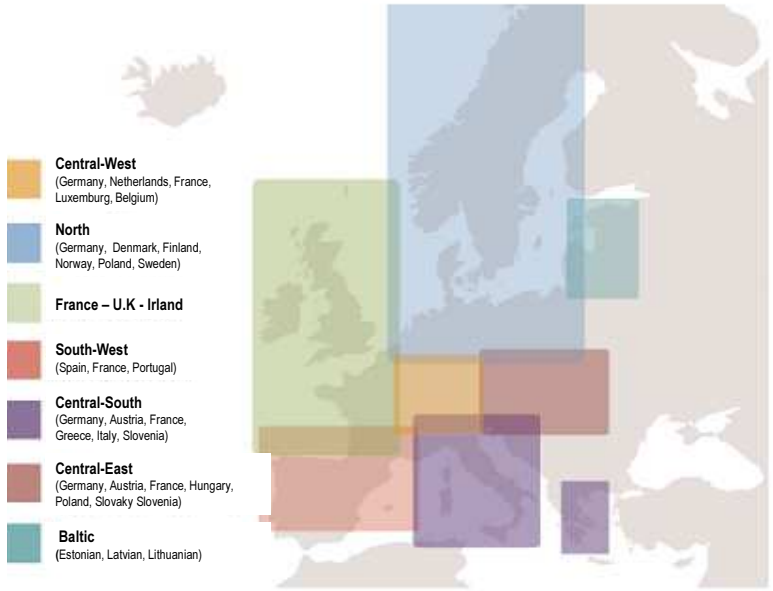

Figure 4.1. Regional electricity markets in Europe. (Source: Commision de Régulation de l'Énergie)

The high penetration of renewable energy in the MIBEL market makes it a good model on which to base the control algorithm which tries to solve the economic dispatch of a smart grid highly composed by renewable energy. There are several advanced electricity markets with similar characteristics, such as the Australian Market , the USA Market, the German Market or the Norwegian Market. The Iberian market sequence is shown in figure 4.2. As can be observed in the figure, there are two main actors in the market: the Market Operator and the System Operator:

- **Market Operator:** Is the entity in charge of performing the settlements of the day-ahead and intraday markets.

- **System Operator:** The role of the System Operator (also called Transmission System Operator) in a wholesale electricity market is to manage the security of the power system in real time and coordinate the supply of and demand for electricity, in a manner that avoids fluctuations in frequency or interruptions of supply. The System Operator service is normally specified in rules or codes established as part of the electricity market. The System Operator is required to maintain a continuous (second-by-second) balance between electricity supply from power stations and demand from consumers, and also ensure the provision of reserves that will allow for sudden contingencies. The System Operator achieves this by determining the optimal combination of generating stations and reserve providers for each market trading period, instructing generators when and how much electricity to generate, and managing any contingent events that threaten the balance between supply and demand. System Operations staff undertake this work using sophisticated energy modelling and communications systems. In addition to its roles of real-time dispatch of generation and managing security, the System Operator also carries out investigations and planning to ensure that supply can meet demand and system security can be maintained during future trading periods. Examples of planning work may include co-ordinating generator and transmission outages, facilitating commissioning of new generating plants and procuring ancillary services to support power system operation.

As a summary of the process, the operation of the Spanish/Iberian Market Operator (OMEL-OMIE) is as follows: the Market Operator receives bids everyday from agents (selling and buying), one day ahead, and clears the market according to the marginal price procedure. The System Operator validates the units schedule considering the electrical systems technical constraints. After that, the hourly merit- order curves of generation and demand are elaborated. Finally, the matching algorithm is run in order to find the crossing point of the supply and demand curves. As a result, a single hourly and marginal price (and traded energy) for the whole market is set. All generating units are rewarded at this clearing price, regardless of the price specified in their bids for the considered hour [192].

In the Iberian market the special regime includes renewable sources and cogeneration. Big hydropower units ($\geq 50MW$) are not included. Electricity generation under the special regime is already a key piece of the Iberian production

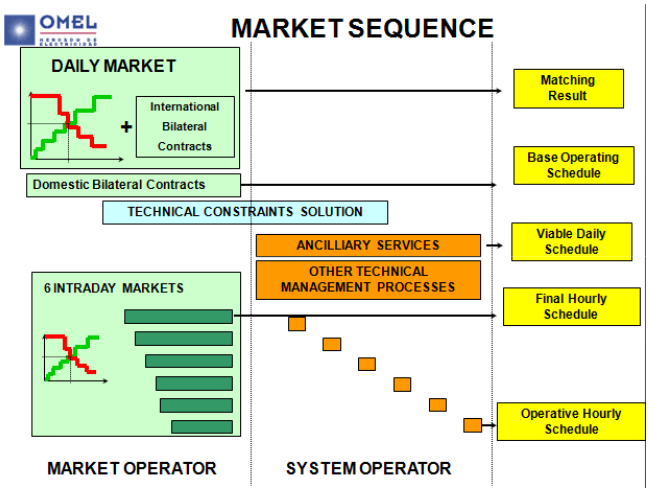

Figure 4.2. Market sequence in the Iberian Electricity Market. (Source: OMIE)

mix, which is essential to reconcile the liberalization of electricity production with goals that society has already outlined in terms of environmental protection and energy efficiency and independence. However, the special regime should not only be required to contribute energy, but also to contribute available capacity, as well as a solid contribution to the development of the market and to the safe operation of the system. This special regime gives special consideration to renewable energy producers who can participate in the market with a regulated tariff or in the free market. In the first case, the average or reference tariff is established through Royal-Decree. Its calculation is based on the revenues needed to satisfy each electric activity's economic remuneration and considering the estimated electricity consumption. This tariff's update determines the change in the tariff for regulated consumers and the access to tariffs for liberalized clients. In the second case, they perceive the clearing market price plus a regulated premium (to compensate renewable producers for their marginal costs and for the risk of using a less mature technology). Due to the transition that renewable producers must do to compare their technologies with classic producers, only the free market (whose participation rules are more difficult) is described.

4.2.1 Day-Ahead Market

The daily market or commonly Day-Ahead Market is a forward market in which each hourly Locational Marginal Pricing (LMP) is calculated for the next oper-

ating day based on generation offers, demand bids and scheduled bilateral transactions (see figure 4.3). Its main purpose is to handle electrical transactions for the following day through the presentation of electricity sale and purchase bids by market participants. Bids made by these sellers are presented to the market operators and will be included in a matching procedure that will affect the daily programming schedule corresponding to the day after the deadline date for the reception of bids for the session, and comprising twenty-four consecutive programming hours. The market operator matches electricity power purchase and sale bids (received before 10 a.m. on each day). The price in each hour will be equal to the price of the last block of the sale bid of the last production unit whose acceptance has been required to meet the demand that has been matched. The market operator obtains the Matching Result from this match; this represents the hourly production and demand schedule on the network established by the market operator. The market operator carries this out by matching electricity sale and purchase bids which determines the volume of electricity production required to cover electricity demand in each hour of the same day. There are several concepts which make the purchase prices higher than the sale prices, such as, losses payment, payments by capacity, traps, net marketing, different tolls distribution, VAT, test equipment rental or the electricity excise duty [193].

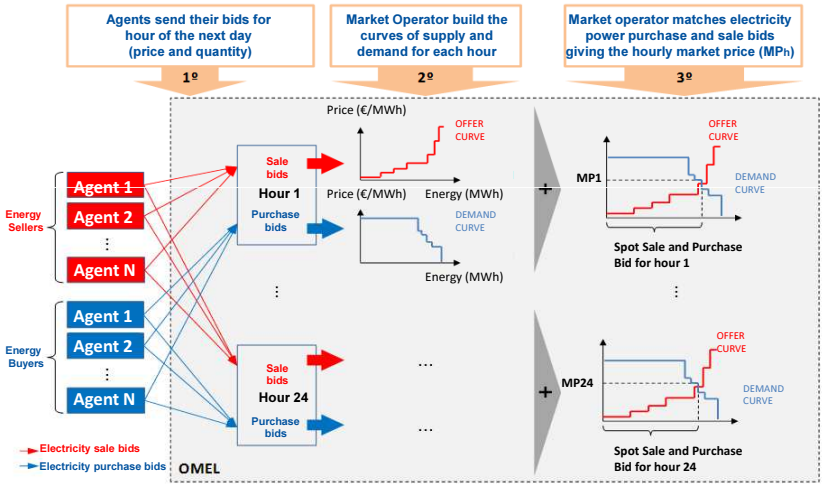

Figure 4.3. Locational marginal price formation in the day-Ahead spot market. (Source: Energía y Sociedad)

4.2.2 Intraday Market

The purpose of the intraday market is to respond, through the presentation of electricity power sale and purchase bids by market agents, to adjustments made to the Final Viable Daily Schedule. The intraday market is currently structured into six sessions with the following hourly distribution per session in table 4.1. The agents authorized to present purchase bids on the daily market may only participate in the intraday market for the hourly periods corresponding to those included in the daily market session in which they have participated [193].

The sale bids for each intraday market session must be such that the final schedule resulting from the complete acceptance of the bid plus the previous schedule of the production or purchasing unit, respects the limitations declared by the system operator for the scheduling horizon, or if it does not comply with these prior to the presentation of the bid, it must be close to complying with them. Similar proceedings are realized with the purchase bids. The purchase bids for each intraday market session must be such that the final schedule resulting from the complete acceptance of the bid plus the previous schedule of the production unit respects the limitations declared by the system operator for the scheduling horizon; if it does not comply with these prior to the presentation of the bid, it must be close to complying with them. The market operator matches electricity power purchase and sale bids. The price in each hourly schedule will be equal to the price of the last block of the sale bid of the last production unit whose acceptance has been required in order to meet, either partially or totally, the purchase bids at a price equal to, or greater than, the marginal price [193].

Table 4.1. Intraday market sessions (Source [193])

Session	First	Second	Third	Fourth	Fifth	Sixth
Opening	16.00h	21.00h	01.00h	04.00h	08.00h	12.00h
Horizon	21-24h	1-24h	5-24h	8-24h	12-24h	16-24h
Schedule	28 hours	24 hours	20 hours	17 hours	13 hours	9 hours

4.2.3 Ancilliary Services

The operation of the system encompasses the activities necessary to ensure the security and continuity of supply, as well as the proper coordination between production and transmission, ensuring that the energy produced by the generators is transported to distribution networks under the quality conditions required by

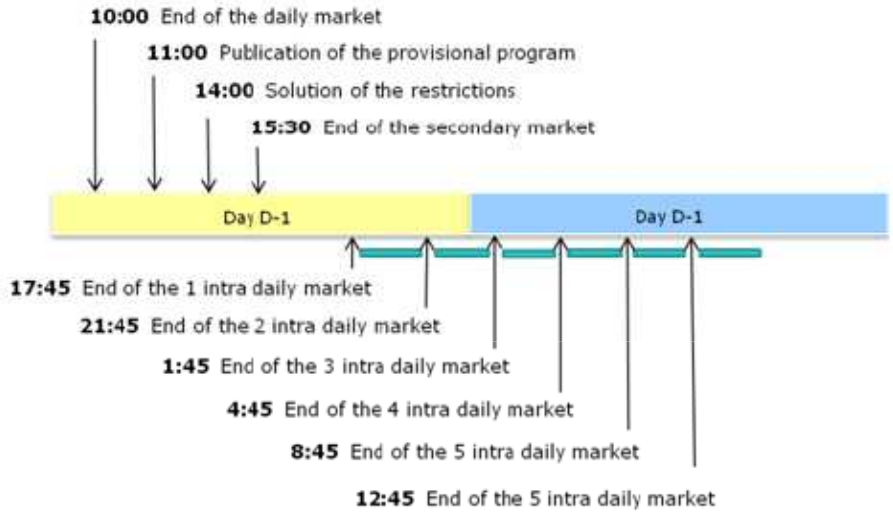

Figure 4.4. Intraday market sequence (Source: OMIE)

the regulations currently in force [193]. The complete sequence of the actions in the power system realized by the Market Operator and the System Operator are defined in figure 4.5

Despite their reduced impact in terms of cost, Ancillary Services are crucial from a technical point of view. One must also bear in mind the general ideas and concerns with a particular emphasis on reserves (including primary, secondary and tertiary reserves) together with methodologies in the literature to allocate some of these services.

The Ancilliary Service Market provides system balancing including: (1) technical restrictions resolution process; (2) deviation management; (3) additional services, which include (3a) those associated with frequency-power regulation (primary, secondary and tertiary reserve), (3b) voltage control of the transmission grid, and (3c) restoration of service [194, 195]. The complete sequence of the electrical market including the market operator and the system operator is shown in figure 4.6.

The resolution of technical restrictions is managed through market mechanisms on three levels: (1a) those associated with the base daily operating schedule (BDOS), (1b) those that arise after intraday markets and (1c) those handled in real time. Deviation management is settled using a competitive dual price system. Within ancillary services: primary reserve is compulsory and is not remunerated;

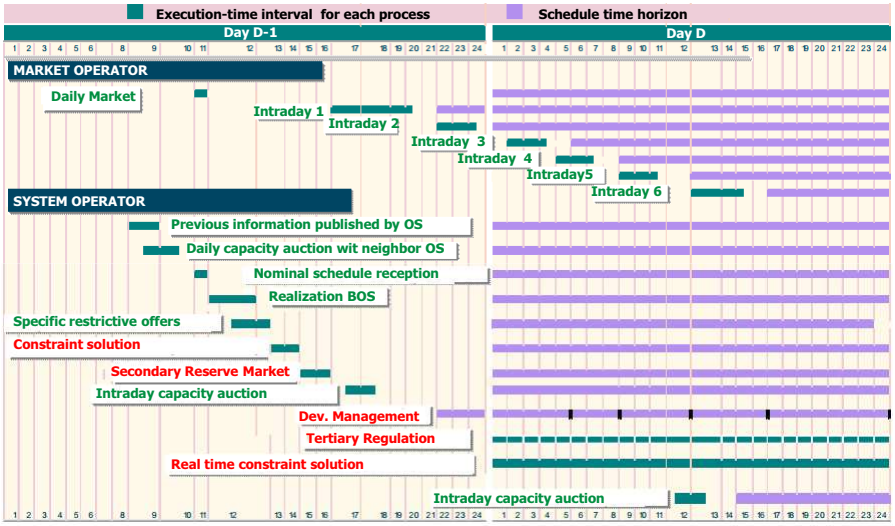

Figure 4.5. Setting services of the system schedule (Source: REE)

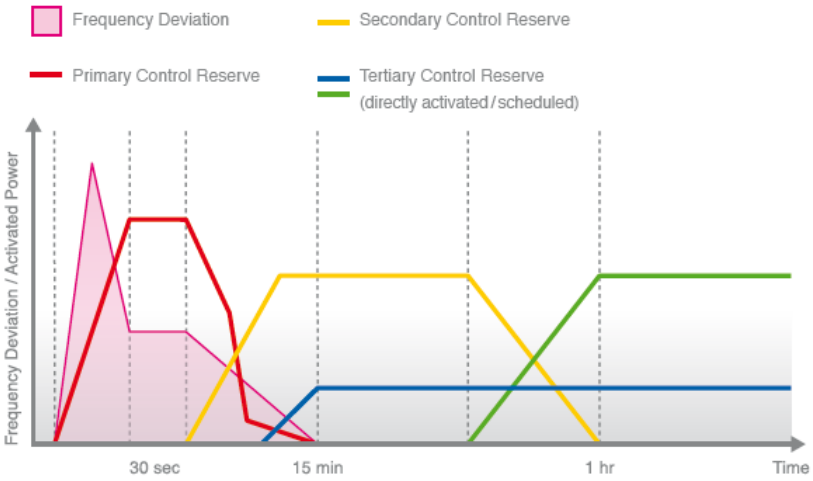

Figure 4.6. Principal of frequency deviation and subsequent activation of reserves (Source: ENTSO-E)

secondary reserve is a marginally remunerated optional service; tertiary reserve must be offered and is also marginally remunerated. Voltage control is comprised of two parts: a voluntary part, which is remunerated in accordance with regulations, and another unpaid and mandatory part for all suppliers of the service; lastly, the manner for remunerating restoration of service is still pending statutory development [194, 195].

Momentary imbalances are initially regulated by Primary Regulation (This primary regulation is obligatory and not remunerated). If the imbalance continues for several minutes, Secondary Regulation will take over, thus freeing up Primary Regulation resources for regulation of new imbalances. If further regulation is necessary, Tertiary Regulation (regulating power) will be activated which, correspondingly, will make secondary regulating resources available [193, 196].In the case of Tertiary Regulation the power variation regarding program must be no longer than 15 minutes and must be maintained at least 2 hours as submitted. Both Secondary and Tertiary Regulation are remunerated at the same price and have not obligatory character. The auction of these complementary services is done by the System Operator at the end of the Daily Market. [193, 197].

The primary regulation automatically corrects (through the speed regulators of the generators) instant generation-demand imbalances and is mandatory and unpaid. It reaches a time horizon of up to 30 seconds. The secondary regulation aims to correct instant deviations with respect to the power exchange schedule in the interconnection between Spain and France, as well as deviations in terms of the frequency of the system. It encompasses a time horizon of between 30 and 15 seconds. The dynamic response requirement corresponds to a time constant of 100 seconds. It is an optional service that is marginally paid based on two concepts: availability (power band) and use (energy), both to increase and to decrease. It is provided through control areas. Each control area consists of a group of plants capable of providing the secondary regulation service certified by REE, and of other generating units not equipped to regulate, so that the control areas also serve as aggregation units of the production unit schedules. In addition, the secondary market refers to band offers; secondary regulation energy is valued at the marginal price of the tertiary regulation that would have been necessary to schedule each hour, both to increase and to decrease, in order to replace this net use of secondary energy. The tertiary reserve replaces the consumed secondary reserve. It is activated manually and is defined as the maximum power variation achieved in a period up to 15 minutes that can be maintained for at least two hours. It is a mandatory service that is paid based on corresponding marginal prices for mobilized reserve to increase and to decrease. Voltage control consists of two parts: a voluntary part that is paid according to regulations and

an unpaid part that is mandatory for all service providers (carriers, distribution network managers and qualified large generators and consumers connected to the transport network). The restoration service is based on the capacity that certain generator sets have to start up without external power in a certain time after a zero of general voltage in the facility and keep generating steadily during the process to restore supply, or to be able to island its ancillary services. This additional service has been defined since the market was created in 1998 but has not yet been developed [194].

Black start corresponds to another service to be provided by machines that can start being energized using autonomous systems, without being connected to the power system. These machines should be reasonably dispersed along the system so that they can be used to start re energizing the whole system after a major black out. Regarding reactive power services, voltage control is the most typical one. It aims at maintaining voltage magnitudes in the nodes of the grid within specified bands typically indicated in the operation codes followed by the system operator. This corresponds typically to a service that is provided in a distributed way from a geographical point of view in the sense that reactive power devices should be spread along the grid to support voltages, to minimize reactive flows and to reduce active losses [190].

In this chapter, only the economic schedule of the microgrid is carried out, so the terms referring to black start, voltage or frequency support are considered in a more technical manner in chapter 5. Although as has been commented the restoration service has not been implemented in the system. Thanks to the microgrid structure, changing the operating mode of the microgrid from grid-connected to islanded-mode will be quite easy. The economic control algorithm of the islanded operation mode is just a subcase of the grid-connected one adding the constraint of zero power exchange with the main grid. From the technical point of view of the microgrid, the transition to the islanded mode means that an ESS acts as grid working in voltage mode imposing the voltage and frequency reference on the rest. The remaining components will be working in grid connected mode injecting active and reactive power carried out in their economic schedule.

4.3 Energy Storage Systems in the Electrical Energy Market

The introduction of ESSs in the paradigm of smart grids introduces new possibilities in the electrical market. The financial benefits of energy storage systems in smart grid include cost reduction of bulk energy arbitrage, revenue increase

of central generation capacity, cost avoidance of ancillary services, revenue increase for transmission access and congestion, reduced demand charges, reduced reliability-related financial losses, reduced power quality-related financial losses and increased revenue from renewable energy sources. Some of these are briefly explained below [6]:

1. Revenue increase for load leveling and peak shaving: Load leveling is rescheduling certain loads to cut electrical power demand, or the production of energy during off-peak periods for storage and use during peak demand periods . Peak shaving consists of reducing electric use during certain periods or moving usage for the off-peak periods of time .

2. Revenue increase of bulk energy arbitrage: Energy arbitrage involves the purchase of inexpensive available electricity during low demand periods to charge the storage systems so that the low priced energy can be used or sold at a later time when the price s higher.

3. Revenue increase for transmission access and congestion: Transmission congestion can be reduced or avoided by using energy storage systems. Further storage systems can be used to increase the energy transfer capacity and stabilize voltage levels.

4. Reduced demand charges: Storage systems can be used to reduce the electricity demand of end-user during the times of peak load demand.

5. Reduced reliability-related financial losses: Storage systems can reduce financial losses associated with power outages. This mainly benefits end-users and applies to commercial and industrial customers primarily because power outages cause moderate to significant losses to them.

6. Reduced power quality-related financial losses: Storage systems can reduce financial losses associated with power quality anomalies. Power quality anomalies of interest are those that cause loads to go off-line and/or that damage electricity using equipment and whose negative effects can be avoided by using storage.

7. Increased revenue from renewable energy sources: Storage can be used to time-shift electric energy generated by renewable sources. Energy is stored when the demand and the price for power are low, in this way the energy can be used when the demand and the price for power are high and output from the intermittent renewable sources is low.

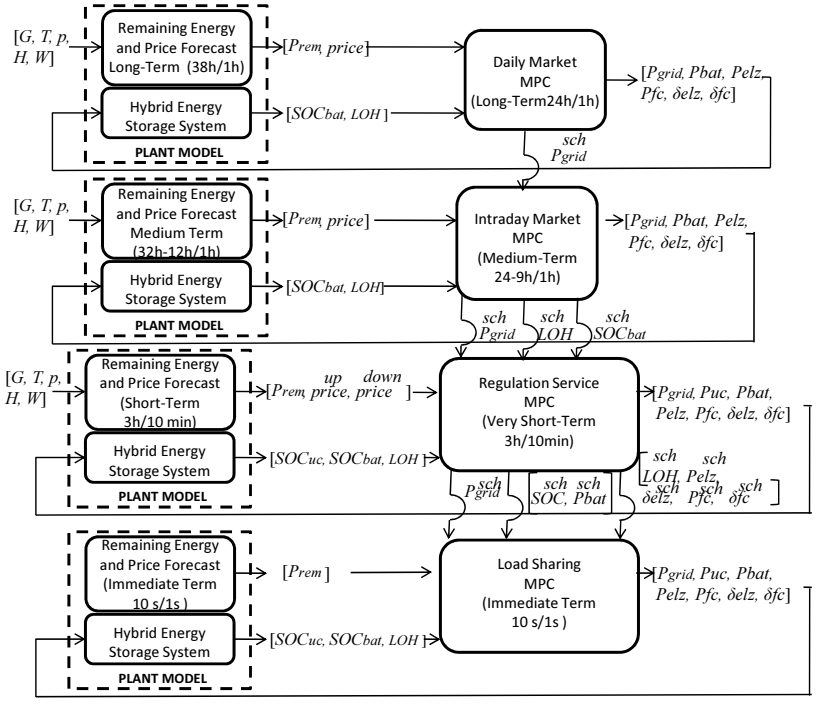

Figure 4.7. Tertiary MPC controller general block diagram

4.4 Tertiary Model Predictive Control-Schedule

The different time-scales of the electricity markets make a whole control algorithm necessary to solve the long term horizon schedule made by the daily market (38 hours ahead), the different sessions of the intraday market (28-9 h), the regulation service market(3 h) but also the real scenario load sharing (seconds) (more information about the electrical market can be found in [193, 197]). The horizon schedule also determines the most appropriate ESS technology to be used. The cost and constraints of each ESS based on the life and load cycling degradation of the each ESS, as well as the deviation schedule penalty with respect to the main grid, are considered using a four level-cascade MPC controller. The block diagram of the different levels of the Tertiary MPC controller are detailed in figure 4.7. In order to clarify the algorithm explanation the tertiary MPC controller has been divided into the schedule and the load sharing. In this section, it is just treated the optimal economical schedule of the microgrid. The controller was implemented in Matlab using the solver CPLEX.

4.4.1 Mixed Logic Dynamic Systems

The MLD MPC results in an optimization problem with a set of linear constraints and with real and integer (Boolean in this case) decision variables. These types of optimization problems are known , in general, as Mixed Integer Programming (MIP) problems. The general MLD form of a hybrid system is [198]:

$$x(t+1) = Ax(t) + B_1u(t) + B_2\delta(t) + B_3z(t) \tag{4.1}$$

$$y(t) = Cx(t) + D_1u(t) + D_2\delta(t) + D_3z(t) \tag{4.2}$$

$$E_2\delta(t) + E_3z(t) \leq E_1u(t) + E_4x(t) + E_5 \tag{4.3}$$

where x is the continuous and binary states, u represents the inputs, y the outputs, δ represents the binary variables and z represents auxiliary binary and continuous variables. With the introduction of a series of basic conversions given in table 4.2, the non-linearity of the system, introduced by the combination of logical and dynamic variables, is transformed into constraints of the control algorithm. Allowing to derive the system in order to find an optimal solution for the given cost function. In table 4.2, m and M represent the lower and upper bounds of the system and $\epsilon > 0$ is the smaller tolerance of the device [198].

4.4.2 Model of the Plant

The model of the plant has two parts: the remaining energy and price forecast model, and the evolution of the state variables of the microgrid (LOH, SOC_{uc}, SOC_{bat}).

4.4.2.1 Forecast of the Remaining Energy in the Microgrid and Price Evolution

The model is based on an artificial neural network (ANN) developed with the auto-regressive integrated moving average model (ARIMA) using the time series method. Its result is the forecasting of wind and solar power generation the load consumption. The model uses as inputs the meteorological variables: solar irradiance (G), ambient temperature (T), atmospheric pressure (P), relative humidity (H) and wind speed, including the wind direction (W). The ANN is a three-layer model (input layer, hidden layer and output layer). The input layer neurons are the profile of the last hour for the indicated measures. The first step of the development is to identify the most similar profile for each neuron at exactly the same time that the prediction is made over the previous two weeks. The next step is to compare, for the same day, the most similar profile for each variable in all the following days during a month for the same instant in the last two years. With

Table 4.2. Conversion of logic relations into Mixed Integer Inequalities [198]

	Relation	**Logic**	**MLD Inequalities**
P1	AND ($\wedge$)	$S_1 \wedge S_2$	$\delta_1 = 1,\ \delta_2 = 1$
P2		$S_3 \Leftrightarrow (S_1 \wedge S_2)$	$-\delta_1 + \delta_3 \leq 0$ $-\delta_2 + \delta_3 \leq 0$ $\delta_1 + \delta_2 - \delta_3 \leq 1$
P3	OR ($\vee$)	$S_1 \vee S_2$	$\delta_1 + \delta_2 \geq 1$
P4	NOT ($\sim$)	$\sim S_1$	$\delta_1 = 0$
P5	IMPLY ($\Rightarrow$)	$S_1 \Rightarrow S_2$	$\delta_1 - \delta_2 \leq 0$
P6	IFF ($\Leftrightarrow$)	$S_1 \Rightarrow S_2$	$\delta_1 - \delta_2 = 0$
P7		$[a^T x \leq 0] \Rightarrow [\delta = 1]$	$a^T x \geq \varepsilon + (m - \varepsilon)$
P8		$[\delta = 1] \Rightarrow [a^T x \leq 0]$	$a^T \leq M - M\delta$
P9		$[a^T x \leq 0] \Leftrightarrow [\delta = 1]$	$a^T \leq M - M\delta$ $a^T \geq \epsilon + (m - \epsilon)\delta$
P10	Mixed product	$z = \delta \cdot a^T x$	$z \leq M\delta$ $z \geq m\delta$ $z \leq a^T x - m(1 - \delta)$ $z \geq a^T x - M(1 - \delta)$

the selected data, the hidden layer simply selects those profiles which are similar to a maximum error value of 15 %. With these selected data the model takes the irradiance, the temperature and the wind speed in the required prediction horizon for each neuron. Finally the average of the prediction made is taken for the selected neurons in the hidden layer. The output layer prediction is an average value where the recent year variables and the temperatures are more weighted than the other neurons. In the case that no neuron profile is similar to the present profile with an error of below 15 %, the most similar temperatures are taken for the prediction. The output of the model gives the prediction of the irradiance, the temperature and the wind speed for the horizon prediction. With these data, the power production for the photovoltaic array P_{pv} and wind turbine generator P_{wt} can be easily predicted following the models explained by Villalva *et al.* [150] and Iov *et al.* [159]. The price forecast and the load profile P_{load} are done by taking a statistical average of the last month using four different profiles. The

first one corresponds with the working days. The second profile corresponds to Friday after noon. The third profile corresponds to Saturday and the forth profile to Sunday. The result of the model gives the prediction for the remaining power, equation (4.4), and the price energy forecast for each instant of discretization of the prediction horizon for every level of control of the microgrid.

$$P_{rem}(t_k) = P_{pv}(t_k) + P_{wt}(t_k) - P_{load}(t_k) \tag{4.4}$$

The renewable energy data have been provided by the meteorological station, from the company Geonica, model MTD 3008, located at the installations of the Spanish National Center on Hydrogen, which has been collecting data every ten minutes since 2009. The load profile corresponds to the collected data of a domestic home located in Puertollano (Ciudad Real, Spain) whose maximum contracted power with the electrical company Union Fenosa is 5 kW. The sources, load and ultracapacitor have been emulated for the experimental results with the equipment given in table 4.3. The maximum load emulation power is just 2.5 kW versus 5 kW of the real measurements. The obtained load profile is divided by 2. The energy price data have been given by the Iberian market operator (OMIE). The original data for the price of the month of March'14 can be seen in figure 4.8. The displayed results correspond to the day of March 31th, 2014.

Precio Final Demanda Nacional (EUR/MWh)

Marzo 2014

Día	1	2	3	4	5	6	7	8	9	10	11	12	13	14	15	16	17	18	19	20	21	22	23	24
S 01	12,26	14,67	13,00	12,32	12,37	11,16	11,99	11,80	10,96	13,85	16,04	14,46	13,52	10,75	11,40	11,27	10,36	10,96	13,54	14,79	19,03	20,03	12,98	10,45
D 02	11,36	12,93	11,81	11,78	11,82	11,49	11,31	11,33	11,44	11,56	10,82	10,51	11,91	12,26	12,23	10,79	10,40	10,19	11,16	12,47	13,70	13,29	11,19	10,54
L 03	10,19	12,85	12,66	12,71	12,80	12,59	12,12	9,73	12,66	13,34	12,50	11,35	11,73	12,26	12,67	12,81	12,44	14,12	15,50	20,89	21,09	20,64	14,59	12,00
M 04	8,75	9,03	9,53	10,29	10,39	10,18	10,49	11,62	14,96	14,69	14,33	13,99	14,66	14,88	14,33	12,93	13,06	15,10	18,16	25,44	26,26	26,88	18,13	13,45
M 05	12,28	12,29	11,24	10,97	11,04	11,24	16,02	23,76	33,18	43,09	45,75	27,74	32,33	33,63	30,17	27,37	28,69	39,72	53,67	93,16	87,51	69,41	54,72	42,20
J 06	42,41	42,08	31,90	32,56	31,70	33,05	42,49	58,33	63,81	63,78	59,49	58,88	60,17	56,58	52,61	48,82	49,53	55,44	69,99	101,49	106,18	101,54	58,72	54,81
V 07	42,94	39,16	35,16	34,87	34,83	37,11	42,25	61,16	63,05	64,25	59,10	56,76	54,40	51,63	49,34	45,70	45,00	52,62	63,03	82,45	81,13	76,21	56,37	49,61
S 08	41,12	30,91	25,21	24,40	17,15	14,95	16,76	25,20	17,48	25,54	27,61	26,32	26,19	25,53	26,36	19,19	14,66	20,62	32,82	46,73	39,96	35,84	28,76	24,76
D 09	21,82	18,62	14,16	14,42	13,25	13,30	12,72	12,87	13,24	13,12	13,06	11,38	12,95	13,26	14,07	14,17	15,41	18,96	32,12	45,14	48,15	49,29	47,00	39,78
L 10	33,55	28,57	23,01	25,14	23,84	24,32	31,54	56,52	58,81	85,13	50,96	47,34	48,56	48,06	46,15	43,89	46,65	52,84	61,56	70,00	62,82	58,33	47,34	39,29
M 11	27,85	23,91	16,69	18,47	18,25	21,13	28,88	47,20	72,04	52,91	49,81	45,78	47,32	48,17	47,92	42,36	43,24	45,91	53,91	69,69	64,14	55,74	45,34	41,49
M 12	37,23	37,98	38,11	39,74	39,61	42,15	45,35	48,97	53,82	52,95	50,34	47,91	48,41	47,05	47,67	47,01	48,02	51,24	55,81	82,45	78,70	71,20	53,83	48,94
J 13	45,07	43,59	38,84	39,32	39,40	42,90	46,90	56,50	59,11	58,55	52,59	51,14	51,71	53,96	58,28	48,84	49,09	51,41	58,49	79,89	79,59	76,35	56,22	48,85
V 14	47,01	43,41	38,84	39,80	39,62	42,31	48,76	55,96	59,40	59,24	58,18	53,39	56,51	55,74	54,02	52,05	51,66	53,00	58,58	73,15	71,43	62,22	53,93	50,49
S 15	45,49	47,14	43,80	42,68	40,27	39,76	39,10	39,35	36,43	37,34	40,61	38,63	38,28	36,13	38,31	33,64	30,08	35,12	44,05	46,45	46,13	44,86	40,76	37,20
D 16	32,58	28,99	19,14	18,35	18,28	18,63	19,83	22,01	22,93	20,57	18,29	23,79	25,41	20,50	21,09	19,49	19,60	27,31	34,62	45,91	51,81	57,73	50,34	42,35
L 17	46,79	45,75	38,93	41,16	41,99	45,22	52,85	57,70	71,91	59,97	57,68	54,33	56,10	56,02	56,45	54,05	54,45	56,87	69,42	85,01	106,10	92,76	64,30	54,87
M 18	61,86	53,77	43,76	42,71	42,35	42,26	47,65	51,83	57,21	57,20	54,11	51,71	54,80	52,57	51,35	46,62	46,56	48,59	54,83	57,11	54,59	51,96	47,62	41,42
M 19	30,95	25,27	15,16	16,78	16,83	19,25	28,36	37,13	47,05	54,31	51,00	50,12	53,40	53,05	54,79	52,83	53,90	55,86	59,45	81,12	73,42	77,30	57,09	51,95
J 20	50,07	48,85	44,47	43,65	41,55	42,52	47,86	50,71	56,73	55,71	53,42	52,97	54,76	53,90	52,76	51,57	51,76	54,39	58,37	65,36	69,37	63,11	52,02	44,20
V 21	39,02	35,61	30,47	30,94	32,36	36,09	39,28	48,14	55,04	52,76	52,39	51,07	51,67	49,04	48,78	41,39	41,28	47,48	54,64	62,69	60,13	58,31	51,72	48,81
S 22	45,64	38,84	28,32	30,03	27,57	30,37	32,78	33,09	32,63	33,71	34,04	28,28	23,83	23,08	19,35	16,38	12,57	14,49	23,30	33,95	38,24	44,28	31,99	31,49
D 23	27,26	26,16	21,30	20,01	19,49	20,17	21,25	20,67	18,98	19,73	19,85	20,60	22,84	23,00	24,21	21,69	22,90	25,39	38,09	52,71	57,02	60,01	54,01	49,35
L 24	44,71	39,82	33,45	33,65	32,49	35,34	39,18	42,39	48,37	46,75	45,37	45,46	45,19	40,97	40,39	37,45	33,13	35,70	42,85	44,13	46,80	43,58	40,22	27,51
M 25	18,58	18,77	16,05	15,88	14,61	16,58	17,84	23,19	27,11	26,08	20,24	18,23	18,69	18,19	18,50	17,75	17,39	19,38	24,57	27,41	31,80	30,88	22,68	18,21
M 26	15,30	15,14	12,48	12,67	12,98	15,42	18,35	21,00	26,39	26,85	26,35	25,85	25,84	26,19	23,36	22,37	27,26	29,64	38,23	60,47	65,70	59,89	47,85	42,44
J 27	45,51	45,90	44,52	43,87	44,77	47,69	51,03	54,04	68,43	69,41	66,12	65,86	65,60	57,49	56,06	53,16	53,75	58,43	81,09	157,20	115,12	91,78	67,87	50,33
V 28	46,17	38,67	37,69	37,76	34,61	36,70	39,45	42,75	51,21	52,27	51,34	49,72	51,72	48,89	48,95	45,62	46,35	47,65	53,95	58,86	59,85	59,08	54,08	49,61
S 29	40,65	37,02	31,49	38,92	35,12	36,48	36,20	37,28	37,66	39,47	37,31	34,12	34,11	33,89	35,35	32,80	32,53	36,20	46,85	50,59	52,54	52,30	45,92	44,42
D 30	45,21	44,25	33,89	32,90	30,73	34,32	34,63	36,03	36,90	38,16	37,25	38,43	35,73	36,22	31,81	26,23	26,91	33,35	39,25	49,92	51,43	51,81	42,87	0,00
L 31	39,19	39,87	33,42	35,30	34,65	36,94	45,04	54,96	59,39	57,22	57,44	57,38	56,49	57,19	48,55	45,29	44,30	46,69	48,24	63,95	62,06	56,57	47,23	38,40

Datos elaborados por OMIE de acuerdo con la Disp. Adicional Quinta de la Orden ITC/1659/2009, de 22 de junio

Figure 4.8. Price of the energy in March 2014. (Source: OMIE)

Table 4.3. Microgrid emulation equipment

Microgrid Component	Nominal Value
Electronic Source (POWERBOX)	$P = 6000$ W
Electronic Load (AMREL)	$P = 2500$ W

4.4.2.2 Linear State Space Model of the Plant

The dynamic of the state variables, which are the level of the storage systems, is given by equations (4.5) and (4.81):

$$SOC_\alpha(t_{k+1}) = SOC_\alpha(t_k) + \frac{\eta_{ch,\alpha} \cdot P_{ch,\alpha}(t_k) \cdot T_s}{C_\alpha} + \frac{P_{dis,\alpha}(t_k) \cdot T_s}{\eta_{dis,\alpha} \cdot C_\alpha}\Bigg|_{\alpha=bat,uc} \tag{4.5}$$

$$LOH(t_{k+1}) = LOH(t_k) + \varsigma_{elz} \cdot P_{elz}(t_k) \cdot \delta_{elz}(t_k) \cdot T_s - \frac{P_{fc}(t_k) \cdot \delta_{fc}(t_k) \cdot T_s}{\varsigma_{fc}} \tag{4.6}$$

4.4.3 Day-Ahead Market MPC

The purpose of the Day-Ahead market is to handle electricity transactions for the following day through the presentation of electricity sale and purchase bids by market participants. Bids made by sellers are presented to the market operator and will be included in a matching procedure that will affect the daily programming schedule corresponding to the following day. The market operator matches electricity power purchase and sale bids (received before 10 a.m. on each day). As can be seen in figure 4.7 the outputs of the controllers are the reference power values for all the ESS, for each hour of the day. The ultracapacitor ESS does not have enough energy density to schedule long-term control horizon so it is not considered. Therefore, the following cost function is minimized (using $T_s = 1\ h$ as sample period):

$$J = \sum_{h_i=1}^{24} \left(J_{grid}(h_i) + J_{bat}(h_i) + J_{elz}(h_i) + J_{fc}(h_i)\right) \tag{4.7}$$

4.4.3.1 Grid Cost Function

The cost function of the grid is given by the economic revenue of selling energy to the grid or by the economic cost of buying energy from the grid.

$$J_{grid} = \sum_{h_i=1}^{24} \left(-\Gamma_{sale}^{DM}(h_i) \cdot P_{sale}(h_i) + \Gamma_{pur}^{DM}(h_i) \cdot P_{pur}(h_i)\right) \cdot T_s \tag{4.8}$$

where the sale and purchase of energy with the grid are expressed with equations (4.9) and (4.10) replacing subscripts α, β and γ with $\alpha = sale$, $\beta = pur$ and $\gamma = grid$.

$$P_\alpha(t_k) = \begin{cases} P_\gamma(t_k) & P_\gamma(t_k) \geq 0 \\ 0 & P_\gamma(t_k) < 0 \end{cases} \tag{4.9}$$

$$P_\beta(t_k) = \begin{cases} 0 & P_\gamma(t_k) > 0 \\ P_\gamma(t_k) & P_\gamma(t_k) \leq 0 \end{cases} \tag{4.10}$$

These piecewise functions are introduced in the MPC controller using the transformation explained by Bemporad and Morari [198] resulting in the MLD constraints expressed in the inequalities (4.37)-(4.41). All the constraints of the controller are exposed in section 4.4.6.

4.4.3.2 Batteries Cost Function

Battery manufacturers quantify the life of this ESS as a function of the number of the charge and discharge cycles. In order to take into account the degradation issues associated with batteries, Arora *et al.* in the study [70] model the batteries degradation like function of a film growing (ι), which increases the internal resistance of the lithium ion battery (see equation 3.37). This depends on the battery current and a series of constant parameters which depend on the battery. In order to take this fact into account, a second term is introduced in the cost function associated to the battery where the cost does not only depend on the cycle used but it also quantifies this film growing.

$$\begin{aligned} J_{bat} = \sum_{h_i=1}^{24} \Bigg(& \frac{\mathrm{CC}_{bat}}{2 \cdot \mathrm{Cycles}_{bat}} P_{bat,ch}(h_i) \cdot T_s \cdot \eta_{bat,ch} \\ & + \mathrm{Cost}_{degr,ch} \cdot P_{bat,ch}^2(h_i) \\ & + \frac{\mathrm{CC}_{bat}}{2 \cdot \mathrm{Cycles}_{bat}} \frac{P_{bat,dis}(h_i) \cdot T_s}{\eta_{dis,bat}} \\ & + \mathrm{Cost}_{degr,dis} \cdot P_{bat,dis}^2(h_i) \Big) \end{aligned} \tag{4.11}$$

The charge and discharge of the batteries can be expressed with equations (4.9) and (4.10) replacing subscripts α, β and γ with $\alpha = ch$, $\beta = dis$ and $\gamma = bat$. Similar assumptions can be done with the ultracapacitor. These expressions result in the constraints expressed in (4.42)-(4.46).

4.4.3.3 Hydrogen Cost Function

Electrolyzer and fuel cell manufacturers give the lifetime expression of these kinds of systems as a function of the number of life hours. Start up and shut down cycles and fluctuating load conditions can seriously affect these devices, as explained in Chapter 3. In the same way, in the case of the batteries, the operation and maintenance cost is minimum, but in this kind of ESS it must be considered.

$$\begin{aligned} J_{elz}(h_i) = &\left(\frac{\text{CC}_{elz}}{\text{Hours}_{elz}} + \text{Cost}_{o\&m,elz}\right)\delta_{elz}(h_i) + \\ &\text{Cost}_{startup,elz}\cdot\sigma^{on}_{elz}(h_i) + \text{Cost}_{shutdown,elz}\cdot\sigma^{off}_{elz}(h_i) \\ &+ \text{Cost}_{degr,elz}\cdot\vartheta^2_{elz}(h_i) \end{aligned} \tag{4.12}$$

$$\begin{aligned} J_{fc}(h_i) = &\left(\frac{\text{CC}_{fc}}{\text{Hours}_{fc}} + \text{Cost}_{o\&m,fc}\right)\delta_{fc}(h_i) + \\ &\text{Cost}_{startup,fc}\cdot\sigma^{on}_{fc}(h_i) + \text{Cost}_{shutdown,fc}\cdot\sigma^{off}_{fc}(h_i) \\ &+ \text{Cost}_{degr,fc}\cdot\vartheta^2_{fc}(h_i) \end{aligned} \tag{4.13}$$

In equations (4.12) and (4.13), a series of auxiliary logical variables have been introduced. The start-up ($\sigma^{on}_j(t_k)$) and shut-down ($\sigma^{off}_j(t_k)$) states for the electrolyzer and the fuel cell are defined by the equations (4.14) and (4.15).

$$\sigma^{on}_j(t_k) = max(\delta_j(t_k) - \delta_j(t_{k-1}), 0)|_{j=elz,fc} \tag{4.14}$$

$$\sigma^{off}_j(t_k) = max(\delta_j(t_{k-1}) - \delta_j(t_k), 0)|_{j=elz,fc} \tag{4.15}$$

Using the Karnaugh map rules, these equations can be expressed as logical relationships:

$$\sigma^{on}_j(t_k) = \delta_j(t_k) \wedge (\sim \delta_j(t_{k-1}))|_{j=elz,fc} \tag{4.16}$$

$$\sigma^{off}_j(t_k) = \delta_j(t_{k-1}) \wedge (\sim \delta_j(t_k))|_{j=elz,fc} \tag{4.17}$$

Using the relationships defined by Bemporad [198], the next inequalities are introduced in the constraints of the MPC controller (4.47)-(4.52). The logical power variation $\vartheta_j(t_k)$ for the electrolyzer and the fuel cell is defined by the power variation in all the instants apart from those where the device is started up or shut down, this casuistic is defined with equation (4.18).

$$\vartheta_j(t_k) = \Delta z(t_k)\cdot(\delta_j(t_k) \wedge \delta_j(t_{k-1}))|_{j=elz,fc} \tag{4.18}$$

where the logical power $z(t_k)$ (equation 4.19) of each device can be defined as the product of the power reference value and the logical on/off state resulting in the introduction of MLD constraints in the controller cited in the expressions (4.53)-(4.55):

$$z_j(t_k) = P_j(t_k) \cdot \delta_j(t_k)|_{j=elz,fc} \tag{4.19}$$

A new auxiliary variable called logic state of degradation by power variation ($\chi_j(t_k)$) is defined, resulting in the constraints expressed in inequalities (4.56)-(4.58). Equation (4.18) gives as result the MLD constrains (4.59)-(4.61).

$$\chi_j(t_k) = (\delta_j(t_k) \wedge \delta_j(t_{k-1})) \tag{4.20}$$

The constraint introduced in (4.47) avoids the fuel cell and electrolyzer working at the same time.

4.4.4 Intraday Market MPC

The purpose of the intraday market is to respond, through the presentation of electricity power sale and purchase bids by market participants, to adjustments made to the Final Viable Daily Schedule. It is structured into different sessions. Market participants may only participate for the hourly periods corresponding to those included in the daily market in which they have participated [193]. In order to simplify the block diagram (Figure 4.7) only the first session has been included in the figure. In a similar way that the Daily Market outputs are considered as inputs for the Intraday Market MPC, the inputs of the rest of sessions correspond with the outputs of the previous session. The sample period used for this control level is $T_s = 1h$.

$$\begin{aligned} J_{grid}(h_i) = &-\Gamma^{DM}_{sale}(h_i) \cdot P^{sch}_{sale}(h_i) + \Gamma^{DM}_{pur}(h_i) \cdot P^{sch}_{pur}(h_i) \\ &+ \Gamma^{IM}_{sale}(h_i) \cdot P^{IM}_{sale}(h_i) \cdot \delta_{grid}(h_i) \\ &- \Gamma^{IM}_{pur}(h_i) \cdot P^{IM}_{pur}(h_i)) \cdot \delta_{grid}(h_i) \end{aligned} \tag{4.21}$$

$$\delta_{grid}(t_k) = \begin{cases} 1 & P^{sch}_{grid}(t_k) \neq 0 \\ 0 & P^{sch}_{grid}(t_k) = 0 \end{cases} \tag{4.22}$$

The intraday market control algorithm can only participate in those instants when energy exchange exists with the grid in the day-ahead market. This is done with the introduction of the logical variable $\delta_{grid}(t_k)$. The product of logical and dynamic variables resulting in the introduction of the auxiliary variables z_{sale} and z_{pur} with the constrains (4.53)-(4.55).

$$P_{grid}(h_i) = P^{sch}_{sale}(h_i) - P^{sch}_{pur}(h_i) + z_{sale}(h_i) - z_{pur}(h_i) \tag{4.23}$$

Taking into account the considerations made for the intraday market level control of the microgrid, the next global cost function is introduced whose schedule horizon (SH) is given by the prediction horizon of each intraday session. Cost functions defined for the batteries, the electrolyzers and the fuel cells in the Daily Market MPC (equations (4.11)-(4.13)) are also valid in the Intraday Market MPC.

$$J = \sum_{h_i=1}^{SH} \left(J_{grid}(h_i) + J_{bat}(h_i) + J_{elz}(h_i) + J_{fc}(h_i) \right) \tag{4.24}$$

4.4.5 Regulation Service Market MPC

Regulation Service helps to match generation and load and adjusts generation output to maintain the desired frequency. There is a penalty deviation cost used as an incentive for market participants to maintain their power balance. The importance of the reference levels marked for each ESS in every hour must be taken into account of by the previous MPC controllers. MPC is executed every ten minutes with a prediction horizon of 3 hours discretized in periods of 10 minutes to track the reference set by the previous MPC using receding horizon. There is a reserved hydrogen storage band of $1Nm^3$ amplification, that is not used in the rest of controllers in order to manage bad forecast scenarios.

$$\begin{aligned} J(h_i, m_j) = & J^{RM}_{grid}(h_i, m_j) + J^{RM}_{uc}(h_i, m_j) \\ & + J^{RM}_{bat}(h_i, m_j) + J^{RM}_{H_2}(h_i, m_j) \end{aligned} \tag{4.25}$$

In the next subsections, equation (4.25) will be particularized for each ESS.

4.4.5.1 Grid Cost Function

The cost function of the grid is given by (4.26).

$$\begin{aligned} & J^{RM}_{grid}(t_k) = \\ & \sum_{j=1}^{j=18} \left(\Gamma^{RM}_{up,reg}(t_{k+j}) \cdot \left(P_{grid}(t_{k+j}) - P^{sch}_{grid}(t_{k+j}) \right) \cdot \delta_{up,reg}(t_{k+j}) \right. \\ & \left. - \Gamma^{RM}_{down,reg}(t_{k+j}) \cdot \left(P_{grid}(t_{k+j}) - P^{sch}_{grid}(t_{k+j}) \right) \cdot \delta_{down,reg}(t_{k+j}) \right) \end{aligned} \tag{4.26}$$

where,

$$\delta_{up,reg}(h_i, m_j) = \begin{cases} 1 & (P_{grid}(h_i, m_j) - P^{sch}_{grid}(h_i)) \geq 0 \\ 0 & (P_{grid}(h_i, m_j) - P^{sch}_{grid}(h_i)) < 0 \end{cases} \tag{4.27}$$

$$\delta_{down,reg}(h_i, m_j) = \begin{cases} 0 & (P_{grid}(h_i, m_j) - P^{sch}_{grid}(h_i)) \geq 0 \\ 1 & (P_{grid}(h_i, m_j) - P^{sch}_{grid}(h_i)) < 0 \end{cases} \tag{4.28}$$

This expression results in the introduction of constraints (4.62)-(4.65) in the MPC controller.

4.4.5.2 Ultracapacitor Cost Function

The ultracapacitor cost function is included to always maintain the ultracapacitor available to balance the energy surplus or deficit between the long-term and the short-term, keeping the ultracapacitor in an intermediate state of charge. This way to control the ultracapacitor avoids also the degradation due to overcharge and undercharge associated to the ultracapacitor (see Chapter 3).

$$J_{uc}(t_k) = \sum_{j=1}^{18} \left(w_{uc} \cdot \left(SOC_{uc}(t_{k+j}) - SOC_{uc}^{ref} \right)^2 \right) \tag{4.29}$$

4.4.5.3 Batteries Cost Function

The functional cost of the regulation service made by the battery is the deviation at the end of the short-term horizon prediction (3 hour) discretized in six periods of ten minutes in the short-term MPC. Note that this deviation is taken only at the end of the control horizon. The aspects concerning the batteries degradation must also be considered by the controller.

$$\begin{aligned} & J_{bat}(t_k) = \\ & w_{bat} \cdot \left(SOC_{bat}(t_{k+18}) - SOC_{bat}^{sch}(t_{k+18}) \right)^2 \\ & + \frac{1}{6} \sum_{j=1}^{j=18} \left(\frac{\mathrm{CC}_{bat}}{2 \cdot \mathrm{Cycles}_{bat}} \left(\frac{P_{bat,dis}(t_{k+j})}{\eta_{dis,bat}} \right. \right. \\ & \left. + P_{bat,ch}(t_{k+j}) \cdot \eta_{bat,ch} \right) \\ & + \mathrm{Cost}_{degr,dis} \cdot P_{bat,dis}^2(t_{k+j}) \\ & \left. + \mathrm{Cost}_{degr,ch} \cdot P_{bat,ch}^2(t_{k+j}) \right) \end{aligned} \tag{4.30}$$

4.4.5.4 Hydrogen Cost Function

The functional cost of the use of hydrogen ESSs in the regulation market level control is a penalty deviation from the final instant of the control horizon com-

bined to the aspects of degradation and useful cost of this system.

$$
\begin{aligned}
& J_{H_2}(t_k) = \\
& w_{H_2} \cdot \left(LOH(t_{k+18}) - LOH^{sch}(t_{k+18})\right)^2 \\
& + \sum_{j=1}^{j=18} \left(\frac{1}{6} \left(\frac{\mathrm{CC}_{elz}}{\mathrm{Hours}_{elz}} + \mathrm{Cost}_{o\&m,elz} \right) \delta_{elz}(t_{k+j}) \right. \\
& + \mathrm{Cost}_{startup,elz} \cdot \sigma_{elz}^{on}(t_{k+j}) \\
& + \mathrm{Cost}_{shutdown,elz} \cdot \sigma_{elz}^{off}(t_{k+j}) \\
& + \mathrm{Cost}_{degr,elz} \cdot \vartheta_{elz}^2(t_{k+j}) \\
& \frac{1}{6} \left(\frac{\mathrm{CC}_{fc}}{\mathrm{Hours}_{fc}} + \mathrm{Cost}_{o\&m,fc} \right) \delta_{fc}(t_{k+j}) \\
& + \mathrm{Cost}_{startup,fc} \cdot \sigma_{fc}^{on}(t_{k+j}) \\
& + \mathrm{Cost}_{shutdown,fc} \cdot \sigma_{fc}^{off}(t_{k+j}) \\
& \left. + \mathrm{Cost}_{degr,fc} \cdot \vartheta_{fc}^2(t_{k+j}) \right)
\end{aligned}
\tag{4.31}
$$

.

4.4.6 System Constraints

4.4.6.1 Physical Constraints

Physical constraints are given by the upper and lower limits of the ESS which can absorb or supply the maximum and minimum levels of energy storage that every ESS has (main grid power exchange is also considered).

$$
\begin{aligned}
P_{pv}(t_k) + P_{wt}(t_k) - P_{load}(t_k) = P_{grid}(t_k) \\
+ z_{elz}(t_k) - z_{fc}(t_k) + P_{bat}(t_k) + P_{uc}(t_k)
\end{aligned}
\tag{4.32}
$$

$$
P_i^{min} \leq P_i(t_k) \leq P_i^{max}|_{i=grid,elz,fc,bat,uc} \tag{4.33}
$$

$$
SOC_i^{min} \leq SOC_i(t_k) \leq SOC_i^{max}|_{i=bat,uc} \tag{4.34}
$$

$$
LOH^{min} \leq LOH(t_k) \leq LOH^{max} \tag{4.35}
$$

$$
0 \leq \delta_i(t_k) \leq 1|_{i=elz,fc} \tag{4.36}
$$

4.4.6.2 MLD Constraints

The conversions introduced by Bemporad and Morari [198] make it possible to include binary and auxiliary variables introduced in an discrete-time dynamic system to describe, in a unified model, the evolution of the continuous and logic

signals of the system.

$$0 \leq \delta_{sale}(t_k) + \delta_{pur}(t_k) \leq 1 \tag{4.37}$$

$$P_{sale}(t_k) - P_{pur}(t_k) = P_{grid}(t_k) \tag{4.38}$$

$$P_{grid}^{min}\delta_{sale}(t_k) \leq P_{sale}(t_k) \leq P_{grid}^{max}\delta_{sale}(t_k) \tag{4.39}$$

$$P_{grid}(t_k) - P_{grid}^{max}(1 - \delta_{sale}(t_k)) \leq P_{sale}(t_k) \tag{4.40}$$

$$P_{sale}(t_k) \leq P_{grid}(t_k) - P_{grid}^{min}(1 - \delta_{sale}(t_k)) \tag{4.41}$$

$$0 \leq \delta_{ch,i}(t_k) + \delta_{dis,i}(t_k) \leq 1|_{i=uc,bat} \tag{4.42}$$

$$P_{ch,i}(t_k) - P_{dis,i}(t_k) = P_i(t_k)|_{i=uc,bat} \tag{4.43}$$

$$P_i^{min}\delta_{ch,i}(t_k) \leq P_{ch,i}(t_k) \leq P_i^{max}\delta_{ch,i}(t_k)|_{i=uc,bat} \tag{4.44}$$

$$P_i(t_k) - P_i^{max}(1 - \delta_{ch,i}(t_k)) \leq P_{ch,i}(t_k)|_{i=uc,bat} \tag{4.45}$$

$$P_{ch,i}(t_k) \leq P_i(t_k) - P_i^{min}(1 - \delta_{ch,i}(t_k))|_{i=uc,bat} \tag{4.46}$$

$$0 \leq \delta_{elz}(t_k) + \delta_{fc}(t_k) \leq 1 - \delta_i(t_k) + \sigma_i^{on}(t_k) \leq 0|_{i=elz,fc} \tag{4.47}$$

$$-(1 - \delta_i(t_k - 1)) + \sigma_i^{on}(t_k) \leq 0|_{i=elz,fc} \tag{4.48}$$

$$\delta_i(t_k) + (1 - \delta_i(t_k - 1)) - \sigma_i^{on}(t_k) \leq 1|_{i=elz,fc} \tag{4.49}$$

$$-\delta_i(t_k - 1) + \sigma_i^{off}(t_k) \leq 0|_{i=elz,fc} \tag{4.50}$$

$$-(1 - \delta_i(t_k)) + \sigma_i^{off}(t_k) \leq 0|_{i=elz,fc} \tag{4.51}$$

$$\delta_i(t_k - 1) + (1 - \delta_i(t_k)) - \sigma_i^{off}(t_k) \leq 1|_{i=elz,fc} \tag{4.52}$$

$$P_i^{min}\delta_i(t_k) \leq z_i(t_k) \leq P_i^{max}\delta_i(t_k)|_{i=pur,sale,elz,fc} \tag{4.53}$$

$$P_i(t_k) - P_i^{max}(1 - \delta_i(t_k)) \leq z_i(t_k)|_{i=pur,sale,elz,fc} \tag{4.54}$$

$$z_i(t_k) \leq P_i(t_k) - P_i^{min}(1 - \delta(t_k))|_{i=pur,sale,elz,fc} \tag{4.55}$$

$$-\delta_i(t_k) + \chi_i(t_k) \leq 0|_{i=elz,fc} \tag{4.56}$$

$$-\delta_i(t_{k-1}) + \chi_i(t_k) \leq 0|_{i=elz,fc} \tag{4.57}$$

$$\delta_i(t_k) + \delta_i(t_{k-1}) - \chi_i(t_k) \leq 1|_{i=elz,fc} \tag{4.58}$$

$$\Delta z_i^{min}(\chi_i(t_k)) \leq \vartheta_i(t_k) \leq \Delta z_i^{max}(\chi_i(t_k))|_{i=elz,fc} \tag{4.59}$$

$$\Delta z_i(t_k) - \Delta z_i^{max}(1 - \chi_i(t_k)) \leq \vartheta_i(t_k)|_{i=elz,fc} \tag{4.60}$$

$$\vartheta_i(t_k) \leq \Delta z_i(t_k) - \Delta z_i^{min}(1 - \chi_i(t_k))|_{i=elz,fc} \tag{4.61}$$

$$(P_{grid}(h_i, m_j) - P_{grid}^{sch}(h_i)) \leq P_{grid}^{max} - P_{grid}^{max} \cdot \delta_{down}(t_k) \tag{4.62}$$

$$(P_{grid}(h_i, m_j) - P_{grid}^{sch}(h_i)) \geq \epsilon + (-\epsilon) \cdot \delta_{down}(t_k) \tag{4.63}$$

$$-(P_{grid}(h_i, m_j) - P_{grid}^{sch}(h_i)) \leq P_{grid}^{max} - P_{grid}^{max} \cdot \delta_{up}(t_k) \tag{4.64}$$

$$-(P_{grid}(h_i, m_j) - P_{grid}^{sch}(h_i)) \geq \epsilon + (-\epsilon) \cdot \delta_{up}(t_k) \tag{4.65}$$

4.5 Tertiary Model Predictive Control-Load Sharing

Several authors consider the load sharing control level as a part of the secondary control of the microgrid. Here, it is considered as the last part of the tertiary control level of the microgrid. This controller is explained in a separated section because as it will be explained, some variables must be defined in a different way. In figure 4.9, the block diagram for the MPC Controller is shown. The controller receives as reference the energy and power reference scheduled by the economical dispatch of the microgrid for the batteries, the electrolyzer and the fuel cell, as well as, the energy exchange with the main grid with the main grid, as done in previous section. Note the fact that the economical schedule gives as reference both the power reference and the energy stored by each ESS. The reason to introduce a double reference gives a freedom degree in the controller allowing to correct deficit scenario with exceeding scenario in comparison with the forecast carried out at the economical dispatch. While the last level of the economical schedule explained in previous section has a control horizon of 3 hours and a T_s =10 min, the Load Sharing MPC Controller has a control horizon of 15 s (value taken due to the start sequence of the electrolyzer) and a T_s =1 s. The use of all the cascade control sequence explained in previous section allows to manage from the long term control horizon given at the day-ahead MPC controller detailed linked to the real operational scenario object of this section. At this control level there is not an ARIMA prediction model for the

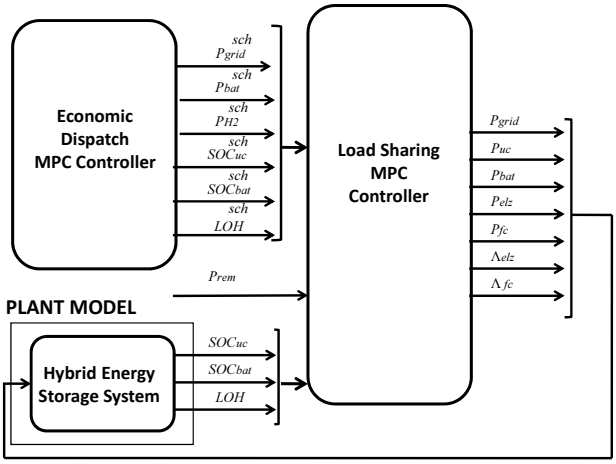

Figure 4.9. Optimal Load Sharing MPC Controller Block Diagram

remaining power P_{rem} of the microgrid. Several model of photovoltaic and wind

turbine generator, as well as load consumption of the microgrid forecast can be found in the literature. The sample time established for the controller is $T_s = 1s$. In this time-order the dynamic of the generators and the loads for the all the sample instants of the control horizon ($j = 1, 2, ..., 15$) can be assumed constant and equal to the sampled value. The next power prediction is introduced in the controller:

$$\begin{aligned} P_{pv}(t_{k+j}) + P_{wt}(t_{k+j}) - P_{load}(t_{k+j}) = \\ P_{pv}(t_k) + P_{wt}(t_k) - P_{load}(t_k) \end{aligned} \tag{4.66}$$

The way to calculate the state of charge of the ultracapacitor and the battery also differs from the previous section and it must be used the current value versus the power value. The model of the ultracapacitor has complex equations to be linearized as detailed in Chapter 3, but the voltage dynamic is quite lower than for the current for the selected sample time $T_s = 1$. So the aproximation considered in equation (4.67) will be included in the MPC controller. In the case of the battery, it can be concluded that for the selected sample time, equation (4.67) is also valid.

$$U_i(t_{k+1}) = U_i(t_k)|_{i=uc,bat} \tag{4.67}$$

The capacity of the ultracapacitor and the batteries can be modelled with the next equation:

$$C_i(t_{k+1}) = C_i(t_k) + (I_{ch,i}(t_{k+1}) - I_i^{dis}(t_{k+1})) \cdot T_s\big|_{i=bat,uc} \tag{4.68}$$

The relationship between the charging and discharging current and the corresponding charging and discharging power can be found.

$$I_i^{ch}(t_{k+1}) = \left.\frac{P_i^{ch}(t_{k+1}) \cdot \eta_i^{ch}}{U_i(t_k)}\right|_{i=bat,uc} \tag{4.69}$$

$$I_i^{dis}(t_{k+1}) = \left.\frac{P_i^{dis}(t_{k+1})}{U_i(t_k) \cdot \eta_i^{dis}}\right|_{i=bat,uc} \tag{4.70}$$

Finally the state of charge of the batteries is given by the next expression:

$$SOC_i(t_{k+1}) = \left.\frac{C_i(t_{k+1})}{C_i^{max}}\right|_{i=bat,uc} \tag{4.71}$$

This consideration gives as result the constraint introduced in the inequality (4.83).

4.5.1 Objective Function

The functional cost of each ESS in this control level is based on the deviation from the power references and the energy stored level from that marked by the economical dispatch of the microgrid. In order to give a freedom grade to the system the ultracapacitor is just referenced to an intermediate state of charge. In all the function cost applied to each system, degradation or anomalous working conditions are avoided, introducing these terms in the objective function of the controller as it will be explained in the following sections.

$$\begin{aligned} \min J(t_{k+1}) = J_{grid}(t_{k+1}) + J_{uc}(t_{k+1}) \\ + J_{bat}(t_{k+1}) + J_{H_2}(t_{k+1}) \end{aligned} \tag{4.72}$$

4.5.1.1 Grid Cost Function

The grid cost function is introduced in the controller giving a high penalty to the deviation of the power exchanged with the main grid $P_{grid}(t_{k+1})$ versus the contracted-schedule with the Market/System Operator.

$$J_{grid}(t_{k+1}) = \sum_{j=1}^{15} \left(w_{grid} \left(P_{grid}(t_{k+j}) - P_{grid}^{sch}(t_{k+j}) \right)^2 \right) \tag{4.73}$$

4.5.1.2 Ultracapacitor Cost Function

The cost function of the ultracapacitor is shown in equation (4.74). In order to be always available if required to compensate the rest of components of the microgrid, the ultracapacitors are kept in an intermediate state of charge. This allows also to protect them from undercharge or overcharge. The second term of the cost function is added to avoid instability points in the ultracapacitor giving a low weighting factor but giving zero as power reference value for the ultracapacitor. If this term is not included, sub-optimal problem solutions can be found overall when the power calculated by the solver is near to zero.

$$\begin{aligned} J_{uc}(t_{k+1}) = \sum_{j=1}^{15} \Big(w_{uc}^{E} \left(SOC_{uc}(t_{k+j}) - SOC_{uc}^{ref}(t_{k+j}) \right)^2 \\ + w_{uc}^{P} \cdot \left(P_{uc}(t_{k+j}) - 0 \right)^2 \Big) \end{aligned} \tag{4.74}$$

4.5.1.3 Batteries Cost Function

The batteries cost function is expressed with equation (4.75). As commented the batteries have a double reference in power and energy. In comparison with the hydrogen, batteries are more flexible due to the fact that start-up and shut-down cycles do not affect to this technology. The power tracking has a lower weight than in the case of the hydrogen while the energy tracking has a higher weight than in the case of hydrogen. With the proposal to protect the batteries from high charging/discharging current ratio, high charging/discharging current values are penalized in the third term of the cost function. The last term of the cost function penalizes the AC current in the batteries.

$$\begin{aligned} J_{bat}(t_{k+1}) = \sum_{j=1}^{15} \Big(& w_{bat}^{P} \left(P_{bat}(t_{k+j}) - P_{bat}^{sch}(t_k + j) \right)^2 \\ & + w_{bat}^{E} \left(SOC_{bat}(t_{k+j}) - SOC_{bat}^{sch}(t_{k+j}) \right)^2 \\ & + w_{bat}^{degr} \cdot \left(I_{bat}(t_{k+j}) \right)^2 \\ & + w_{bat}^{ripple} \left(\Delta I_{bat}(t_{k+j}) \right)^2 \Big) \end{aligned} \tag{4.75}$$

4.5.1.4 Hydrogen Cost Function

The hydrogen ESS is composed by the electrolyzer, the fuel cell and the metal hydride tank. The different variables to be considered in the cost function associated to the degradation states of the electrolyzer and the fuel cell have been introduced in previous sections. The electrolyzer management system (ELMS) is charged to maintain the correct water level in the separator in order to avoid drying conditions in the membrane, feeding the stack with enough water to produce the electrolysis reaction. Before the electrolyzer is in the state of hydrogen production the ELMS carries out the stages of water filling of the separators and nitrogen purge in all the gas circuit. This procedure, known as 'Start up' secuence, takes the ELMS a starting time of 10 s before it can absorb energy from the microgrid which must be considered at this time scale. In a similar way to the electrolyzer, fuel cells have also a start up sequence. During the 'stand by' state, the air fan is switched off and the hydrogen inlet valve is closed. The period required for nominal conditions to be reached is known as the start-up sequence. During start up, the fan switches on and the hydrogen inlet valve opens. During this time, no current is delivered by the fuel stack. The starting time of the fuel cell is set in 2 seconds. Due to the 'Starting-up' sequence, $\delta_i(t_k)|_{i=elz,fc}$ must be expressed as function of the logical control signal to switch on/off the devices $\Lambda_i(t_k)|_{i=elz,fc}$. The fuel cell and the electrolyzer just reach the energized

state if $\Lambda_i(t_k)|_{i=elz,fc}$ is active in all the instants of the required time $\varphi_i|_{i=elz,fc}$ for the starting sequence. The relationship between $\delta_i(t_k)|_{i=elz,fc}$ and $\Lambda_i(t_k)|_{i=elz,fc}$ is defined in equation (4.76):

$$\delta_i(t_k) = 1 \Leftrightarrow \varphi_i - \sum_{s_j=0}^{s_j=\varphi_i} \left(\Lambda_i(t_k - s_j)\right)|_{i=elz,fc} \leq 0 \tag{4.76}$$

Using the conversions defined in [198] this equation can be transformed into the constrains expressed in inequalities (4.89) and (4.90), defined in section 4.5.2.2, where the coefficients m, M and ϵ follow the notation given in [198].

The start-up ($\sigma_j^{on}(t_k)$) and shut-down ($\sigma_j^{off}(t_k)$) states for the electrolyzer and the fuel cell are defined with the equations (4.77) and (4.78).

$$\sigma_j^{on}(t_k) = max(\Lambda_j(t_k) - \Lambda_j(t_{k-1}), 0)|_{j=elz,fc} \tag{4.77}$$
$$\sigma_j^{off}(t_k) = max(\Lambda_j(t_{k-1}) - \Lambda_j(t_k), 0)|_{j=elz,fc} \tag{4.78}$$

Using the Karnaugh map rules, this equation can be expressed as a logical relationship:

$$\sigma_j^{on}(t_k) = \Lambda_j(t_k) \wedge (\sim \Lambda_j(t_{k-1}))|_{j=elz,fc} \tag{4.79}$$
$$\sigma_j^{off}(t_k) = \Lambda_j(t_{k-1}) \wedge (\sim \Lambda_j(t_k))|_{j=elz,fc} \tag{4.80}$$

Using the conversions defined by [198] the next inequatilies are introduced in the constraints of the MPC controller (4.91)-(4.96), defined in section 4.5.2.2. The dynamic of the metal hydride tank is instantaneous for the selected sample time, so the level of hydrogen in the tank can be modelled as follows:

$$\begin{aligned} LOH(t_{k+1}) = LOH(t_k) + \varsigma_{elz} \cdot P_{elz}(t_k) \cdot \delta_{elz}(t_k) \cdot T_s \\ - \frac{P_{fc}(t_k) \cdot \delta_{fc}(t_k) \cdot T_s}{\varsigma_{fc}} \end{aligned} \tag{4.81}$$

The hydrogen cost function is defined by the equation (4.82). As well as in the case of the batteries, the economical dispatch of the microgrid gives both references the schedule in energy and in power at each instant. In order to protect from the main causes of degradation, the start up and shut down states are penalized in the controller. As commented in previous section in the cost function the power fluctuation is penalty in all the states, but when the fuel cell

or the electrolyzer change the state from start up to energized state.

$$\begin{aligned} J_{H_2}(t_{k+1}) = \sum_{j=1}^{15} \Big(& w_{tank}^{E} \left(LOH(t_{k+j}) - LOH^{sch}(t_{k+j}) \right)^2 \\ & + w_{elz}^{P} \left(z_{elz}(t_{k+j}) - z_{elz}^{sch}(t_{k+j}) \right)^2 \\ & + w_{fc}^{P} \left(z_{fc}(t_{k+j}) - z_{fc}^{sch}(t_{k+j}) \right)^2 \\ & + w_{elz}^{ripple} \left(\vartheta_{elz}(t_{k+j}) \right)^2 + w_{fc}^{ripple} \left(\vartheta_{fc}(t_{k+j}) \right)^2 \\ & + w_{elz}^{startup} \cdot \sigma_{elz}^{on}(t_{k+1}) + w_{elz}^{shutdown} \cdot \sigma_{elz}^{off}(t_{k+j}) \\ & + w_{fc}^{startup} \cdot \sigma_{fc}^{on}(t_{k+j}) + w_{fc}^{shutdown} \cdot \sigma_{fc}^{off}(t_{k+j}) \Big) \end{aligned} \tag{4.82}$$

where the variables z and ϑ_{elz} were introduced in section 4.4.3.3 with their associated MLD constraints.

4.5.2 System Constraints

4.5.2.1 Physical constraints

Physical constraints are given by the upper and lower limit power than the ESS can absorbe or supply or the maximum and minimum level of energy storage that every ESS has got (main grid power exchange is also considered).

$$\begin{aligned} P_{pv}(t_k) + P_{wt}(t_k) - P_{load}(t_k) = P_{grid}(t_{k+j}) + z_{elz}(t_{k+j}) \\ - z_{fc}(t_{k+j}) + P_{bat}(t_{k+j}) + P_{uc}(t_{k+j})|_{j=1,\dots,15} \end{aligned} \tag{4.83}$$

$$\Delta P_i^{min} \leq \Delta P_i(t_k) \leq \Delta P_i^{max}|_{i=elz,fc} \tag{4.84}$$

$$P_i^{min} \leq P_i(t_k) \leq P_i^{max}|_{i=grid,elz,fc,bat,uc} \tag{4.85}$$

$$SOC_i^{min} \leq SOC_i(t_k) \leq SOC_i^{max}|_{i=bat,uc} \tag{4.86}$$

$$LOH^{min} \leq LOH(t_k) \leq LOH^{max} \tag{4.87}$$

$$0 \leq \Lambda_i(t_k) \leq 1|_{i=elz,fc} \tag{4.88}$$

4.5.2.2 MLD constraints

The conversions introduced by Bemporad and Morari [198] makes it possible to include binary and auxiliary variables introduced into a discrete-time dynamic system in order to describe in a unified model the evolution of the continuous and logic signals of the system. As explained the MLD constraints associated to

z and ϑ_{elz} must be also considered (see section 4.4.6.2).

$$\varphi_i - \sum_{s_j=0}^{s_j=\varphi_i} (\Lambda_i(t_k - s_j)) \leq M - M\delta_i|_{i=elz,fc} \tag{4.89}$$

$$\varphi_i - \sum_{s_j=0}^{s_j=\varphi_i} (\Lambda_i(t_k - s_j)) \geq \epsilon + (m - \epsilon)\delta_i|_{i=elz,fc} \tag{4.90}$$

$$-\Lambda_i(t_k) + \sigma_i^{on}(t_k) \leq 0|_{i=elz,fc} \tag{4.91}$$

$$-(1 - \Lambda_i(t_{k-1})) + \sigma_i^{on}(t_k) \leq 0|_{i=elz,fc} \tag{4.92}$$

$$\Lambda_i(t_k) + (1 - \Lambda_i(t_{k-1})) - \sigma_i^{on}(t_k) \leq 1|_{i=elz,fc} \tag{4.93}$$

$$-\Lambda_i(t_{k-1}) + \sigma_i^{off}(t_k) \leq 0|_{i=elz,fc} \tag{4.94}$$

$$-(1 - \Lambda_i(t_k)) + \sigma_i^{off}(t_k) \leq 0|_{i=elz,fc} \tag{4.95}$$

$$\Lambda_i(t_{k-1}) + (1 - \Lambda_i(t_k)) - \delta_i^{off}(t_k) \leq 1|_{i=elz,fc} \tag{4.96}$$

4.6 Experimental Results

In this section the most significant cases of each level of the MPC schedule controller will be detailed. The different cost factors utilized in the experimental results can be seen in table 4.4.

4.6.1 Day-Ahead Market

The results of the ARIMA model and the daily market MPC controller are shown in figures 4.10 and 4.12. If there is a surplus of energy, the system tries to sell energy to the grid but when there is a deficit of energy in the microgrid the system tries to use the hybrid energy storage system. The number of hours of use and the switching states of the electrolyzer and the fuel cell are minimized, as well as the peak power in the charge and discharge of the battery. The SOC of the batteries is also controlled imposing constraints on the controller protecting them from high states of charge or discharge. As can be seen in figure 4.12, the purchase of energy to the grid is done when the prices are lower, in the same way that the energy sale to the grid is done at maximum price periods. The power reference given to the fuel cell and the electrolyzer is maintained nearly constant giving minimum variation to these devices and thus minimizing degradation due to the operation of the electrolyzer and the fuel cell.

Table 4.4. Cost Factor values utilized by the MPC scheduler. Data based on the next sources [199, 200, 201]

PEM Electrolyzer
$\varsigma = 0.23\ Nm^3/kWh$, CC= 8.22 €/$kW$, $\text{Cost}_{o\&m,elz} = 2\ m€/h$
$\text{Cost}_{startup,elz} = 0.123$ €, $\text{Cost}_{shutdown,elz} = 0.0062$ €
$\text{Cost}_{degr,elz} = 0.05$ €/W, Lifetime= 10000 hours
PEM Fuel Cell
$\varsigma = 1.320\ kWh/Nm^3$, CC=30 €/$kW$, $\text{Cost}_{o\&m,fc} = 1\ m€/h$
$\text{Cost}_{startup,fc} = 0.01$ €, $\text{Cost}_{shutdown,fc} = 0.005\ m€$,
$\text{Cost}_{degr,fc} = 0.01$ €/W, Lifetime= 10000 hours
Batteries
$\eta_{ch} = 0.90$, $\eta_{dis} = 0.95$, CC=125 €/kWh, Life cycles=3000,
$\text{Cost}_{degr,dis} = 10^{-9}$ €/W^2h, $\text{Cost}_{degr,ch} = 10^{-9}$ €/W^2h
Ultracapacitor
$\eta_{ch} = 0.97$, $\eta_{dis} = 0.99$

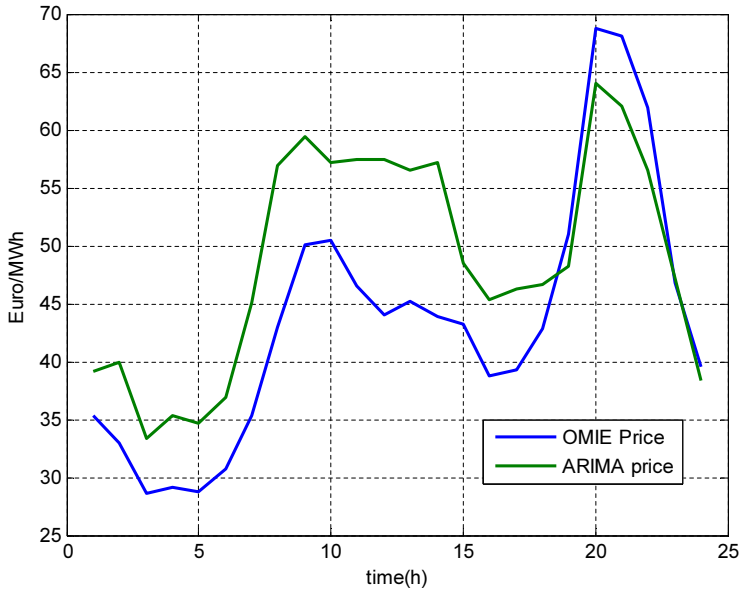

Figure 4.10. Comparison between the energy price data given by OMIE and the ARIMA model

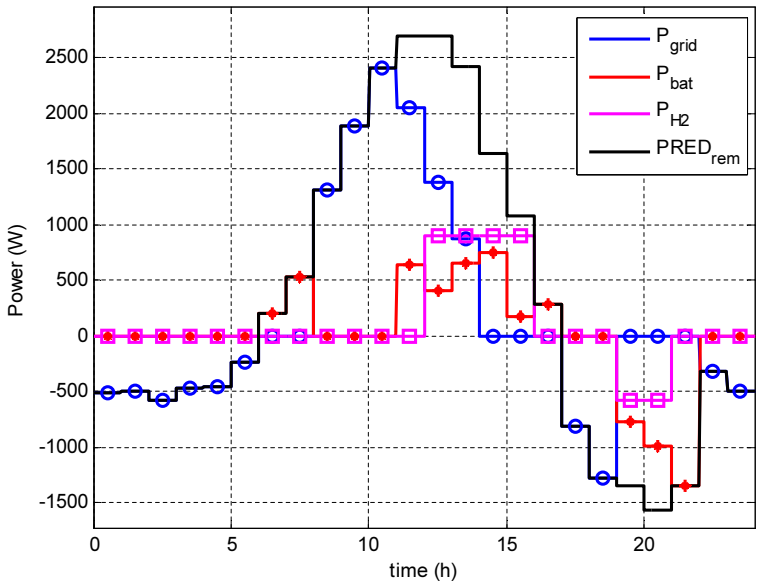

Figure 4.11. Daily market MPC controller schedule

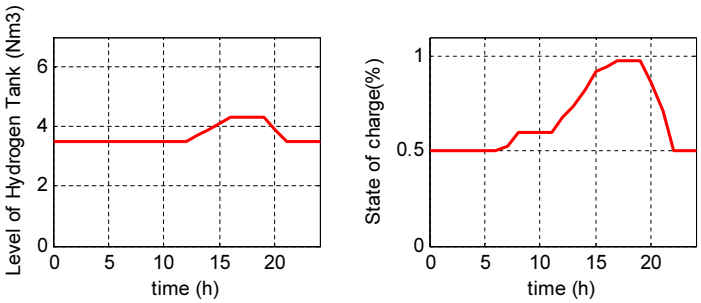

Figure 4.12. Evolution of the state variables LOH and SOC at the Daily Market

4.6.2 Intraday Market

The ARIMA-forecast model results are more accurate when the prediction horizon is lower. For the selected day, a bad forecast scenario is given for the daily market session (38 hours ahead) but this is corrected in the medium term horizon (28 hours ahead) given in the first session of the intraday market. A new schedule is given for the first session of the intraday market as shown in figure 4.13 where the price forecast is based on the results of the previous session of the market. Respecting degradation issues and the different constraints of each ESS, the economic benefit of the microgrid is given, shifting the hours of energy storage to a time when the prices are lower than the price forecast scenario of the daily market. Although the horizon prediction of the remaining power would be shorter, the renewable energy prediction and the load forecast are always subject to errors. The rest of the control levels of the microgrid must manage these kinds of events so as not to generate economic losses in the microgrid at a time when degradation issues for the different ESS are considered.

Two cases are shown for the intraday market algorithm results: the surplus scenario and the deficit scenario shown infigures 4.13 and 4.15, with the evolution of the state variables for both cases (Figures 4.14 and 4.16). The total energy exchange with the main grid is given, adding the results of the daily market (cyan) and the intradaily market (blue). Note that in the surplus case, the maximum price value for the intraday market can be different to the daily market, so the maximum power sale of the intraday market must be carried out at this moment. A re-schedule of the energy stored is done according to the new prediction data. Note that for the case of the deficit scenario, energy must be purchased in the intraday market to fulfill the schedule in the daily market.

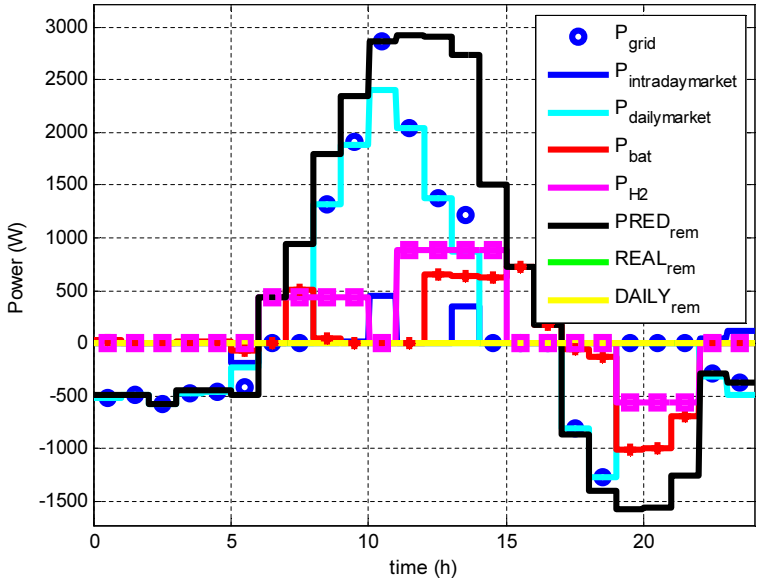

Figure 4.13. Intraday market MPC controller schedule in surplus scenario

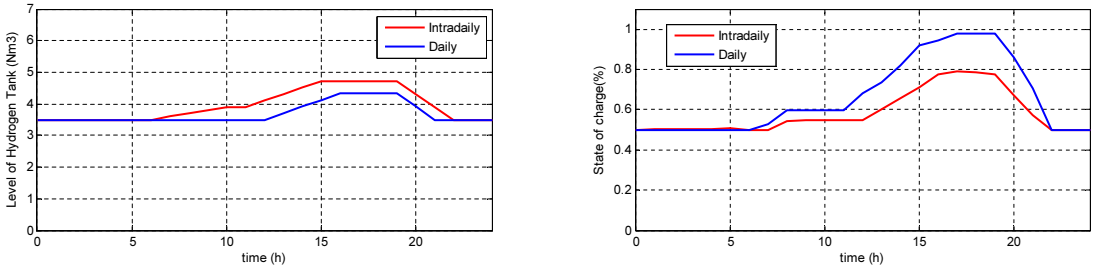

Figure 4.14. Day-Ahead and intraday market MPC controller schedule level for LOH and SOC in surplus scenario

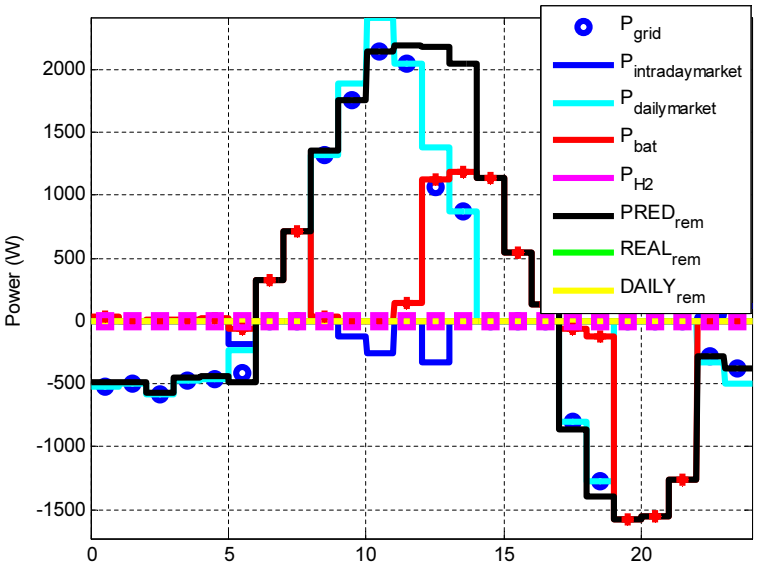

Figure 4.15. Intraday market MPC controller schedule in deficit scenario

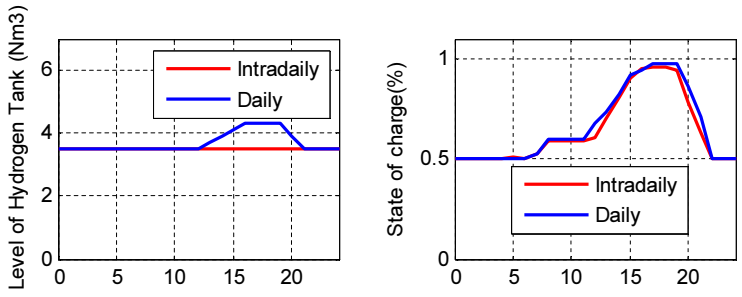

Figure 4.16. Day-Ahead and intraday market MPC controller schedule level for LOH and SOC in deficit scenario

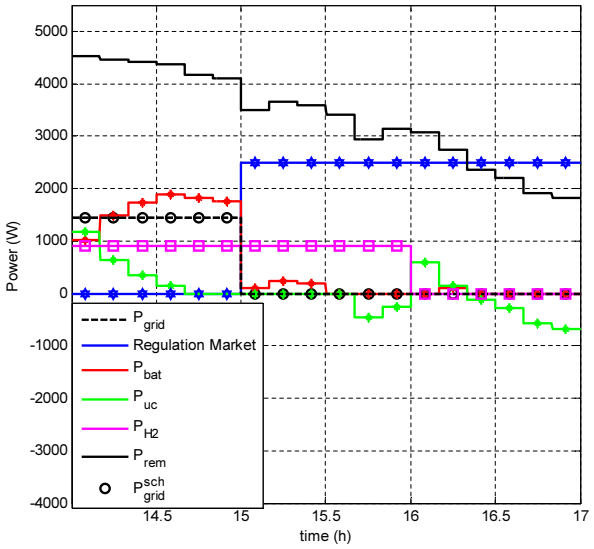

Figure 4.17. Regulation service market MPC controller schedule level. Case of Regulation with the grid

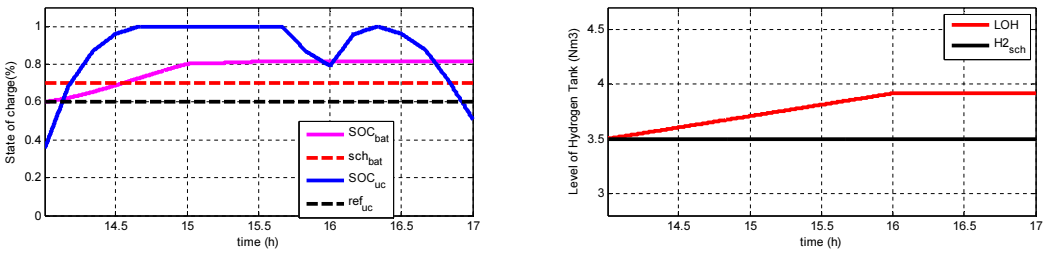

Figure 4.18. Regulation service market MPC controller schedule level. Case of Regulation with the grid. Evolution of the state variables of the microgrid

4.6.3 Regulation Service Market

The Regulation Service MPC is the last schedule control level before the real scenario optimal load sharing. It is launched every ten minutes with a control horizon of 3 hours in order to ensure the schedule is going to be reached. The short term horizon of this controller includes the action of the ultracapacitor ESS. As can be seen in figure 4.17, the algorithm gives a constant reference for the electrolyzer for all the working hours minimizing the degradation effects. Depending on regulation prices, the down-regulation/up-regulation with the main grid can be maximized or minimized but must be kept constant during 2 hours. The peak current charge of the batteries is also minimized which offers a smooth current profile to this kind of ESS. The ultracapacitor ESS is maintained over the reference SOC and the level of stored energy in batteries and hydrogen is followed (see figure 4.18). Although the MPC is designed to minimize the schedule variation with the grid but the grid requires it in the exposed figure 4.17 and 4.18 is manifested that when it is required because the level of stored energy it too high or too low respect of the schedule the MPC controller active the energy exchange with the main grid.

4.6.4 Load Sharing

Real operational scenario in renewable energy microgrids differs from the forecast developed by the economic dispatch, having to achieve the contracted schedule carried out with the grid Market/System operator. This MPC controller is charged to follow the schedule carried out protecting the hybrid ESS. The different weighting factors and constraint limits of the different components of the microgrid managed by the controller are exposed in table 4.5. The weigthing factor assignment criterion has been that the maximum weight is given to the schedule tracking with the main grid. The second level in power tracking importance is given to the hydrogen ESS in order to minimize the number of working hours, although the energy tracking has an order below the energy tracking respect the battery. In the degradation costs the biggest importance is given to the hydrogen technologies, followed by the battery and finally the ultracapacitor.

In figure 4.19, are shown the power scheduled for each component of the microgrid as result of the economical dispatch MPC controller. In figures 4.20 and 4.21, the results of a 24 hour-experimental test applied to the controller can be observed. It corresponds with the 31th of March of 2014. This day was selected because the weather profile had periods of wind early in the morning, was cloudy in the noon and sunny in the evening As can be seen in the figure 4.21, due to the stochastic behaviour of the renewable energy resources only the

Table 4.5. Constraints Limits and Weighting Factors Imposed to the Controller

Microgrid Component	**Controller's Values**
Grid	$P_{grid}^{max} = 6000$ W, $P_{grid}^{min} = -2500$ W, $w_{grid}^{P} = 10^{10}/(P_{grid}^{max})^2$
Ultracapacitor	$P_{uc}^{max} = 3000$ W, $P_{uc}^{min} = -3000$ W, $SOC_{uc}^{max} = 1p.u.$ $SOC_{uc}^{min} = 0.1p.u.$ $w_{uc}^{P} = 1/(P_{uc}^{max})^2$, $w_{uc}^{E} = 10^8$ $SOC_{uc}^{ref} = 0.5$
Electrolyzer	$P_{elz}^{max} = 900$ W, $P_{elz}^{min} = 300$ W, $w_{elz}^{P} = 10^7/(P_{elz}^{max})^2$ $\Delta P_{elz}^{max} = 20$ W, $\Delta P_{elz}^{min} = -20$ W, $w_{elz}^{ripple} = 10^9/(P_{elz}^{max})^2$ $w_{elz}^{startup} = 10^6$, $w_{elz}^{shutdown} = 10^{10}$
Fuel Cell	$P_{fc}^{max} = 750$ W, $P_{fc}^{min} = 300$ W, $\Delta P_{fc}^{max} = 10$ W, $\Delta P_{fc}^{min} = -10$ W, $w_{fc}^{P} = 10^7/(P_{fc}^{max})^2$ $w_{fc}^{ripple} = 10^9/(P_{fc}^{max})^2$ $w_{fc}^{startup} = 10^6$, $w_{fc}^{shutdown} = 10^{10}$
Metal Hydride	$LOH^{max} = 7$ Nm^3, $LOH^{min} = 0$ Nm^3 $w_{tank}^{E} = 10^6/(LOH^{max})^2$
Pb-Acid Battery	$P_{bat}^{max} = 2500$ W, $P_{bat}^{min} = -2500$ W $SOC_{bat}^{max} = 1p.u.$ $SOC_{bat}^{min} = 0.2p.u.$ $w_{bat}^{P} = 10^2/(P_{bat}^{max})^2$, $w_{bat}^{E} = 10^8$ $w_{bat}^{degr} = 10^5/(P_{bat}^{max}/U_{bat}^{nom})^2$, $w_{bat}^{ripple} = 10^4/(P_{bat}^{max})^2$

power schedule applied to the grid is followed exactly at all the instants of the day. The day begun with smooth power variations due to the wind, as can be seen from 0-5h, a smooth power profile is demanded to the batteries while the power fluctuations are absorbed by the ultracapacitor while its state of charge is maintained over SOC_{uc}^{ref} given by the controller. In the period from 5h to 6h high power fluctuations in the P_{rem} of the microgrid where found while the

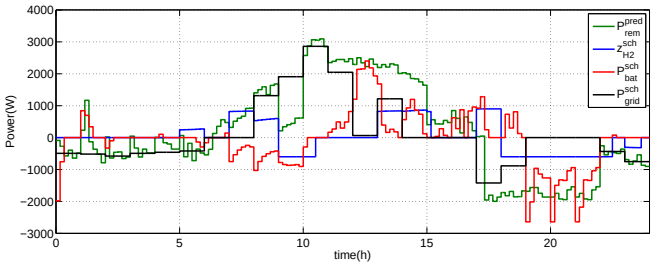

Figure 4.19. Schedule carried out in the economical dispatch MPC controller

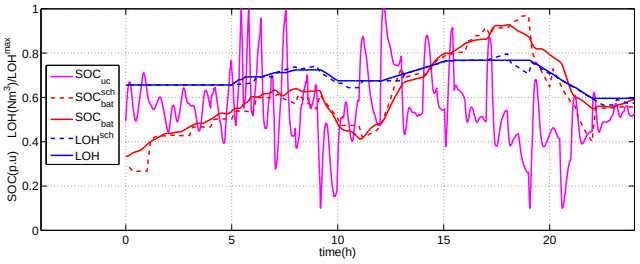

Figure 4.20. Experimental results of the evolution of the state variables SOC_{uc}, SOC_{bat} and LOH

electrolyzer was scheduled to be actived. As can be observed in this period, the ultracapacitor absorbes the highest requirement in power fluctuations. A smoother power profile is demanded to the battery, while the start-up and shut-down cycles of the electrolyzer are minimized. This can be overall observed at 5.45 when although the remaining power of the microgrid is decreasing the electrolyzer shut down is delayed until 6.00. In a similar way, the control system is able to start up the electrolyzer although it was not scheduled at 6.30 in order to minimize P_{bat}^{ch} at this moment. Although high changes in the remaining power profile appear at 7.00 the electrolyzer is smoothly shut down and the power battery is smoothly changed while all the power oscillation is absorbed by the ultracapacitor. In all the cases, although high power oscillations exist, the schedule with the grid is followed satisfactory. Similar results can be observed for the cases when the fuel cell is started up, such as the period interval of 18.00 when the fuel cell start up is delayed until 19.00. At 20.30 a high load step is demanded, the MPC changes the power of the ultracapacitor and smoothly the fuel cell power and the battery. Finally the ultracapacitor is again charged to be available for the next high power step fluctuation. In figure 4.20, the evolution of the state variables SOC_{uc}, SOC_{bat} and LOH are shown. While a correct tracking in the SOC_{bat} and

LOH, high oscillations are found over the reference of SOC_{uc}. The maximum and minimum level of the state variables imposed to the controller are respected.

4.7 Comparison with other Control Methods

Every element in the microgrid has its own casuistry, constraints and cost. That imposes on the controller multiple variables to optimize and multiple constraints to fulfill. Several studies associated to the management of microgrids with hybrid storage propose the hysteresis method ([91, 92, 93]) where the hydrogen ESS is activated depending on the SOC of the batteries and the batteries are activated depending on the SOC of the ultracapacitor. But this method does not take into account the associated cost of the use of each ESS. The use of heuristical methods to solve a similar objective algorithm would have too many subcases which increases the complexity associated and makes the guarantee to find the optimal schedule difficult. This complexity is increased with the use of a high number of constraints. The use of these kinds of algorithms are appropriate when there is not a large number of variables to optimize and constraints to fulfill, but when the complexity grade of the control algorithm is elevated there is not a guarantee of reaching the optimal solution giving as results local minimums. The mathematical formulation used by MPC allows minimizing a cost function with an optimization solver guaranteeing that the optimal solution is found even in the presence of the MLD framework. The main disadvantages of the use of MPC controllers are the formulation complexity and the fact that an optimization solver package is necessary. None of the works presented in the literature have considered the degradation issues incorporated into the cost function.

In order to quantitatively evaluate the performance of the proposed controller, a comparison for the daily market schedule with three control strategies is carried out. The first strategy is based on the manual case where a fixed hybridization (FH) degree between the battery and the fuel cell is imposed. This strategy sells to the grid when the price prediction is higher than a price reference and buys from the grid when this prediction is lower than a fixed reference. The second strategy is based on the hysteresis method using also the price hysteresis band. The third strategy is based on MILP as utilized in [102, 103, 104, 105] where just operational costs without degradation issues are introduced. The result of these three strategies can be observed in figures 4.24 and 4.25 which can be compared with the results obtained for the MIQP proposed controller in figures 4.22 and 4.23. In table 4.6, several key performance indicators are detailed for each one of the strategies under study. Similar efficiency is found for the MILP and the

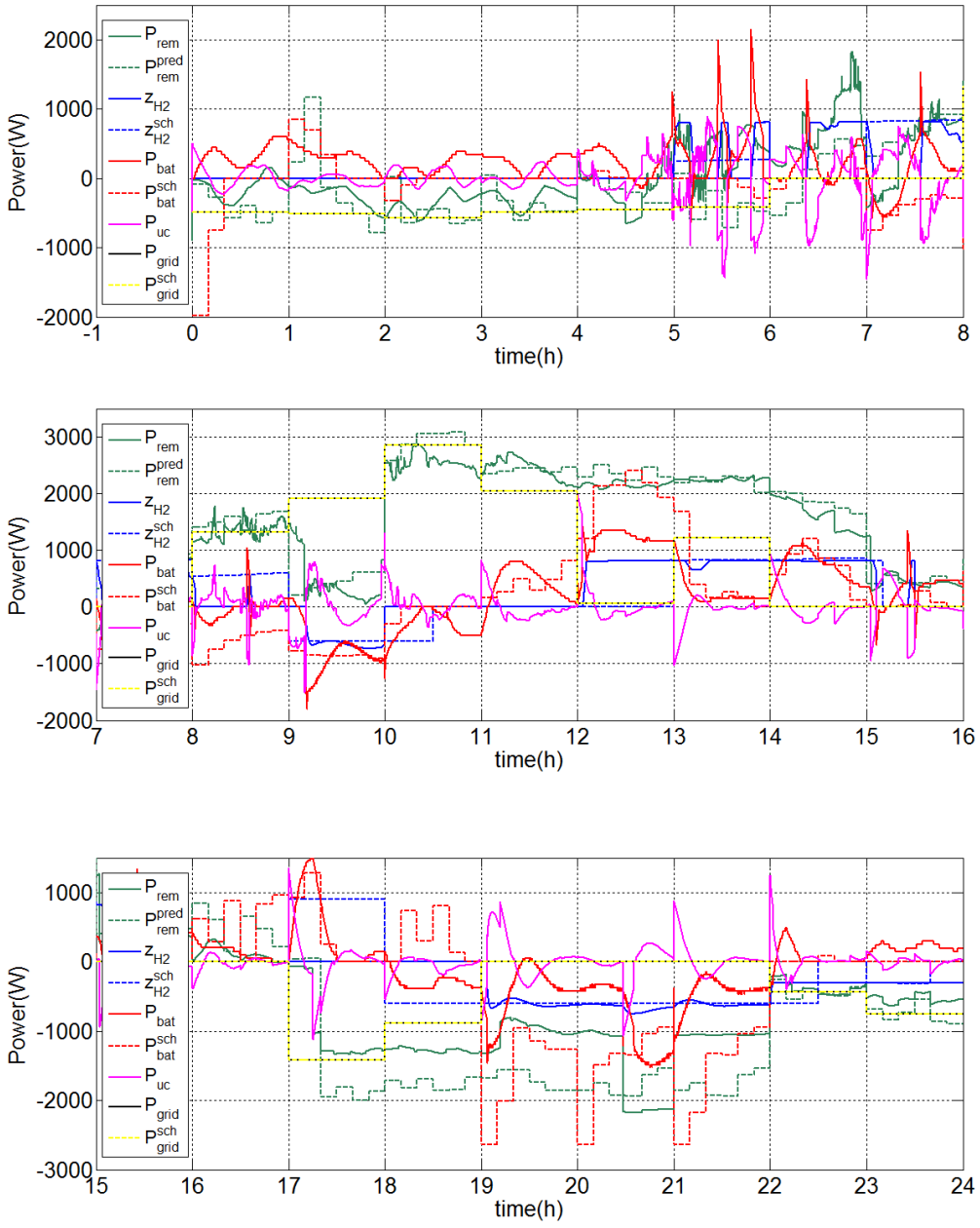

Figure 4.21. Experimental results of the output power for each component of the microgrid

MIQP but a better distribution of the ESS for minimum degradation is found in the MIQP. The MIQP controller proposed in this study is the only one of the four proposed strategies that is always the most favourable (8/11) or the second most favourable (3/11) controller for all the key indicators studied. Note that the values of the microgrid utilized for this comparison correspond with the article published by Garcia-Torres and Bordons [189].

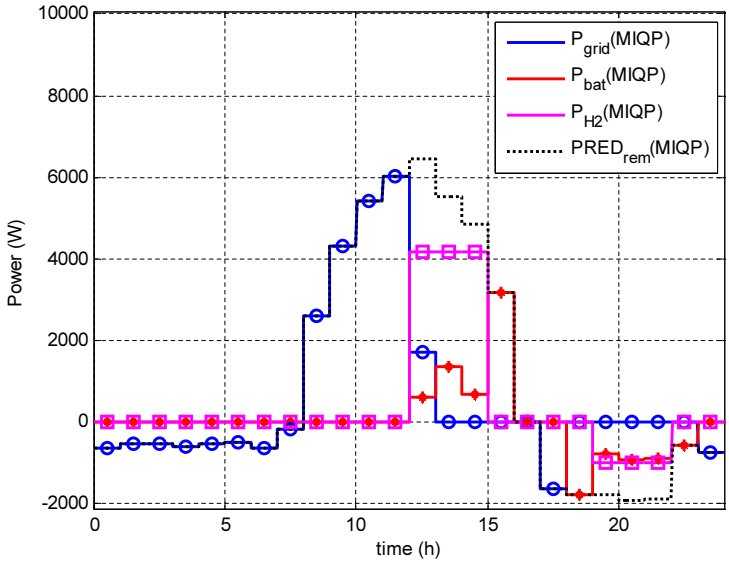

Figure 4.22. Daily market schedule results with the proposed MIQP controller

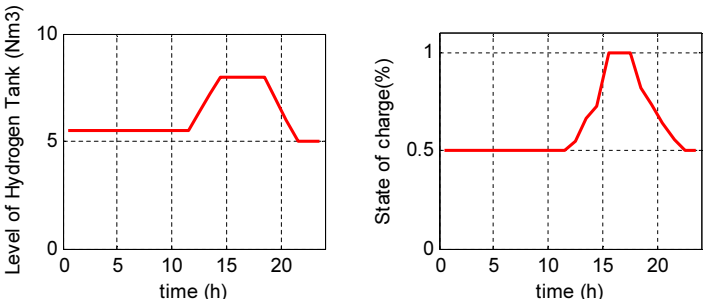

Figure 4.23. Schedule level for LOH and SOC for the proposed MIQP controller

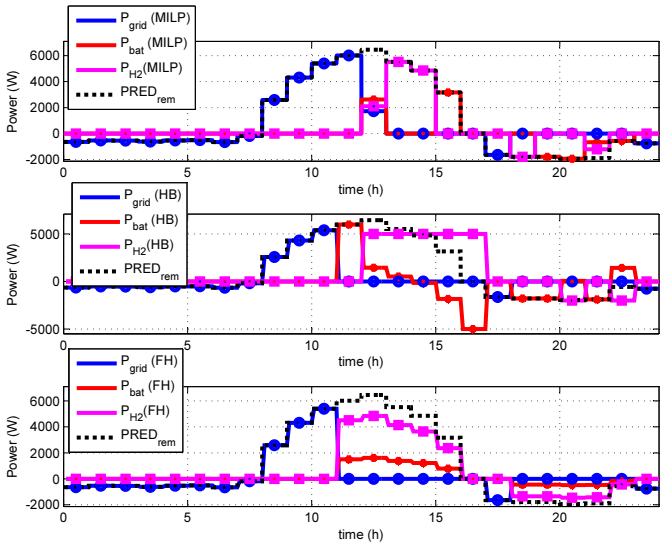

Figure 4.24. Daily market schedule results for different controllers

Table 4.6. Comparison of the key performance value of the controllers

	MIQP	**MILP**	**HB**	**FH**
Economic Balance Grid(€)	0.9685*	0.9685*	0.4686	0.4686
Hours of the ELZ	3*	3*	5**	5**
Start up/shut down ELZ	1*	1*	1*	1*
Reference changes ELZ	2*	4**	2*	6
Hours of the FC	2*	2*	2*	4**
Start up/shut down FC	1*	2**	2**	1*
Reference changes FC	2*	4**	4**	6
Charge cycle(%)	50*	50*	56.12**	50*
Discharge cycle(%)	50**	50**	100	16.25*
Maximum charge BAT	3160**	3160**	6004	1613*
Maximum discharge BAT	1784**	1931	4994	482.75*

(*) Most favourable controller

(**) Second most favourable

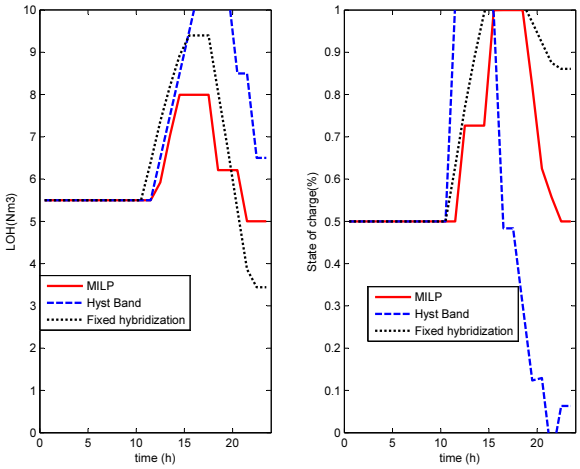

Figure 4.25. Schedule level for LOH and SOC for different controllers

4.8 Conclusions

In this chapter, an MPC controller for the optimal economical schedule of a microgrid has been presented and validated. This formulation integrates the operational costs in the optimization problem, including degradation of all the components of the hybrid ESS, especially the hydrogen-based storage. This allows an optimal scheduling policy linked to the time-varying price of energy. The results show an optimal behavior of the microgrid whose non-dispatchable generation is converted into dispatchable using the ESS. Followed an MPC controller for the optimal load sharing of a microgrid at real operational scenario has been presented and validated in an experimental plant. This formulation integrates the penalties over degradation situations of all the components of the hybrid ESS. This allows an optimal behaviour of the global ESS despite differences between the predicted scenario given in the economical schedule and the real time scenario at the same time that the grid contracted schedule is satisfactory respected. The results show an optimal behaviour of the microgrid whose non-dispatchable generation is converted into dispatchable using the ESS.

The complementarity between the three ways to store energy is also manifested in this chapter. When the hydrogen storage is active the overcharge and the undercharge of the battery and the ultracapacitor can be controlled. The high stress current ratio in the battery is also neglected with the use of the hydrogen ESS. The fluctuating operation conditions in hydrogen are avoided with the use of batteries and ultracapacitor. The proposed control algorithm can contribute to improve the given lifetime of the ESS. The method can be expanded to other

ways to store energy.

The results obtained of the function cost minimization conclude that the hydrogen ESS is appropriate for great quantities of energy storage requirements in short-functional periods while batteries are appropriate for low quantities in the energy storage requirements with long-functional periods. Ultracapacitors are the most appropriate technology to correct rapid fluctuations in the disposal of energy in the microgrid. The complementarity between the three ways to store energy is also manifested in this chapter. When the hydrogen storage is active the overcharge and the undercharge of the battery and the ultracapacitor can be controlled. The high stress current ratio in the battery is also neglected with the use of the hydrogen ESS. The fluctuating operation conditions in hydrogen are avoided with the use of batteries and ultracapacitor.

According to the economic values used in the study to make the ESS competitive, their life must be increased, decreasing in this way their associated cost. This chapter shows how the control algorithm can contribute to this objective.

Chapter 5

Microgrid Power Quality Enhancement

5.1 Introduction

Microgrids appear as a key solution to manage smart grids with high penetration of renewable energy generation and unbalanced nonlinear loads. Their flexibility allows the energy exchange with the utility network in grid-connected mode or the transition to an islanded operation mode from the main grid in case of disturbances or faults. While in grid-connected mode the main grid imposes the frequency and voltage. While in islanded mode the microgrid itself must balance the load between all the connected components to the microgrid and must supervise that the power flow inside the microgrid is done according to the power quality levels that all the devices of the microgrid require.

ESSs are usually interfaced with power inverters whose control algorithm is based on classic methods whose transient response under fluctuating conditions could even introduce more power quality problems while the reference is reached.

The MPC techniques applied to power converters are characterised by their fast dynamic response, being a model of the plant necessary to predict the output in the control horizon utilized by the controller. Usually, a prediction horizon of "1" is used in order to avoid excessive computations. MPC based algorithms applied to power converters use Park's or Clarke's transformation with a correct horizon. However, these methods are only valid for balanced and harmonic-free three-phase voltages and currents, it is still necessary to compute the positive-sequence active and reactive powers associated with a periodic set of three-phase

voltages and currents equations where the power quality conditions are not appropriate.

Usually ESSs are characterised by their low voltage output. Therefore it is necessary to introduce power conversion composed by a booster step followed usually by a two-level voltage source inverter (2L-VSI). Current ripple applied to the ESS is one of the main causes of degradation which must be taken into account.

In order to improve power quality in these kinds of applications, a new control strategy based on Model Predictive Control (MPC) and an on-line Fourier analysis of the voltage and current measurements, evaluated per cycle of the fundamental frequency, is presented in this chapter. This new technique is applied to Voltage Source Inverters (VSI) in islanded and grid-connected modes. Although the time horizon is "1", the memory of the last fundamental frequency cycle is used. The current ripple effects are also minimized in order to improve the lifetime of the ESS using MPC techniques applied to DC/DC converters.

5.2 Power Quality in the Smart Grid

Power quality will be an important factor in the transition towards the smart grid, according to the different national policies the generation should meet the growing demand cleanly, reliably, sustainably and at low cost [3]. In electric power systems, any deviation with respect to the theoretical sinusoidal waveform (produced in the generation centres) is considered to be a perturbation in the power quality of the electrical grid to. The deviation can be given in any of the parameters of the wave: frequency, amplitude, waveform and symmetry between phases. Depending on its grade and the sensitivity of the receptors, this perturbation may have a repercussion on other devices. Adequate quality supply provides the necessary compatibility between all the devices connected to the same grid.

While reliability indices are not yet standardised, voltage characteristics of European public distribution system concerning the supplier's side are regulated by standard EN 50160. Standard EN 50160 defines the main features of voltage supplied by public distribution grids, distribution for low and medium voltage under normal exploitation conditions . There is still shortage in the regulatory framework of the reliability and commercial dimensions of quality, but this will acquire further importance in an integrated, multi-function and multi-communication platform like smart grid [4].

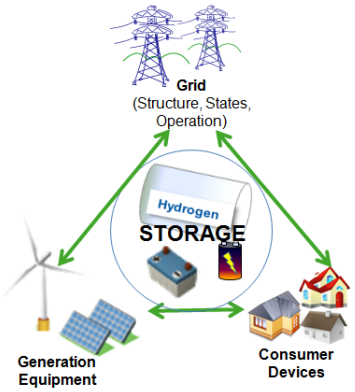

Figure 5.1. Power quality interaction in the Smart Grid

5.2.1 Analysis of power quality issues in the different components of the smart grid

In traditional power systems, power quality in a node of the grid is associated with the short circuit power at this point of the grid. Under constant emission higher short circuit power results in better voltage quality. The controllability of fossil-fuel power plants on which the centralised generation and lineal loads are based(with a high resistive component) just cause low level power quality anomalies in comparison with short circuit power in the upstream network [3]. But this scenario has been modified in recent years marking the transition to the smart grid. With independency of the scenario, power quality would be defined by the interaction between the generation equipment, the consumer devices and the grid. All anomalies should be compensated by the energy storage systems (Figure 5.1).

The documents presented by the European Technology Platform for Electricity Networks: *Vision and Strategy for Europe's Electricity Networks of the Future* [202], *Strategic Research Agenda* [203] and *Strategic Deployment Document for Europe's Electricity Networks of the Future* [204] draw the energy landscape for the next decades.

5.2.1.1 Generation Equipment

The penetration index for renewable generation should be $20\% - 35\%$ in the year 2020 [202, 203, 204]. The high penetration for solar and wind generation reached

in several countries such as Spain and Germany have brought about several instability problems associated with the randomness and fluctuations of these kind of generation systems. Photovoltaic power systems, the associated inverter act in the grid as non-linear loads with a high contribution of harmonic injection in the grid. These kind of effects are increased in low irradiance periods [205]. In the case of wind generation, the reactive consumption and the its inertia increase the instability associated with power quality [156]. The penetration of micro-generation (typically defined as generation with a rated power of less than 16 A per phase) in the low-voltage networks is expected to increase continuously. This could increase the negative-sequence and the zero-sequence voltage in the low voltage gird. In weak distribution networks, existing limits could be overcome rather quickly. Reconsidering the limits for negative-sequence voltages and introducing limits for zero-sequence voltage could be needed [3].

5.2.1.2 Consumer Devices

The transformation of the energetic scenario is not only conceived from the point of view of generation. In the document *Vision and Strategy for Europe's Electricity Networks of the Future* [202], targets are created the, known as the "20-20-20" targets which set three key objectives for 2020:

1. A 20% reduction in EU greenhouse gas emissions from 1990 levels.
2. Raising the share of EU energy consumption produced from renewable resources to 20%.
3. A 20% improvement in the EU's energy efficiency.

From the point of view of consumption loads, the first repercussion has been the replacement of incandescent bulbs with energy saving and LED bulbs. Seen from the electrical network point of view, each of the new lamp technologies results in the replacement of a resistive load by a rectifier load. The fundamental current is reduced significantly whereas the harmonic currents are increased. High penetration together with high coincidence of operation may lead to an increase of low order harmonics [4]. There is also a increase in the use of electronic devices by the consumers whereby voltage quality levels are affected but these electronic devices are also quite sensitive and are strongly affected by the voltage quality [3]. Due to the continuous decrease of resistive loads, providing damping stability issues may become important for low-voltage networks. In conjunction, the increasing capacitive load (The EMC filters of electronic equipment) can bring about resonance points with decreasing resonant frequencies, as well as, damping periods [4].

5.2.1.3 Distribution Network

Nowadays the IEC electromagentic compatibility standards impose a reference impedance (cf. IEC 60725) used as a link between compatibility levels (voltages) and emission limits (currents). In future grids with high penetration of renewable generation, significant different scenarios may be possible, from supply by a strong upstream network to an islanded (self-balanced) operation. This may lead to a significantly higher variability in the short-circuit power than today [3]. The grid might need a new lower management level to correctly balance generation and consumption in a microgrid topology. These microgrids must work in both connected or islanded mode, having the ability to change from connected to islanded mode and vice verse when power quality levels require this action.

5.2.1.4 Energy Storage Systems

Energy storage systems appear as the solution to compensate the imbalances introduced by non-controlability and perturbations on power qualities that new generation equipment and consumer devices could introduce in the distribution grid. Even in the future, the capability to store energy will probably be an index of power quality at a given point of the grid. Technical roles and functions of electric storage systems in smart grids include grid voltage support, frequency support, grid transient stability, load levelling and peak shaving, spinning reserve, power quality improvement, power reliability, ride through support and unbalanced load compensation. Some of these functions are briefly explained below [6]:

1. Grid voltage support: Storage power can be used to maintain the voltages of electrical distribution system within the acceptable range. This involves a trade-off between the amount of real and reactive power produced by generators.

2. Grid frequency support: Storage power can be used to reduce any sudden, large load generation imbalance in electrical distribution systems. It will keep the grid frequency within the permissible tolerance.

3. Spinning reserve: Spinning reserve is defined as the amount of generation capacity that can be used to produce active power over a given period of time, which has not yet been committed to the production of energy during this period. Therefore, the storage power can be used as spinning reserve.

4. Grid transient stability: Storage systems injects or absorbs real power to reduce any power oscillation due to any rapid events.

5. Power quality improvement: Power quality is basically related to the changes in magnitude and shape of voltage and current. This results in different issues including harmonics, power factor, transients, flicker, sag and swell. Distributed storage systems can easily mitigate these problems

6. Power reliability: Reliability can be represented as the percentage of interruption in the delivery of electric power/energy to customers. Distributed storage systems can help to provide reliable electricity to consumers.

7. Ride through support: Ride through means the electric unit stays connected during system disturbances. Distributed storage systems have the potential of providing energy to ride-through.

8. Unbalanced load compensation: this can be done in combination with four-inverters and also by injecting and absorbing power individually at each phase to supply unbalanced loads. combination with four-wire inverters and also by injecting and absorbing power individually at each phase to supply unbalanced loads unbalanced loads.

5.2.2 Distributed Storage Interface

Energy storage systems are usually direct energy conversion sources producing DC voltages/currents. Their low voltage output normally requires a booster converter followed by an inverter in order to achieve the voltage levels required in the standards similar to EN-50160. Depending on the selected power conversion topology, it would be classified as a voltage source or a current source. Taking into account the control applied to the power conversion, a new classification can be established based on current and voltage control. Regarding inverters, the voltage source inverters(VSI) design is imposed on the industry due to their efficiency. They also have higher reliability and faster dynamic response. In the case of the DC/DC booster converter the current ripple effects over the ESS make a current source converter (CSC) recommendable instead of a voltage source converter. The control algorithm is the basis of the operation of the power electronic device, following the two main control families applied to power electronics are briefly explained.

5.2.2.1 Current Control

The main objectives of the current controller are to provide a relatively high bandwidth to ensure accurate current tracking, shorten the transient period as much

as possible; and force the VSI to equivalently act as a current source amplifier within the current loop bandwidth. In addition, the current loop is responsible for the injected-current power quality and over-current protection. Grid voltage harmonics, unbalance, transients and grid parameters directly affect the current control performance and might impair the power quality and even the stability of the inverter system. However, it is only recently that the effects of supply harmonics on the control effectiveness of inverter based distributed generators have begun to be investigated. Small distortions in the grid voltage remarkably increase the total harmonic distortion in the injected current and eventually, inverter instability can occur due to possible interaction between grid distorsion and inverter's power circuit filter. Therefore, grid disturbances suppression is one of the important properties that should be found in the current controller in a VSI-based distributed generator [9].

The major techniques to regulate the output current of a current-controlled VSI include either a variable switching frequency, such as the hysteresis control scheme, or fixed-switching schemes, such as the ramp comparison stationary and synchronous frame proportional-integral (PI), and deadbeat predictive current control schemes [9].

5.2.2.2 Voltage Control

Generally, there are two modes of voltage control inverter-based DG units: voltage control in grid-connected mode and voltage control in the islanded mode. In grid connected-mode, voltage control can be an option to regulate the grid voltage at the PCC. While this is not allowed in stiff grids, it is a favourable solution in weak grids. There are certain requirements in this mode of operation: firstly, a low total harmonic distorsion (THD) of the output voltage must be obtained under different load conditions. This is an important objective as the harmonic current produced by nonlinear loads can remarkably distort the output voltage of the inverter, affecting the power quality exported to other loads. Secondly, the inverter should provide effective voltage regulation performance in terms of low voltage dip and fast recovery in the case of load transients and network disturbances. These voltage performance requirements become more challenging when the unbalanced nature of grid/load voltages is considered. Severe and random voltage disturbances might be initiated by time-varying loads, such as arc furnaces, non-dispatchable generation, such as fluctuating output power of wind and photovoltaic generation [9].

5.2.3 Microgrid Operation Modes

Microgrids have essentially two operation modes, the grid connected mode and the islanded mode, the transition between both modes is also important. The main difference between both modes is established by the voltage and frequency control. In the case of the grid connected mode the voltage and the frequency references are imposed by the main grid, while in the islanded mode it is set up by the microgrid itself.

5.2.3.1 Grid-Connected Mode

In this mode the microgrid must be capable to export/import energy to/from the main grid at the voltage amplitude and frequency imposed by the main grid, generators, load; and the ESS must absorb or inject power with these voltage and frequency levels. The microgrid power exchange with the main grid is scheduled in the economic dispatch of the microgrid.

The main problem in this mode is the slow response of the control signals when a change of the output power occurs. The absence of synchronous machines connected to the low-voltage power grid requires power blancing during transients to be provided by the ESS of the microgrid [46].

5.2.3.2 Islanded Mode

The microgrid can work in this mode due to different criteria, such as the non-existence of the main grid, a fault in the main grid, or a period of maintenance. There is usually an Intelligent Power Switch (IPS) which is not active during this working mode. In this mode the microgrid itself must carry out the load balance between all the components of the microgrid and must supervise that the power flow inside the microgrid is done according to power quality levels that all the components of the microgrid require [46].

5.2.3.3 Transition between Grid-Connected and Islanded Mode

When a power supply shutdown occurs, the restoration process must be reduced as much as possible in order to ensure a high reliability level. Restoration stages are aimed at the plant restart, power generation of the main grid and system frequency synchronization. During this stage, some details must be considered such as reactive power balance, commutation of the transient voltages, balancing power generation, starting sequence, and coordination of generation units [46].

The IPS must continuously supervise both the utility grid and the microgrid status. When a fault in the main grid has been detected by the IPS, it must disconnect the microgrid. In such a case, this switch can readjust the power reference at nominal values. In addition to this, the IPS keeps in closed-state in grid-connected mode if maximum permissible deviations are not exceeded, (typically, 2% for frequency and 5 % for amplitude), changing to opened-state in opposite conditions. When the microgrid is in islanded mode operation and the IPS detects main grid fault-free stability, syncrhonszation with voltage, amplitude, phase and frequency must be developed by connection operation [46].

5.3 Primary Model Predictive Control Design

The primary control of the ESS in the microgrid must follow in an optimal way the power reference given by the economical dispatch of the microgrid. The optimal load sharing MPC gives as reference the P_i^{sch} for each ESS of the microgrid. The Q_i^{sch} relationship with the P_i^{sch} is usually given with a power factor reference $\cos(\varphi_{ref})$.

Usually ESSs are characterised by their low voltage output which makes it necessary a power conversion composed by a booster converter followed usually by a two-level Voltage Source Inverter (2L-VSI), see figure 5.2. The most common booster topology is the isolated full bridge or the double isolated full bridge when the bidirectional characteristic is needed of the converter. Besides the converter topology, the use of a hybrid ESS makes advanced control necessary in order to make the output of the power electronic device associated to each ESS accurate. This fact is even greater when the objective is to improve the power quality supply of the system with high penetration of renewable energies or weak grids. But as explained in Chapter 3, the demanded current ripple to the ESS is a degradation cause for batteries, ultracapacitors and electrolyzers and fuel cells. Primary control must perform an accurate tracking of the active and reactive power reference given by the tertiary control of the microgrid. However it must take into account the current ripple degradation issue associated with ESSs. These must be the two objectives of the primary control. As explained in figure 5.3, each one of the explained objectives is inside one of the two parts which the power electronic device associated to the integration of the ESS can be divided into. While degradation aspects can be located inside the DC/DC converter, power quality issues are maintained in the DC/AC inverter, see figure 5.3.

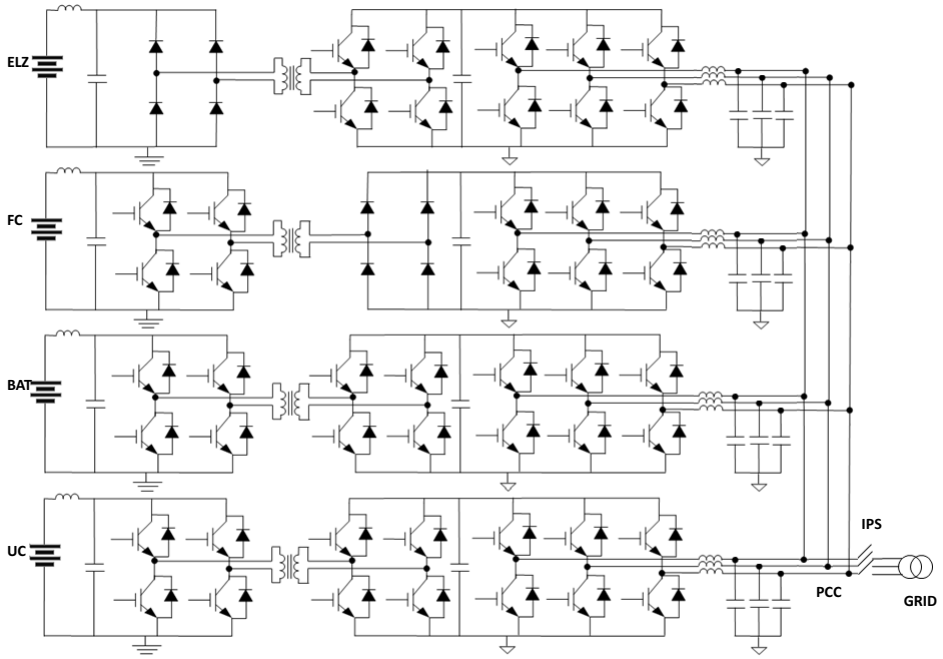

Figure 5.2. Power electronic of the hybrid ESS of the microgrid

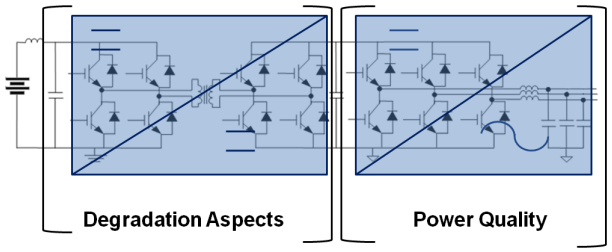

Figure 5.3. Power quality and degradation aspects in the power converter of the ESS

5.3.1 CSC Model Predictive Control under Minimum Current Ripple Criteria

As commented in Chapter 3, current ripple is one of the factors that affect the useful life of the ESS. In this section a new algorithm based on the MPC technique is developed including in the cost function of the controller the minimization of the current ripple applied to the ESS between two consecutive instants [206].

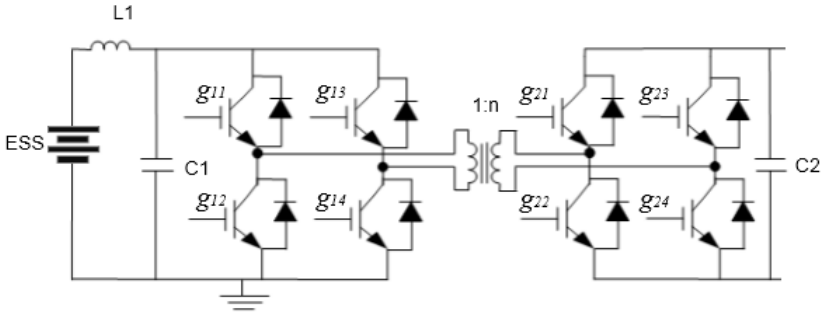

Figure 5.4. Variables and nomenclature used in the CSC

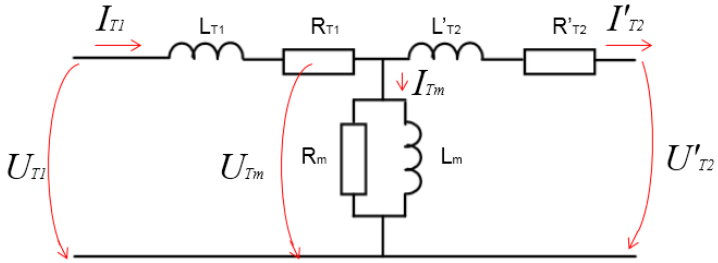

Figure 5.5. HF Transformer equivalent circuit

5.3.1.1 Topology Description

In figure 5.2, the topology of the power electronics associated with each ESS is shown. Both batteries and ultracapacitors have a bidirectional behaviour so they are integrated by the isolated double full bridge DC/DC current source converter with a high frequency (HF) transformer, the second bridge output is connected to a DC-link capacitor whose output it connected to the 2L-VSI. The fuel cell just injects power into the grid so its power electronics associated is composed by an isolated full bridge booster DC/DC CSC. The steps of the fuel cell converter are a full Insulated Gate Bipolar Transistor (IGBT) H-Bridge followed by a high frequency transformer whose output is linked to a H-bridge diode rectifier connected to its correspondent 2L-VSI. The input of the electrolyzer DC/DC converter is connected with a full bridge diodes-rectifier followed by a HF transformer and a full IGBT bridge which is fed by a 2L-VSI. The electrolyzer can only receive energy, so the selected topology for its integration in the microgrid is the isolated full bridge buck DC/DC CSC. Note that all the 2L-VSI are commonly connected to the same Point of Common Coupling (PCC) which is also connected to the outputs of the MPPT (Maximum Power Point Tracking) of the inverters

Table 5.1. Parameters of the Current Source Converter

Parameter	Value
Filter inductance L_1	1 $[mH]$
Filter inductance resistance R_{L_1}	0.1 $[\Omega]$
Filter capacitor C_1	1 $[mF]$
Filter capacitor resistance R_{C_1}	0.1 $[\Omega]$
Filter capacitor C_2	1 $[mF]$
Filter capacitor resistance R_{C_2}	0.1 $[\Omega]$
Nominal frequency of the HF Transformer f_N	100 $[kHz]$
Primary Nominal Voltage of the HF Transformer U_{T1}	100 $[V_{rms}]$
Primary Inductance of the HF Transformer L_{T1}	6366.2 $[\mu H]$
Resistor of the Primary Inductance of the HF Transformer RL_{T1}	5 $[m\Omega]$
Secondary Nominal Voltage of the HF Transformer U_{T2}	1000 $[V_{rms}]$
Secondary Inductance of the HF Transformer L_{T2}	63.663 $[\mu H]$
Resistor of the Secondary Inductance of the HF Transformer RL_{T2}	0.5 $[m\Omega]$
Magnetiszation Inductance of the HF Transformer L_{Tm}	1.5915 $[\mu H]$
Magnetiszation Resistor of the HF Transformer R_{Tm}	1 $[k\Omega]$
DC link voltage U_{dc}	700 $[V]$

associated to the wind turbine and solar panels. The PCC is connected to an inductive filter followed by an IPS which is connected to the galvanic isolation transformer where the power flow between the grid and the microgrid is carried out.

Depending on whether the battery and the ultracapacitor are in charge or discharge mode the isolated double full bridge can be divided into two circuits the buck isolated full bridge (similar to the electrolyzer inverter represented in figure 5.2) and the booster isolated full bridge CSI (similar to the fuel cell inverter represented in the same figure). In figure 5.4, the nomenclature used in the model can be found. In figure 5.5, the equivalent model used for the HF transformer can be found.

This topology is selected for the ultracapacitor and the battery in order to maintain similarities with the electrolyzer and the fuel cell. However, the output voltage in the case of the battery and the ultracapacitor can be obtained just by adding several serial units, or selecting a simpler topology. In any case, the concepts introduced in this section for the control algorithm can be easily applied

to other topologies.

5.3.1.2 Predictive Model of the Isolated Full Bridge Booster CSC

The output of each leg of the inverter is connected to a high frequency transformer followed by a full diode H-Bridge whose output is connected to an The isolated full bridge booster DC/DC CSC is composed of two legs with IGBT's comprising two switches each one. The switches states are a function of the associated gate-signals. The gate signals applied to the switches situated on the same leg of the inverter are related, being the value of the negative terminal connected gate signal the opposed of the positive terminal gate signal. Each gate signal can only adopt two values 0 if the power switch is at OFF-state and 1 when the power switch is at ON-state. Taking into consideration the topology of two legs, $2^2 = 4$ possible states of the converter can be. The nomenclature used for the different states of the converter is expressed in table 5.2. Another possibility is state $g_{11} = 1, g_{13} = 1$ but as is seen in the model, it has the same effect on the output of the converteras "0". Due to the bidirectional behaviour of the double isolated full bridge, a new state is defined labelled as "Diode" when the four signal gates of the converter are "0" the behaviour of the bridge is output capacitor C_2. The current and voltage

Table 5.2. State definition of the Isolated Full Bridge Booster CSC

State	Description
"-1"	$g_{11} = 0, g_{12} = 1, g_{13} = 1, g_{14} = 0$
"0"	$g_{11} = 0, g_{12} = 1, g_{13} = 0, g_{14} = 1$
"1"	$g_{11} = 1, g_{12} = 0, g_{13} = 0, g_{14} = 1$
"Diode"	$g_{11} = 0, g_{12} = 0, g_{13} = 0, g_{14} = 0$

of the input capacitor $C1$ can be modelled as follows:

$$I_{C_1}(t_{k+1}) = \frac{U_{C_1}(t_{k+1}) - U_{C_1}(t_k)}{T_s} \tag{5.1}$$

$$\begin{aligned} U_{C_1}(t_{k+1}) = U^{ESS}(t_{k+1}) - L_1 \frac{I_{L_1}(t_{k+1}) - I_{L_1}(t_k)}{T_s} \\ - R_{L_1} \cdot I_{L_1}(t_{k+1}) \end{aligned} \tag{5.2}$$

Primary voltage and current of the transformer can be expressed as a function of the inductor current. The input voltage for the converter and the gate signals for the next instant can be expressed with the next equations:

$$U_{T_1}(t_{k+1}) = (g_{11}(t_{k+1}) - g_{13}(t_{k+1})) \cdot U_{C_1}(t_{k+1}) \tag{5.3}$$

$$I_{T_1}(t_{k+1}) = (g_{11}(t_{k+1}) - g_{13}(t_{k+1})) \cdot (I_{L_1}(t_{k+1}) - I_{C_1}(t_{k+1})) \tag{5.4}$$

Equation (5.4) is only valid for states "1" and "-1". Secondary voltage and current of the transformer can be expressed as a function of the current output of the converter with the following expressions using the equivalent circuit of the transformer (Figure 5.5).

$$U_{T_m}(t_{k+1}) = U_{T_1}(t_{k+1}) - L_{T_1}\frac{I_{T_1}(t_{k+1}) - I_{T_1}(t_k)}{T_s} - R_{T_1} \cdot I_{T_1}(t_{k+1}) \tag{5.5}$$

$$I_{T_m}(t_{k+1}) = \frac{U_{T_m}(t_{k+1})}{R_{T_m}} + \frac{T_s \cdot U_{T_m}(t_{k+1})}{L_{T_m}} + I_{L_{T_m}}(t_k) \tag{5.6}$$

$$U_{T_2}(t_{k+1}) = U_{T_m}(t_{k+1})\frac{U_{N_2}}{U_{N_1}} + L_{T_2}\frac{I_{T_2}(t_{k+1}) - I_{T_2}(t_k)}{T_s} + R_{T_2} \cdot I_{T_2}(t_{k+1}) \tag{5.7}$$

$$I_{T_2}(t_{k+1}) = (I_{T_1}(t_{k+1}) - I_{T_m}(t_{k+1}))\frac{U_{N_1}}{U_{N_2}} \tag{5.8}$$

The full bridge diode rectifier is polarised when the condition $|U_{T_2}(t_{k+1})| > U_{C_2}(t_{k+1})$, in this case the next expression, is fulfilled:

$$I_{C_2}(t_{k+1}) = |I_{T_2}(t_{k+1})| - \sum_{j=a,b,c} g_{j_1}(t_{k+1}) \cdot I_{Lj}(t_{k+1}) \tag{5.9}$$

$$U_{C_2}(t_{k+1}) = |U_{T_2}(t_{k+1})| - R_{on}^{diode} \cdot |I_{T_2}(t_{k+1})| - U_f^{diode} \tag{5.10}$$

$$I_{C_2}(t_{k+1}) = C_2 \frac{U_{C_2}(t_{k+1}) - U_{C_2}(t_k)}{T_s} \tag{5.11}$$

When the diodes rectifier is not polarized ($|U_{T_2}(t_{k+1})| \leq U_{C_2}(t_{k+1})$)

$$-\sum_{j=a,b,c} g_{j_1}(t_{k+1}) \cdot I_{Lj}(t_{k+1}) = C_2 \frac{U_{C_2}(t_{k+1}) - U_{C_2}(t_k)}{T_s} \tag{5.12}$$

5.3.1.3 Predictive Model of the Isolated Full Bridge Buck CSC

The isolated full bridge buck DC/DC CSC has a similar topology to the booster although the current sense is the opposite, so inductor L_1 is the output of the converter and capacitor C_2 is the input. Once again, the gate signals applied to the switches situated in a same leg of the inverter are related, the value of the negative terminal connected gate signal is the opposite of the positive terminal gate signal. Each gate signal can only adopt two values 0 if the power switch at OFF-state and 1 when the power switch is at ON-state. The defined states are similar but the gates are g_{21}, g_{22}, g_{23} and g_{24} see table 5.3. Another possibility is state $g_{21} = 1, g_{23} = 1$ but as is seen in the model, it has the same effect on the output of the converter as "0" state.T he output of each leg of the inverter is connected to the high frequency transformer follows by full diode H-Bridge whose output is connected to an output capacitor C_1 followed by the output inductor $L1$.

In this case, the predicted primary voltage and current of the transformer for

Table 5.3. State definition of the Isolated Full Bridge Buck CSC

State	Description
"-1"	$g_{21} = 0, g_{22} = 1, g_{23} = 1, g_{24} = 0$
"0"	$g_{21} = 0, g_{22} = 1, g_{23} = 0, g_{24} = 1$
"1"	$g_{21} = 1, g_{22} = 0, g_{23} = 0, g_{24} = 1$
"Diode"	$g_{21} = 0, g_{22} = 0, g_{23} = 0, g_{24} = 0$

the next instant t_{k+1} can be expressed as a function of the gate signals with the following equations:

$$\begin{aligned} U_{T_2}(t_{k+1}) = (g_{21}(t_{k+1}) - g_{23}(t_{k+1})) \\ \cdot U_{C_2}(t_{k+1}) \end{aligned} \tag{5.13}$$

$$I_{T_2}(t_{k+1}) = (g_{21}(t_{k+1}) - g_{23}(t_{k+1})) \cdot \left(\sum_{j=a,b,c} g_{j_1}(t_{k+1}) \cdot I_{Lj}(t_{k+1}) - I_{C_2}(t_{k+1}) \right) \tag{5.14}$$

Equation (5.14) is only valid for states "1" and "-1". Primary voltage and current of the transformer can be expressed with the next expressions using the equivalent circuit of the transformer (Figure 5.5).

$$U_{T_m}(t_{k+1}) = (U_{T_2}(t_{k+1}) - L_{T_2}\frac{I_{T_2}(t_{k+1}) - I_{T_2}(t_k)}{T_s} - R_{T_2} \cdot I_{T_2}(t_{k+1}))\frac{U_{N_1}}{U_{N_2}} \tag{5.15}$$

$$I_{T_1}(t_{k+1}) = (I_{T_2}(t_{k+1}) + I_{T_m}(t_{k+1}))\frac{U_{N_2}}{U_{N_1}} \tag{5.16}$$

Being the expression of I_{T_m} and U_{T_1} for this case similar to equation (5.6) and (5.5) respectively. The condition to polarise the diode H-Bridge for this case is $|U_{T_1}(t_{k+1})| > U_{C_1}(t_{k+1})$. The current input to the electrolyzer or the charge of the batteries or ultracapacitor can be expressed:

$$I_{L_1}(t_{k+1}) = I_{C_1}(t_{k+1}) + |I_{T_1}(t_{k+1})| \tag{5.17}$$

$$U_{C_1}(t_{k+1}) = |U_{T_1}(t_{k+1})| - R_{on}^{diode} \cdot |I_{T_2}(t_{k+1})| - U_f^{diode} \tag{5.18}$$

$$I_{C_1}(t_{k+1}) = C_1\frac{U_{C_1}(t_{k+1}) - U_{C_1}(t_k)}{T_s} \tag{5.19}$$

When the diodes rectifier is not polarised ($|U_{T_1}(t_{k+1})| \leq U_{C_1}(t_{k+1})$)

$$I_{L_1}(t_{k+1}) = I_{C_1}(t_{k+1}) \tag{5.20}$$

$$I_{C_1}(t_{k+1}) = C_1\frac{U_{C_1}(t_{k+1}) - U_{C_1}(t_k)}{T_s} \tag{5.21}$$

5.3.1.4 Control Algorithm

With the relationships expressed in sections 5.3.1.2 and 5.3.1.3, it is possible to express all the state variables of the converter as a function of the control variables of the converter (g_{ij}). The next cost function is minimised by the controller:

$$\begin{aligned}\min_{g_{11},g_{13},g_{21},g_{23}} \quad J = w_0 \cdot \left(I_{L_1}(t_{k+1}) - I_{control}\right)^2 + w_1 \cdot \left(g_{11} + g_{13} + g_{21} + g_{23}\right)^2 \\ + w_2 \cdot \left(I_{TM}(t_{k+1})\right)^2 + w_3 \cdot \left(\Delta I_{L_1}(t_{k+1})\right)^2\end{aligned} \tag{5.22}$$

The first terminus is the most important and the most weighted by the controller. It penalties the deviation between the control current $I_{control}$ calculated by the controller as a function of the reference voltage given to the DC-link capacitor $U^{ref}_{dc-link}$. In the case of the booster CSC, it is expressed as follows:

$$I_{control}(t_{k+1}) = \frac{\left(U^{ref}_{dc-link}\right)^2}{\eta_{conv}(t_k) \cdot R_{th}(t_k) \cdot U_{ESS}(t_{k+1})} \tag{5.23}$$

where $\eta_{conv}(t_k)$ is the efficiency of the converter and $R_{th}(t_k)$ the equivalent resistance of the converter both are calculated with the following expressions:

$$\eta_{conv}(t_k) = \frac{\sum_{t_j=t_k-T}^{t_j=t_k} U_{out}(t_j) \cdot I_{out}(t_j)}{\sum_{t_j=t_k-T}^{t_j=t_k} U_{ESS}(t_j) \cdot I_{L1}(t_j)} \tag{5.24}$$

$$R_{th}(t_k) = \frac{\sum_{t_j=t_k-T}^{t_j=t_k} U_{out}(t_j)}{\sum_{t_j=t_k-T}^{t_j=t_k} I_{out}(t_j)} \tag{5.25}$$

Period T is defined as the time between two transitions from a state different to zero to the state "0". In the case of the buck converter, the control current is calculated with the following expressions:

$$I_{control}(t_{k+1}) = \frac{\eta_{conv}(t_k) \cdot \left(U^{ref}_{dc-link}\right)^2}{R_{th}(t_k) \cdot U_{ESS}(t_{k+1})} \tag{5.26}$$

$$\eta_{conv}(t_k) = \frac{\sum_{t_j=t_k-T}^{t_j=t_k} U_{ESS}(t_j) \cdot I_{L1}(t_j)}{\sum_{t_j=t_k-T}^{t_j=t_k} U_{out}(t_j) \cdot I_{out}(t_j)} \tag{5.27}$$

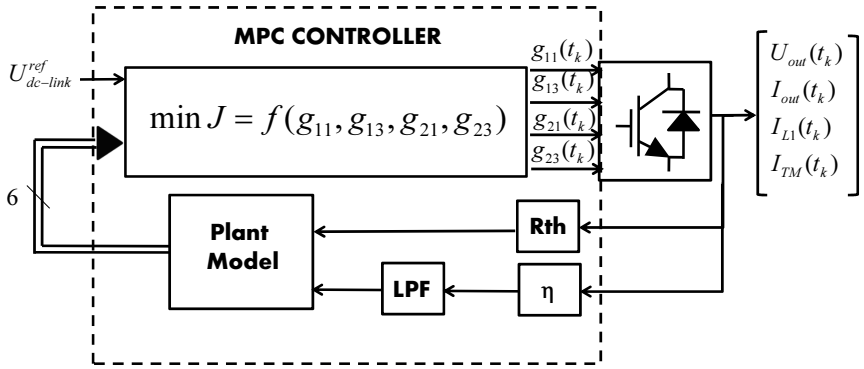

Figure 5.6. Block diagram of the control algorithm for the CSC

The expression for Thevenin's equivalent resistor shown in equation 5.25 is valid for both cases. The second terminus penalties different states to "0", in order to create a cyclical wave in the transformer. The third terminus of the cost function penalties the magnetization current in the high frequency transformer. The fourth terminus minimises the current ripple of the ESS. In figure 5.6, the block diagram for the proposed controller is represented. As can be seen in the block diagram, in order to give stability to the controller the performance calculus input is filtered with a low pass filter (LPF).

5.3.2 VSI Current Predictive Control Based on Fourier Transform

This method was introduced in [207]. In the primary control level of the microgrid an active and reactive power reference is followed and it is supposed that the frequency and voltage level of the microgrid are imposed by the grid itself or by the master of the microgrid (this will be introduced in section 5.4).

5.3.2.1 Park's Transformation

In electrical engineering, Park's transformation or dqo-transformation is a mathematical transformation that rotates the reference frame of three-phase systems in an effort to simplify the analysis of three-phase circuits. The dqo transformation can be thought of in geometric terms as the projection of the three separate sinusoidal phase quantities onto two axes rotating with the same angular velocity

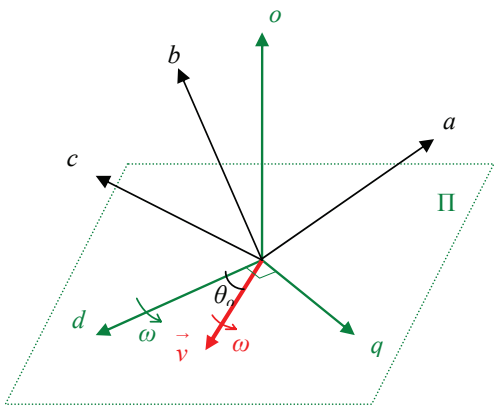

Figure 5.7. Park's transformation

as the sinusoidal phase quantities. The two axes are called the direct, or d, axis; and the quadrature or q, axis; that is, with the q-axis being at an angle of 90 degrees from the direct axis, see figure 5.7. The mathematical expression for this transformation can be expressed as shown in equation (5.28):

$$\begin{bmatrix} U_d(t) \\ U_q(t) \\ U_o(t) \end{bmatrix} = \frac{1}{\sqrt{3}} \begin{bmatrix} \cos(\omega t) & \cos(\omega t - \frac{2\pi}{3})) & \cos(\omega t + \frac{2\pi}{3})) \\ \sin(\omega t) & \sin(\omega t - \frac{2\pi}{3})) & \sin(\omega t + \frac{2\pi}{3})) \\ 1 & 1 & 1 \end{bmatrix} \cdot \begin{bmatrix} U_a(t) \\ U_b(t) \\ U_c(t) \end{bmatrix} \tag{5.28}$$

Usually the d-axis is aligned with the voltage reference. Using the dqo framework, the expressions for the instantaneous active and reactive power, as well, as the harmonic current in the inverter can be expressed as shown in equations 5.29 and 5.30.

$$P_{inst}(t) = \frac{3}{2}(U_d(t)I_d(t) + U_q(t)I_q(t_k) + 2U_o(t)I_o(t)) \tag{5.29}$$

$$Q_{inst}(t) = \frac{3}{2}(U_q(t)I_d(t) - U_d(t)I_q(t)) \tag{5.30}$$

The dqo equations to evaluate the active and reactive power are only accurate for balanced and harmonic-free three-phase voltages and currents.

5.3.2.2 Fourier Expressions

As explained in the previous section, the instantaneous active power and reactive power expressed with Park's transformation can only be computed for balanced and harmonic-free three-phase voltages. While it is still necessary to compute the active and reactive powers associated with a periodic set of three-phase voltages

and currents equations. This is done through the Fourier analysis of the current and voltage signals per phase. As is well-known, a signal $y(t)$ can be expressed by a Fourier series of the form:

$$y(t) = \frac{a_0}{2} + \sum_{n=0}^{\infty} a_n \cos(n\omega t) + b_n \cos(n\omega t) \tag{5.31}$$

where n represents the rank of the harmonics (n = 1 corresponds to the fundamental component). The magnitude and phase of the selected harmonic component can be calculated by the next equations:

$$|H_n| = \sqrt{a_n^2 + b_n^2} \tag{5.32}$$

$$\underline{/H_n} = \arctan\left(\frac{b_n}{a_n}\right) \tag{5.33}$$

where,

$$a_n^y = \frac{2}{T}\int_{t-T}^{t} y(t)\cos(n\omega t)dt$$

$$b_n^y = \frac{2}{T}\int_{t-T}^{t} y(t)\sin(n\omega t)dt$$

being $T = 1/f$ the corresponding period to the fundamental frequency. (Note that the upper index y is related to the signal $y(t)$ in which the Fourier analysis is developed). Using expressions 5.32 and 5.33, for the voltage and current signals, the value of this signal expressed in the Fourier's domain $\mathscr{U}(t)$ and $\mathscr{I}(t)$. can be obtained

The equivalent Thevenin's impedance calculated for the fundamental frequency can be estimated in polar coordinates:

$$\left|Z_n^{th}(t)\right| = \frac{\sqrt{(a_n^U(t))^2 + (b_n^U(t))^2}}{\sqrt{(a_n^I(t))^2 + (b_n^I(t))^2}} \tag{5.34}$$

$$\varphi_n^{th}(t) = \underline{/Z_n^{th}}(t) = \arctan\left(\frac{b_n^U(t)}{a_n^U(t)}\right) - \arctan\left(\frac{b_n^I(t)}{a_n^I(t)}\right) \tag{5.35}$$

The upper index v and i are related to the output voltage and output current of the inverter. The expression for active and reactive powers of the voltage-current pairs calculated at fundamental frequency can be computed (being $\varphi_{j,n}^{th}(t_{k+1})$ the phase of Thevenin's impedance evaluated at $n = 1$):

$$P_m(t) = \frac{\sqrt{(a_n^U(t))^2 + (b_n^U(t))^2}}{\sqrt{2}} \frac{\sqrt{(a_n^I(t))^2 + (b_n^I(t))^2}}{\sqrt{2}} \cos(\varphi_n^{th}(t)) \tag{5.36}$$

$$Q_m(t) = \frac{\sqrt{(a_n^U(t))^2 + (b_n^U(t))^2}}{\sqrt{2}} \frac{\sqrt{(a_n^I(t))^2 + (b_n^I(t))^2}}{\sqrt{2}} \sin(\varphi_n^{th}(t)) \tag{5.37}$$

Expressions and are valid for all the cases, including non-balanced and non-harmonic-free three-phase voltages and currents systems.

5.3.2.3 Predictive Model of the Current and Voltage of the VSI

The inverter modelled corresponds to a two-level voltage source inverter (2L-VSI) (see figure 5.8 and table 5.4). It is composed of three-legs, each one is made up of two power switches, one connected to the positive terminal of the DC voltage source (or dc-link capacitor) and the other switch connected to the negative terminal. The switches states are functions of the associated gate signals. The gate signals applied to the switches situated at the same leg of the inverter are related, the value of the negative terminal connected gate signal is the opposite of the positive terminal gate signal. Each gate signal can only adopt two values: "0" if the power switch is at OFF-state and "1" when the power switch is at ON-state. Taking into consideration that there are three legs there are $2^3 = 8$ possible states of the inverter. The output of each leg of the inverter is connected to an LC-filter. In order to obtain a rough estimation of the real value of the inductor and the capacitor, their associated resistances are also considered.

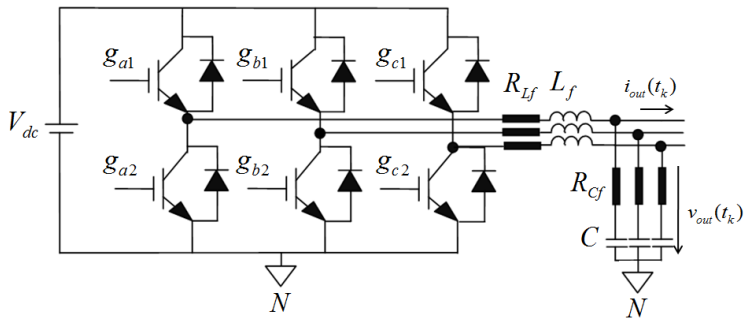

Figure 5.8. Voltage source inverter with output LC filter

The inverter can be modelled as a function of its decision variables (gate signals of each leg (g_{a1},g_{b1},g_{c1})) and its state variables, inductor currents or capacitor voltages of the output filter (I_{La},I_{Lb},I_{Lc},U_{Ca},U_{Cb},U_{Cc}). The output voltage and current of the inverter can be obtained as a function of the decision variables and the state variables evolution, obtaining the relationship expressed in the following

Table 5.4. Parameters of the Inverter

Parameter	Value
Filter inductance L	$1[mH]$
Filter inductance resistance R_L	$0.1[\Omega]$
Filter capacitor C	$0.5\ [mF]$
Filter capacitor resistance R_C	$0.1[\Omega]$
DC link voltage U_{dc}	$700\ [V]$

equations.

$$U_j^{out}(t_{k+1}) = U_{dc}(t_{k+1}) \cdot g_{j1}(t_{k+1}) - L_j \frac{I_L(t_{k+1}) - I_L(t_k)}{T_s} - R_L \cdot I_{L_j}(t_{k+1})\Big|_{j=a,b,c} \tag{5.38}$$

$$I_{C_j}(t_k+1) = C \frac{U_{C_{jN}}(t_{k+1}) - U_{C_{jN}}(t_k)}{T_s}\Bigg|_{j=a,b,c} \tag{5.39}$$

$$U_{C_j}(t_{k+1}) = U_j^{out}(t_{k+1}) - R_C \cdot I_{C_j}(t_{k+1})\Big|_{j=a,b,c} \tag{5.40}$$

$$I_j^{out}(t_{k+1}) = I_{L,j}(t_{k+1}) - I_{C,j}(t_{k+1})|_{j=a,b,c} \tag{5.41}$$

Using the inherent property of Park's transformation (being a rotational reference frame of three-phase systems), the dqo output voltage for the next instant is supposed to be similar to when the control decision is taken, resulting in the approximation given by equation (5.42):

$$\begin{bmatrix} U_a^{out}(t_{k+1}) \\ U_b^{out}(t_{k+1}) \\ U_c^{out}(t_{k+1}) \end{bmatrix} = \begin{bmatrix} \cos(\omega t_{k+1}) & -\sin(\omega t_{k+1}) & 1 \\ \cos(\omega t_{k+1} - \frac{2\pi}{3}) & -\sin(\omega t_{k+1} - \frac{2\pi}{3}) & 1) \\ \cos(\omega t_{k+1} + \frac{2\pi}{3}) & -\sin(\omega t_{k+1} + \frac{2\pi}{3}) & 1) \end{bmatrix} \begin{bmatrix} U_d^{out}(t_k) \\ U_q^{out}(t_k) \\ U_o^{out}(t_k) \end{bmatrix} \tag{5.42}$$

Using equations (5.38)-(5.42), the output current and voltage of the inverter can be obtained. Applying the Fourier's transformation to this signal Fourier's expression for the fundamental harmonic $n = 1$ of both signals ($\mathscr{U}_{j,n}^{out}(t_{k+1})$,$\mathscr{I}_{j,n}^{out}(t_{k+1})$) per each phase $j = a, b, c$.can be obtained. With this value the active and reactive powers of the voltage-current pairs at fundamental frequency can be computed, being $\varphi_{j,n}^{th}(t_{k+1})$ the phase of equivalent Thevenin's impedance evaluated at $n = 1$, for each phase of the inverter:

$$P_{m,j}(t_{k+1}) = \frac{1}{2} \left|\mathscr{U}_{j,n}^{out}(t_{k+1})\right| \left|\mathscr{I}_{j,n}^{out}(t_{k+1})\right| \cos(\varphi_{j,n}^{th}(t_{k+1}))\Big|_{j=a,b,c} \tag{5.43}$$

$$Q_{m,j}(t_{k+1}) = \frac{1}{2}\left|\mathscr{U}_{j,n}^{out}(t_{k+1})\right|\left|\mathscr{I}_{j,n}^{out}(t_{k+1})\right|\sin(\varphi_{j,n}^{th}(t_{k+1}))\Big|_{j=a,b,c} \tag{5.44}$$

Using Park's transformation the instantaneous expression for active and reactive power in dqo-coordinates: can be gathered

$$P_{inst}(t_{k+1}) = \frac{3}{2}\left(U_d^{out}(t_{k+1})I_d^{out}(t_{k+1} + U_q^{out}(t_{k+1})I_q^{out}(t_{k+1}) + 2U_o^{out}(t_{k+1})I_o^{out}(t_{k+1})\right) \tag{5.45}$$

$$Q_{inst}(t_{k+1}) = \frac{3}{2}(U_q^{out}(t_{k+1})I_d^{out}(t_{k+1}) - U_d^{out}(t_{k+1})I_q^{out}(t_{k+1})) \tag{5.46}$$

5.3.2.4 Control Algorithm

The block diagram of the control algorithm is shown in figure 5.9. The objective function to be minimized by the controller is expressed in equation (5.47).

$$\begin{aligned}\min_{g_{a1},g_{b1},g_{c1}} J = w_0 \cdot \Bigg[& \left(\sum_{j=a,b,c}(P_{m,j}(t_{k+1})) - P^{sch}(t_{k+1})\right)^2 \\ & + \left(\sum_{j=a,b,c}(Q_{m,j}(t_{k+1})) - Q^{sch}(t_{k+1})\right)^2\Bigg] \\ & w_1 \cdot \left[\left(P_{inst,j}(t_{k+1}) - P^{sch}(t_{k+1})\right)^2\right] \\ & + w_2 \cdot \left(\sum_{j=a,b,c}\Delta g_j(t_{k+1})\right)^2 + w_3 \cdot (I_{out,o}(t_{k+1}))^2\end{aligned} \tag{5.47}$$

The end goal of the control algorithm is to track with high precision the established schedule in active and reactive power for the inverter. The valid expression for this tracking is the expressed in equations (5.43) and (5.44). For this reason the maximum weight cost in the cost function is assigned to the terminus. The single use of this terminus will cause some instable situations due to the quadratic component of the decision variables in expression (5.43) and (5.44). These instable conditions are corrected using the second and third terminus of the objective function. The second terminus punishes deviations from the schedule of values obtained for Park's expression for active and reactive power. The third terminus punishes the control effort of signal g_i. This schedule must be completed with minimum harmonic current for that reason the fourth terminus of the objective function exists.

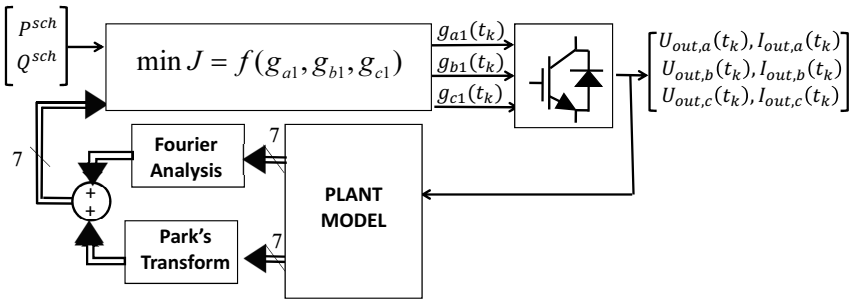

Figure 5.9. Grid connected MPC controller block diagram

5.4 Secondary Model Predictive Control Design

Two main modes are given in the Secondary Control level of the microgrid corresponding with the two main working modes of the microgrid: grid-connected and islanded. In both cases, one of the ESSs must act as master of the microgrid, carrying out the final balance of the microgrid. In the case of islanded, the microgrid master ESS must impose the voltage and frequency reference levels in order to synchronise wotj the rest of components of the microgrid. When the microgrid is working in connected mode, the master must be the ultimate responsible of fulfilling the contracted schedule with the main grid. This control level is also charged to make the transition between both modes. The inertia under transient conditions of classic methods based on PI-Controllers result in several power qualities losses. With the proposed method the transient periods are minimised using the fast response of the MPC controllers.

5.4.1 VSI Voltage Predictive Control Based on Fourier Transform

This method was presented in [208]. It is a new control strategy based on Model Predictive Control and a Fourier analysis is presented in this paper applied to the voltage/frequency controls of a Voltage Source Inverter. At each sample instant, the current demand in the microgrid is predicted via the estimation of the equivalent Thevenin's impedance in the microgrid. Thus it allows the inverter controller to select the most appropriate gate signal combination to maintain the frequency and voltage reference in the microgrid.

5.4.1.1 Predictive Model of the Current and Voltage of the Inverter

The inverter is modelled as a function of its decision variables, gate signals of each leg (g_{a1},g_{b1},g_{c1}) and its state variables, inductor currents and capacitor voltages of the output filter (I_{La},I_{Lb},I_{Lc},U_{Ca},U_{Cb},U_{Cc}). The output voltage and current of the inverter can be obtained as functions of the decision variables and the state variables evolution, obtaining the relationship expressed in the following equations .

$$\begin{aligned} U_{out,j}(t_{k+1}) = U_{dc}(t_{k+1}) \cdot g_{j1}(t_{k+1}) - L_j \frac{I_L(t_{k+1}) - I_L(t_k)}{T_s} \\ -R_L \cdot I_{L_j}(t_{k+1})\big|_{j=a,b,c} \end{aligned} \tag{5.48}$$

$$I_{C_j}(t_k+1) = C \frac{U_{C_{jN}}(t_{k+1}) - U_{C_{jN}}(t_k)}{T_s}\bigg|_{j=a,b,c} \tag{5.49}$$

$$U_{C_j}(t_{k+1}) = U_{out,j}(t_{k+1}) - R_C \cdot I_{C_j}(t_{k+1})\big|_{j=a,b,c} \tag{5.50}$$

$$I_{out_j}(t_{k+1}) = I_{L,j}(t_{k+1}) - I_{C,j}(t_{k+1})\big|_{j=a,b,c} \tag{5.51}$$

$$\begin{aligned} U_{out,j}(t_{k+1}) = R_j^{th}(t_k) \cdot I_{out,j}(t_{k+1}) \\ +L_j^{th}(t_k) \frac{I_{out,j}(t_{k+1}) - I_{out,j}(t_k)}{T_s}\bigg|_{j=a,b,c} \end{aligned} \tag{5.52}$$

5.4.1.2 Control Algorithm

Using the inherent property of Park's transformation (a rotational reference frame of three-phase systems), the reference voltage for the next sample instant can be fixed to a constant value for all the instants. Finally the cost function of the control algorithm is explained in equation (5.53):

$$\begin{aligned} J = \left(U_{out,d}(t_{k+1}) - U_d^{ref}\right)^2 + \left(U_{out,q}(t_{k+1}) - U_q^{ref}\right)^2 \\ + \left(U_{out,o}(t_{k+1}) - U_o^{ref}\right)^2 \end{aligned} \tag{5.53}$$

where the d-axis is aligned with the voltage reference.

The computation of the control action (gate signals) is performed by evaluating the cost function for each value of the gate signals and using those which are smaller than J. Note that a prediction horizon of 1 is used in order to avoid excessive computations.

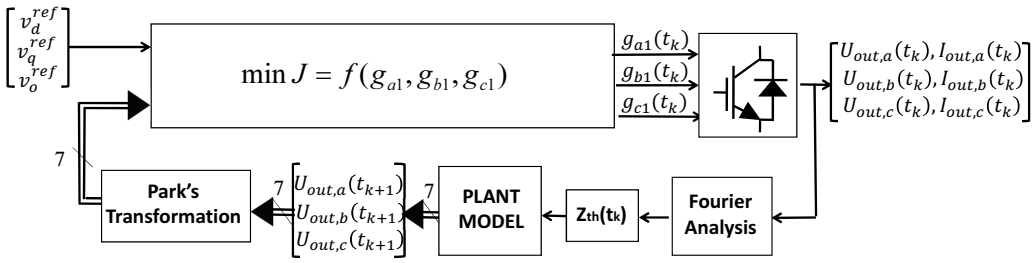

Figure 5.10. Block diagram of the control algorithm for the Voltage Predictive Control based on the Fourier Transform algorithm applied to the VSI

5.4.2 VSI Current Predictive Control Based on Fourier Transform

In grid-connected mode the microgrid master must carry out the final balance of the microgrid in order to fulfil the power requirement of the schedule carried out with the main grid at the economic dispatch level, explained in Chapter 4. The algorithm is similar to the case explained in section 5.3.2 but the ESS which acts as master of the microgrid (in this case the ultracapacitor) has as reference the active and reactive power obtained by the following equations:

$$P_{uc}^{sch}(t_{k+1}) = P_{grid}^{sch}(t_{k+1}) - P_{\mu grid}(t_k) \tag{5.54}$$

$$Q_{uc}^{sch}(t_{k+1}) = Q_{grid}^{sch}(t_{k+1}) - Q_{\mu grid}(t_k) \tag{5.55}$$

where $P_{\mu grid}(t_k)$ and $Q_{\mu grid}(t_k)$ represent the rest of components of the microgrid excluding the one which acts as master.

5.5 Simulation Results

The different controllers have been modelled using Simpower©toolbox of Matlab for several cases. The sample period for the simulation is $T_sim = 1\mu s$, using a sample period for the controller of $T_s = 30\mu s$. The parameters utilized for the model of the converter are shown in tables 5.1 and 5.4.

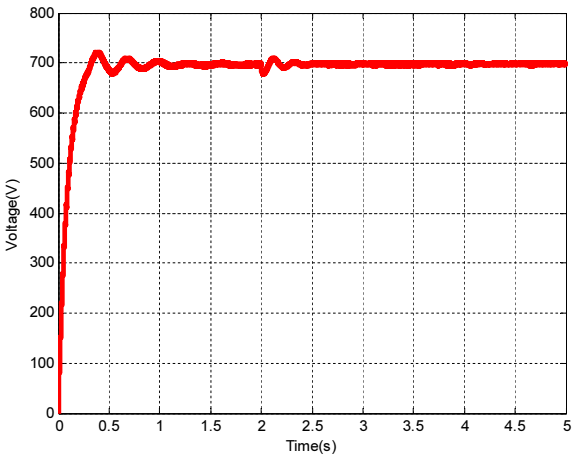

Figure 5.11. Voltage output of the Isolated Full Bridge Booster CSC with the MPC controller with minimum current ripple criteria

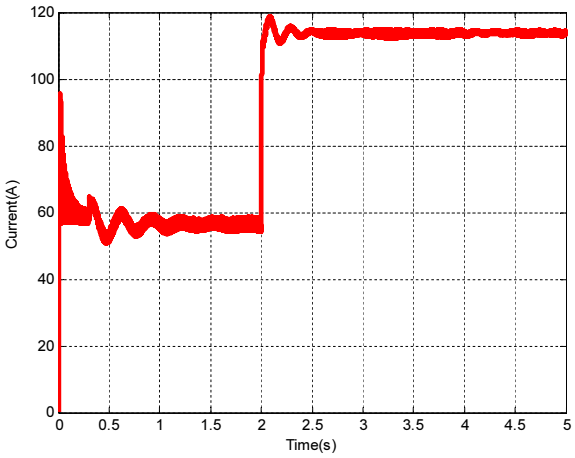

Figure 5.12. Current of the ESS at the input of the Isolated Full Bridge Booster CSC with the MPC controller with minimum current ripple criteria

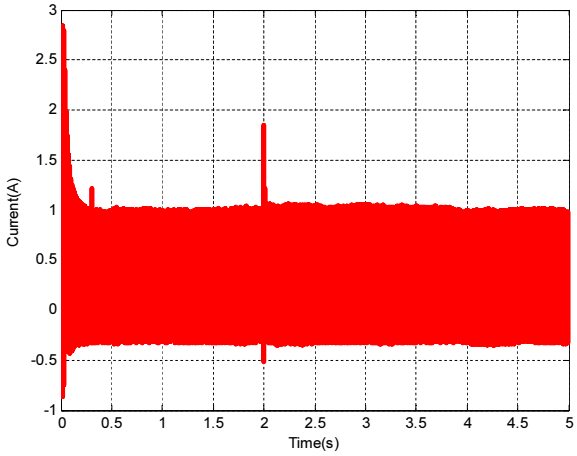

Figure 5.13. Magnetiszation current of the HF transformer of the Isolated Full Bridge Booster CSC with the MPC controller with minimum current ripple criteria

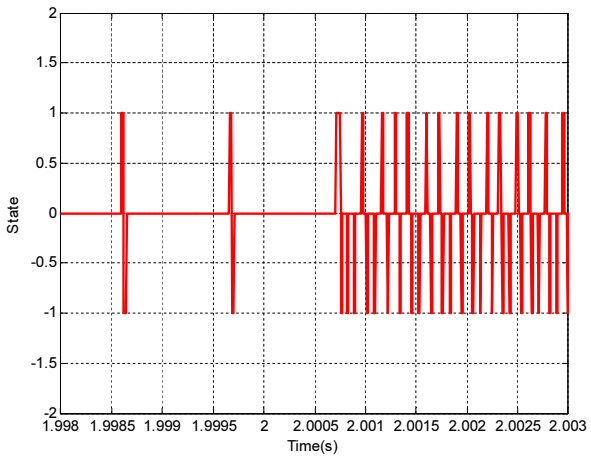

Figure 5.14. State transition at the Isolated Full Bridge Booster CSC with the MPC controller with minimum current ripple criteria

5.5.1 CSC with MPC controller under Minimum Current Ripple Criteria

This simulation is used to validate the behaviour of the proposed MPC controller applied to CSC. The simulation is run over 5 seconds. The values of the controller

coefficients have been set at $w_0 = 1$, $w_1 = 0.001$, $w_2 = 0.01$ and $w_3 = 10$. The input voltage of the converter is set to 100 V and the reference output voltage is set to 700 V. The converter feeds a load of 4 kW over the first two seconds. At time t=2s the load is increased up to 8kW. In figure 5.11, the fast response can be seen in order to track the reference of the controller even when the load is changed. In figure 5.12, the low current ripple of the converter can be observed with the proposed controller even at instant t=2s when the change in the demanded power is carried out. The MPC controller also allows to minimise the magnetisation current of the transformer which entails an increase in the performance of the converter (see figure 5.13). In figure 5.14, the transition states of the converter are shown, the waveform of the states can be different at each instant, providing a higherperformance than PWM-based controllers. As can be seen, one of the advantages of the MPC controller is its possibility to carry out a multivariable control.

5.5.2 VSI Current Predictive Control Based on Fourier Transform

The behaviour of the proposed controller explained in section 5.3.2 will be explained and validated with this simulation. In order to evaluate the behaviour of the controller it has been compared with a classic PI-Controlled inverter. The results of the comparison can be observed in figure 5.15. The simulation is run over two seconds. At the beginning, the reference in active and reactive power is set to $P_{ref} = 1000$ W and $Q_{ref} = 500$ Var. At $t = 1$ s the references are changed into $P_{ref} = -1000$ W and $Q_{ref} = -500$ Var. While the PI-controller needs a transient period in order to track the new reference, the MPC controller based on Fourier Transform method only needs one cycle of the fundamental frequency to achieve the active and reactive power. Besides this, there is no-coupling with the track carried out between the active and the reactive power. The weighting factors applied to the controller have been $w_0 = 10$, $w_1 = 1$, $w_2 = 1000$ and $w_3 = 1000$. The results of the simulation can be observed in figure 5.15. The current wave form for phase a is also compared between the hysteresis method and the MPC strategy giving better results for the current wave form in the MPC controller, as well as, a lower THD value. MPC THD value is 1.5% versus THD=2.15% in the case of the PI-controller (See figure 5.16). The spectra analyses of the current output of the inverter in phase "a" at t=1.5 s is shown in figure 5.17.

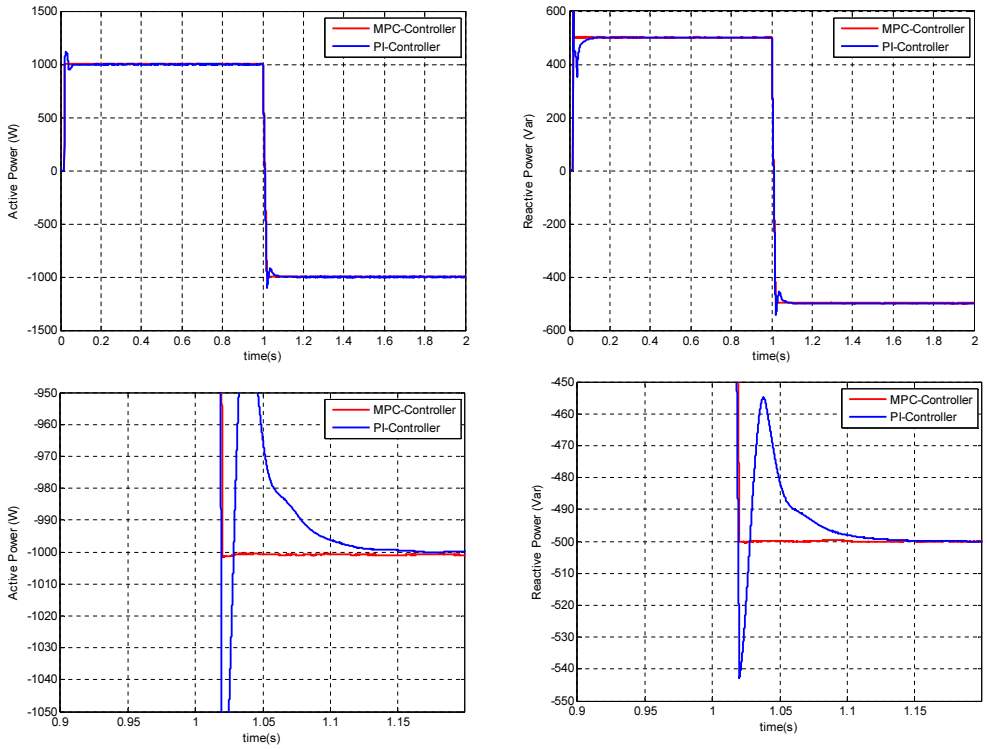

Figure 5.15. Comparison of the response between the MPC controller applied to the classic PI-controller applied to a VSI under a change in the reference of active and reactive power

5.5.3 VSI Voltage Predictive Control Based on Fourier Transform

The first simulation was carried out in order to compare the behaviour of the proposed controller with classic PI-PWM controllers under linear loads. The inverter is connected at each phase to a linear load composed by a resistor (10Ω) in series with an inductor ($1mH$). The results of the simulation (figure 5.18) show a faster response of the MPC-controller versus the PI-PWM controller. Once again, while the PI-PWM needs a transient period to reach the voltage reference, the MPC-controller only needs one cycle of the fundamental frequency to carry out the calculus of the equivalent Thevenin's impendance to send the optimal signal to the drivers of the IGBTs which compose the VSI.

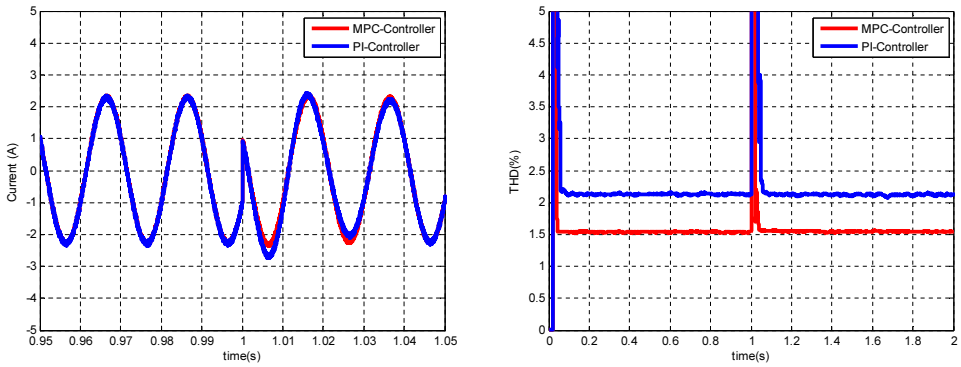

Figure 5.16. Comparison of current output between the MPC controller applied to the classic PI-controller applied to a VSI under a change in the reference of active and reactive power

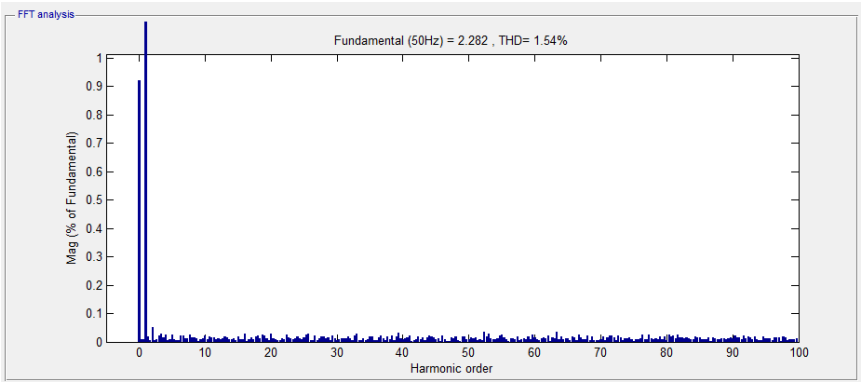

Figure 5.17. Spectra analysies of the current output MPC control-based inverter in the phase a at t=1.5s

The second simulation carried out has been used to evaluate the behaviour of the proposed controller under non-linear loads. The simulink scheme for this case is explained in figure 5.19. A circuit breaker manages the connection at instant $t = 0s$ and the disconnection at $t = 2s$ of a non-linear load composed by a diode full-bridge rectifier whose output is connected to a capacitor ($C_{nonlinear} =$

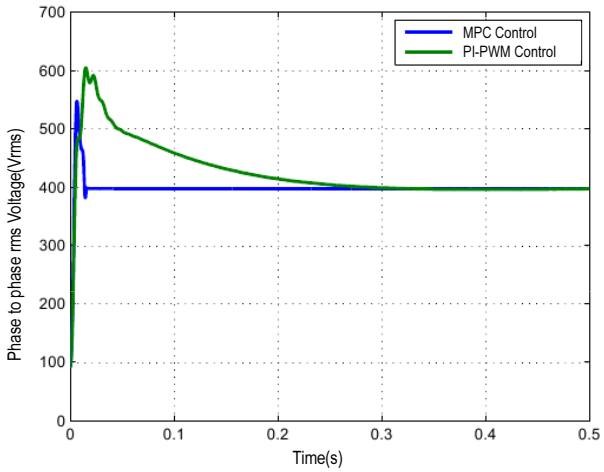

Figure 5.18. Comparison of the phase-to-phase rms output voltage of the inverter between the MPC and the PI-PWM controllers

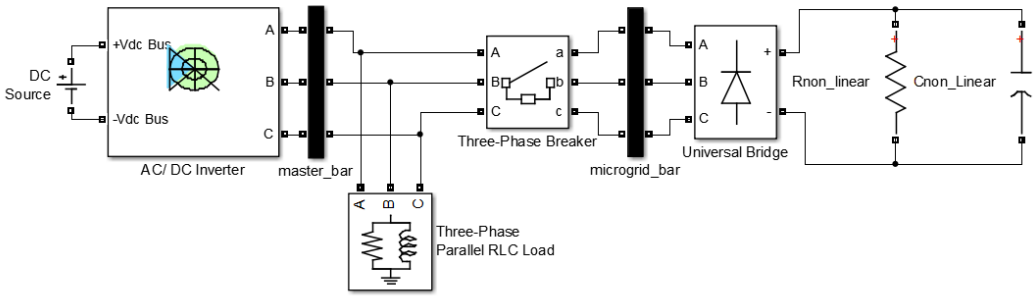

Figure 5.19. Simpower model simulation with non-linear loads connected to the inverter

$3000\mu F$) in parallel position with resistance ($R_{nonlinear} = 60\Omega$). During all the simulation, a three-phase parallel RLC load is also connected. The values used for the RLC load have been active power ($P = 10kW$) and inductive reactive power ($Q_L = 100$ positive VAr). In figure 5.20, the results of the output voltage of the inverter can be observed for all instants of the simulation with the measurement of phase-to-phase rms voltage. The results show a low voltage ripple for all instant ($\leq 1\%$ when only linear loads are connected) and fast dynamic response when the non-linear load is connected. The output voltage waveform is shown in figure 5.21.

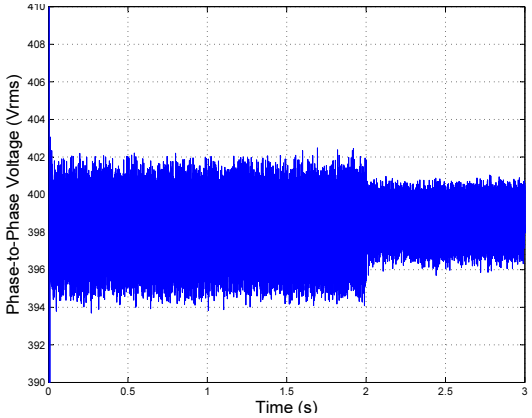

Figure 5.20. Measurement of the phase-to-phase rms output voltage of the inverter with the MPC controller with connected linear and non-linear loads

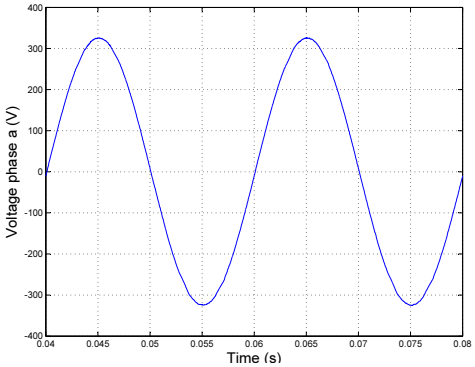

Figure 5.21. Measurement of the output voltage of the inverter in the phase a with the MPC controller with connected non-linear loads

The spectra analyses of the voltage output at phase a of the inverter have been developed for both linear and non-linear connected loads. Non-linear loads produce an increase in the THD value of 0.45 % and low content of harmonics up to $n = 20$. In the case of linear loads, the result of the spectra analysis carried out over three frequency cycles at instant $t = 2.5$ has a THD value of 0.28 % (see figure 5.23) with all the harmonic-contained weight next to the fundamental harmonic.

In figure 5.24 and figure 5.25, the values of the current predicted by the controller and of that obtained by Simpower are shown with accurate results, even with the current spikes due to the capacitor of the non-linear load.

The third simulation is run during a period of 2s where the behaviour of the islanded inverter is evaluated when a grid-tied inverter (controlled by the PI-

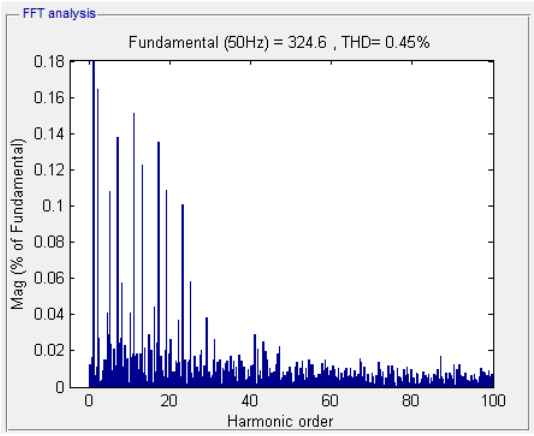

Figure 5.22. Spectra analyses for the output voltage of the phase a in the MPC control-based-islanded inverter at instant $t = 0.5$ s (Non-Linear loads connected)

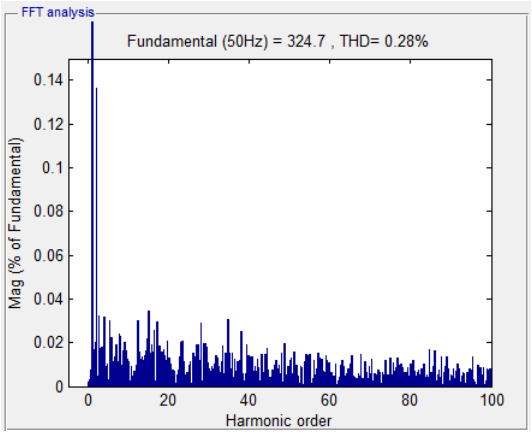

Figure 5.23. Spectra analyses for the output voltage of phase a in the MPC control-based-islanded inverter at instant $t = 2.5$ s (Linear loads connected)

Hysteresis current control method) is connected to the islanded microgrid. The model is shown in figure 5.26. The islanded inverter acts as a grid, regulating the voltage and the frequency in the islanded-microgrid where a non-linear source interfaced with a grid-connected inverter is connected.

In order to evaluate the dynamic behaviour of the islanded inverter, the ref-

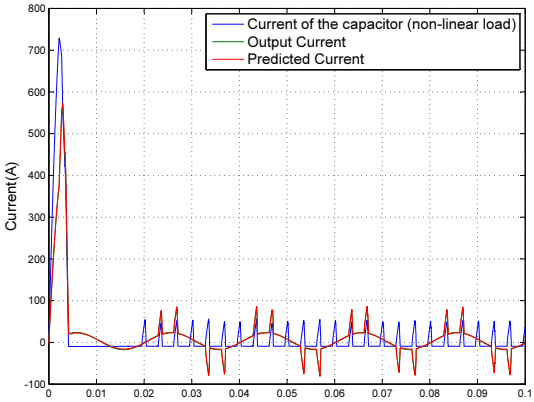

Figure 5.24. Predicted current, output current of the inverter and current of the capacitor of non-linear loads

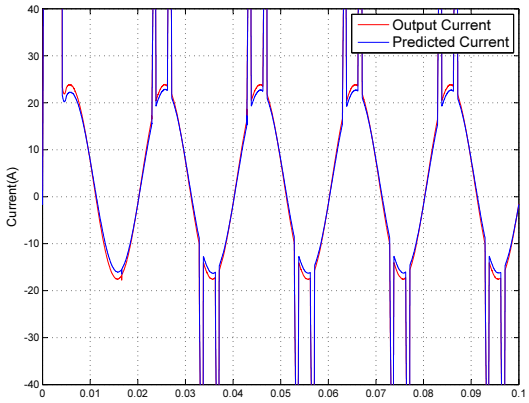

Figure 5.25. Predicted current versus output current of the inverter with the presence of non-linear loads

erence values for active and reactive power of the grid-connected inverter are modified in $t = 1s$ (see figure 5.27). As can be observed in the figure 5.28 the inverter has an immediate response to the new situation.

The voltage output waveform is demonstrated in figure 5.29. The harmonic analysis for this situation is displayedin figure 5.30. The results indicate a major weight of the harmonic over the fundamental component and low harmonic-content for the rest, being the measurement of the total harmonic distortion THD = 0.26%.

The comparison between the current predicted by the model and the one

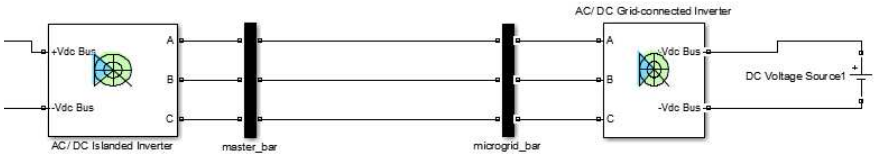

Figure 5.26. Simpower model simulation with the grid-tied inverter connected to the islanded inverter with voltage MPC

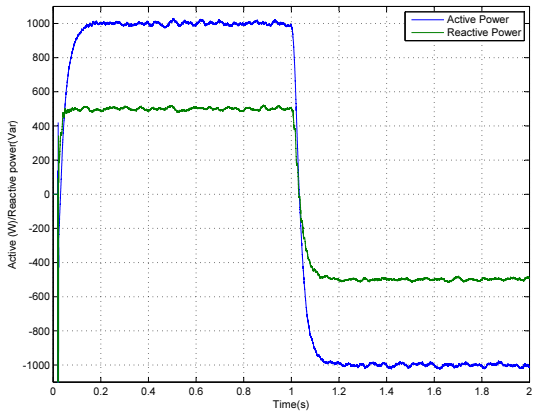

Figure 5.27. Active/Reactive Power injected by the grid-connected inverter

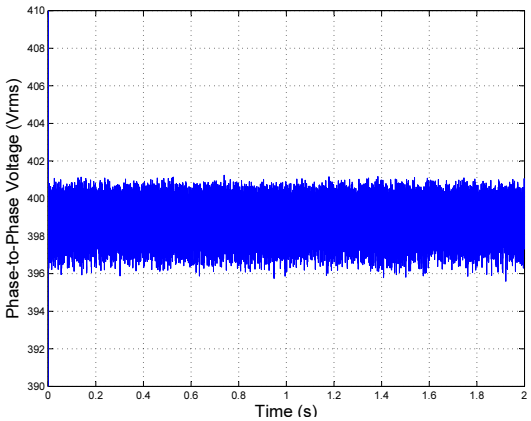

Figure 5.28. Measurement of the phase-to-phase rms output voltage of the islanded inverter with a grid-connected inverter

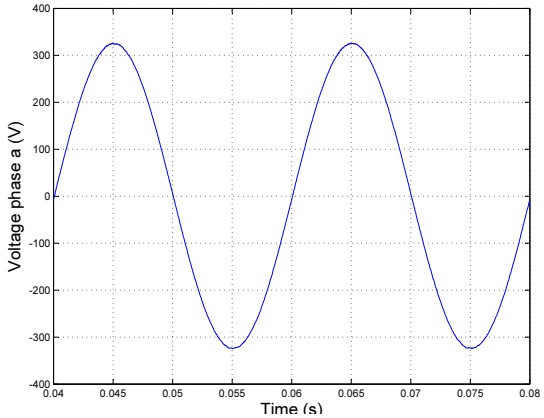

Figure 5.29. Measurement of the output voltage of the islanded inverter in the phase a with a grid-tied inverter connected

obtained by the simulation is presented in figure 5.31 with accurate results even for the most difficult case that is produced when the active and reactive power reference of the grid-tied inverter is modified (t=1s).

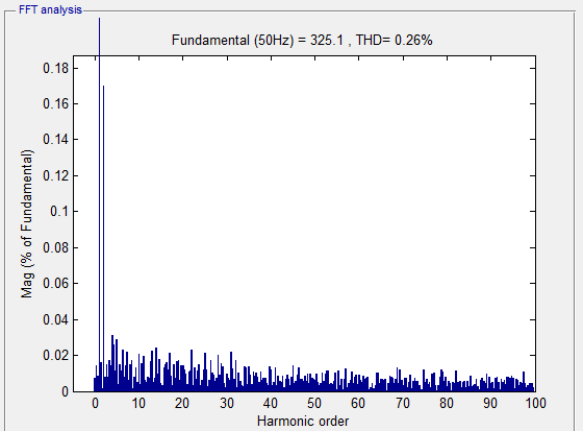

Figure 5.30. Spectra analyses for the output voltage of phase a for a three-phase voltage source at instant $t = 0.5$ s (Non-Linear connected sources)

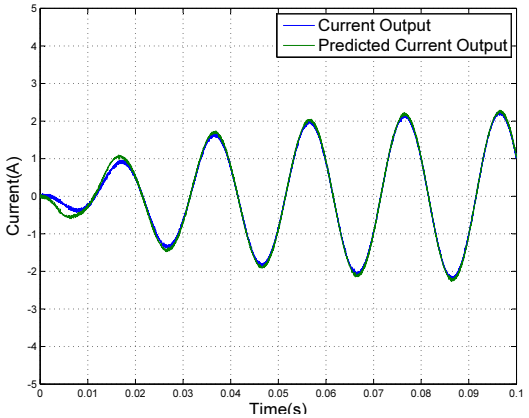

Figure 5.31. Current predicted versus current output of the inverter with the presence of non-linear sources

5.6 Conclusions

The behaviour of a controller applied to the voltage control of a VSI has been developed and analysed under simulation. The results show a better and faster response under transient in comparison with the classic PI-PWM controller of VSI.

A model predictive control based algorithm needs a model to implement the controller. Although the inverter needs to be modelled with this method, the load is modelled on-line by the controller with accurate results for current prediction in all of the cases with the developed technique.

The inverter has been designed to act as a master of a microgrid when the islanded-mode of operation is needed. The most critical cases of non-linear loads non-linear sources have been tested showing an accurate response for each one of the cases explained.

Future developments will be based on expanding the technique to cases of harmonics introduction and unbalanced loads. This should be carried out using an active control of the fourth wire(neutral) of the inverter and the real application to a VSI i(to evaluate the final results of the MPC controller).

Chapter 6

Conclusions

6.1 Closing Remarks

New control algorithms for renewable energy microgrids with hybrid energy storage systems, during both grid-connected and micro-grid modes of operation, have been proposed and presented in this thesis. The proposed control algorithms are designed to carry out a robust ESS interface that guarantees stability and high power quality injection. This is to be done under the challenging and uncertain nature of distribution systems and future smart grids and provides an optimal economic operation of the microgrid under minimum degradation criteria applied to the different ESSs considered.

In Chapter 3, the modelling and analysis of each component of the microgrid is carried out, focusing on the main integration problems in the microgrid from the point of view of energy forecasting, power quality or degradation issues.

The different problems concerning the economic dispatch are solved in Chapter 4. In this chapter, an MPC controller for the optimal economic dispatch of a microgrid has been presented and validated. This formulation integrates operational costs in the optimization problem, including degradation of all the components of the hybrid ESS, especially the hydrogen-based storage. This allows an optimal scheduling policy linked to the time-varying price of energy.

Power quality issues are detailed in Chapter 5, where new control algorithms applied to ESS power converters are carried out, developing the voltage and current predictive control based on Fourier Transform techniques. An MPC control algorithm applied to DC-DC converters is also developed to minimize the current ripple of the ESS.

6.2 Contributions

The main contributions of this dissertation can be highlighted with the next items:

1. To introduce a new MLD formulation for the economic dispatch of renewable energy microgrids with hybrid storage energy systems. Besides the capital cost of each ESS the different degradation issues are included to minimize the total cost of using the ESS in the microgrid.

2. To introduce the tri-hybrid ESS composed by hydrogen, a battery and an ultracapacitor in the microgrid management through a MPC controller which minimizes the disadvantages of each ESS whilst harnessing advantages.

3. To solve the different time-scales of the economic schedule of the microgrid with the objective of integrating the renewable energy system in the electrical market.

4. To develop a new control technique applied to power inverters based on the MPC where the short horizon control is solved using periodical signals based on Fourier Transform.

5. To integrate the MPC technique in DC-DC converters so as to minimizse the current ripple effect in different ESSs.

Throughout the thesis we have published the articles cited in the bibliography [43, 189] and the works presented at international conferences [187, 188, 206, 207, 208].

6.3 Future studies

Concluded this work the next directions are given in order to follow up the research topics:

1. To expand the hybrid MPC controller with stochastic and distributed MPC techniques applied to microgrids networks or microgrids with external agents such as the electrical vehicles, is one of the most interesting lines considered.

2. To introduce other ESSs in the MPC algorithm such as flywheel, SMES, molten salts or graphene batteries. These should be one of the next lines to develop.

3. The proposed method in Chapter 5, MPC based on Fourier Transform applied to VSI must be expanded to the cases of unbalanced loads and harmonic injection in the microgrid. Thus it will be necessary to expand the method with an active control over the fourth or neutral wire. The method must be also extended to LCL filters and implemented on a real system.

4. To introduce power electronic controllers to DC-microgrids or the HVDC smart grid.

5. The direct application of optimal load sharing methods to the fuel cell vehicle.

References

[1] J. Rifkin, *The third industrial revolution.* Palgrave MacMillan, 2011. 1

[2] F. Katiraei, R. Iravani, N. Hatziargyriou, and A. Dimeas, "Microgrids management," *Power and Energy Magazine, IEEE*, vol. 6, no. 3, pp. 54–65, 2008. 2, 29, 30, 31

[3] M. H. Bollen, J. Zhong, F. Zavoda, J. Meyer, A. McEachern, and F. Lopez, "Power quality aspects of smart grids," in *Procedings of International Conference on Renewable Energies and Power Quality*, 2010. 2, 3, 4, 39, 142, 143, 144, 145

[4] I. R. Aleksandar Janjic, Zoran Stajic, "Power quality requirements for the smart grid design," in *International Journal of Circuits, Systems and Signal Processing*, 2011. 2, 3, 4, 39, 142, 144

[5] R. Lasseter, A. Akhil, C. Marnay, J. Stephens, J. Dagle, R. Guttromson, A. Meliopoulous, R. Yinger, and J. Eto, "The certs microgrid concept," *White paper for Transmission Reliability Program, Office of Power Technologies, US Department of Energy*, 2002. 2, 3, 30

[6] T. Logenthiran and D. Srinivasan, "Intelligent management of distributed storage elements in a smart grid," in *Power Electronics and Drive Systems (PEDS), 2011 IEEE Ninth International Conference on.* IEEE, 2011, pp. 855–860. 4, 105, 145

[7] C. Dötsch, "Energy storage," in *Technology Guide.* Springer, 2009, pp. 362–367. 5, 7, 12, 14, 20, 21, 22, 23, 25, 26, 28

[8] P. Flynn *et al.*, "Meeting the energy needs of future warriors, committee on soldier power/energy systems, board on army science and technology, national research council of the nation academies, ed," 2004. 6

[9] Y. A.-R. I. Mohamed, "New control algorithms for the distributed generation interface in grid-connected and micro-grid systems," Ph.D. dissertation, University of Waterloo, 2008. 12, 41, 147

[10] G. Boyle, *Renewable energy*. OXFORD university press, 2004. 13

[11] M. Deshmukh and S. Deshmukh, "Modeling of hybrid renewable energy systems," *Renewable and Sustainable Energy Reviews*, vol. 12, no. 1, pp. 235–249, 2008. 13

[12] V. Sharma and H. Chawla, "Integrated renewable systems," in *Power, Control and Embedded Systems (ICPCES), 2012 2nd International Conference on*. IEEE, 2012, pp. 1–6. 13

[13] P. Balamurugan, S. Ashok, and T. Jose, "Optimal operation of biomass/wind/pv hybrid energy system for rural areas," *International Journal of Green Energy*, vol. 6, no. 1, pp. 104–116, 2009. 13

[14] T. Ackermann, S. Cherevatskiy, T. Brown, R. Eriksson, A. Samadi, M. Ghandhari, L. Söder, D. Lindenberger, C. Jägemann, S. Hagspiel *et al.*, "Smart modeling of optimal integration of high penetration of pv–smooth pv." 13, 56, 57

[15] EPIA, "Connecting the sun, solar photovoltaics on the road to large/scale grid integration," European Photovoltaic Industry Association, Tech. Rep., September 2012. 13, 14

[16] A. Jger-Waldau, "Pv status report 2012," EU JRC Scientific and Policy Report, Tech. Rep., October 2012. 13

[17] M.-J. Wilkes, J., "Wind in power: 2012 european statistics," *European Wind Energy Association*, 2013. 14

[18] K. Eger, J. Gtz, R. Sauerwein, A. von Jagwitz, D. Boda, R. del Olmo Arce, C. Matrose, M. Gdde, and F. Chatzipapadopoulos, "Microgrid scenario building blocks," *Future Internet for Smart Energy (FINSENY) and Seventh Framework Programme, Aug*, vol. 5, 2011. 14

[19] M. T. G. R. Papapetrou, Michael and G. Garcia, "European regulatory and market framework for electricity storage infrastructure, store project, deliverable 4.2 (june 2013)." 15, 16, 17

[20] H. Chen, T. N. Cong, W. Yang, C. Tan, Y. Li, and Y. Ding, "Progress in electrical energy storage system: A critical review," *Progress in Natural Science*, vol. 19, no. 3, pp. 291–312, 2009. 18, 19, 20, 21, 22, 24, 26, 28

[21] T. Nanahara, "Pumped hydro storage," *Journal Japan Institute of Energy*, vol. 81, no. 9; ISSU 905, pp. 811–818, 2002. 20

[22] A. Mohd, E. Ortjohann, A. Schmelter, N. Hamsic, and D. Morton, "Challenges in integrating distributed energy storage systems into future smart grid," in *Industrial Electronics, 2008. ISIE 2008. IEEE International Symposium on*. IEEE, 2008, pp. 1627–1632. 20, 21, 22, 24

[23] F. Crotogino, "Compressed air storage," in *Internationale Konferenz" Energieautonomie durch Speicherung Erneuerbarer Energien*, 2006. 20, 21

[24] R. A. Jouneghani, M. Pipattanasomporn, and S. Rahman, "Flywheel energy storage systems for ride-through applications in a facility microgrid." 21

[25] M. G. Molina, "Dynamic modelling and control design of advanced energy storage for power system applications," *Universidad Nacional de San Juan Argentina*. 21, 22, 23

[26] C. Abbey and G. Joos, "Supercapacitor energy storage for wind energy applications," *Industry Applications, IEEE Transactions on*, vol. 43, no. 3, pp. 769–776, 2007. 22

[27] M. H. Ali, B. Wu, and R. A. Dougal, "An overview of smes applications in power and energy systems," *Sustainable Energy, IEEE Transactions on*, vol. 1, no. 1, pp. 38–47, 2010. 23

[28] J. Jin, W. Xu, X. Chen, X. Zhou, J. Zhang, W. Gong, A. Ren, and Y. Xin, "Developments of smes devices and potential applications in smart grids," in *Innovative Smart Grid Technologies-Asia (ISGT Asia), 2012 IEEE*. IEEE, 2012, pp. 1–6. 23

[29] D. S. Padimiti and B. H. Chowdhury, "Superconducting magnetic energy storage system (smes) for improved dynamic system performance," in *Power Engineering Society General Meeting, 2007. IEEE*. IEEE, 2007, pp. 1–6. 23

[30] D. Linden and T. B. Reddy, "Handbook of batteries," *New York*, 2002. 24

[31] B. Dunn, H. Kamath, and J.-M. Tarascon, "Electrical energy storage for the grid: a battery of choices," *Science*, vol. 334, no. 6058, pp. 928–935, 2011. 24

[32] G. Sikha, P. Ramadass, B. Haran, R. White, and B. N. Popov, "Comparison of the capacity fade of sony us 18650 cells charged with different protocols," *Journal of power sources*, vol. 122, no. 1, pp. 67–76, 2003. 25, 35, 73

[33] M. B. Stevens, "Hybrid fuel cell vehicle powertrain development considering power source degradation," Ph.D. dissertation, University of Waterloo, 2008. 25, 35, 72, 73, 85, 86

[34] M. Ball and M. Wietschel, "The future of hydrogen–opportunities and challenges," *International Journal of Hydrogen Energy*, vol. 34, no. 2, pp. 615–627, 2009. 26

[35] S. Dunn, "Hydrogen futures: toward a sustainable energy system," *International journal of hydrogen energy*, vol. 27, no. 3, pp. 235–264, 2002. 26

[36] A. Züttel, "Hydrogen storage methods," *Naturwissenschaften*, vol. 91, no. 4, pp. 157–172, 2004. 26, 27

[37] A. P. Bergen, "Integration and dynamics of a renewable regenerative hydrogen fuel cell system," Ph.D. dissertation, University of Victoria, 2008. 27, 35

[38] A. Roy, "Dynamic and transient modelling of electrolysers by renewable energy sources and cost analysis of electrolytic hydrogen," 2006. 35

[39] S. Yamamoto, S. Sugawara, and K. Shinohara, "Fuel cell stack durability for vehicle application," in *Polymer Electrolyte Fuel Cell Durability*. Springer, 2009, pp. 467–482.

[40] K. W. Suh, "Modeling, analysis and control of fuel cell hybrid power systems," *Department of Mechanical Engineering, The University of Michigan*, 2006. 36, 37, 85, 86

[41] J. T. Pukrushpan, A. G. Stefanopoulou, and H. Peng, *Control of fuel cell power systems: principles, modeling, analysis and feedback design*. Springer Verlag, 2004. 27, 36, 83, 85, 87, 88

[42] A. M. Marcolini, "Técnicas de optimización aplicadas a la supervisión de límites de operación ya la determinación de actuaciones preventivas en sistemas eléctricos de potencia: tesis doctoral," Ph.D. dissertation, Universidad de Sevilla, 2010. 29

[43] C. Bordons, F. Garcia-Torres, and L. Valverde, "Gestión óptima de la energía en microrredes con generación renovable," *Revista Iberoamericana de Automática e Informática Industrial RIAI*, vol. 12, no. 2, pp. 117–132, 2015. 29, 180

[44] A. E.-M. M. M. Aly and A. El-Aal, "Modelling and simulation of a photovoltaic fuel cell hybrid system," Ph.D. dissertation, 2005. 30

[45] M. A. Pedrasa and T. Spooner, "A survey of techniques used to control microgrid generation and storage during island operation," in *Proceedings of the 2006 Australasian Universities Power Engineering Conference (AUPEC'06)*, 2006, pp. 1–6. 30, 42

[46] J. C. Vásquez Quintero *et al.*, "Decentralized control techniques applied to electric power distributed generation in microgrids," 2009. 31, 34, 40, 41, 148, 149

[47] J. M. Guerrero, J. C. Vasquez, J. Matas, L. G. de Vicuña, and M. Castilla, "Hierarchical control of droop-controlled ac and dc microgridsa general approach toward standardization," *Industrial Electronics, IEEE Transactions on*, vol. 58, no. 1, pp. 158–172, 2011. 31

[48] K. De Brabandere, K. Vanthournout, J. Driesen, G. Deconinck, and R. Belmans, "Control of microgrids," in *Power Engineering Society General Meeting, 2007. IEEE.* IEEE, 2007, pp. 1–7. 31, 32

[49] J. M. Guerrero, P. C. Loh, M. Chandorkar, and T.-L. Lee, "Advanced control architectures for intelligent microgrids, part i: Decentralized and hierarchical control," *IEEE Transactions on Industrial Electronics*, vol. 60, no. 4, pp. 1254–1262, 2013. 33, 34, 39

[50] Y. Wang, Z. Lu, Y. Min, Z. Bo, L. Hossenlopp, and A. Grid, "Four-level hierarchical control system for micorgrid." 32

[51] D. E. Olivares, A. Mehrizi-Sani, A. H. Etemadi, C. A. Cañizares, R. Iravani, M. Kazerani, A. H. Hajimiragha, O. Gomis-Bellmunt, M. Saeedifard, R. Palma-Behnke *et al.*, "Trends in microgrid control," 2014. 32

[52] H. Kumar Nunna and S. Doolla, "Multiagent-based distributed-energy-resource management for intelligent microgrids," *Industrial Electronics, IEEE Transactions on*, vol. 60, no. 4, pp. 1678–1687, 2013. 32

[53] C. Colson and M. H. Nehrir, "Comprehensive real-time microgrid power management and control with distributed agents," *IEEE Transactions on Smart Grid*, vol. 4, no. 1, pp. 617–627, 2013.

[54] M. Fathi and H. Bevrani, "Statistical cooperative power dispatching in interconnected microgrids," *IEEE Transactions on Sustainable Energy*, vol. 4, no. 3, pp. 586–593, 2013.

[55] J. Wu and X. Guan, "Coordinated multi-microgrids optimal control algorithm for smart distribution management system," *Smart Grid, IEEE Transactions on*, vol. 4, no. 4, pp. 2174–2181, 2013. 32

[56] K. Lee, J. C. Eidson, H. Weibel, and D. Mohl, "Ieee 1588-standard for a precision clock synchronization protocol for networked measurement and control systems," in *Conference on IEEE*, vol. 1588, 2005. 33

[57] F. Katiraei and M. Iravani, "Power management strategies for a microgrid with multiple distributed generation units," *Power Systems, IEEE Transactions on*, vol. 21, no. 4, pp. 1821–1831, 2006. 33

[58] M. Prodanovic and T. C. Green, "High-quality power generation through distributed control of a power park microgrid," *Industrial Electronics, IEEE Transactions on*, vol. 53, no. 5, pp. 1471–1482, 2006.

[59] M. N. Marwali, J.-W. Jung, and A. Keyhani, "Control of distributed generation systems-part ii: Load sharing control," *Power Electronics, IEEE Transactions on*, vol. 19, no. 6, pp. 1551–1561, 2004.

[60] A. Mehrizi-Sani and R. Iravani, "Potential-function based control of a microgrid in islanded and grid-connected modes," *Power Systems, IEEE Transactions on*, vol. 25, no. 4, pp. 1883–1891, 2010. 33

[61] J. M. Guerrero, L. Garcia de Vicuna, J. Matas, M. Castilla, and J. Miret, "Output impedance design of parallel-connected ups inverters with wireless load-sharing control," *Industrial Electronics, IEEE Transactions on*, vol. 52, no. 4, pp. 1126–1135, 2005. 33

[62] J. M. Guerrero, J. Matas, L. G. De Vicuña, M. Castilla, and J. Miret, "Wireless-control strategy for parallel operation of distributed-generation inverters," *Industrial Electronics, IEEE Transactions on*, vol. 53, no. 5, pp. 1461–1470, 2006.

[63] J. M. Guerrero, J. C. Vasquez, J. Matas, M. Castilla, and L. G. de Vicuña, "Control strategy for flexible microgrid based on parallel line-interactive ups systems," *Industrial Electronics, IEEE Transactions on*, vol. 56, no. 3, pp. 726–736, 2009.

[64] K. De Brabandere, B. Bolsens, J. Van den Keybus, A. Woyte, J. Driesen, and R. Belmans, "A voltage and frequency droop control method for parallel inverters," *Power Electronics, IEEE Transactions on*, vol. 22, no. 4, pp. 1107–1115, 2007. 33

[65] S. Vazquez, S. M. Lukic, E. Galvan, L. G. Franquelo, and J. M. Carrasco, "Energy storage systems for transport and grid applications," *Industrial Electronics, IEEE Transactions on*, vol. 57, no. 12, pp. 3881–3895, 2010. 35

[66] A. Tani, M. B. Camara, and B. Dakyo, "Energy management based on frequency approach for hybrid electric vehicle applications: Fuel-cell/lithium-battery and ultracapacitors," *Vehicular Technology, IEEE Transactions on*, vol. 61, no. 8, pp. 3375–3386, 2012.

[67] L. Wang and H. Li, "Maximum fuel economy-oriented power management design for a fuel cell vehicle using battery and ultracapacitor," *Industry Applications, IEEE Transactions on*, vol. 46, no. 3, pp. 1011–1020, 2010.

[68] W.-S. Liu, J.-F. Chen, T.-J. Liang, R.-L. Lin, and C.-H. Liu, "Analysis, design, and control of bidirectional cascoded configuration for a fuel cell hybrid power system," *Power Electronics, IEEE Transactions on*, vol. 25, no. 6, pp. 1565–1575, 2010.

[69] E. Schaltz and P. O. Rasmussen, "Design and comparison of power systems for a fuel cell hybrid electric vehicle," in *Industry Applications Society Annual Meeting, 2008. IAS'08. IEEE.* IEEE, 2008, pp. 1–8. 35, 36

[70] P. Arora, R. E. White, and M. Doyle, "Capacity fade mechanisms and side reactions in lithium-ion batteries," *Journal of the Electrochemical Society*, vol. 145, no. 10, pp. 3647–3667, 1998. 35, 73, 111

[71] L. A. Flores Oropeza, "Estudio y análisis de soluciones tipológicas de convertidores cc-cc bidireccionales para su aplicación en vehículos híbridos," Ph.D. dissertation, Industriales, 2004. 36

[72] D. Ketata and L. Krichen, "Dynamic modeling and control of a hybrid unit based on a pemfc-supercapacitor." 36

[73] G. Samson, T. M. Undeland, O. Ulleberg, and P. Vie, "Optimal load sharing strategy in a hybrid power system based on pv/fuel cell/battery/supercapacitor," in *Clean Electrical Power, 2009 International Conference on*. IEEE, 2009, pp. 141–146.

[74] Y. Zhang, Z. Jiang, and X. Yu, "Control strategies for battery/supercapacitor hybrid energy storage systems," in *Energy 2030 Conference, 2008. ENERGY 2008. IEEE*. IEEE, 2008, pp. 1–6.

[75] J. J. Awerbuch and C. R. Sullivan, "Control of ultracapacitor-battery hybrid power source for vehicular applications," in *Energy 2030 Conference, 2008. ENERGY 2008. IEEE*. IEEE, 2008, pp. 1–7. 36

[76] T. Zhou and B. Francois, "Modeling and control design of hydrogen production process for an active hydrogen/wind hybrid power system," *International Journal of Hydrogen Energy*, vol. 34, no. 1, pp. 21–30, 2009. 36

[77] F. Garcia, A. Ferreira, and J. Pomilio, "Control strategy for battery-ultracapacitor hybrid energy storage system," in *Applied Power Electronics Conference and Exposition, 2009. APEC 2009. Twenty-Fourth Annual IEEE*. IEEE, 2009, pp. 826–832. 36

[78] W.-S. Lin and C.-H. Zheng, "Energy management of a fuel cell/ultracapacitor hybrid power system using an adaptive optimal-control method," *Journal of Power Sources*, vol. 196, no. 6, pp. 3280–3289, 2011. 36

[79] P. Thounthong, S. Raël, and B. Davat, "Energy management of fuel cell/battery/supercapacitor hybrid power source for vehicle applications," *Journal of Power Sources*, vol. 193, no. 1, pp. 376–385, 2009. 36

[80] P. Thounthong, V. Chunkag, P. Sethakul, S. Sikkabut, S. Pierfederici, and B. Davat, "Energy management of fuel cell/solar cell/supercapacitor hybrid power source," *Journal of power sources*, vol. 196, no. 1, pp. 313–324, 2011. 36

[81] A. Vahidi and W. Greenwell, "A decentralized model predictive control approach to power management of a fuel cell-ultracapacitor hybrid," in *American Control Conference, 2007. ACC'07.* IEEE, 2007, pp. 5431–5437. 37

[82] W. Greenwell and A. Vahidi, "Predictive control of voltage and current in a fuel cell–ultracapacitor hybrid," *Industrial Electronics, IEEE Transactions on*, vol. 57, no. 6, pp. 1954–1963, 2010. 37

[83] A. Arce, A. J. del Real, and C. Bordons, "Mpc for battery/fuel cell hybrid vehicles including fuel cell dynamics and battery performance improvement," *Journal of Process Control*, vol. 19, no. 8, pp. 1289–1304, 2009. 37

[84] C. Bordons, M. A. Ridao, A. Pérez, A. Arce, and D. Marcos, "Model predictive control for power management in hybrid fuel cell vehicles," in *Vehicle Power and Propulsion Conference (VPPC), 2010 IEEE.* IEEE, 2010, pp. 1–6. 37

[85] P. Pinson, C. Chevallier, and G. N. Kariniotakis, "Trading wind generation from short-term probabilistic forecasts of wind power," *Power Systems, IEEE Transactions on*, vol. 22, no. 3, pp. 1148–1156, 2007. 37, 93

[86] H. Holttinen, "Optimal electricity market for wind power," *Energy Policy*, vol. 33, no. 16, pp. 2052–2063, 2005. 37, 93

[87] M. Korpås, "Distributed energy systems with wind power and energy storage," Ph.D. dissertation, Norwegian University of Science and Technology, 2004. 37, 38

[88] T. Geer, J. Manwell, and J. McGowan, "A feasibility study of a wind/hydrogen system for marthas vineyard, massachusetts," in *American Wind Energy Association Windpower 2005 Conference*, 2005. 37

[89] R. Dufo-López, J. L. Bernal-Agustín, and J. Contreras, "Optimization of control strategies for stand-alone renewable energy systems with hydrogen storage," *Renewable energy*, vol. 32, no. 7, pp. 1102–1126, 2007. 37, 49, 51, 52, 53

[90] S. Chakraborty and M. G. Simoes, "Pv-microgrid operational cost minimization by neural forecasting and heuristic optimization," in *Industry Applications Society Annual Meeting, 2008. IAS'08. IEEE.* IEEE, 2008, pp. 1–8. 38

[91] Ø. Ulleberg, "The importance of control strategies in pv–hydrogen systems," *Solar Energy*, vol. 76, no. 1, pp. 323–329, 2004. 38, 134

[92] M. Little, M. Thomson, and D. Infield, "Electrical integration of renewable energy into stand-alone power supplies incorporating hydrogen storage," *International Journal of Hydrogen Energy*, vol. 32, no. 10, pp. 1582–1588, 2007. 134

[93] L. Valverde, F. Rosa, and C. Bordons, "Design, planning and management of a hydrogen-based microgrid," *Industrial Informatics, IEEE Transactions on*, vol. 9, no. 3, pp. 1398–1404, 2013. 38, 134

[94] W. Gu, Z. Wu, and X. Yuan, "Microgrid economic optimal operation of the combined heat and power system with renewable energy," in *Power and Energy Society General Meeting, 2010 IEEE.* IEEE, 2010, pp. 1–6. 38

[95] H. Kanchev, D. Lu, F. Colas, V. Lazarov, and B. Francois, "Energy management and operational planning of a microgrid with a pv-based active generator for smart grid applications," *Industrial Electronics, IEEE Transactions on*, vol. 58, no. 10, pp. 4583–4592, 2011. 38

[96] T. Zhou and B. François, "Energy management and power control of a hybrid active wind generator for distributed power generation and grid integration," *Industrial Electronics, IEEE Transactions on*, vol. 58, no. 1, pp. 95–104, 2011. 38

[97] C. O. Adika and L. Wang, "Autonomous appliance scheduling for household energy management," *Smart Grid, IEEE Transactions on*, vol. 5, no. 2, pp. 673–682, 2014. 38

[98] G. Ferrari-Trecate, E. Gallestey, P. Letizia, M. Spedicato, M. Morari, and M. Antoine, "Modeling and control of co-generation power plants: a hybrid system approach," *Control Systems Technology, IEEE Transactions on*, vol. 12, no. 5, pp. 694–705, 2004. 38

[99] R. Negenborn, M. Houwing, B. De Schutter, and J. Hellendoorn, "Model predictive control for residential energy resources using a mixed-logical dynamic model," in *Networking, Sensing and Control, 2009. ICNSC'09. International Conference on.* IEEE, 2009, pp. 702–707. 38

[100] A. del Real, A. Arce, and C. Bordons, "Hybrid model predictive control of a two-generator power plant integrating photovoltaic panels and a fuel cell," in *Decision and Control, 2007 46th IEEE Conference on*. IEEE, 2007, pp. 5447–5452. 38

[101] L. Valverde, C. Bordons, and F. Rosa, "Power management using model predictive control in a hydrogen-based microgrid," in *IECON 2012-38th Annual Conference on IEEE Industrial Electronics Society*. IEEE, 2012, pp. 5669–5676. 38

[102] F. De Angelis, M. Boaro, D. Fuselli, S. Squartini, F. Piazza, and Q. Wei, "Optimal home energy management under dynamic electrical and thermal constraints," *Industrial Informatics, IEEE Transactions on*, vol. 9, no. 3, pp. 1518–1527, 2013. 38, 134

[103] Q. Jiang, M. Xue, and G. Geng, "Energy management of microgrid in grid-connected and stand-alone modes," *Power Systems, IEEE Transactions on*, vol. 28, no. 3, pp. 3380–3389, 2013. 134

[104] P. Yang and A. Nehorai, "Joint optimization of hybrid energy storage and generation capacity with renewable energy," *Smart Grid, IEEE Transactions on*, vol. 5, no. 4, pp. 1566–1574, 2014. 134

[105] P. Malysz, S. Sirouspour, and A. Emadi, "An optimal energy storage control strategy for grid-connected microgrids," *Smart Grid, IEEE Transactions on*, vol. 5, no. 4, pp. 1785–1796, 2014. 38, 134

[106] M. Trifkovic, M. Sheikhzadeh, K. Nigim, and P. Daoutidis, "Modeling and control of a renewable hybrid energy system with hydrogen storage," *Control Systems Technology, IEEE Transactions on*, vol. 22, no. 1, pp. 169–179, 2014. 38

[107] R. Palma-Behnke, C. Benavides, F. Lanas, B. Severino, L. Reyes, J. Llanos, and D. Sáez, "A microgrid energy management system based on the rolling horizon strategy." *IEEE Trans. Smart Grid*, vol. 4, no. 2, pp. 996–1006, 2013. 38

[108] A. Khodaei, "Microgrid optimal scheduling with multi-period islanding constraints," *Power Systems, IEEE Transactions on*, vol. 29, no. 3, pp. 1383–1392, 2014. 38

[109] A. Vaccaro, V. Loia, G. Formato, P. Wall, and V. Terzija, "A self organizing architecture for decentralized smart microgrids synchronization, control and monitoring," *IEEE Transaction on Industrial Informatics*, vol. 11, no. 1, pp. 289 – 298, 2015. 38

[110] Z. Wang, B. Chen, J. Wang, M. M. Begovic, and C. Chen, "Coordinated energy management of networked microgrids in distribution systems." 38

[111] B. Jiang and Y. Fei, "Smart home in smart microgrid: A cost-effective energy ecosystem with intelligent hierarchical agents." 38

[112] D. T. Nguyen and L. B. Le, "Risk-constrained profit maximization for microgrid aggregators with demand response," 2014. 38

[113] M. Patsalides, D. Evagorou, G. Makrides, Z. Achillides, G. E. Georghiou, A. Stavrou, V. Efthimiou, B. Zinsser, W. Schmitt, and J. H. Werner, "The effect of solar irradiance on the power quality behaviour of grid connected photovoltaic systems," in *International Conference on Renewable Energy and Power Quality*, 2007, pp. 1–7. 39

[114] M. A. Eltawil and Z. Zhao, "Grid-connected photovoltaic power systems: Technical and potential problemsa review," *Renewable and Sustainable Energy Reviews*, vol. 14, no. 1, pp. 112–129, 2010.

[115] F. Díaz-González, A. Sumper, O. Gomis-Bellmunt, and R. Villafáfila-Robles, "A review of energy storage technologies for wind power applications," *Renewable and Sustainable Energy Reviews*, vol. 16, no. 4, pp. 2154–2171, 2012.

[116] J. Soens, "Impact of wind energy in a future power grid," *Leuven, Belgica, Katholieke Universiteit Leuven*, 2005. 63

[117] T. Sun, "Power quality of grid-connected wind turbines with dfig and their interaction with the grid," Ph.D. dissertation, Aalborg University, Denmark, 2004. 39

[118] J. M. Guerrero, P. C. Loh, T.-L. Lee, and M. Chandorkar, "Advanced control architectures for intelligent microgridspart ii: Power quality, energy storage, and ac/dc microgrids," *Industrial Electronics, IEEE Transactions on*, vol. 60, no. 4, pp. 1263–1270, 2013. 39

[119] I. Wasiak, R. Pawelek, and R. Mienski, "Energy storage application in low-voltage microgrids for energy management and power quality improvement," *Generation, Transmission & Distribution, IET*, vol. 8, no. 3, pp. 463–472, 2014. 39

[120] N. A. Ahmed, M. Miyatake, and A. Al-Othman, "Power fluctuations suppression of stand-alone hybrid generation combining solar photovoltaic/wind turbine and fuel cell systems," *Energy Conversion and Management*, vol. 49, no. 10, pp. 2711–2719, 2008. 39

[121] X. Li, D. Hui, X. Lai, and T. Yan, "Power quality control in wind/fuel cell/battery/hydrogen electrolyzer hybrid micro-grid power system," *Applications and Experiences of Quality Control, InTech, Vienna*, pp. 579–594, 2011. 39

[122] R. Majumder, "Modeling, stability analysis and control of microgrid," 2010. 40

[123] M. Savaghebi, J. C. Vasquez, A. Jalilian, and J. M. Guerrero, "Secondary control for compensation of voltage harmonics and unbalance in microgrids," in *Power Electronics for Distributed Generation Systems (PEDG), 2012 3rd IEEE International Symposium on*. IEEE, 2012, pp. 46–53. 40

[124] A. Ghosh, R. Majumder, G. Ledwich, and F. Zare, "Power quality enhanced operation and control of a microgrid based custom power park," in *Control and Automation, 2009. ICCA 2009. IEEE International Conference on*. IEEE, 2009, pp. 1669–1674. 40

[125] Q. Fu, A. Nasiri, V. Bhavaraju, A. Solanki, T. Abdallah, and D. C. Yu, "Transition management of microgrids with high penetration of renewable energy," *Smart Grid, IEEE Transactions on*, vol. 5, no. 2, pp. 539–549, 2014. 41

[126] E. Mojica-Nava, C. A. Macana, and N. Quijano, "Dynamic population games for optimal dispatch on hierarchical microgrid control," *Systems, Man, and Cybernetics: Systems, IEEE Transactions on*, vol. 44, no. 3, pp. 306–317, 2014. 41

[127] M. B. Delghavi, "Advanced islanded-mode control of microgrids," 2011. 41

[128] Z. Jiang and X. Yu, "Active powervoltage control scheme for islanding operation of inverter-interfaced microgrids," in *Power & Energy Society General Meeting, 2009. PES'09. IEEE*. IEEE, 2009, pp. 1–7. 41, 42

[129] J. Rodriguez, J. Pontt, C. A. Silva, P. Correa, P. Lezana, P. Cortés, and U. Ammann, "Predictive current control of a voltage source inverter," *Industrial Electronics, IEEE Transactions on*, vol. 54, no. 1, pp. 495–503, 2007. 41, 43

[130] T. Geyer, G. Papafotiou, and M. Morari, "Hybrid model predictive control of the step-down dc–dc converter," *Control Systems Technology, IEEE Transactions on*, vol. 16, no. 6, pp. 1112–1124, 2008. 41

[131] K. H. Kwan, K. T. Tan, and P. L. So, "An unified power quality conditioner for load sharing and power quality improvement," in *Electromagnetic Compatibility (APEMC), 2012 Asia-Pacific Symposium on*. IEEE, 2012, pp. 963–967. 41

[132] J. Peas Lopes, C. Moreira, and A. Madureira, "Defining control strategies for microgrids islanded operation," *Power Systems, IEEE Transactions on*, vol. 21, no. 2, pp. 916–924, 2006. 42

[133] C. K. Sao and P. W. Lehn, "Control and power management of converter fed microgrids," *Power Systems, IEEE Transactions on*, vol. 23, no. 3, pp. 1088–1098, 2008. 42

[134] H. Karimi, H. Nikkhajoei, and R. Iravani, "A linear quadratic gaussian controller for a stand-alone distributed resource unit-simulation case studies," in *Power Engineering Society General Meeting, 2007. IEEE*. IEEE, 2007, pp. 1–6. 42

[135] Y. Li, D. M. Vilathgamuwa, and P. C. Loh, "Design, analysis, and real-time testing of a controller for multibus microgrid system," *Power electronics, IEEE transactions on*, vol. 19, no. 5, pp. 1195–1204, 2004. 42

[136] M. B. Delghavi and A. Yazdani, "Islanded-mode control of electronically coupled distributed-resource units under unbalanced and nonlinear load conditions," *Power Delivery, IEEE Transactions on*, vol. 26, no. 2, pp. 661–673, 2011. 42

[137] G. Escobar, A. A. Valdez, J. Leyva-Ramos, and P. Mattavelli, "Repetitive-based controller for a ups inverter to compensate unbalance and harmonic distortion," *Industrial Electronics, IEEE Transactions on*, vol. 54, no. 1, pp. 504–510, 2007. 42

[138] G. Willmann, D. F. Coutinho, L. F. A. Pereira, and F. B. Libano, "Multiple-loop h-infinity control design for uninterruptible power supplies," *Industrial Electronics, IEEE Transactions on*, vol. 54, no. 3, pp. 1591–1602, 2007. 42

[139] Z. Zeng, H. Yang, Q. Tang, and R. Zhao, "Objective-oriented power quality compensation of multi-functional grid-tied inverters and its application in micro-grids," 2015. 42

[140] H. Han, Y. Liu, Y. Sun, J. Guerrero *et al.*, "An improved droop control strategy for reactive power sharing in islanded microgrid," 2014. 42

[141] J. He, Y. Li, and F. Blaabjerg, "An islanding microgrid reactive power, imbalance power, and harmonic power sharing scheme," 2015. 42

[142] A. Ovalle, G. Ramos, S. Bacha, A. Hably, and A. Rumeau, "Decentralized control of voltage source converters in microgrids based on the application of instantaneous power theory," 2014. 42

[143] S. Seidi Khorramabadi and A. Bakhshai, "Critic-based self-tuning pi structure for active and reactive power control of vscs in microgrid systems." 42

[144] S. Kouro, P. Cortés, R. Vargas, U. Ammann, and J. Rodríguez, "Model predictive controla simple and powerful method to control power converters," *Industrial Electronics, IEEE Transactions on*, vol. 56, no. 6, pp. 1826–1838, 2009. 43

[145] S. Vazquez, J. Leon, L. Franquelo, J. Rodriguez, H. Young, A. Marquez, and P. Zanchetta, "Model predictive control: A review of its applications in power electronics," *Industrial Electronics Magazine, IEEE*, vol. 8, no. 1, pp. 16–31, 2014. 43

[146] P. Cortés, G. Ortiz, J. I. Yuz, J. Rodríguez, S. Vazquez, and L. G. Franquelo, "Model predictive control of an inverter with output filter for ups applications," *Industrial Electronics, IEEE Transactions on*, vol. 56, no. 6, pp. 1875–1883, 2009. 43

[147] P. Cortes, J. Rodriguez, S. Vazquez, and L. G. Franquelo, "Predictive control of a three-phase ups inverter using two steps prediction horizon," in *Industrial Technology (ICIT), 2010 IEEE International Conference on*. IEEE, 2010, pp. 1283–1288. 43

[148] S. S. Soman, H. Zareipour, O. Malik, and P. Mandal, "A review of wind power and wind speed forecasting methods with different time horizons," in *North American Power Symposium (NAPS), 2010*. IEEE, 2010, pp. 1–8. 47, 62

[149] E. Lorenzo, *Electricidad solar. Ingeniera de los sistemas fotovoltaicos*. Instituto de Energa Solar. Universidad Politcnica de Madrid. Ed. Progensa. Sevilla., 2004. 49

[150] M. G. Villalva, J. R. Gazoli *et al.*, "Comprehensive approach to modeling and simulation of photovoltaic arrays," *Power Electronics, IEEE Transactions on*, vol. 24, no. 5, pp. 1198–1208, 2009. 53, 54, 108

[151] H. S. Rauschenbach, "Solar cell array design handbook-the principles and technology of photovoltaic energy conversion," 1980. 53, 54

[152] W. De Soto, S. Klein, and W. Beckman, "Improvement and validation of a model for photovoltaic array performance," *Solar energy*, vol. 80, no. 1, pp. 78–88, 2006. 54

[153] A. Driesse, S. Harrison, and P. Jain, "Evaluating the effectiveness of maximum power point tracking methods in photovoltaic power systems using array performance models," in *Power Electronics Specialists Conference, 2007. PESC 2007. IEEE*. IEEE, 2007, pp. 145–151. 54

[154] F. Nakanishi, T. Ikegami, K. Ebihara, S. Kuriyama, and Y. Shiota, "Modeling and operation of a 10 kw photovoltaic power generator using equivalent electric circuit method," in *Photovoltaic Specialists Conference, 2000. Conference Record of the Twenty-Eighth IEEE*. IEEE, 2000, pp. 1703–1706. 54

[155] R. Faranda, S. Leva, and V. Maugeri, "Mppt techniques for pv systems: energetic and cost comparison," in *Power and Energy Society General Meeting-Conversion and Delivery of Electrical Energy in the 21st Century, 2008 IEEE*. IEEE, 2008, pp. 1–6. 55

[156] A. Larsson, "Phd. dissertations, the power quality of wind turbines," Ph.D. dissertation, Chalmers University of Technology, Department of Electric Power Engineering, 2000. 59, 144

[157] E. Hau and H. von Renouard, *The wind resource*. Springer, 2006. 60

[158] M. Yin, G. Li, M. Zhou, and C. Zhao, "Modeling of the wind turbine with a permanent magnet synchronous generator for integration," in *Power Engineering Society General Meeting, 2007. IEEE.* IEEE, 2007, pp. 1–6. 60, 61

[159] F. Iov, A. D. Hansen, P. Sorensen, and F. Blaabjerg, "Wind turbine blockset in matlab/simulink," *Aalborg University, March*, 2004. 60, 61, 108

[160] G. Sybille, "Simpowersystems users guide, version 2014a, published under sublicense from hydro-québec, and the mathworks, inc," 2014. 61

[161] M. Shirazi, A. H. Viki, and O. Babayi, "A comparative study of maximum power extraction strategies in pmsg wind turbine system," in *Electrical Power & Energy Conference (EPEC), 2009 IEEE.* IEEE, 2009, pp. 1–6. 61

[162] T. Ackermann *et al.*, *Wind power in power systems.* Wiley Online Library, 2005, vol. 140. 63

[163] Å. Larsson, *The Power Qualities of Wind Turbines.* Chalmers University of Technology, 2000. 63

[164] A. Burke, "Ultracapacitors: why, how, and where is the technology," *Journal of power sources*, vol. 91, no. 1, pp. 37–50, 2000. 65, 66, 67

[165] J. Bauman, "Advances in fuel cell vehicle design," Ph.D. dissertation, University of Waterloo, 2008. 66

[166] B. Wu, C.-C. Lin, Z. Filipi, H. Peng, and D. Assanis, "Optimal power management for a hydraulic hybrid delivery truck," *Vehicle System Dynamics*, vol. 42, no. 1-2, pp. 23–40, 2004. 66

[167] S. Basu and T. M. Undeland, "Voltage and current ripple considerations for improving lifetime of ultra-capacitors used for energy buffer applications at converter inputs," in *Power Electronics Specialists Conference, 2007. PESC 2007. IEEE.* IEEE, 2007, pp. 1453–1457. 67

[168] N. Xu and J. Riley, "Nonlinear analysis of a classical system: The double-layer capacitor," *Electrochemistry Communications*, vol. 13, no. 10, pp. 1077–1081, 2011. 68

[169] K. B. Oldham, "A gouy–chapman–stern model of the double layer at a (metal)/(ionic liquid) interface," *Journal of Electroanalytical Chemistry*, vol. 613, no. 2, pp. 131–138, 2008. 68

[170] R. L. Hartmann II, "An aging model for lithium-ion cells," Ph.D. dissertation, The University of Akron, 2008. 70, 71, 72

[171] S. Hossain and D. Linden, "Handbook of batteries," *McGraw-Hill, New York*, 1995. 70, 71

[172] G. L. Plett, "Extended kalman filtering for battery management systems of lipb-based hev battery packs: Part 1. background," *Journal of Power sources*, vol. 134, no. 2, pp. 252–261, 2004. 71

[173] J. P. Christophersen, G. L. Hunt, C. D. Ho, and D. Howell, "Pulse resistance effects due to charging or discharging of high-power lithium-ion cells: A path dependence study," *Journal of Power Sources*, vol. 173, no. 2, pp. 998–1005, 2007. 72

[174] A. Ruddell, A. Dutton, H. Wenzl, C. Ropeter, D. Sauer, J. Merten, C. Orfanogiannis, J. Twidell, and P. Vezin, "Analysis of battery current microcycles in autonomous renewable energy systems," *Journal of Power sources*, vol. 112, no. 2, pp. 531–546, 2002. 73

[175] L. Valverde, F. Rosa, A. del Real, A. Arce, and C. Bordons, "Modeling, simulation and experimental set-up of a renewable hydrogen-based domestic microgrid," *International Journal of Hydrogen Energy*, vol. 38, no. 27, pp. 11 672–11 684, 2013. 73, 74, 77, 78

[176] F. Barbir, "Pem electrolysis for production of hydrogen from renewable energy sources," *Solar Energy*, vol. 78, no. 5, pp. 661–669, 2005. 75, 76

[177] H. Görgün, "Dynamic modelling of a proton exchange membrane (pem) electrolyzer," *International journal of hydrogen energy*, vol. 31, no. 1, pp. 29–38, 2006. 75, 76

[178] J. Cargnelli, "Recent advances in pem water electrolysis," *First International Workshop on durability and degradation issues of PEM electrolysis, Freiburg, Germany*, 2013. 76

[179] W. Grove, "A small voltaic battery of great energy," *Philosophical Magazine*, vol. 15, pp. 287–293, 1839. 80

[180] E. Leksono, J. Pradipta, and T. A. Tamba, "Modelling and identification of oxygen excess ratio of self-humidified pem fuel cell system," *Mechatronics, Electrical Power, and Vehicular Technology*, vol. 3, no. 1, pp. 39–48, 2012. 84

[181] J. Ishaku, N. Lotfi, H. Zomorodi, and R. G. Landers, "Control-oriented modeling for open-cathode fuel cell systems," in *American Control Conference (ACC), 2014*. IEEE, 2014, pp. 268–273. 84, 87

[182] F. Barreras, A. M. López, A. Lozano, and J. E. Barranco, "Experimental study of the pressure drop in the cathode side of air-forced open-cathode proton exchange membrane fuel cells," *International Journal of Hydrogen Energy*, vol. 36, no. 13, pp. 7612–7620, 2011. 84

[183] L. Zhang, D. Xu, and W. G. Hurley, "Modelling and simulation of a portable fuel cell system," in *Power Electronics and Motion Control Conference (EPE/PEMC), 2010 14th International*. IEEE, 2010, pp. T12–96. 84

[184] F. De Bruijn, V. Dam, and G. Janssen, "Review: durability and degradation issues of pem fuel cell components," *Fuel cells*, vol. 8, no. 1, pp. 3–22, 2008. 86

[185] B. P. Systems, *NexaTM .Power Module Users Manual*, 2003. 86

[186] A. Del Real, A. Arce, and C. Bordons, "Development and experimental validation of a pem fuel cell dynamic model," *Journal of Power Sources*, vol. 173, no. 1, pp. 310–324, 2007. 87

[187] F. Garcia and C. Bordons, "Optimal economic dispatch for renewable energy microgrids with hybrid storage using model predictive control," in *Industrial Electronics Society, IECON 2013-39th Annual Conference of the IEEE*. IEEE, 2013, pp. 7932–7937. 94, 180

[188] ——, "Regulation service for the short-term management of renewable energy microgrids with hybrid storage using model predictive control," in *Industrial Electronics Society, IECON 2013-39th Annual Conference of the IEEE*. IEEE, 2013, pp. 7962–7967. 94, 180

[189] F. Garcia-Torres and C. Bordons, "Optimal economical schedule of hydrogen-based microgrids with hybrid storage using model predictive control," *IEEE Transaction on Industrial Electronics*, 2015. 94, 136, 180

[190] J. T. Saraiva, H. Heitor, N. Correia, and R. Araujo, "Ancillary servicesthe current situation in the iberian electricity market and future possible developments," in *PowerTech, 2011 IEEE Trondheim*. IEEE, 2011, pp. 1–8. 95, 104

[191] Everis and Mercados, "From regional markets to a single european market, studied conducted by the european commission," Tech. Rep., 2009. 95, 96

[192] J.-M. Roldan-Fernandez, M. Burgos-Payan, A.-L. Trigo-Garcia, J.-L. Diaz-Garcia, and J.-M. Riquelme-Santos, "Impact of renewable generation in the spanish electricity market," in *European Energy Market (EEM), 2014 11th International Conference on the*. IEEE, 2014, pp. 1–5. 97

[193] O.-P. E. S. (OMIE). 99, 100, 101, 103, 106, 113

[194] MIBEL, "Description of the operation of the mibel," Regulatory Council, Tech. Rep., Madrid, 2009. 101, 103, 104

[195] P. Bennerstedt and J. Grelsson, "Spain's electricity market design: A case study," 2012. 101, 103

[196] "Final report, store project (june 2013)," 2011. 103

[197] "Creating the internal energy market in europe," *European Wind Energy Association*, 2012. 103, 106

[198] A. Bemporad and M. Morari, "Control of systems integrating logic, dynamics, and constraints," *Automatica*, vol. 35, no. 3, pp. 407–427, 1999. 107, 108, 111, 112, 116, 122, 123

[199] J. Spendelow, J. Marcinkoski, and S. Satyapal, "Doe hydrogen and fuel cells program record 14012," *Department of Energy (DOE)*, 2014. 125

[200] "Multi-year research, development and demonstration plan (hydrogen production)," *Department of Energy (DOE)*, 2014. 125

[201] D. Howel, "Battery status and cost reduction prospects. in ev everywhere grand challenge battery workshop," *Department of Energy (DOE)*, 2012. 125

[202] "Vision and strategy for europe's electricity networks of the future," Tech. Rep., 2006. 143, 144

[203] "Strategic research agenda," Tech. Rep., 2008. 143

[204] "Strategic deployment document for europe's electricity networks of the future," Tech. Rep., 2010. 143

[205] M. Patsalides, "The effect of solar irradiance on the power quality behaviour of grid connected photovoltaic systems," in *International Conference on Renewable Energies and Power Quality*, 2007. 144

[206] F. Garcia, "Model predictive control based current source converter for minimizing degradation aspects in fuel cell applications." in *ELECTRIMACS*. IMACS, 2014, pp. 640–645. 150, 180

[207] F. Garcia and C. Bordons, "Model predictive control based inverters for energy storage integration in renewable energy microgrids." in *ELECTRIMACS*. IMACS, 2014, pp. 31–36. 158, 180

[208] F. Garcia-Torres, C. Bordons, and S. Vazquez, "Voltage predictive control for microgrids in islanded mode based on fourier transform," in *ICIT*. IEEE, 2015, pp. 2358–2363. 164, 180